

Polymer Phase Separation in Competition Solvents

DISSERTATION

vorgelegt

der Fakultät Mathematik und Naturwissenschaften der
Technischen Universität Dresden

von

Master in Wissenschaften

Huaisong Yong

geboren am 09.06.1986 im Sichuan von China

zur Erlangung des akademischen Grades

Doctor rerum naturalium

(Dr. rer. nat.)

Gutachter: Prof. Dr. Andreas Fery
Prof. Dr. Jens-Uwe Sommer

Eingereicht am: 15. Dezember 2020

Tag der Verteidigung: 26. April 2021

Die Dissertation wurde in der Zeit von April 2017 bis
Dezember 2020 im Leibniz-Institut für Polymerforschung Dresden e.V. angefertigt.

Gutachter: **Prof. Dr. Andreas Fery**

Die Fakultät für Chemie und Lebensmittelchemie

Technische Universität Dresden

Leibniz-Institut für Polymerforschung Dresden e. V.

Prof. Dr. Jens-Uwe Sommer

Die Fakultät für Physik

Technische Universität Dresden

Leibniz-Institut für Polymerforschung Dresden e. V.

Abstract

Cononsolvency occurs if a mixture of two good solvents causes the collapse or demixing of polymers into a polymer-rich phase in a certain range of compositions of these two solvents. The better solvent is usually called cosolvent and another common solvent is called solvent. So far, the phase-transition mechanism behind cononsolvency is still rather controversially debated in literature. In this thesis, I experimentally investigated the cononsolvency effect of poly(N-isopropylacrylamide) (PNiPAAm) brushes with different grafting density in aqueous alcohol mixtures. I have used Vis-spectroscopic ellipsometry measurements and proved the hypothesis that the cononsolvency transition of PNiPAAm brushes consists of a volume phase-like equilibrium transition.

I found a strong collapse transition in PNiPAAm brushes followed by a reentry behavior as observed by ellipsometry measurements. Using a series of alcohols with increasing alkyl-chain length I have demonstrated that the cononsolvency effect is enhanced and shifted to smaller volume fractions of the alcohol. Particularly for the alcohol with increasing hydrophobic property this is correlated with an increasing tendency of demixing between the cosolvent and water. This is apparently in contrast to the hypothesis of strongly associative solvents being the origin of the cononsolvency effect. The hypothesis of preferential adsorption, on the other hand, can account for this case by assuming an increasing hydrophobically driven adsorption of the cosolvent on the polymer chains. The recently proposed adsorption-attraction model based on the concept of preferential adsorption, can be used to predict the corresponding phase-transition behavior. In particular the model predictions for variation of the grafting density is in agreement with the experimental findings. However, to reflect the imperfect mixing of the longer alcohols in water as well as finite miscibility of the polymers in the common solvent, extensions of the model have to be considered. I have shown that the simplest extension of the model taking into account the Flory-Huggins parameter for polymer and water can account for the qualitative changes observed for temperature changes in my experiments.

Both a theoretical analysis and experimental observations show that the phase-transition mechanism of cononsolvency depends on the relative strengths of various interactions in the polymer solutions. A cononsolvency transition can be driven by a strong cosolvent-solvent attraction or by the preferential adsorption of cosolvent onto the polymer. By an extension of the adsorption-attraction model, I report on a comprehensive and quantitative theoretical study of the cononsolvency effect of neutral polymers such as PNiPAAm brushes, macro-gels and single long chains. The extended adsorption-attraction model is able to describe and predict the phase-transition behaviors of these systems in various aqueous alcohol solutions quantitatively. My analysis showed that besides the dominant role of polymer-cosolvent preferential adsorption and the monomer-cosolvent-monomer triple contacts (cosolvent-assisted temporary cross-linking effect) that define the strength of the collapse-transition in the cosolvent-poor region, other effects are shown to be of relevance: The non-ideal mixing between polymer and solvent plays a role in shifting the collapse transition to the lower-concentration region of cosolvent, and an increase of the demixing tendency between cosolvent and solvent on the polymer chains reduces the window width of the cononsolvency transition. Using data from my own experiments and literature I can show that the cononsolvency response of brushes, gels and single long polymer chain can be consistently described with the same model. The model parameters are consistent with their microscopic interpretation. In addition, weakening of the cononsolvency transition in cosolvent-poor aqueous solutions at high hydrostatic pressure can be explained by the suppression of demixing tendency between cosolvent and water, and between polymer and water in the case of PNiPAAm.

An investigation of the grafting-density effect in the cononsolvency transition of grafted PNiPAAm polymer, showed that a decrease of grafting density at the collapse state as well as the temperature is fixed, the swollen polymer chains can show various morphologies not limited to collapse brush. In addition, my experimental results clearly showed that the strongest collapse state can be only realized by polymer brushes with moderate grafting densities. My results display the universal character of the cononsolvency effect with respect to series of cosolvents and show that PNiPAAm brushes display a well-defined and sharp collapse transition. This is most pronounced for 1-propanol as cosolvent which is still fully miscible in wa-

ter. Potential applications are switches built from implementation of brushes in pores and similar concave geometries can be realized by harnessing the cononsolvency effect of stimuli-responsive polymers such as PNiPAAm.

As an example of application of cononsolvency effect of grafted polymers, different molecular-weight PNiPAAm polymers are grafted around the rim of solid-state nanopores by using grafting-to method. I demonstrate that small amounts of ethanol admixed to an aqueous solution can trigger the translocation of fluorescence DNA through polymer-decorated nanopores. I can identify the cononsolvency effect as being responsible for this observation which causes an abrupt collapse of the brush by increasing the alcohol content of the aqueous solution followed by a reswelling at higher alcohol concentration. For the first time, I provide a quantitative method to estimate hydrodynamic thickness of a polymer layer which is grafted around the rim of nanopores. Regardless of the grafting density of a grafted PNiPAAm polymer layer around the rim of nanopores, in the alcohol-tris buffer mixtures, the polymer layer displays solvent-composition responsive behaviors in the range of metabolic pH values and room temperatures. Although in this study PNiPAAm was chosen as a model synthetic polymer, I believe in that the conclusions made for PNiPAAm can be also in general extended to other synthetic polymers as well as to biopolymers such as proteins. As a proof of concept of using synthetic polymers to mimic biological functions of cell-membrane channels, my study clearly transpired that cononsolvency effect of polymers can be used as a trigger to change the size of nanopores in analogy to the opening and closure of the gates of cell-membrane channels.

Contents

Chapter 1 Background and motivation.....	4
1.1 Liquid-liquid phase separation	4
1.2 Polymer phase separation in a pure solvent	5
1.3 Polymer phase separation in mixtures of two good solvents	10
1.4 Characterizing cononsolvency transition in experimental study	14
1.5 Research motivation	16
Chapter 2 Phase behaviors of PNiPAAm brushes in alcohol/water mixtures: A combined experimental and theoretical study.....	17
2.1 Introduction	17
2.2 Materials and Methods	17
2.2.1 Materials	17
2.2.2 Preparation of Polymer Brushes	18
2.2.3 VIS-Spectroscopic Ellipsometry Measurement	18
2.2.4 Determining a polymer brush's overlap grafting density	19
2.2.5 Test of PNiPAAm solubility in short-chain polyols	20
2.3 The adsorption-attraction model	20
2.4 Equilibrium behavior of cononsolvency transition of PNiPAAm brushes.....	22
2.5 Role of volume of solvent molecules in the swelling of PNiPAAm brushes	24
2.6 Cononsolvency transition of PNiPAAm brushes in aqueous solutions of a series of alcohol	24
2.7 Isomer effect of alcohol in the cononsolvency transition of PNiPAAm brushes	27
2.8 Role of alcohol-water interaction in the cononsolvency transition of PNiPAAm polymers.....	28
2.9 Temperature effect in the cononsolvency transition of PNiPAAm brushes	30
2.10 Grafting-density effect in the cononsolvency transition of PNiPAAm brushes	33
2.11 Octopus-shape-micelle morphology of grafted PNiPAAm polymers	34
2.12 Chapter summary	35
2.13 Chapter appendix	37
2.13.1 Data extraction and reprocessing for the molar Gibbs free energy of mixing	37
2.13.2 Temperature effect in the cononsolvency transition of PNiPAAm gels.....	37
Chapter 3 The extended adsorption-attraction model	41
3.1 Introduction	41

3.2	<i>An extension of the adsorption-attraction model</i>	43
3.3	<i>Numerical solution of the extended adsorption-attraction model</i>	47
3.4	<i>Validation of the extended adsorption-attraction model</i>	50
3.4.1	<i>Cononsolvency transition of polymer brushes and macro-gels in different alcohol-water mixtures</i> 51	
3.4.2	<i>An analysis of the enthalpic interaction between cosolvent and solvent</i>	57
3.4.3	<i>The window width of the cononsolvency transition</i>	60
3.4.4	<i>Pressure effect in the cononsolvency transition of PNiPAAm polymers.....</i>	61
3.4.5	<i>Cononsolvency transition of a single long polymer.....</i>	65
3.5	<i>Chapter summary</i>	66
3.6	<i>Chapter appendix</i>	67
3.6.1	<i>Chemical potential change of mixing two components.....</i>	67
3.6.2	<i>The Enthalpic Wilson model</i>	68
3.6.3	<i>Estimation of effective Flory-interaction parameter</i>	73
3.6.4	<i>Crosslink-density effect in the cononsolvency transition of poly(N-isopropylacrylamide) micro-gel</i> <i>and macro-gel</i>	74
3.6.5	<i>Pressure effect on the dimensionless chemical potential change (μ).....</i>	75
3.6.6	<i>Pressure effect on the cosolvent-solvent interaction (χ_{cs})</i>	76
3.6.7	<i>Pressure effect on the polymer-solvent interaction (χ_{ps}).....</i>	77
3.6.8	<i>Chemical potential change of DMSO/water mixtures.....</i>	78
Chapter 4 Gating the translocation of DNA through poly(N-isopropylacrylamide) decorated nanopores using the cononsolvency effect in aqueous environments		80
4.1	<i>Introduction.....</i>	80
4.2	<i>Methods.....</i>	80
4.2.1	<i>Preparation of polymer-grafted gold membrane.....</i>	80
4.2.2	<i>Translocation experiments of fluorescence λ-DNA through nanopores.....</i>	82
4.2.3	<i>Method of identification and counting of DNA translocation events</i>	84
4.3	<i>Results and discussion</i>	86
4.3.1	<i>Grafting density effect on the swollen behaviors of PNiPAAm polymers around the rim of</i> <i>nanopores</i>	86
4.3.2	<i>Switching effect of polymer chains around the rim of nanopores in the tri-buffer/ethanol mixtures</i> 88	
4.3.3	<i>Switching effect of polymer brushes on the flat surface in the tri-buffer/ethanol mixtures.....</i>	92

4.3.4	<i>An attempt of numerical fit of experimental data using the extended adsorption-attraction model</i>	94
4.4	<i>Chapter summary</i>	95
4.5	<i>Chapter appendix</i>	96
4.5.1	<i>An estimation of grafting density</i>	96
4.5.2	<i>The method of processing data</i>	97
Chapter 5 Concluding remarks and outlooks		100
5.1	<i>Concluding remarks</i>	100
5.2	<i>Outlooks: A preliminary discussion of the cononsolvency transition of polymer solutions</i>	102
References and notes		108
List of figures		119
List of tables		128
Acknowledgements		130
List of publications		131
Erklärung		132

Chapter 1 Background and motivation

1.1 Liquid-liquid phase separation

A liquid-liquid phase separation is a reversible process of a homogenous fluid de-mixing into multiple phases. When polymers are exposed to mixed solvents, various coacervate phases can be formed by variation of solution composition, temperature, and pressure [1-4]. The maximum number of distinct coexisting phases that can emerge within a liquid-liquid phase separation is given by the phase rule, which can be derived from classical thermodynamics [5]. Accordingly, a mixture of n nonreactive components can coexist in as much as a maximum of $n+2$ distinct phases. In mixtures with reactive components, this maximum is decreased by k , the number of linearly independent chemical reactions in the system, which is equal to the rank of the stoichiometry matrix. An extraordinary but general signature of a liquid-liquid phase separation is the coexistence of two stable distinct phases, i.e., a dilute phase and a condense phase. In contrast, three- or more- phases can only stably coexist over a narrower range of thermodynamic variables; for example, in a single-component system, it will only be at the triple point where three phases can coexist with one another [6].

In order for a liquid-liquid phase separation to be thermodynamically favoured, it needs to result in a decrease in the mixture's Gibbs free energy [5, 6]. Let $x_l \equiv (x_{l1}, x_{l2}, \dots, x_{ln})$ be the composition vector of a homogeneous liquid mixture (name it as l) with that x_{li} is the molar fraction of the i -th component. Upon a phase separation, the initial phase l will separate into two coexisting phases, a dilute phase (name it as d) and a condense phase (name it as c). Note that x_l will be located on a tie line connecting x_d and x_c , i.e., there will be a partition constant $0 < \lambda < 1$ so that $x_l = \lambda x_d + (1 - \lambda)x_c$. Since the two phases d and c will be at an equilibrium, $\mu_d(x_d) = \mu_c(x_c)$ with $\mu_\alpha \equiv (\mu_{\alpha 1}, \mu_{\alpha 2}, \dots, \mu_{\alpha n})$ being a chemical potential vector for phase $\alpha = d, c$. The change in the free energy of the system as a result of a phase separation will therefore be given by:

$$\Delta g = \lambda g_d(x_d) + (1 - \lambda)g_c(x_c) - g_l(x_l) = \lambda x_d \mu_d(x_d) + (1 - \lambda)x_c \mu_c(x_c) - x_l \mu_l(x_l). \quad (1.1)$$

Here $g_\alpha(x_\alpha)$ is the molar Gibbs free energy of phase $\alpha = d, c, l$. The described phase separation will be thermodynamically favoured if $\Delta g = x_l(\mu_d(x_d) - \mu_l(x_l)) = x_l(\mu_c(x_c) - \mu_l(x_l)) < 0$. Also, the constraints imposed on chemical potentials and the overall composition of the two phases imply that x_d and x_c and λ can be uniquely determined from the temperature, pressure and composition of the original mixture. In general, it is possible to obtain empirical or semi-empirical expressions for μ_α , which can then be utilized to predict the possibility- or like thereof- phase separation for any given mixture. In a liquid-liquid phase separation under a given temperature and pressure the following Gibbs-Duhem equation holds:

$$\sum_{i=1}^n x_{\alpha i} d\mu_{\alpha i} = 0 \text{ with a constraint of } \sum_{i=1}^n x_{\alpha i} = 1, \quad (1.2)$$

where $d\mu_{\alpha i}$ is an infinitesimal increase in chemical potential for the i -th component in the α -phase.

Figure 1.1 is a graphical presentation when there are only two components in the liquid mixtures, a particular example is the liquid mixture containing a polymer and solvent.

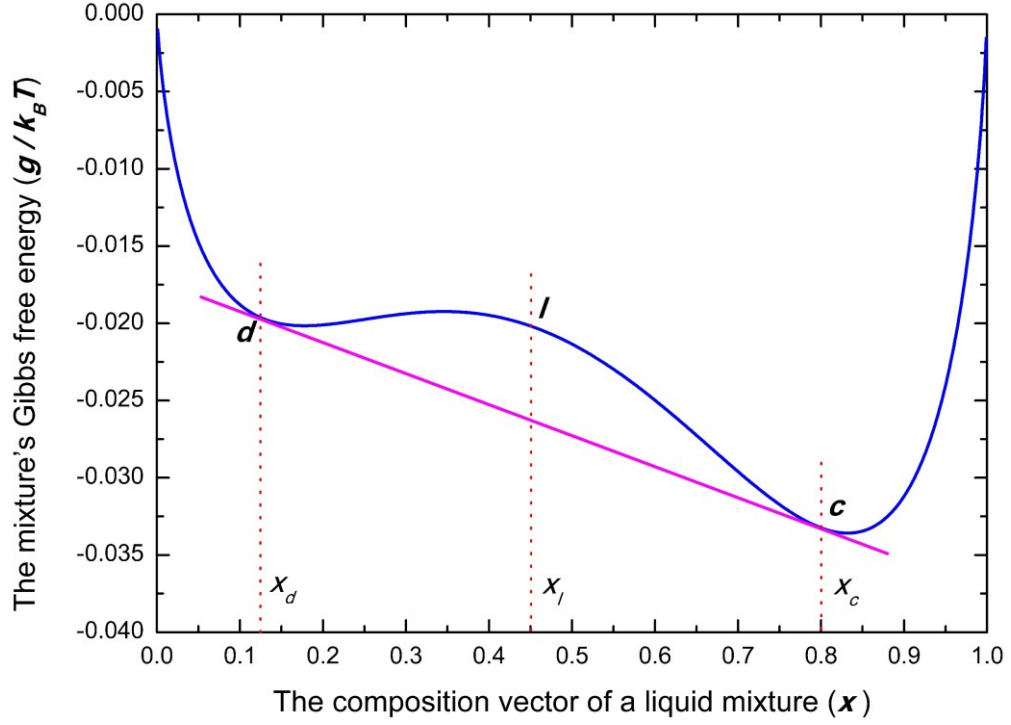


Figure 1.1(Figure 1) A graphical plot of the mixture's Gibbs free energy (g) in respect to the composition vector of the liquid mixture (x). For simplicity, in the figure I plot the situation when the system only has two components. It is noted that if $x_d < x_l < x_c$, the system will undergo a phase separation when it goes to thermodynamic equilibrium.

1.2 Polymer phase separation in a pure solvent

When a polymer is mixed with a pure solvent, segregation effects in the polymer solution are usually caused by repulsive interactions between monomers and solvent. This is rationalized by the Flory-Huggins mean-field model [7, 8] where the interaction between the different components such as solvent and monomers is represented by a phenomenological χ -parameter. This model can be written in the following form for a simple polymer solvent mixture:

$$G_{FH} = \frac{c \ln(c)}{N} + (1-c) \ln(1-c) + \chi_{ps} c(1-c). \quad (1.3)$$

Here, the volume fraction of each polymer chain consisting of N monomers in the solution is denoted by c , and the free energy per volume of the polymer solution, G_{FH} , is taken in units of $k_B T$. In this representation the χ -parameter, χ_{ps} , corresponds to the effective (typically repulsive) interaction

between the monomers and the solvent. In mean-field theories for homopolymer solutions, the parameter χ_{ps} is defined as:

$$\chi_{ps} = \frac{z(2\varepsilon_{ps} - \varepsilon_{pp} - \varepsilon_{ss})}{2k_B T}. \quad (1.4)$$

In **Eq.(1.4)**, the term ε_{ij} refers to a mean-field energy for an interaction between species i and j ; the subscripts p and s refer to the polymer and solvent, respectively. The algebraic sum of energies is made dimensionless by normalization using the parameter $k_B T$, which quantifies the thermal energy at temperature T ; z is a coordination number that represents the average number of nearest-neighbor interactions that each monomeric unit within the polymer can make.

Consider adding a small amount of polymer molecules to a liquid of pure solvent ($c \ll 1$). The free energy (G_{FH}) in **Eq.(1.3)** can be expanded into a power series in composition (c) of the polymer molecules. For small values of composition ($c \ll 1$), the free energy (G_{FH}) in **Eq.(1.3)** can be rewritten into its virial expansion [9]:

$$G_{FH} = \frac{c \ln(c)}{N} + \nu_1 c + \frac{1}{2} \nu_2 c^2 + \frac{1}{6} \nu_3 c^3 + \frac{1}{12} \nu_4 c^4 + \dots \quad (1.5)$$

Here, the first virial coefficient is $\nu_1 = \chi_{ps} - 1$, the second virial coefficient is $\nu_2 = 1 - 2\chi_{ps}$ with both the third and the fourth virial coefficients being $\nu_3 = 1$, $\nu_4 = 1$. When the second virial coefficient is negative (the third virial coefficient is positive), the polymer solution is unstable and it decomposes into a dilute and condense polymer phases. This type phase separation is well-known and well-studied as type-I phase transition. It is noted that from the virial expansion, the two-body interaction (v , or conventionally termed as excluded volume) between polymer and solvent can be estimated by $v = \nu_2 b^3 = (1 - 2\chi_{ps})b^3$ and the three-body-interaction (w) between polymer and solvent is calculated [9] by $w = \nu_3 b^6/3 = b^6/3$, where b is a monomer size of the polymer.

In a polymer solution [9, 10] comprising a polymer and a poor solvent where the second virial coefficient (ν_2) is negative (see **Eq.(1.5)**), there exists a system-specific χ_{ps} -dependent concentration threshold designated as the saturation concentration or c_{sat} beyond which the system separates into a condense polymer-rich phase (sometimes in the form of precipitate) that coexists with a very dilute liquid supernatant (polymer-poor phase, with the concentration c_{sat}), see **Figure 1.2**. The volume fractions of the polymer in the coexisting dilute and condense phases are designated as c_{dilute} and c_{dense} , respectively, where $c_{dilute} = c_{sat}$. For $c_{dilute} < c < c_{dense}$, the numbers of the polymer molecules in the two phases are determined by the so-called lever rule: $n_{dilute} = n_{total}(c_{dense} - c)/(c_{dense} - c_{dilute})$ and $n_{dense} = n_{total}(c - c_{dilute})/(c_{dense} - c_{dilute})$, where n_{dilute} and n_{dense} are the numbers of polymer molecules in the dilute and condense phases respectively, and n_{total} is the total number of polymer molecules: $n_{total} = n_{dilute} + n_{dense}$. For homopolymer solutions, the magnitude of the system-specific Flory-Huggins interaction parameter between the polymer and solvent χ_{ps} , which is larger than $0.5 + 1/\sqrt{N}$ in a poor

solvent, will determine the values of c_{dilute} at the order of $(2\chi_{ps} - 1) \exp(-(2\chi_{ps} - 1) N^{2/3})$ and c_{dense} at the order of $(2\chi_{ps} - 1)$ via the so-called common tangent construction for free energy G_{FH} with respect to polymer concentration c .

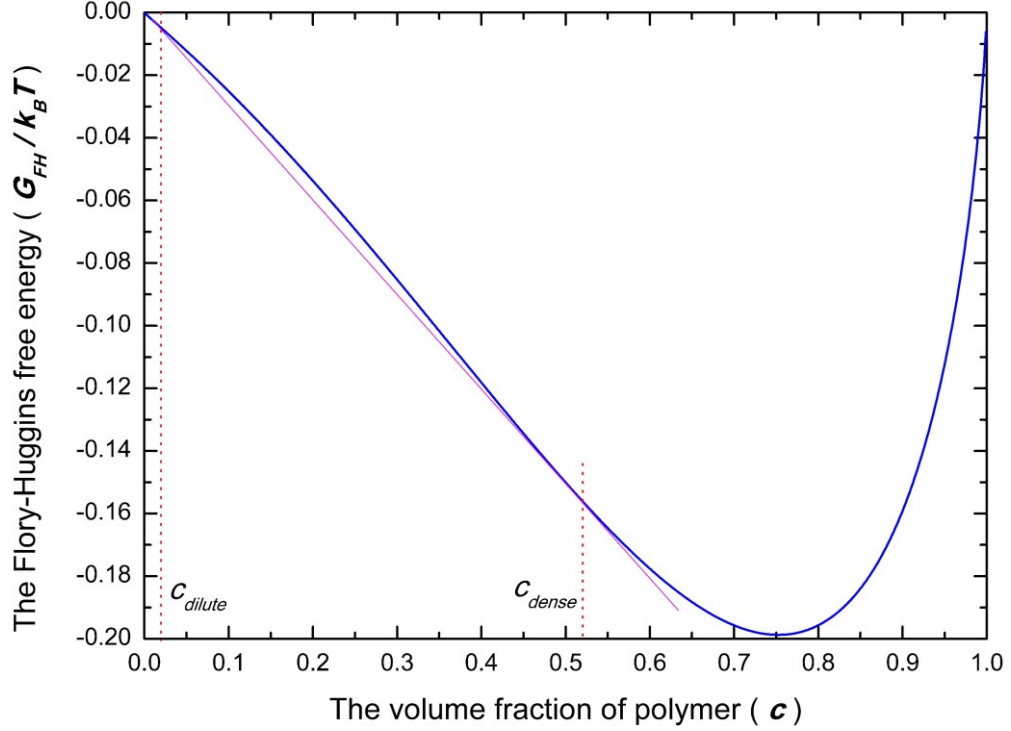


Figure 1.2 (Figure 2) A graphical plot of the Flory-Huggins free energy (G_{FH} , Eq.(1.3)) with respect to the volume fraction of polymer (c) for polymer solutions. It is noted that if $c \leq c_{dilute}$ or $c \geq c_{dense}$, there is no phase separation. Parameter used in the plot are $N = 100$ and $\chi_{ps} = 0.8$.

Here, it is worth noting that a binary mixture comprising a polymer and a solvent, a positive Flory-Huggins χ -parameter implies that the polymer and the solvent tend to lower the free energy when they separate each other into two phases: one polymer-rich phase and a solvent-rich phase. This leads to that for both phases, enthalpy contribution is small and the free energy (G_{FH}) is low, see Eq.(1.3). What's more, to lower the overall free energy, a discontinuous Flory-Huggins phase transition and coexistence between a condensed phase and a very diluted phase of the polymer is the consequence of the balance between the entropy of translation of the polymers in the diluted state and the interaction enthalpy in the condensed state, see Eq.(1.3). On accounting of this reason, for polymer chains immobilized on a substrate (brushes), by cross-linking (gels), or in the semi-diluted state ($c \geq c_{dense}$, see Figure 1.2) such as caused by a finite osmotic pressure (osmotic membrane), the first term in Eq.(1.3) vanishes, or can be ignored, thus no phase coexistence can occur. In these cases, the degradation of the solvent quality merely leads to a monotonous and smooth increase of density.

Let us consider polymer brushes as an example to prove the above statement in detail, other cases can be verified by the same method. For polymer brushes, with an ansatz of mean-field Alexander-de Gennes approach [11] for elastic energy of a brush layer, we rewrite Eq.(1.3) as:

$$G_{FH} = \frac{1}{2} \frac{\sigma_d^2}{c} + (1-c) \ln(1-c) + \chi_{ps} c(1-c). \quad (1.6)$$

Here, parameter σ_d is the dimensionless grafting density of the polymer brush with the physical constraint of $0 < \sigma_d \leq 1$. The condition for the two-phase coexistence of a polymer-brush system can be probed by a study of spinodal phase decomposition in terms of the second derivative ($d^2 G_{FH}/dc^2$) of the free energy (G_{FH}), which corresponds to the surface of free energy (G_{FH}) being concave in mathematics ($d^2 G_{FH}/dc^2 < 0$), then we get the boundary,

$$\frac{d^2 G_{FH}}{dc^2} = \frac{\sigma_d^2}{c^3} + \frac{1}{1-c} - 2\chi_{ps} < 0. \quad (1.7)$$

It is inconvenient to get analytical solutions for monomer concentration (c) from parameters σ_d and χ_{ps} in the Eq.(1.7); however, it is much easier to handle its inverse function. We get,

$$\chi_{ps} > \frac{\sigma_d^2}{2c^3} + \frac{1}{2(1-c)}. \quad (1.8)$$

It does not matter what is the value of the parameter $0 < \sigma_d \leq 1$ that we choose, the function of χ_{ps} with respect to c doesn't exist a physical solution ($0 < c < 1$) at $\chi_{ps} = 1/2$ for a polymer brush, this contrasts remarkably with the case of polymer solutions. Actually, with a very sparse grafting density such as $\sigma_d \geq 0.01$, Eq.(1.8) already doesn't have a physical solution when the value of χ_{ps} locates in a rather conventional physical range ($1/2 < \chi_{ps} \leq 0.59$) for poor solvent, see **Figure 1.3**. Therefore, it is impossible to occur phase coexistence for polymer brushes under the Flory-Huggins approach like for polymer solutions. For this situation, the degradation of the solvent quality (the increase of χ_{ps} around 1/2) merely leads to a monotonous and smooth increase of density, see **Figure 1.3**. Even though, it is worth mentioning that when the dispersity of a brush layer is significantly far away from a uniform polymer brush, Flory-Huggins approach can no longer deal with this case properly, computer-simulation studies [12, 13] showed that it is possible for polydisperse and bi-disperse brushes to happen phase coexistence in a common thermal solvent (the value of χ_{ps} is around 1/2).

In a good solvent [9, 10], χ_{ps} is smaller than $0.5 + 1/\sqrt{N}$, which implies that a polymer-solvent interaction is favored over a polymer-polymer interaction. As a result, a homogeneous, one-phase mixture is preferred irrespective of the value of polymer concentration c . In a θ -solvent, also known as an indifferent solvent where the second virial coefficient $\nu_2 = 0$, i.e., $\chi_{ps} = 0.5 + 1/\sqrt{N}$, and the polymer-solvent, polymer-polymer, and solvent-solvent interactions are perfectly counterbalanced. Accordingly, the entropy of mixing is the only relevant term, and this favors the formation of an ideal-like, one-phase mixture in a θ -solvent. When a polymer is mixed with a solvent, the good-, θ -

and poor-solvent states can be realized by changing temperature T . In particular, the temperature for a polymer-solvent system that realizes a θ -solvent state is usually called the θ -temperature. For the case of a polymer is mixed with a pure solvent, the θ -solvent state is unique. Whereas for a multi-component system of polymers with solvents, how to determine/predict θ -solvent state is still rather complex, it could have many different θ -solvent states which generally depend on both the concentration of each component and interactions between these components. For example, if a polymer is mixed within two poor solvents, solubility of the polymer can be improved when compared with its solubility in each pure poor solvent, this phenomenon is well-known as cosolvency [14]. For the cosolvency system, when the polymer concentration is fixed, only changing solvent composition, there may be as much as two solvent-composition dependent θ -solvent states at which the chain conformations are nearly ideal.

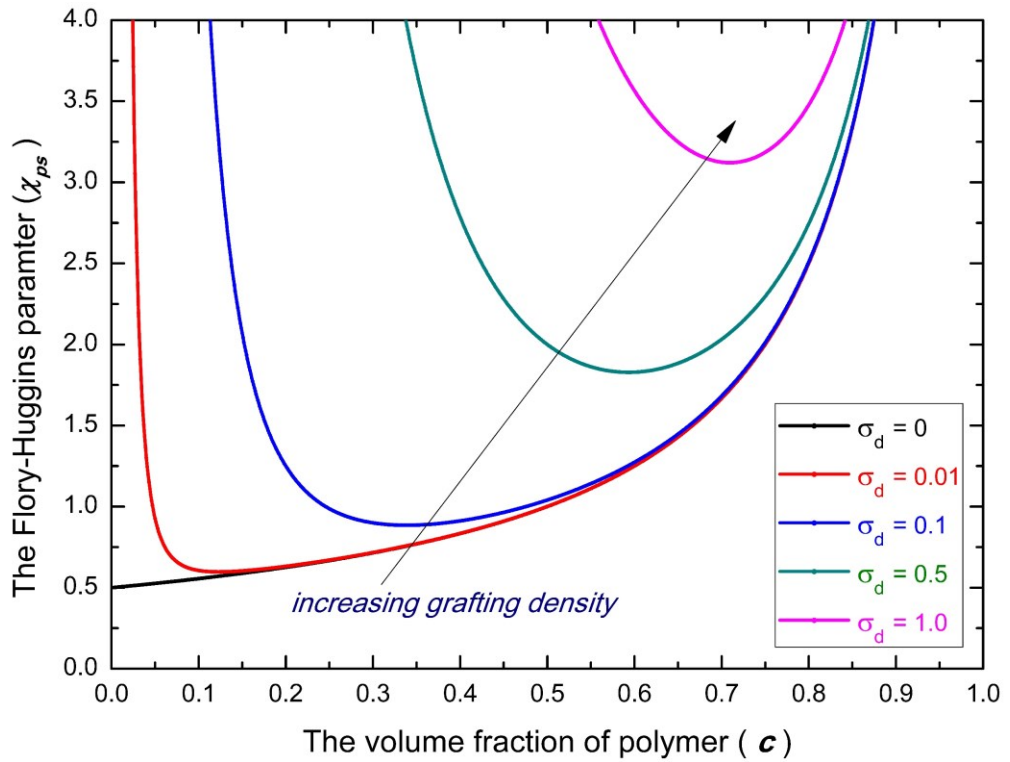


Figure 1.3(Figure 3) A graphical plot of the Flory-Huggins parameter (χ_{ps} , Eq.(1.8)) with respect to the volume fraction of polymer (c) for uniform polymer brushes. Note that in the plot I restrict the value of χ_{ps} in its conventional physical range ($0 \leq \chi_{ps} \leq 4.0$).

Here, it is worth pointing out that an obvious fact that is not captured by the Flory-Huggins theory is the large localized density fluctuation in the dilute solution [15, 16]. The instantaneous picture of the solution has much higher polymer density where the chains are located and pure solvents elsewhere, which is significantly different from the random-mixing picture envisioned in the Flory-Huggins theory. For polymers in poor solvents, such localized density fluctuation takes the form of single-chain globules and multichain clusters. Another important fact not reflected in the Flory-Huggins theory is the change in chain conformation according to different solvent qualities. Even though, after counting these facts except that a larger dilute-phase concentration (c_{dilute})

with a lower condense-phases concentration (c_{dense}) are expected, the solvent-quality rule still holds for θ -solvent where $\chi_{ps} = 0.5 + 1/\sqrt{N}$.

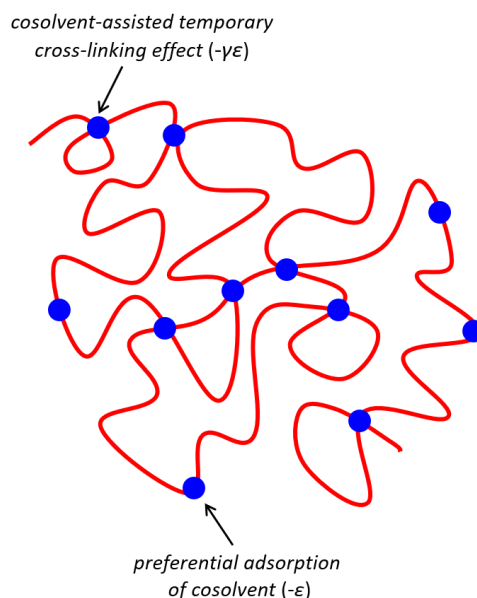
To realize a phase transition for a binary solution of a polymer and a solvent, the solvent quality is usually degraded by changing temperature. There are two different polymer phase transitions upon a change of temperature. The first one is by a decrease of temperature; it is the so-called upper critical solution temperature (UCST) transition which can be well approximated by the Flory-Huggins theory, where the second virial coefficient is negative but the third virial coefficient is positive for free energy expansion, see **Eq.(1.5)**. In contrast, another one is the so-called lower critical solution temperature (LCST) transition by an increase of temperature which in general cannot be well described by the the Flory-Huggins theory.

1.3 Polymer phase separation in mixtures of two good solvents

Following the standard Flory-Huggins model of the liquid-liquid phase transition of a polymer solution, the translation entropy of the polymers is essential in order to stabilize the diluted polymer phase in coexistence with a polymer-condensed phase. This results in that degrading the solubility of immobilized UCST-polymers, such as polymer brushes, in common thermal solvents can only lead to a smooth crossover from the good-solvent state to the poor-solvent state, see **Figure 1.3**. In principle, switchable surfaces can only be efficient if small variations of environmental parameters can induce a large response such as volume phase transitions in polymer brushes. Switch-like response of immobilized neutral polymers can therefore only be obtained in “uncommon” solvents which do not obey a simple Flory-Huggins phase-transition behavior. For water soluble polymers there are three well-known routes to achieve this goal: The transition at the lower critical solution temperature **[17]**, the cononsolvency effect **[18]** and nanoparticles induced phase transition in polymer solutions **[19-21]**. In previous two cases, a subtle interplay of interactions between polymer and solution gives rise to a so-called type-II phase transition where the third virial coefficient is negative but the second virial coefficient stays positive for free energy expansion **[22-24]**, which causes a jump-like collapse of the polymer layer. Thermo-responsive switch-like behavior of brushes, for instance, has been detected with polymers displaying a LCST behavior such as poly(N-isopropylacrylamide). In this case a phenomenological concentration-dependent Flory-parameter has been introduced in order to account for the unusual phase behaviors **[17, 22]**.

While thermo-responsive brushes received much attention, their switching-behavior is determined by the LCST-transition temperature which in turn is fixed and limited by their polymer chemistry **[17, 22]**. An interesting alternative are multi-component solvents which offer the possibility to induce a phase transition as a response to the chemical composition in a broad range of temperatures, a special but simple case of polymer phase transition in multi-component solvent system is cononsolvency transition **[18]**. Cononsolvency occurs if a mixture of two good solvents causes the collapse or demixing of polymers into a polymer-rich phase in a certain range of compositions of these two solvents. The better solvent is usually called cosolvent and another common solvent is called solvent. It is noted that under certain situation, solutes such as nanoparticles and

salts play similar roles like cosolvent in the reentrant condensation of polymers [25], thus for convenience these solutes are termed as cosolutes. Two typical examples for this situation are: (i) phase transition of ultra-high molecular weight poly(ethylene oxide) in silica nanoparticle's aqueous solutions [21] where silica nanoparticle is the cosolute, as well as (ii) phase transition of bovine serum albumin protein aqueous solution on addition of salts where tri/tetra-valent salt is the cosolute [26].



Scheme 1.1(Figure 4) A mechanism where phase transition of polymer occurs if one component (it is usually termed as cosolvent) of a binary solvent mixture displays a strong tendency to adsorb at the polymer and can form temporary crosslinks.

Theoretical understanding of the cononsolvency transition is related to the theory of polymers in competitive solutions. The key of understanding cononsolvency relies on correctly determining the roles of various interactions among solvent molecules and/or polymer. Different from a convenient but heuristic black-box early discussion [27] on the phenomenological χ -parameter of various interactions in phase transitions of polymer brushes in mixed solvents, in recent theoretical discussions, in the case of weak cosolvent-solvent attraction, a comprehensive understanding of cononsolvency is largely based on the assumption of a preferential adsorption of the cosolvent onto polymer chains and monomer-cosolvent-monomer triple contact, see **Scheme 1.1**. The concept of preferential adsorption has been already used in a long time to discuss cononsolvency mechanism in experimental studies [28], by contrast, a rationalization of this concept just happened quite recently in theoretical studies. As an **ad hoc** example of a rationalization of preferential adsorption, Tanaka, Koga and Winnik [29] pioneeringly proposed that cononsolvency of temperature-responsive polymers can be explained based on the competition between the two solvents in forming hydrogen bonds with the LCST polymers. They found that the total coverage of the polymer chain by the bound solvent molecules is not a monotonic function but passes through a minimum at the composition where the competition is the strongest. This study correctly captured the competition adsorption behaviors of two solvents on the polymer chains in the cononsolvency transition, however, it is not correct to say that the competition source for the cononsolvency of LCST polymers is

from hydrogen bonds formation with polymers, this will be further investigated in depth in **Chapter 2**.

Meanwhile, it is also well-known that polymers with UCST behaviors, such as standard polymers polystyrene [30] and poly(methyl methacrylate) [31], also display the cononsolvency behavior. What is more, a polymer can also be cosolvent or cosolute in the cononsolvency transition of another polymer, such as polyethylene glycol aqueous solutions in the cononsolvency transition of poly(N-isopropylacrylamide) gels [32-34]. These observations point to the possible generic origin of this enigmatic or mysterious phenomenon. The general cornerstone concept of preferential adsorption is initially rationalized for single polymer chain by Mukherji, Kremer and Marques [35] that a simple theoretical description of cononsolvency was formulated by considering the fraction of φ of monomers is **simply** adsorbed by cosolvent molecules and a thin film of solvent on the polymer chains is formed like a Langmuir monolayer. The theoretical description [35] of cononsolvency was further formulated by considering the fraction of φ_b of monomers is bridged by cosolvent molecules, while the rest fraction of $(1 - \varphi - \varphi_b)$ monomers is occupied by the common solvent molecules. If we assume all sizes are equal for cosolvent, common solvent and monomer, then the adsorption free energy per unit of monomer f_{ads} , for a single polymer chain, reads in the units of $k_B T$:

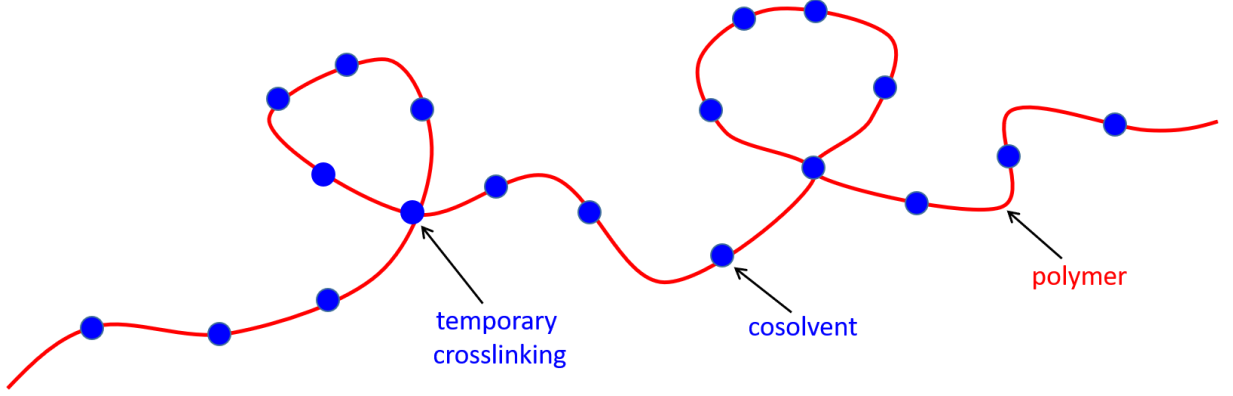
$$f_{ads} = \varphi \ln(\varphi) + 2\varphi_b \ln(2\varphi_b) + (1 - \varphi - 2\varphi_b) \ln(1 - \varphi - 2\varphi_b) - \varepsilon\varphi - \varepsilon_b\varphi_b - \mu(\varphi + \varphi_b), \quad (1.9)$$

where μ represents the chemical potential change of the cosolvent when mixing with the solvent, the preferential-adsorption energy of one cosolvent molecule with respect to the polymer is denoted as ε and the bridging energy between two monomers is denoted as ε_b . A main consequence for this formulation is that a single chain undergoing a phase transition has to bend itself and form loops due to that monomers have to keep connectivity and not break the polymer chain, see **Scheme 1.2**. Although the formulation of **Eq.(1.9)** captures the essence of cononsolvency phase transition, some questions cannot be directly answered from this formulation. For instance, regardless the architecture of the polymer material, such as a single chain, polymer brushes and polymer gels, cononsolvency transition of the same kind polymer all show very sharp collapse transition in the cosolvent-poor solvent mixture; in addition, the minimum location of cosolvent composition for the collapse transition is nearly independent of the architecture of the polymer material. In particular, as for dense polymer bushes and gels, it is unnecessary to form loops to occur a cononsolvency phase transition, since under these situations the possibility of forming loops is significantly oppressed by topological constraint of confined polymer chains and the loop-formation effect actually is expected to be trivial.

An alternative formulation [23, 24] of the cornerstone concept where phase transition of polymer occurs if cosolvent displays a strong tendency to adsorb onto the polymer and form temporary crosslinks, is that cosolvent molecules can be shared by two or more monomers, decreases the free energy of the total system, regardless whether these monomers belong to the same chain or to different chains. Within the mean-field approximation this can be written in terms of a free energy per monomer unit f_{attr} , reads in the units of $k_B T$:

$$f_{attr} = -2\gamma\varepsilon\varphi(1-\varphi)c, \quad (1.10)$$

where φ denotes the fraction of monomers that is adsorbed by cosolvent molecules and c is monomer concentration in the polymer phase. ε denotes the preferential-adsorption energy of one cosolvent molecule with respect to the polymer. The strength of a temporary crosslink is given by $\gamma\varepsilon$, in which the parameter γ represents the size effect when cosolvent bridges monomers in [refs. \[23, 24\]](#).



Scheme 1.2(Figure 5) Illustration of cosolvent-assisted loop formation on a single polymer chain.

This mean-field approach has shown that the bridging between monomers induced by the cosolvent can be mapped onto a concentration-dependent Flory interaction parameter for the polymer. As for the simplest scenario for polymer brushes [\[23\]](#), it can be written as a free energy per monomer unit $f(c)$, reads in the units of $k_B T$:

$$f(c) = \frac{1}{2} \frac{\sigma_d^2}{c^2} + \left(\frac{1}{c} - 1 \right) \ln(1-c) - \frac{1}{8} (\varepsilon + \mu)^2 - \chi(c)c, \quad (1.11)$$

with a concentration-dependent Flory interaction parameter $\chi(c)$,

$$\chi(c) = \frac{\gamma\varepsilon}{2} \left[1 - \frac{1}{4} \frac{(\mu + \varepsilon)^2}{1 + \gamma\varepsilon c} \right]. \quad (1.12)$$

Here, parameter μ is the chemical potential of the cosolvent, which is the same as defined in [Eq.\(1.9\)](#).

It is noted that the free energy, $f(c)$, in [Eq.\(1.11\)](#) can be rewritten into its virial expansion:

$$f(c) = -\frac{1}{8} (\varepsilon + \mu)^2 + \frac{1}{2} \frac{\sigma_d^2}{c^2} + \frac{1}{2} v_2 c + \frac{1}{6} v_3 c^2 + \frac{1}{12} v_4 c^3 + \dots, \quad (1.13)$$

with virial coefficients,

$$\begin{aligned}
v_2 &= 1 - \gamma\epsilon + \frac{1}{4}\gamma\epsilon(\epsilon + \mu)^2 \\
v_3 &= 1 - \frac{3}{4}\gamma^2\epsilon^2(\epsilon + \mu)^2 \\
v_4 &= 1 + \frac{3}{2}\gamma^3\epsilon^3(\epsilon + \mu)^2
\end{aligned} \tag{1.14}$$

As a rather moderate example of $\mu = -3.0$ which corresponds that the volume fraction of cosolvent in a solvent mixture is about 5% and we choose $\gamma, \epsilon = 1.0$, we reach a state where the third virial coefficient $v_3 = -2.0$, is negative but the second virial coefficient $v_2 = 1.0$, remains positive. In this approximation the model justifies the notation of type-II phase transition as it was introduced by de Gennes [36] and was discussed in early literature aimed to particularly explain the LCST behaviours of hydrophilic polymers such as polyethylene glycol [37, 38] and poly(N-isopropylacrylamide) [17, 22].

Minimizing free energy in Eq.(1.11) with respect to the monomer concentration (c), one can predict that an increase of the polymer concentration increases the interaction strength which in turn can cause a jump-like transition for polymer brushes at sufficiently high bridging effect between monomer and cosolvent ($\gamma\epsilon$). This model further predicted the cononsolvency response of polymer brushes with respect to the relevant parameters such as solvent selectivity (ϵ) and grafting density (σ_d). For more detail of this model, please refer to ref.[23]. This model has been successfully applied to qualitatively explain computer-simulation results for phase transitions of polymer brushes where including of nanoparticles behave like cosolvents (cosolutes) [39]. However, so far, in real polymer systems, the assumption of preferential adsorption and bridging effect between cosolvent and polymer is only a feasible concept if the individual solvent components are fully miscible and phase decomposition and criticality within the solvent mixture actually can be usually avoided. The cornerstone assumption and the analytical solution of Eq.(1.11) are ready to be experimentally examined.

1.4 Characterizing cononsolvency transition in experimental study

While cononsolvency transition has been explained by various theoretical concepts, these concepts need to be checked by experiments. When we are interested in the molecular mechanism of liquid-liquid phase transition, a useful methodology is detecting changes of observable variables that coupling or correlating with the phase transition such as volume change. Without exception, this methodology has also been applied to study cononsolvency transition for a long time. Cononsolvency transition shows behaviors of the first-order phase transition. In particular, the volume of a PNIPAAm macrogel shows step (noncontinuous) change when the gel is immersed in DMSO/water and 1-propanol/water mixtures [40]. Therefore, the most convenient method to study cononsolvency of a macrogel is to use a microscope to measure the volume change when the composition of solvent mixtures is changed, this was a direct method used in early literatures [33, 34, 40-42]. In the liquid-liquid phase transition, interaction between solvent and polymer also changes, chromatography and spectroscopy methods are useful to detect these changes, these methods can

at least qualitatively determine relative strength of various interactions among solvent molecules and/or polymer. The composition difference of cosolvent in and outside of a gel in cononsolvency transition was qualitatively or quantitatively determined by chromatography and spectroscopy methods in literatures [28, 33, 40, 43-46]. The measurements showed that in the cononsolvency transition of gels, alcohol and acetone molecules enrich in the gels [28, 40, 43-46] while this enrichment is not obvious for DMSO [40, 44] and liquid polyethylene glycol (such as PEG 200) [33] molecules.

In contrast to gels, it is inconvenient to directly measure volume change of polymer brushes in phase transition. Instead, observing morphology change becomes a convenient method such as using atomic force microscopy to study friction force change between a gold colloid and a polymer brush [47, 48]. When the grafting density of a polymer layer is not too low, the problem of measuring the volume of the polymer layer can be transformed into measuring the thickness of the polymer layer with an *ansatz* that the polymer layer shows homogenous morphologies and the lateral-structure effect of the polymer layer can be neglected. For this situation, in-situ spectroscopic ellipsometry was used to measure brush thickness and study cononsolvency transition of polymer brushes [47, 49, 50]. When the grafting density of a polymer layer is very low, at a poor-solvent state the swollen polymer chains can show various morphologies such as coexistence of two phases, octopus-shape micelle and collapsed globule [51, 52]; under this situation it is no longer enough to correctly characterize phase transition by merely measuring the thickness of the polymer layer, since the polymer layer is inhomogeneous. As an alternative, quartz crystal microbalance can be at least qualitatively used to study mass change in the phase transition of a polymer layer [53, 54]. In addition, some special methods such as surface forces apparatus [55] was already applied to characterize cononsolvency transition of polymer brushes.

As for polymer solutions, in an experimental study, it is hard to accurately measure the change of volume or monomer concentration comparing with polymeric gels and polymer brushes. Instead, a measurement of quantities that indirectly characterize volume phase transition is usually implemented, for examples, a measurement of osmotic pressure [56] or a measurement of LCST/UCST transition temperatures [30, 57] by visible light transmission in the cononsolvency transition. Even though, a direct measurement of volume change of polymer chains in polymer solutions is possible. Actually, the volume of a polymer chain such as hydrodynamic radius was successfully used to quantify cononsolvency transition of a single chain [58, 59] by scattering methods. Scattering methods were also applied to investigate solution structures such as change of polymer conformations in cononsolvency transition [60-63]. However, it is still challenging for scattering methods to quantify phase transition of polymer solutions, since currently a few case studies showed that scattering methods could not correctly characterize sol-gel behaviors (percolation transition) [56] of cononsolvency transition, for details please refer to refs.[64, 65].

In principle, any experimental method that complies to the methodology of detecting changes of observable variables that coupling or correlating with phase transition, can be used to study cononsolvency transition of polymers. Following this methodology, an emergent experimental technique that based upon translocation dynamics of fluorescence λ -DNA [66], is expected to be able to

at least qualitatively determine the swollen thickness of polymer layers which are grafted around the rim of nanopores. It is worth pointing out that to my best knowledge this task cannot be achieved by other already known standard analytic methods. This experimental technique will be used to study phase behaviors of poly(N-isopropylacrylamide) layers around the rim of nanopores, for the details please see **Chapter 4**

1.5 Research motivation

By a holistic combination of experimental and theoretical studies, it is the aim of this thesis to provide a systematic study of the cononsolvency effect in polymers especially polymer brushes under the variation of the cosolvent-content in a cosolvent-water binary mixture to better understand the origin of the cononsolvency effect. In particular, for the first time, we systematically study a series of alcohols as cosolvents as well as various grafting densities of poly(N-isopropylacrylamide) brushes. We also study temperature effect in the cononsolvency transition of poly(N-isopropylacrylamide) polymers.

In this thesis, the phase behaviors of poly(N-isopropylacrylamide) brushes in binary good solvents will be experimentally studied in **Chapter 2**, and a minimalist comparison between curated results from both experiments and theories will be also discussed in **Chapter 2**. In **Chapter 3**, for the first time, a mean-field theory will be proposed to consistently and quantitatively predict cononsolvency behaviors of polymer brushes, gels and single long polymers. An application for the cononsolvency effect of grafted polymers such as polymer brushes around the rim of nanopores will be studied for the first time in **Chapter 4**. Concluding remarks and outlooks on cononsolvency of polymer will be made in **Chapter 5**.

Chapter 2 Phase behaviors of PNiPAAm brushes in alcohol/water mixtures: A combined experimental and theoretical study

(Note: Some results presented in this chapter were already published by the author in the journals “Macromolecules, 2019, 52(16), 6285-6293” and “Materials, 2018, 11(6), 991”.)

2.1 Introduction

Compared to polymer solutions and gels, for polymer brushes only limited experimental results regarding the cononsolvency effect have been published [47-50, 53-55, 67, 68]. In addition, what is still missing up to now is a physical understanding of the equilibrium behavior and nature of the cononsolvency effect on real polymer brushes. As an indication for a reentry-transition Yu et al., [47] and Zhang et al., [48] found that the friction force between a gold colloid and a polymer brush displays a significant increase in the range of cononsolvency. Generally, polymer brushes are a particular interesting system to apply cononsolvency-induced transitions for potential applications ranging from wetting, over friction to microfluidics. From the theoretical point of view polymer brushes are ideal model systems because of their simple architecture where each chain is anchored to the substrate. Due to the height of synthetic brushes which is typically in the order of 100 nm, a quick response to the change of solvent composition is possible. Precise measurements of the brush thickness using optical methods allow for a comparison to theoretical predictions and simulation.

It is the aim of this chapter to provide a systematic study of the cononsolvency effect in poly(N-isopropylacrylamide) (PNiPAAm) brushes under variation of the alcohol-content in an alcohol-water binary mixture to better understand the origin of the cononsolvency effect and to compare the results to the theory. In particular I study a series of alcohols as cosolvents as well as various grafting densities. I observe sharp collapse transitions in accordance with the theoretical prediction. I find that alcohols with stronger hydrophobic effect in water that gives rise to a stronger transition and shift the collapse to lower volume fractions of the alcohol. Using thermodynamic data for the alcohol-water mixtures from literature I can conclude that the increase of cononsolvency effect is correlated with the increasing tendency of demixing, i.e. repulsion, between the two solvents, which favors the explanation of cononsolvency effect by the mechanism of preferential adsorption.

2.2 Materials and Methods

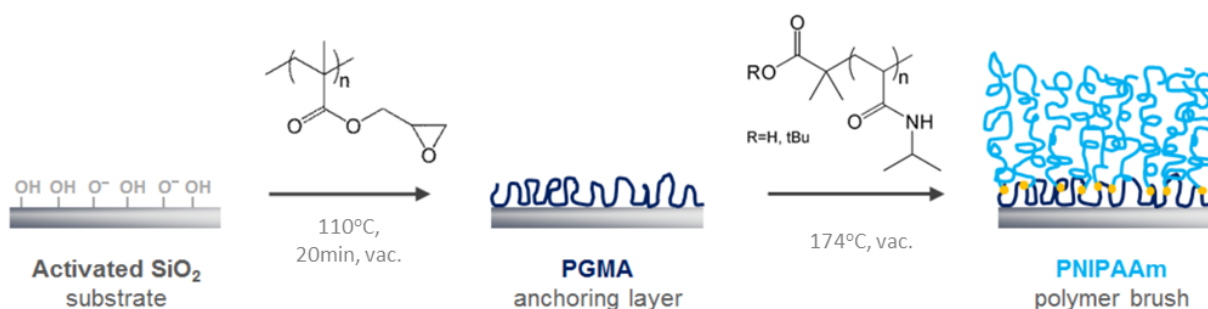
2.2.1 Materials

Poly(glycidyl methacrylate) (PGMA, $M_n = (1.0-2.0) \times 10^4$ g/mol) was purchased from Sigma-Aldrich (Darmstadt, Germany). Dry methanol (MeOH, $\geq 99.8\%$), absolute ethanol (EtOH, $\geq 99.8\%$), dry 1-propanol (1-PrOH, $\geq 99.7\%$) and 1-butanol (1-BuOH, $\geq 99.8\%$) were purchased from Sigma-Aldrich (Darmstadt, Germany). Glycerol ($\geq 99.0\%$), ethylene glycol ($\geq 99.8\%$), 1,3-propanediol ($\geq 99.6\%$) and 1,4-butanediol ($\geq 99.0\%$) were purchased from Sigma-Aldrich (Darmstadt, Germany). Tetrahydrofuran (THF, $\geq 99.98\%$) and chloroform (CHCl_3 , $\geq 99\%$) were purchased from Acros Organics (Darm-

stadt, Germany). Purified water (H_2O) was used from a Milli-Q Direct-8 system from Merck Millipore (Darmstadt, Germany). All chemicals were used as received, if not otherwise specifically noted. Highly polished single-crystal silicon wafers of $\{100\}$ orientation (Si-Mat Silicon Materials, Kaufering, Germany) were used as a substrate. End-functionalized PNiPAAm polymers (P01: $M_n = 3.80 \times 10^4$ g/mol, $M_w/M_n = 1.38$; P14: $M_n = 5.02 \times 10^4$ g/mol, $M_w/M_n = 1.28$; AK13P3: $M_n = 6.1 \times 10^4$ g/mol, $M_w/M_n = 1.40$) with a terminal (*tert*-butyl protected) carboxy group were synthesized and characterized as described by [ref.\[69\]](#).

2.2.2 Preparation of Polymer Brushes

Silicon substrates ($13 \times 20 \text{ mm}^2$) were treated with EtOH in an ultrasonic bath for 10 min, dried with a stream of nitrogen, and treated with oxygen plasma (440-G Plasma System, Technics Plasma GmbH, Wettenberg, Germany) for 1 min at 100 W. Next a thin layer of PGMA (about 2.5 nm) was deposited by spin coating (Spin 150, SPS Coating, Ingolstadt, Germany) a PGMA solution in CHCl_3 (0.3 mg/ml) with subsequent annealing at 110°C in a vacuum oven for 20 min to react the silanol groups of the substrate with a fraction of the epoxy groups of PGMA, thus forming an anchoring layer equipped with the remaining epoxy groups for the following “grafting-to” process [\[70\]](#). Afterwards, a filtered solution of end-functionalized PNiPAAm in THF (9.0 mg/ml) was spin coated onto the PGMA layer and subsequently annealed at 174°C in a vacuum oven (**Scheme 2.1**). The density of the chains attached to the surface grows with grafting-reaction time and approaches values around 0.2 chains/ nm^2 , which are typical for “grafting-to” brushes [\[69\]](#). To remove non-covalently bonded polymers, the resulting films were immersed first in H_2O , then extracted in H_2O overnight, rinsed with EtOH, and dried in a stream of nitrogen.



Scheme 2.1(Figure 6) Preparation of PNiPAAm brushes on silicon substrates using the “grafting-to” approach.

2.2.3 VIS-Spectroscopic Ellipsometry Measurement

A spectroscopic ellipsometer (alpha-SE, Woollam Co., Inc., Lincoln, NE, USA) equipped with a rotating compensator was used to extract the relative phase shift (Δ) and the relative amplitude ratio ($\tan\Psi$) of the polymer brush films in the dry state, as well as in-situ in purified H_2O and H_2O /alcohol mixtures within a batch cuvette (TSL Spectrosil, Hellma, Muellheim, Germany) at constant

temperature [71]. All solvent mixtures were prepared at the same day or one day before measurements and sealed in glass vials at room temperature. I always use the same brush by rinsing the solvent and introducing another solvent with help of a syringe-pump apparatus. The cuvette was flushed at least three times with the current solvent mixture right before measurement to avoid changes in the composition of the ambient. All measurements were performed between 400 and 800 nm at an angle of incidence Φ_0 of 70° , which is close to the Brewster angle of silicon. To evaluate the index of refraction and the thickness of the brush films in dry (h) state and in situ (H), a multi-layer-box-model consisting of silicon, silicon dioxide, anchoring layer PGMA, and a polymer brush was assumed [69]. The refractive indices of the environment (water and H₂O/alcohol mixtures) were measured using a digital multiple wavelength refractometer (DSR-lambda, Schmidt + Haensch, Berlin, Germany). All data was acquired and analysed using the CompleteEASE[®] software package (version 4.46). For the brush sample used in this work, I did three-time repeatable ellipsometry measurements. Result differences of these measurements were small, and as such, data reproducibility of my ellipsometry measurements were quite good.

2.2.4 Determining a polymer brush's overlap grafting density

From the determined film thickness (h) in the dry state, polymer brush parameters like grafting density (σ) and distance between anchoring points (S) can be calculated by using the simple relation:

$$\sigma = \frac{1}{S^2} = \frac{N_A \rho_p h}{M_n}, \quad (2.1)$$

where M_n is the number-average molecular weight of the polymer, N_A is the Avogadro's number, ρ_p is the polymer's melt density [72]. Here, ρ_p is 1.1 g/cm³ for PNiPAAm homo-polymer. For the interpretation of my measurements we have to assume a lateral homogeneous polymer profile in the dry state. This is the case for the brush regime of strongly overlapping chains. To determine whether the grafted polymers are in the brush regime, the distance between grafting sites, S , should be small enough. For the case of a good solvent, S should be much smaller than twice the radius of gyration of the chains (R_G):

$$\frac{S}{2} < R_G = \alpha N^{0.588}, \quad (2.2)$$

where α is a prefactor proportional to the monomer size and N is the degree of polymerization; for the PNiPAAm polymer, α is estimated to be 0.3 nm [73] and 0.588 is the universal scaling exponent of chain sizes in good solvent [9]. However, in the collapsed state, this condition is not sufficient. Here, so-called octopus-micelles can be formed if the grafting density is below the stretching threshold of σ^{**} [52],

$$\sigma^{**} = \frac{N_A \rho_p \alpha}{M_0 \sqrt{N}}, \quad (2.3)$$

where M_0 is the molecular weight of repeat units of the polymer. If $\sigma > \sigma^{**}$, the chains will form stretched brushes. This condition gives the lower boundary for the grafting density, which is necessary for a homogeneous brush in the collapsed state. One might also use the overlap radius of gyration of the chains (R_p) between collapsed single chains as a rough lower estimate for a homogeneous brush under the condition that chains collapse mostly, i.e., $R_p = \alpha N^{1/3}$ and $S/2 < R_p$, where the radius of gyration under poor solvent conditions is taken. I note that this estimate slightly underestimates the necessary grafting density. Basic physical parameters of PNiPAAm brushes used in this study are listed in **Table 2.1**.

Table 2.1(Table 1) Layer parameters (number-average molecular weight M_n , dry layer thickness h , and corresponding brush criteria such as critical grafting density σ^{**} , the radius of gyration of the chains in good solvent and poor solvent R_G and R_p respectively) of polymer films, which were used in this study.

Polymer layers	M_n (g/mol)	PDI	h (nm)	σ^{**} (chains/nm ²)	$2R_G$ (nm)	$2R_p$ (nm)
PGMA	$(1-2) \times 10^4$	-	2.5 ± 0.1	-	-	-
PNiPAAm: P01	3.80×10^4	1.38	/	0.0958	18.3	4.2
PGMA	$(1-2) \times 10^4$	-	2.7 ± 0.1	-	-	-
PNiPAAm: P14	5.02×10^4	1.28	/	0.0834	21.6	4.6
PGMA	$(1-2) \times 10^4$	-	2.7 ± 0.1	-	-	-
PNiPAAm: AK13P3	6.1×10^4	1.40	/	0.0756	24.2	4.9

2.2.5 Test of PNiPAAm solubility in short-chain polyols

Table 2.2(Table 2) Solubility of PNiPAAm in short-chain polyols at the temperature of 25°C.

	Glycerol	ethylene glycol	1,3-propanediol	1,4-butanediol
PNiPAAm: P01	non-solvent	poor solvent	good solvent	good solvent
PNiPAAm: P14	non-solvent	poor solvent	good solvent	good solvent
PNiPAAm: AK13P3	non-solvent	poor solvent	good solvent	good solvent

2.3 The adsorption-attraction model

Let us briefly summarize the essential concept of the adsorption-attraction model [23] as a realization of the preferential adsorption concept [35]. Preferential adsorption of the cosolvent onto the polymer chains leads to an adsorption layer of cosolvent around the polymers. The probability that a monomer unit is covered by cosolvent is given by φ , which depends on the volume fraction of the cosolvent, ρ , but also on the state of the polymer brush. The latter is described within the mean-field model by Alexander and de Gennes and thus characterized by the average volume fraction of monomers in the brush layer, c , which essentially depends on the grafting density, σ . The central assumption of this model is that cosolvent molecules can be shared by two monomers which decreases the free energy of the total system. Within the mean-field approximation this can be written in terms of a free energy per monomer unit as:

$$f_{attr} = -2\varepsilon\gamma\varphi(1-\varphi)c, \quad (2.4)$$

where $\gamma\varepsilon$ denotes the gain of free energy due to a monomer-cosolvent-monomer triple contact, and parameter γ represents the size effect when cosolvent bridges monomers in [ref.\[23\]](#). The above equation has the form of a Flory-Huggins interaction term, where the Flory parameter is given as a function $\chi(\varphi)$. From this we can conclude that a maximum coupling is related with $\varphi \approx 1/2$, and that both extreme cases, namely $\varphi \rightarrow 0$ and $\varphi \rightarrow 1$, lead to vanishing coupling. Given values of $\gamma\varepsilon$ larger than unity we can already predict collapse and re-entry transition for small and large cosolvent concentration respectively without detailed calculation since extreme values of the cosolvent concentration lead $\varphi = 0$ and $\varphi = 1$ and thus to a vanishing interaction parameter and good solvent conditions for the brush. On the other hand, close to the half-occupied regime, $\varphi \approx 1/2$, a collapsed state of the polymer brush can be expected. This model has been discussed analytically and numerically in much detail for the ideal case that all components are pairwise ideally miscible by [ref.\[23\]](#).

For an quantitative description of a particular system the equation of state of the cosolvent including the adsorption on the polymer has to be considered. For the real case the cosolvent-solvent mixture will not be ideal and also the common solvent will not be athermal with respect to the polymer. One aspect of changing the length of the hydrophobic tail of the alcohol is to reduce its mixing entropy. If we denote the ratio between the volume of one alcohol molecule and one water molecule by λ , this gives rise to an adsorption free energy per monomer according to the lattice gas approximation:

$$f_{ads} = \frac{\varphi}{\lambda} \ln(\varphi) + (1-\varphi) \ln(1-\varphi) - \mu\varphi - \varepsilon\varphi, \quad (2.5)$$

where ε denotes the adsorption energy (selectivity) of the cosolvent with respect to the polymer and μ represents the chemical potential change of the cosolvent when mixing with water.

Furthermore, we used the following free energy for the brush:

$$f_{brush} = t \frac{\sigma^2}{c^2} + \left(\frac{1}{c} - 1 - \nu\varphi \right) \ln(1 - c - \nu\varphi c), \quad (2.6)$$

where t is a numerical prefactor which accounts for the specific conformations of chains in a polymer brush diverging from Alexander-de Gennes approach [\[11\]](#), and ν is the added volume fraction by full saturation of the polymer by cosolvent.

The overall free energy per monomer then is given by,

$$f(\varphi, c) = f_{ads} + f_{attr} + f_{brush}. \quad (2.7)$$

To obtain the equilibrium state, minimization with respect to the order parameter of the adsorption, φ , and the brush concentration, c , has to be performed. We note that because of the non-linear coupling between cosolvent and monomers, [Eqs.\(2.4\) and \(2.6\)](#), there exists no analytic solution for the general case. We further note that minimization with respect to φ only leads to a free energy in an effective solvent which can be expressed as concentration-dependent Flory-Huggins parameter $\chi(c)$ [\[23\]](#).

2.4 Equilibrium behavior of cononsolvency transition of PNiPAAm brushes

Although previous experimental studies [47-50, 53-55, 67, 68] claimed that the cononsolvency transition of polymer brushes show features of a phase transition, so far, direct experimental evidence is missing. In order to check whether the cononsolvency transition of polymer brushes is an equilibrium transition, I measured swollen brush thickness as a function of time. The grafting density is chosen well above the overlap grafting density for the corresponding degree of polymerization, for details of determining brush's overlap density see the [section 2.2.4](#). Typical real-time measurements of Vis-spectroscopic ellipsometry for swollen brush thickness of PNiPAAm are shown in **Figure 2.1a-c**. Except for the condition where the ethanol volume fraction is around 50%, it is clearly seen that after about 5 min of continuous measurement, the brush system became stable. For the condition of the ethanol volume fraction around 50%, in current measurement, the time needed to wait for the brush system to become stable was more than 20 min. Thus, the data shown in **Figure 2.1a-c** supported the equilibrium nature of the cononsolvency transition that I report in this thesis.

Here, I point out that these differences in waiting time to reach equilibrium state may depend on the specific characteristics of a polymer-brush sample such as local heterogeneity. As the PNiPAAm polymer is thermally sensitive, even the enthalpy change via changing solvent composition can lead to changes in the polymer's conformations [74, 75]. I also observed that with an increasing ethanol fraction, especially for the regime of high ethanol concentration, scatter in the real-time brush thickness increased. This might be explained due to lower optical contrast between the ambient ethanol and the thin PNiPAAm film. Note that all data about swollen brush thickness in the following are averaged values of real-time ellipsometry data in the stable regime, except when specifically indicated.

Figure 2.1d summarises results for the PNiPAAm brush thickness as a function of ethanol volume fraction (y_E). We were able to qualitatively distinguish five solvent composition regimes: (i) the brush thickness of PNiPAAm was hardly affected by the change of y_E when it was lower than 0.05; (ii) for the range of $0.05 < y_E < 0.15$, there was a sharp collapse transition of brushes, reaching a maximum decrease of thickness in a very narrow composition range of $0.15 \leq y_E \leq 0.17$ (**Scheme 2.2**); (iii) for the range of $0.17 < y_E < 0.3$, there was no obvious change of brush thickness in this regime; (iv) for the range of $0.3 < y_E < 0.8$, there was a re-entrant transition of brushes from a collapsed state to a swollen state; and (v) for the range of $y_E > 0.8$, the brushes were fully re-swelling in ethanol-rich solvents. The brush thickness in pure ethanol ($y_E = 1$) was always thicker than in pure water ($y_E = 0$). This was a direct consequence of the stronger attraction between the alcohol and the monomer as compared to water and the monomer. This can be related with a larger excluded volume coefficient, and thus to stronger swelling. I also note that this phenomenon could be partially attributed to the molecular volume of ethanol being larger than the water's (**Scheme 2.2**, please see more details in the [section 2.5](#)).

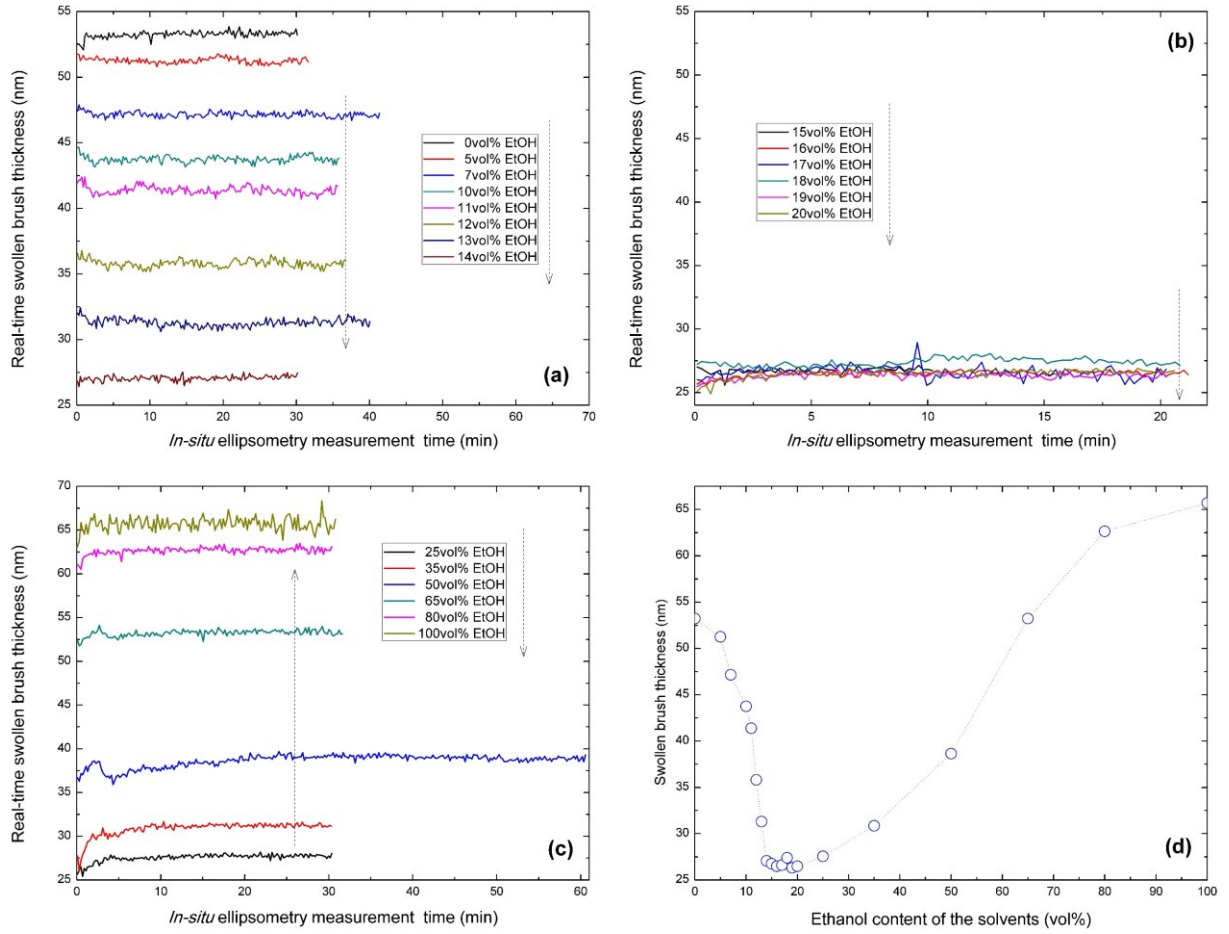
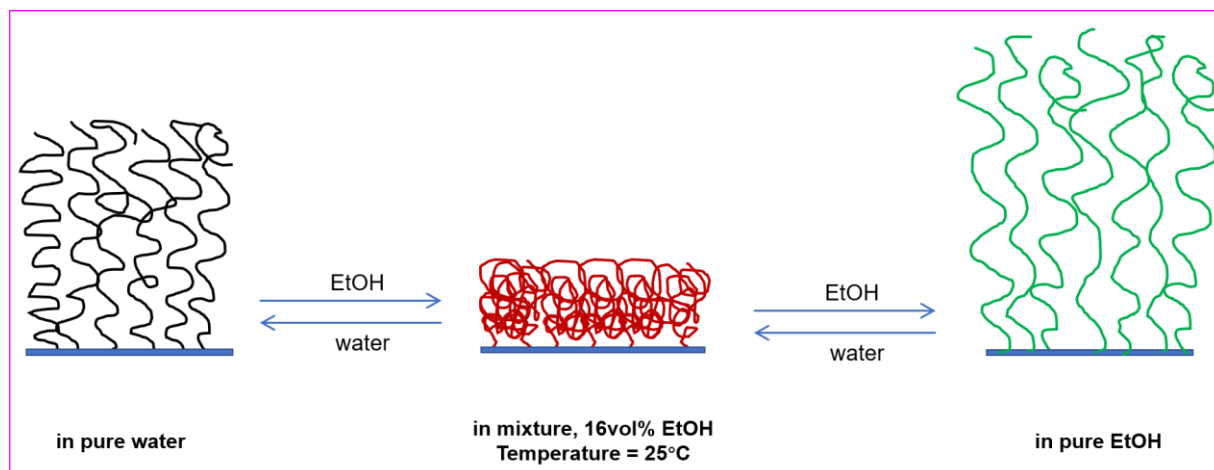


Figure 2.1(Figure 7) Swollen brush thickness of a PNiPAAm brush in aqueous ethanol mixtures as a function of (a-c) measurement time and (d) ethanol fraction obtained via Vis-spectroscopic ellipsometry at the temperature of 25°C. Note that the dashed line in Figure 2.1d is only used to guide eyesight. The error bars in Figure 2.1d are neglected because they are quite small (around 0.5 nm). Parameters of the PNiPAAm brush are: grafting density $\sigma = 0.20$ chains/nm², $M_n = 5.02 \times 10^4$ g/mol, $M_w/M_n = 1.28$.

In previous studies, Y. Yu et al. [47] also measured swollen thicknesses of PNiPAAm brushes with respect to a composition change of ethanol. Different from my results, they concluded that there was a non-sharp re-entrant transition of brushes by using ellipsometry measurements, reaching a maximum decreasing of thickness in a very broad composition range of $0.2 < y_E < 0.3$. The ellipsometry analysis of ref. [47] showed that the difference in swollen brush thickness in pure water and ethanol is negligible, which is in contrast with the corresponding AFM (Atomic force microscopy) measurement. My own experience indicated that these discrepancies may be due to insufficient equilibration of the brush system in their ellipsometry measurements. Nevertheless, their AFM measurement results of the composition range which is about between 0 and 15%vol [47] for the collapse transition with increasing ethanol concentration are consistent with my ellipsometry measurement results.



Scheme 2.2(Figure 8) Main cononsolvency transition regimes of a PNiPAAm brush in ethanol/water mixtures.

2.5 Role of volume of solvent molecules in the swelling of PNiPAAm brushes

Based on scaling theory [76], the brush's height, H , on a flat surface can be expressed as:

$$H = kb^{\frac{1}{\nu_1}} S^{1-\frac{1}{\nu_1}} N, \quad (2.8)$$

where b is the effective monomer size, S is the average distance between two adjacent grafted polymer chains, N is the degree of polymerization, k is a numerical prefactor that depends on temperature and polymer's chemical structure, and ν_1 is the Flory exponent.

The size of a water molecule is about 0.28 nm, the size of an ethanol molecule is about 0.44 nm, and the size of a PNiPAAm repeat unit is about 0.70 nm. Here, I assume that in pure solvents, every repeat unit of PNiPAAm adsorbs a solvent molecule. Then, the actual monomer size of PNiPAAm in pure ethanol is about 1.14 nm ($= 0.70 \text{ nm} + 0.44 \text{ nm}$), and the actual monomer size of PNiPAAm in pure water is about 0.98 nm ($= 0.70 \text{ nm} + 0.28 \text{ nm}$). Then the ratio of brush height in pure ethanol H_E to the brush height in pure water H_W is $H_E/H_W = (1.14/0.98)^{1/0.588}$. I apply $\nu_1 = 0.588$ which is the universal scaling exponent as found in computer simulations for chain sizes in good solvent [9], we get $H_E/H_W = 1.30$. My experimental result of H_E/H_W was 1.24 ($=65.7/53.2$).

The difference between 1.30 and 1.24 is about 5%, therefore my theoretical calculation was consistent with my experimental results. Note that in my calculations, for pure solvents, I assume every repeat unit of PNiPAAm adsorbs a solvent molecule. This assumption implies that the brush thickness in pure ethanol ($y_E = 1$) is always thicker than in pure water ($y_E = 0$) partially due to the fact that molecular volume of ethanol is larger than water's.

2.6 Cononsolvency transition of PNiPAAm brushes in aqueous solutions of a series of alcohol

In **Figure 2.2** we display my results for brushes in various alcohol-water binary mixtures. The grafting density is chosen well above the overlap grafting density for the corresponding degree of

polymerization, for details of determining brush's overlap density see the [section 2.2.4](#). We note that most of the studies of cononsolvency, for instance for gels, were restricted to methanol or ethanol as cosolvent [\[18, 77, 78\]](#). We observed in all cases the characteristic collapse-reentry-transition scenario consistent with the adsorption-attraction model of cononsolvency [\[23\]](#). **Figure 2.2** shows that different alcohols lead to different volume/height changes of the PNiPAAm brushes. With the increase of carbon chain length of alcohol, the location of the minimum of the re-entrant transition curve shifts to lower alcohol-concentrations, and the minimum value of collapsed brush thickness (H/H_0) becomes much smaller. These observations are in line with results of PNiPAAm micro- and macro-gels in alcoholic aqueous solutions reported by Bischofberger et al. [\[79\]](#), Crowther et al. [\[80\]](#) and Amiya et al. [\[41\]](#). Experimental evidences in **Figure 2.2** show that increasing the alcohol's hydrophobicity enhances the strength of the collapse transition of PNiPAAm brushes in the water-rich regime.

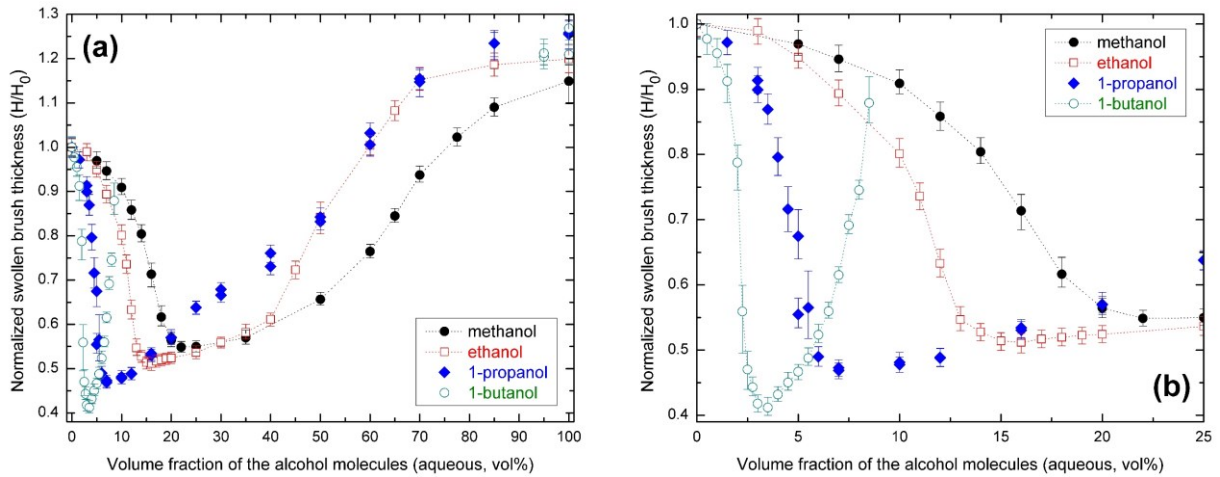


Figure 2.2(Figure 9) Normalized PNiPAAm brush thickness as a function of the volume fraction of cosolvent (a) Cononsolvency transition of the same PNiPAAm brush in different alcohol aqueous solutions, at the temperature of 25°C. Parameters of the PNiPAAm brush are: grafting density $\sigma = 0.143$ chains/nm², $M_n = 6.1 \times 10^4$ g/mol, $M_w/M_n = 1.40$. (b) A zoom-in of Figure 2.2a for the alcohol's volume fraction ranging from 0 to 25%. Note that the dotted lines in the figures are guides to the eyes.

To test the preferential-adsorption concept [\[35\]](#) and the adsorption-attraction model [\[23\]](#) quantitatively, we fitted experimental results of cononsolvency transition of the same PNiPAAm brush in different alcohol-water mixtures as already shown in **Figure 2.2**, the fitted results are shown in **Figure 2.3**. Here, we used MATLAB (a multi-paradigm numerical computing environment) unconstrained multivariable function to obtain these numerical solutions, values of fitting parameters used in the theoretical model are listed in **Table 2.3**. These fitted values are qualitatively in agreement with physical properties of these alcohol-water mixtures and experimental observations for cononsolvency transition of PNiPAAm in various alcohol-water mixtures. Consistently with the expectation, the volume ratio λ increases monotonously with the length of the alcohol, as well as the selectivity ε , the cosolvent added volume v , while the fit parameter for the

brush elasticity stays almost constant (the parameter describing the coupling efficiency γ was fixed and set to unity).

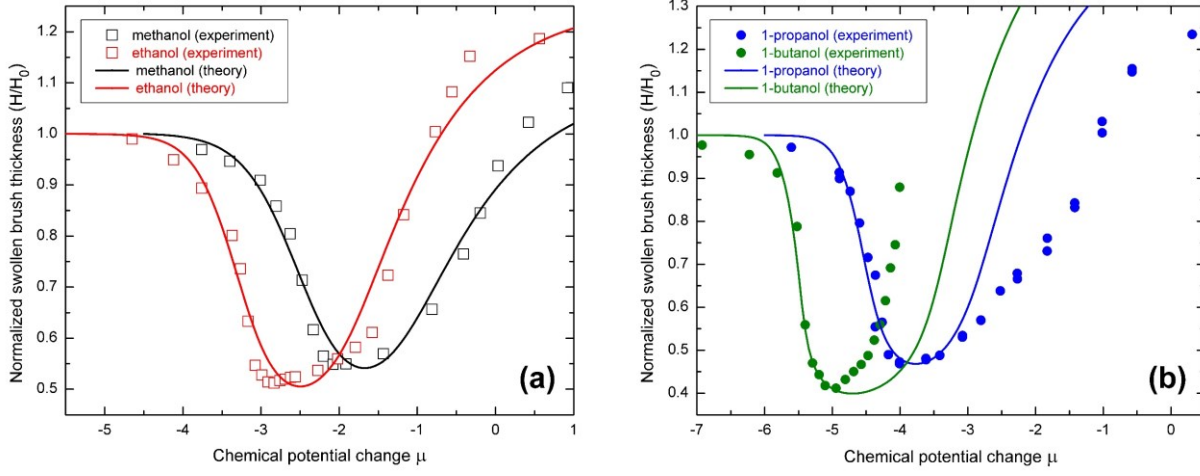


Figure 2.3(Figure 10) Theoretical fits of cononsolvency behavior of the same PNiPAAm brush in different alcohol-water mixtures. The ideal chemical potential change has been calculated based on lattice model as $\mu = \ln(y/(1-y))$, where y is the molar fraction of alcohol. The parameters of the PNiPAAm brush are: grafting density $\sigma = 0.143$ chains/nm², $M_n = 6.1 \times 10^4$ g/mol, $M_w/M_n = 1.40$. While the numerical fit has been optimized in the full range of cosolvent volume fractions for short alcohols (Figure 2.3a), we restricted the fit to the collapse region for the longer alcohols (Figure 2.3b).

Table 2.3(Table 3) Fitting parameters for the adsorption-attraction model.

Alcohol	λ	γ	ϵ	t	ν
methanol	3.0	1.0	1.20	0.7	0.15
ethanol	4.0	1.0	1.60	0.8	0.40
1-propanol	6.0	1.0	2.26	0.9	0.80
1-butanol	7.0	1.0	2.82	1.0	1.00

Fits for methanol and ethanol (**Figure 2.3a**) give a good quantitative description of collapse behavior but increasingly deviate in the regime of the reentry transition. One reason for this is the assumption of ideal mixing of the polymer with the individual solvents. Furthermore, the contribution of the cosolvent to the mixing entropy within the brush phase, second term in **Eq.(2.6)**, is neglected (assuming a dominating contribution from the “bound” cosolvent expressed by the adsorption excess on the polymer, φ). The results for longer alcohols (**Figure 2.3b**) deviate substantially from the theoretical prediction in the regime of cosolvent concentrations beyond the collapse region, and the fit has been obtained here by considering the data points at low cosolvent concentrations up to the collapsed state. An important reason for this deviation is the non-ideal thermodynamics of the solvent mixture for more hydrophobic alcohols. This will be discussed in more detail further below, see the **section 2.8**.

2.7 Isomer effect of alcohol in the cononsolvency transition of PNiPAAm brushes

In **Figure 2.4** and **Figure 2.5** we display my results for brushes in propanol isomer aqueous solutions and butanol isomer aqueous solutions. The grafting density is chosen well above the overlap grafting density for the corresponding degree of polymerization, for details of determining brush's overlap density see the **section 2.2.4**. **Figure 2.4** and **Figure 2.5** show that with increasing the propanol isomers' hydrophobicity, the location of the minimum of the re-entrant transition curve shifts to lower alcohol-concentrations. Experimental evidence in **Figure 2.2**, **Figure 2.4** and **Figure 2.5** show that increasing the alcohol's hydrophobicity enhances the strength of the collapse transition of PNiPAAm brushes in the water-rich regime, this phenomenon can be qualitatively predicted by the adsorption-attraction model [23] by assuming an increasing hydrophobically driven adsorption of the cosolvent on the polymer chains. However, for the same brush, **Figure 2.4** shows that propanol isomers lead to almost the same volume/height changes of the PNiPAAm brush for the collapse state; this observation is also found in **Figure 2.5** for butanol isomers except 1-butanol. Currently, the reason behind this discrepancy between propanol and butanol isomers is still unclear and cannot be properly explained by the adsorption-attraction model [23] (also see **section 2.3**).

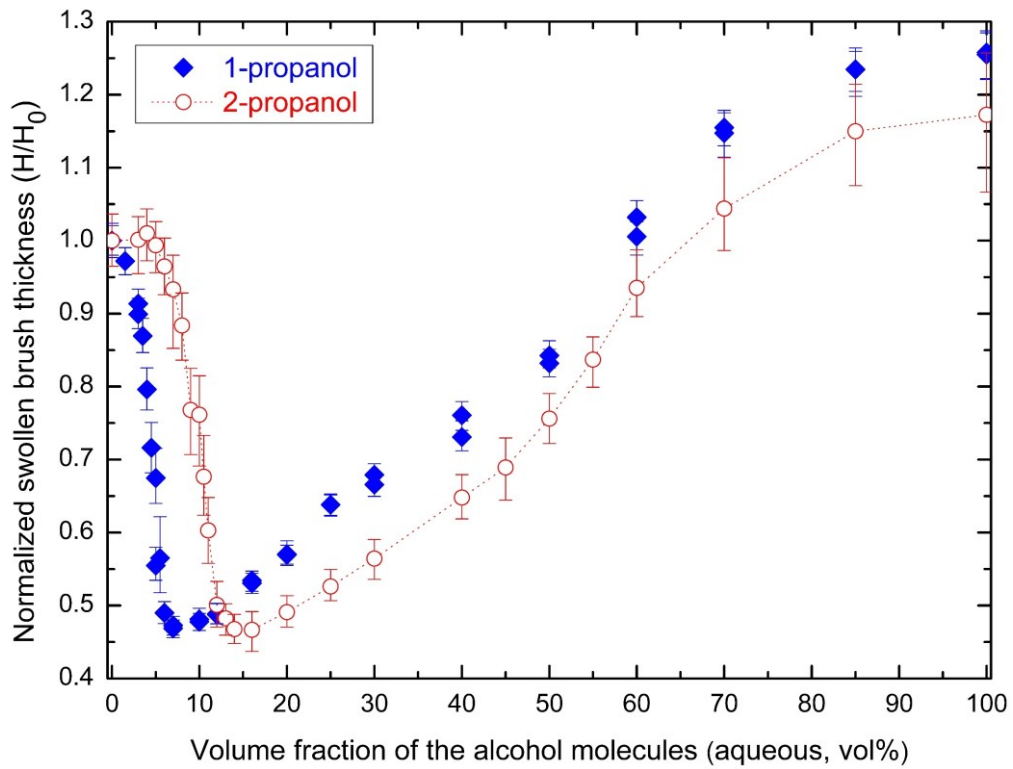


Figure 2.4(Figure 11) Normalized PNiPAAm brush thickness as a function of the volume fraction of cosolvent: Cononsolvency transition of the same PNiPAAm brush in propanol isomer aqueous solutions, at the temperature of 25°C. Parameters of the PNiPAAm brush are: grafting density $\sigma = 0.143$ chains/nm², $M_n = 6.1 \times 10^4$ g/mol, $M_w/M_n = 1.40$. Note that the dotted line in the figure are guides to the eyes.

Previous studies pointed out that the NH amide proton of PNiPAAm was unimportant in the polymer's cononsolvency transition [81]. Thus, my experimental observations of PNiPAAm

brushes in propanol/water and butanol/water mixtures imply that the origin of cononsolvency of PNiPAAm in alcohol-water mixtures favors a hydrophobically driven adsorption of the alcohol molecules on the PNiPAAm polymer chains. This indication is particularly obvious for the cononsolvency transition of PNiPAAm brushes in butanol isomers aqueous solutions. Actually, 1-butanol, 2-butanol and iso-butanol are not miscible with water at intermediate compositions at room temperature, thus only limited data of PNiPAAm brush thickness is available for these mixtures. Even though, in the narrow water-rich regime (as volume fraction of butanol is less than 25%), the PNiPAAm brushes can show a full landscape of cononsolvency transition, this peculiar phase-transition behavior can mainly be attributed to a hydrophobically driven adsorption of the butanol molecules on the PNiPAAm polymer chains.

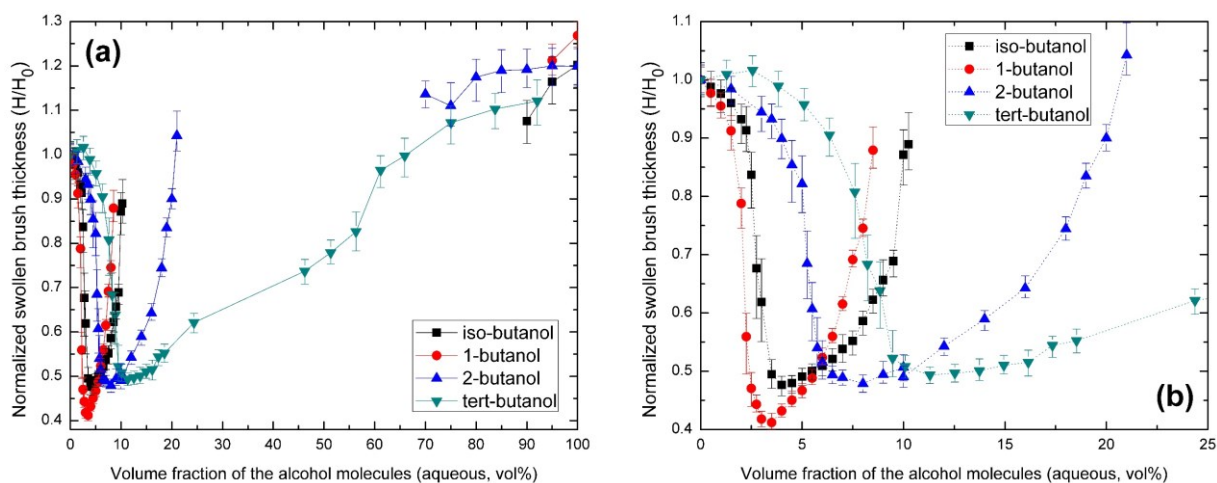


Figure 2.5(Figure 12) Normalized PNiPAAm brush thickness as a function of the volume fraction of cosolvent (a) Cononsolvency transition of the same PNiPAAm brush in butanol isomer aqueous solutions, at the temperature of 25°C. Parameters of the PNiPAAm brush are: grafting density $\sigma = 0.143$ chains/nm², $M_n = 6.1 \times 10^4$ g/mol, $M_w/M_n = 1.40$. (b) A zoom-in of Figure 2.5a for the alcohol's volume fraction ranging from 0 to 25%. Note that the dotted and solid lines in the figures are guides to the eyes.

2.8 Role of alcohol-water interaction in the cononsolvency transition of PNiPAAm polymers

The role of different interactions in the cononsolvency transition of polymer is still debated [82, 83]. Let us briefly outline the arguments leading to the two orthogonal scenarios for the origin on the cononsolvency effect discussed in the literature: The preferential adsorption model (PAM) [35] assumes that the better solvent forms temporal bridges between monomers. The alternative assumption is that of a cosolvent-solvent association frequently related with the picture of formation of cosolvent-solvent “clusters”, short as cluster model (CM) [54, 58, 59, 82, 83]. Support for the PAM model came from atomistic simulations of PNiPAAm-methanol-water systems [75, 84]. Furthermore, the idea of preferential adsorption can be cast into generic theoretical frameworks based on extensions of the Flory-Huggins model [7, 8] for polymer solutions as described above. In particular these models are able to predict the cononsolvency transition including the reentry behavior [19, 23, 24, 35, 39]. The assumption of preferential adsorption is supported in experiments by Wang et al.

[46] and Mukae et al. [28]. These authors used Fourier transform infrared spectroscopy and spectroscopy of variable-temperature high-resolution ^1H MAS NMR to investigate cononsolvency effect of PNiPAAm gels in alcohol-water solutions. Their results demonstrated that the polymer preferentially interacts with alcohol molecules and that alcohols with higher hydrophobicity exhibits higher preferential absorption on PNiPAAm molecules.

On the other hand, the CM model requires association between both solvents which in turn changes the solubility of the polymer. In the language of the Flory-Huggins model, this needs a negative interaction parameter between the two solvent components. This concept has been reconsidered recently by Dudowicz et al. [85] who have shown that a strong negative Flory parameter between the two solvents is necessary to obtain a demixing transition between the polymer and the associating solvent phase. Besides, the idea of the formation of solvent “complexes” or “clusters” has been put forward in previous works [54, 58, 59, 82, 83]. It should be noted that the CM model strongly focused on water as an *ad hoc* common solvent aiming at the specific molecular properties of water such as hydrogen bonding or hydrophobic ordering.

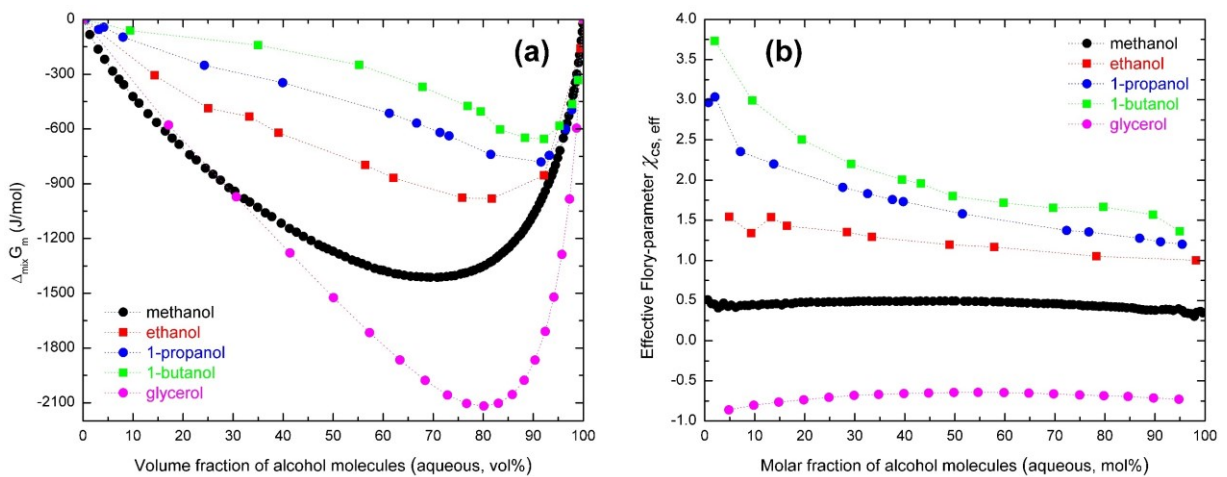


Figure 2.6(Figure 13) Free energy change of mixing alcohols with water: (a) Molar Gibbs free energy change of mixing $\Delta_{\text{mix}}G_m$, when mixing different alcohols with water at the temperature of 25°C. (b) Effective Flory-interaction parameter between the two solvents χ_{CS} , when mixing different alcohols with water at the temperature of 25°C. Data are extracted and reprocessed from refs. [86-89], note that the dotted lines in the figures are only used to guide eyesight.

Considering this controversy about the origin of cononsolvency effect, the analysis of the cosolvent-solvent interaction based on thermodynamic measurements can be the key. While the CM model is based on attraction, i.e. a negative Flory-interaction parameter; a positive interaction parameter, i.e. an imperfect mixture of the solvents would lead to an enhancement of the co-nonsolvency effect in the PAM model.

Molar Gibbs free energy change of mixing $\Delta_{\text{mix}}G_m$ was assessed when mixing different alcohols with water by using data of excess free energy of mixing reported by several authors [86-89], for details see the section 2.13.1. Figure 2.6 shows that at any fixed alcohol concentration, a simple

order relation exists for the mixing free energy: " $\Delta_{mix}G_m$ (methanol, H₂O) \leq $\Delta_{mix}G_m$ (ethanol, H₂O) \leq $\Delta_{mix}G_m$ (1-propanol, H₂O) \leq $\Delta_{mix}G_m$ (1-butanol, H₂O) \leq 0". This is in accordance with a simple picture that longer carbon chain length of the alcohol leads to an enhanced hydrophobic behavior. Actually, 1-butanol is not miscible with water at intermediate compositions at room temperature, thus only limited data of the mixing thermodynamics, and of PNiPAAm brush height is available for these mixtures. We note that the origin of the effective alcohol-water interaction can contain both enthalpic and entropic contributions. In order to quantify the effective interaction between the two solvents, we thus use the molar excess Gibbs free energy of mixing [90] $\Delta_{mix}G_m^E$. Using the data from refs. [86-89] we can extract the effective Flory-parameter between the two solvents $\chi_{cs, eff}$ calculated as:

$$\chi_{cs, eff} = \frac{\Delta_{mix}G_m^E}{RTx(1-x)}, \quad (2.9)$$

where x is alcohol's molar fraction in the alcohol-water mixtures, R is the gas constant and T is the absolute temperature. In **Figure 2.6b** we display the corresponding results. This clearly indicates a positive interaction parameter for methanol, ethanol, 1-propanol and 1-butanol at all concentrations. In the series of alcohols only glycerol displays a perfect mixing. It is remarkable that the effective Flory-parameter for glycerol and water is negative at all concentration, but glycerol is a poor solvent [91] for PNiPAAm, and does not lead to a cononsolvency transition of PNiPAAm in glycerol-water mixtures. We can thus state that an increasing demixing tendency between alcohol and water is correlated with an enhancement of the cononsolvency transition of PNiPAAm.

In this respect we note that recently published data for iso-propanol/water mixtures indicate a difference in the cononsolvency behavior of iso-propanol and 1-propanol [92]. This can be related with the more hydrophilic behavior of iso-propanol [89]. Thus, by ignoring all other effects of the different molecular architecture of both alcohols we would expect a stronger collapse transition of the system of water/1-propanol/PNiPAAm brush in water-rich region, as compared with the system of water/iso-propanol/PNiPAAm brush. This prediction is already verified by my experimental study of cononsolvency transition of PNiPAAm brushes in propanol isomers aqueous solutions and butanol isomers aqueous solutions, see **section 2.7**.

2.9 Temperature effect in the cononsolvency transition of PNiPAAm brushes

We have also investigated the effect of temperature variation for the cononsolvency transition of the PNiPAAm brush (**Figure 2.7**) in ethanol aqueous solutions. The data for the absolute brush thickness as a function of the volume fraction of cosolvent are displayed in **Figure 2.7a**. In the water-rich region, the brush thickness decreases if temperature increases which indicates a LCST behavior of the PNiPAAm brush in pure water. On the other hand, in the ethanol-rich region the brush thickness slightly increases for the temperature change from 15°C to 25°C. This indicates that re-entry transition may be related with an UCST (upper critical solution temperature) behavior of the

PNiPAAm brush in water-ethanol mixtures. We note that similar phenomena were also reported for PNiPAAm solutions [57] and micro-gels [79].

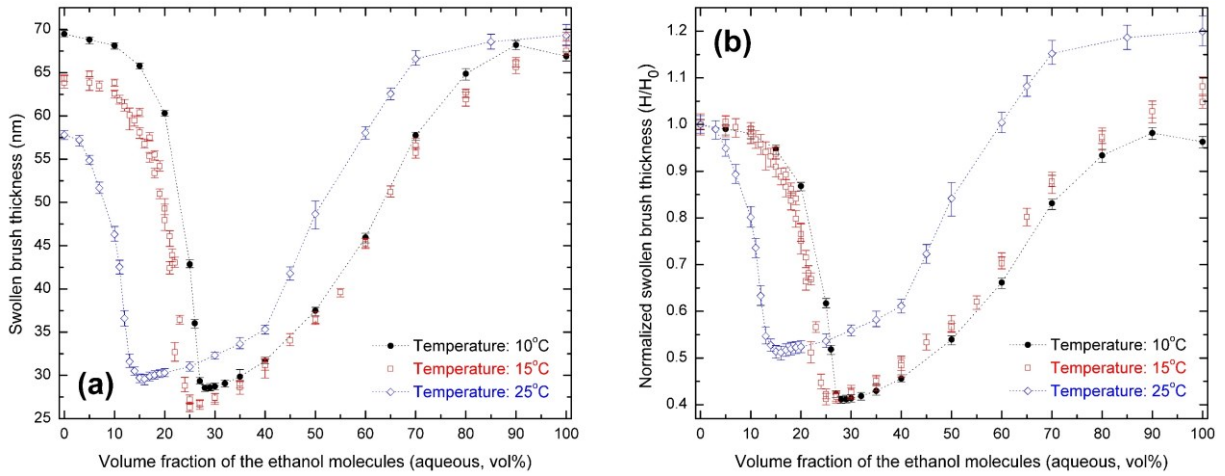


Figure 2.7(Figure 14) Temperature effect on the cononsolvency transition of the same PNiPAAm brush in ethanol aqueous solutions under different temperatures: (a) Swollen brush thickness (unit in nanometre) as a function of temperature. (b) Normalized brush thickness (H/H_0) as a function of temperature. Parameters of the PNiPAAm brush are: grafting density $\sigma = 0.143$ chains/nm², $M_n = 6.1 \times 10^4$ g/mol, $M_w/M_n = 1.40$. Note that the dotted lines in the figures are guides to eyes.

In **Figure 2.7b** we display again the normalized swollen brush thickness for the same system. For temperature changes well below the LCST-transition of PNiPAAm in pure water, which is around 32 °C, only a weak shift of the collapse transition is observed (data for 10 °C and 15 °C). When approaching the LCST temperature, at 25 °C, the collapse becomes weaker and is considerably shifted towards smaller volume fractions of ethanol. This result may be explained by the non-ideal behavior of the polymer in water. By considering the adsorption-attraction model an increase of temperature leads to a decrease of the thermodynamic interaction strength between cosolvent and monomers ϵ , see **Eq.(2.4)** and **Eq.(2.5)**, by $\Delta T/T$ which amounts to about 5%. Such a small change of ϵ is not sufficient to explain the shift between the results for 10 °C and 15 °C, moreover, the model predicts the opposite direction of the shift towards higher volume fractions of cosolvent with increasing temperature. Thus, the rather strong changes of transition in the water-rich regime at higher temperatures should be related to the decrease in solvent quality of the PNiPAAm being close to the LCST transition. My observations on brushes are comparable with those made for PNiPAAm gels, see **section 2.13.2**.

To account for the non-ideal mixing of PNiPAAm in water we have extended the model given in **section 2.3**. The simplest way to account for solvent quality and non-ideal mixing of the polymer-water system is to add a standard Flory-Huggins interaction term of the form:

$$f_{int} = \chi_{ps}(1-c), \quad (2.10)$$

in Eq.(2.7). Here, χ_{ps} denotes the Flory-parameter for the polymer-water system. This is of course a strong simplification of the LCST-behavior which in general cannot be simply reflected by a constant Flory-parameter [17, 22, 93]. Nevertheless, this allows us to study qualitatively the effect of thermal solvent, particularly close to the critical point of mixing, $\chi_{ps} = 0.5$, on the cononsolvency behavior. We hasten to note that in the case of polymers immobilized by grafting to a substrate there is no transition expected due to reduction of solvent quality only. Thus, even at and above $\chi_{ps} = 0.5$ the brush (in the absence of cosolvent) does not show a sharp collapse transition. In **Figure 2.8** we display the numerical solution of the extended model for the parameters suitable for ethanol and for $\chi_{ps} = 0.3$, $\chi_{ps} = 0.4$ and $\chi_{ps} = 0.5$ respectively. With decreasing solvent quality, the transition shifts to smaller concentrations of cosolvent and the collapsed state is (relatively) weakened (with respect to the reference state in pure water). This coincides with the general observations made for the experiments in **Figure 2.7b**. To quantitatively work out the extension of the adsorption-attraction model to imperfect mixing of solvents one has to take into account a more realistic model for the LCST-transition of PNiPAAm.

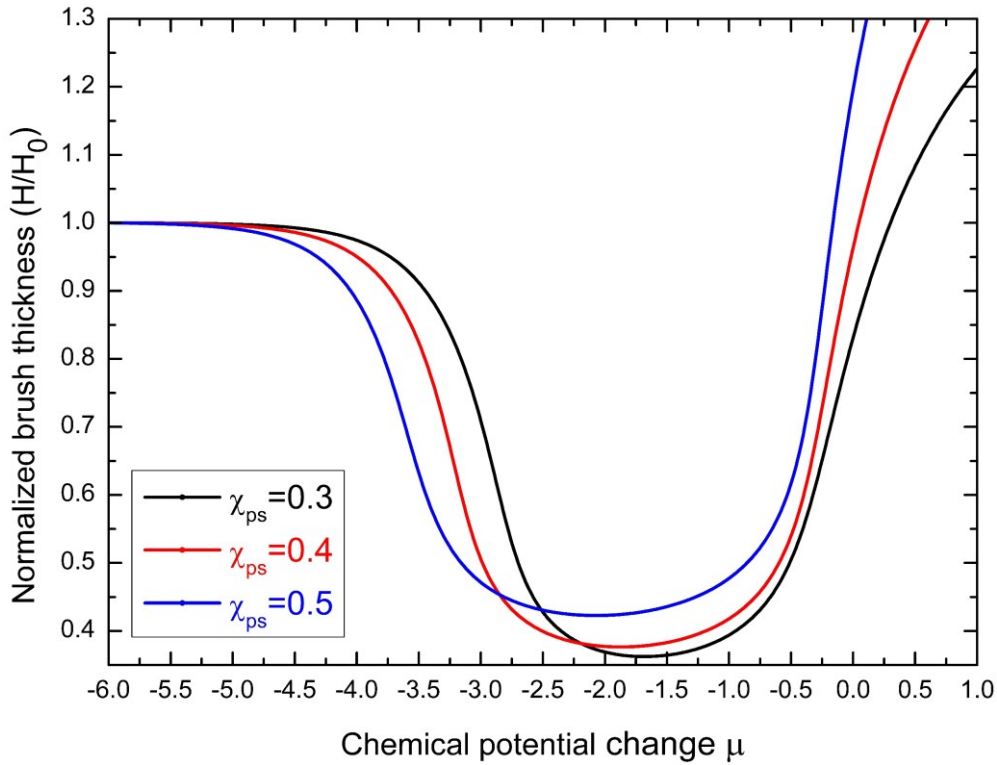


Figure 2.8(Figure 15) Normalized brush thickness (H/H_0) in the cononsolvency transition of a polymer brush as a function of the chemical potential change μ for $\chi_{ps} = 0.3$, $\chi_{ps} = 0.4$ and $\chi_{ps} = 0.5$. Note that in Figure 2.8 except changing the Flory-parameter χ_{ps} , other model parameters are fixed as $\sigma = 0.143$ chains/nm², $\gamma = 1.0$, $t = 1.0$, $\epsilon = 1.5$, $\lambda = 3$ and $\nu = 0.2$.

It is noted that both LCST and cononsolvency transitions of PNiPAAm polymers show behaviors of a type-II phase transition where the third virial coefficient is negative but the second virial coefficient stays positive for free energy expansion [22-24]. The reason behind this general phenomenon

can be attributed to that PNiPAAm achieves LCST transition by a kind of water-depleted physical crosslinking (attraction) of its side hydrophobic chains [94, 95], while the polymer achieves cononsolvency transition by a kind of cosolvent-assisted physical crosslinking (attraction) of its side hydrophobic chains (see Eq.(2.4)). Therefore, both phase transitions can indeed overlap with each other when temperature varies in the PNiPAAm/cosolvent/water solutions, such as PNiPAAm in the alcohol-water mixtures. The overlap of water-depleted and cosolvent-assisted physical crosslinkings can explain the phenomenon where LCST transition of PNiPAAm in cosolvent-water mixtures is enhanced by an increase of cosolvent concentration in the cosolvent-poor region [57].

2.10 Grafting-density effect in the cononsolvency transition of PNiPAAm brushes

Figure 2.9a shows that increasing the grafting density weakens the collapse, but the grafting density has only a very small effect on the solvent-composition location of the maximum collapsed state. These observations are quantitatively predicted by the adsorption-attraction model [23] (also see section 2.3), the details of the fit parameters are shown in Table 2.3. It is worth noting that once the parameters of the adsorption-attraction-model are fixed the prediction of the results for different grafting densities are parameter-free. Two aspects can be deduced from the model directly [23]: First, the increase of grafting density weakens the collapse transition up to a change in signature into a smooth crossover for very high grafting densities. This gives rise to a phase boundary of the discontinuous transition in the parameter space formed by solvent selectivity and grafting density. Second, the model predicts only a weak shift of the state of minimal brush height. Both predictions of the theory can be detected in the experiments. The corresponding model predictions are displayed as solid lines in Figure 2.9a.

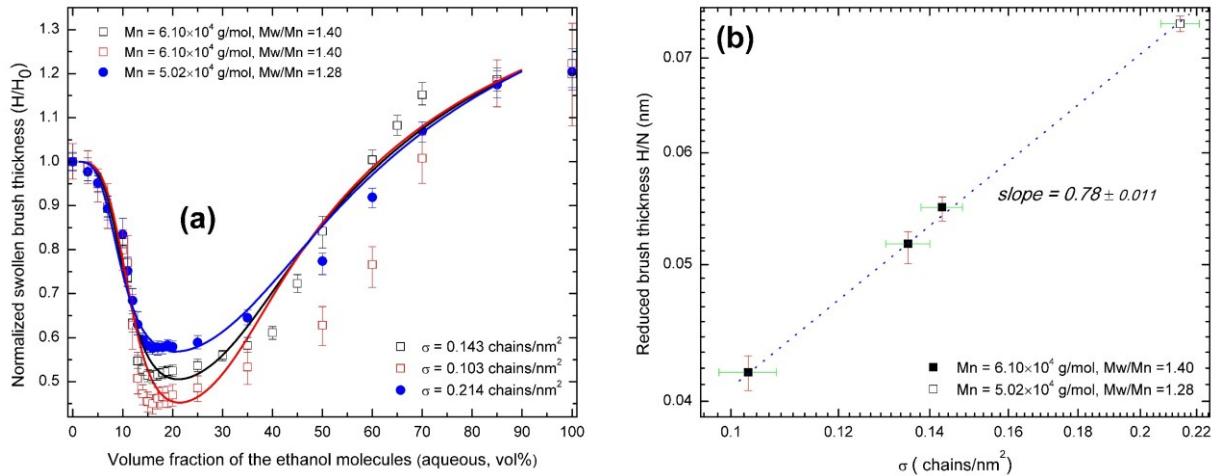


Figure 2.9(Figure 16) Grafting-density effect in the cononsolvency transition of PNiPAAm brushes: (a) Cononsolvency transition of PNiPAAm brushes with different grafting densities in ethanol aqueous solutions, at the temperature of 25°C. The solid lines are numerical fits based on the adsorption-attraction model 23. (b) Reduced brush thickness in the collapsed state of PNiPAAm brushes vs. grafting density at the temperature of 25°C (in the 16% volume fraction of ethanol aqueous solutions). Parameters of the PNiPAAm brushes plotted in Figure 2.9a from above to bottom are: grafting density $\sigma = 0.214$ chains/nm², $M_n = 5.02 \times 10^4$ g/mol,

$M_w/M_n = 1.28$; $\sigma = 0.143$ chains/nm², $M_n = 6.1 \times 10^4$ g/mol, $M_w/M_n = 1.40$; $\sigma = 0.103$ chains/nm², $M_n = 6.1 \times 10^4$ g/mol, $M_w/M_n = 1.40$.

In **Figure 2.9b** we display the brush thickness divided by the average monomer number of the brush N , for the state of maximum collapse as a function of the grafting density. We note that for brushes above the stretching threshold the relation of $H / N \propto \sigma^{1/2}$ is fulfilled because of mass conservation. The apparent scaling exponent $\nu_2 = 0.78 \pm 0.011$ observed in double logarithmic representation corresponds to the value reported for brushes [96] immersed in ordinary poor solvent. It is noted that a recent computer-simulation study [97] also reported a similar apparent scaling exponent for collapsed bushes in cononsolvency transition. This implies that while both ethanol and water are good solvents for the polymer, at a volume fraction around 16% of ethanol, the ethanol aqueous solution behaves similar to poor solvent. This is accordance with results for single PNiPAAm chains in ethanol-water mixtures observed by using fluorescence correlation spectroscopy [98].

2.11 Octopus-shape-micelle morphology of grafted PNiPAAm polymers

The phase behaviors of grafted polymers in poor solvent can be quite different from its free polymer in solutions. Merely with a decrease of a grafted PNiPAAm polymer's grafting density, when the temperature is fixed and higher than its LCST temperature (at a poor-solvent state), the polymer chains can show various morphologies such as collapsed brush, coexistence of two phases, octopus-shape micelle and collapsed globule [51, 52], similar behavior is also observed in my study of grafted PNiPAAm polymers in ethanol/water mixtures.

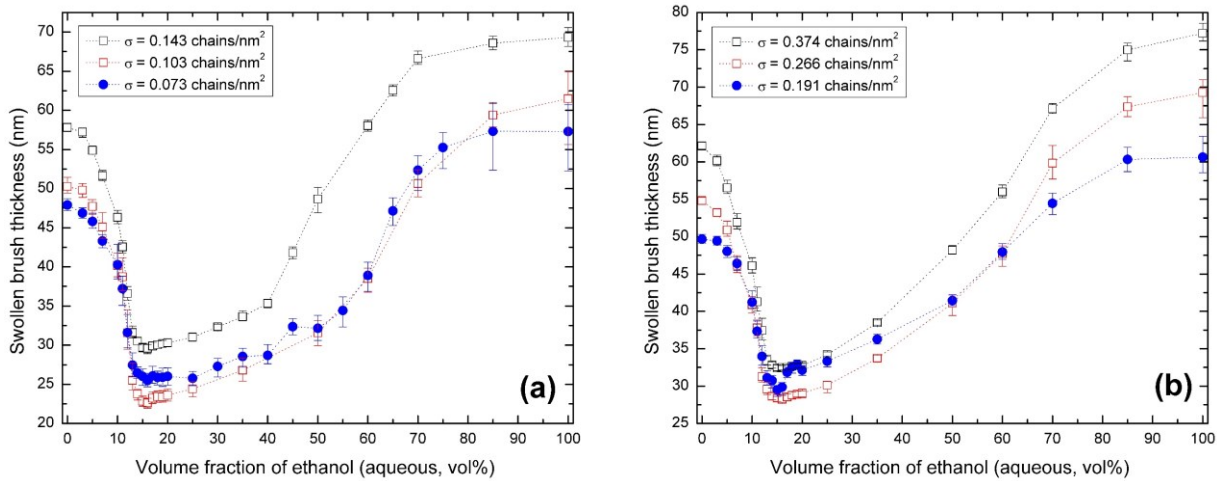


Figure 2.10(Figure 17) Grafting-density effect in the cononsolvency transition of grafted PNiPAAm polymers in ethanol aqueous solutions, absolute swollen brush thickness at the temperature of 25°C: (a) with molecular weight of $M_n = 6.1 \times 10^4$ g/mol, $M_w/M_n = 1.40$ for all polymer layers; (b) with molecular weight of $M_n = 3.8 \times 10^4$ g/mol, $M_w/M_n = 1.38$ for all polymer layers. Note that the dotted lines in the figures are guides to eyes.

The data for the absolute brush thickness as a function of the volume fraction of ethanol are displayed in **Figure 2.10**. The absolute swollen brush thickness at the collapse state clearly showed

that when the brush layer's grafting density (σ) is lower than a threshold grafting density (σ^* , how to determine this threshold see Eq.(2.3)), the collapsed polymer layer (blue filled-circles in **Figure 2.10**) is thicker than a brush layer (red open-square in **Figure 2.10**) whose grafting density is higher than the threshold grafting density. In **Figure 2.11**, we again display the reduced (de-swollen) brush thickness for the same systems as shown in **Figure 2.10**. From **Figure 2.10** and **Figure 2.11**, it shows that when the grafting density (σ) reaches a critical threshold (σ^*) for a polymer layer, a decrease of grafting density weakens the collapse, this is quite different from phase behaviors of a classic polymer brush for which the brush thickness (H) is proportional to grafting density (σ) and the average number of monomers (N) in each polymer chain at the poor-solvent state. It indicates that the polymer layer which has the lowest grafting density (blue filled-circles in **Figure 2.10** and **Figure 2.11**), may be located in the so-called octopus-shape micelle region [51, 52]. It is noted that computer simulation studies on cononsolvency transition of grafted polymer layers have also revealed octopus-shape micelle morphologies [39, 97]. In **Figure 2.10** and **2.11**, it is interestingly observed in my current experimental data that the grafting density has only a very small effect on the solvent-composition location of the maximum collapsed state, it doesn't matter the polymer layer is located in brush or octopus-shape micelle regions. From **Figure 2.10** and **Figure 2.11**, it is also noted that a short polymer chain may be much easier to behave like an octopus-shape micelle rather than a classic polymer brush when its grafting density is reduced.

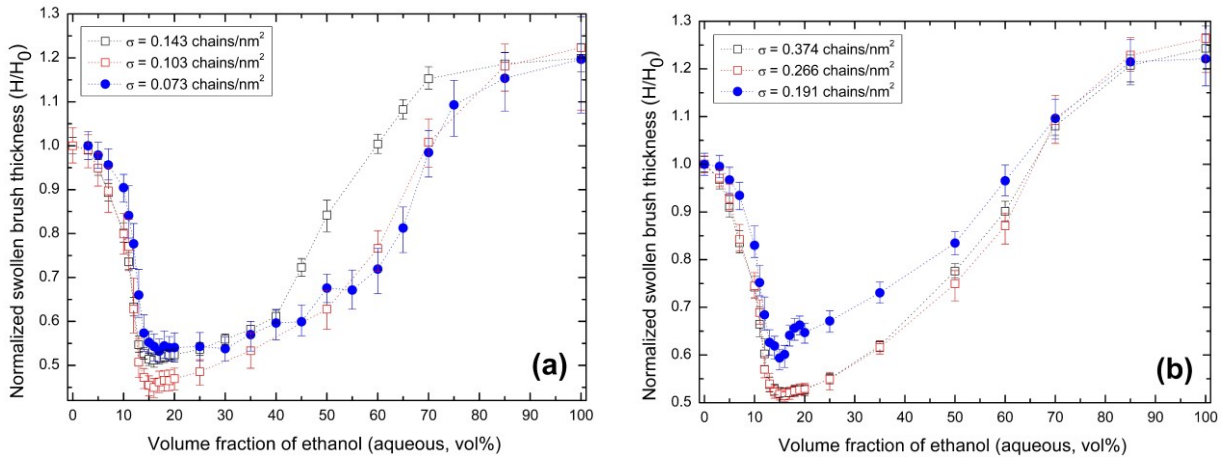


Figure 2.11(Figure 18) Grafting-density effect in the cononsolvency transition of grafted PNiPAAm polymers in ethanol aqueous solutions, normalized swollen brush thickness at the temperature of 25°C: (a) with molecular weight of $M_n = 6.1 \times 10^4$ g/mol, $M_w/M_n = 1.40$ for all polymer layers; (b) with molecular weight of $M_n = 3.8 \times 10^4$ g/mol, $M_w/M_n = 1.38$ for all polymer layers. Note that the dotted lines in the figures are guides to eyes.

2.12 Chapter summary

We investigated the cononsolvency effect of PNiPAAm brushes with different grafting densities in aqueous alcohol mixtures. We have used Vis-spectroscopic ellipsometry measurements to prove the hypothesis that the cononsolvency transition of PNiPAAm brushes consists of a volume phase-like equilibrium transition. We found a strong collapse transition in PNiPAAm brushes followed by a reentry behavior as observed by ellipsometry measurements.

Using a series of alcohols with stronger hydrophobic effect in water we have demonstrated that the cononsolvency effect is enhanced and shifted to smaller volume fractions of the alcohol. Particularly for the longer alcohols this is correlated with an increasing tendency of demixing between the two solvents. This is apparently in contrast to the hypothesis of strongly associative solvents being the origin of the cononsolvency effect. The preferential adsorption model, on the other hand, can account for this case by assuming an increasing hydrophobically driven adsorption of the cosolvent on the polymer chains. The recently proposed adsorption-attraction model can be used to predict the corresponding transition behavior. In particular the model predictions for variation of the grafting density is in agreement with the experimental findings. However, to reflect the imperfect mixing of the longer alcohols in water as well as finite miscibility of the polymers in the common solvent, extensions of the model have to be considered. We have shown that the simplest extension of the model taking into account the Flory-Huggins parameter for polymer and water can account for the qualitative changes observed for temperature changes in my experiments. A particular interesting aspect for future work is to relate the LCST-behavior with cononsolvency since both effects go beyond the standard Flory-Huggins model. An extension of the adsorption-attraction model that it can quantitatively account demixing effect between cosolvent and solvent will be developed in **Chapter 3**.

However, it is still worth pointing out that in some cases where water can be a better solvent rather than organic solvents, examples for this situation are such as poly(N, N-dimethylacrylamide) [99] and poly(2-(methacryloyloxy)ethyl phosphorylcholine) [50] in alcohol-water mixtures, where a preferential adsorption of water rather than alcohol should be considered as a candidate of phase-transition mechanism of cononsolvency transition. Even though, for these cases the interaction between water and monomer strongly depends on monomer concentration and on the unique thermodynamics of correlated water-organic solvent clusters in the solution. This means that an assumption of a constant preferential-adsorption energy (ϵ) between water and polymer is no longer valid. As for these cases, the rationalization of preferential adsorption by Tanaka, Koga and Winnik [29] may be suitable, where the cononsolvency of polymers is explained based on the competition between the two solvents in forming hydrogen bonds with the polymers.

An investigation of grafting-density effect in the cononsolvency transition of grafted PNiPAAm polymers, showed that a decrease of grafting density at the collapse state when the temperature is fixed, the polymer chains can show morphologies not limited to collapse brush. In addition, my experimental results clearly showed that the strongest collapse state can be only realized by polymer brushes with moderate grafting densities. My results display the universal character of the cononsolvency effect with respect to series of cosolvents and show that polymer brushes display a well-defined and sharp collapse transition. This is most pronounced for 1-propanol as cosolvent which is still fully miscible in water. Potential applications are switches built from implementation of brushes in pores and similar concave geometries are expected to be realized by harnessing the cononsolvency effect of stimuli-responsive polymers [100]. An application study for the cononsolvency effect of grafted polymers around the rim of nanopores will be discussed in **Chapter 4**.

2.13 Chapter appendix

2.13.1 Data extraction and reprocessing for the molar Gibbs free energy of mixing

Molar Gibbs free energy of mixing $\Delta_{mix}G_m$, when mixing different alcohols with water molecules is written as,

$$\frac{\Delta_{mix}G_m}{RT} = \frac{\Delta_{mix}G_m^E}{RT} + x \ln(x) + (1-x) \ln(1-x), \quad (2.11)$$

where $\Delta_{mix}G_m$ defines the molar excess Gibbs free energy of mixing, x is the molar fraction of alcohol in the alcohol-water mixtures, R and T are gas constant and absolute temperature respectively. Data of $\Delta_{mix}G_m$ can be extracted from **refs. [86-89]**. Alcohol's molar fraction x , can be converted into volume fraction y , by using,

$$y = \frac{M_w \rho_a x}{M_a \rho_w + (M_w \rho_a - M_a \rho_w) x}, \quad (2.12)$$

where M_w and M_a are water's and alcohol's molar mass respectively, ρ_w and ρ_a are water's and alcohol's volumetric mass density respectively. **Eq.(2.12)** is used to transform data of alcohol concentration for the **Figure 2.6a** of main text.

2.13.2 Temperature effect in the cononsolvency transition of PNiPAAm gels

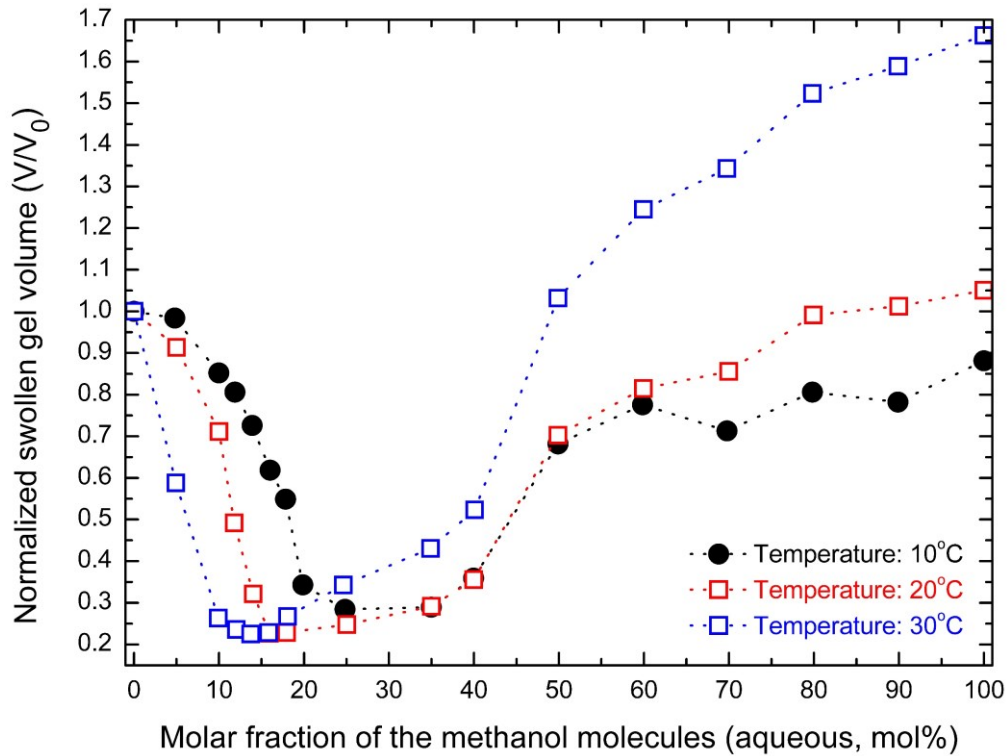


Figure 2.12(Figure 19) Cononsolvency transition of the same PNiPAAm micro-gel in methanol aqueous solutions under different temperatures. Data are extracted and reprocessed from **ref. [101]**, note that the dotted lines in the figure are only used to guide eyesight.

We firstly studied the temperature effect in the cononsolvency transition of polymer brushes. To compare my results with possible similar literature results, in this section we review literature data about temperature effect in the cononsolvency transition of PNiPAAm gels. We find that my extended model (see [section 2.9](#)) can also be used to explain the temperature effect in the cononsolvency transition of gels.

Kojima et al. [\[101\]](#) reported the average hydrodynamic radius, R_h of PNiPAAm micro-gels in methanol-water mixtures under different temperatures. Here we replotted these data as normalized swollen gel volume ($\frac{V}{V_0} = \left(\frac{R_h}{R_{h,0}}\right)^3$) in **Figure 2.12**. Note that $R_{h,0}$ is the average hydrodynamic radius of PNiPAAm micro-gels in pure water, and V_0 is the gel's swollen volume in pure water.

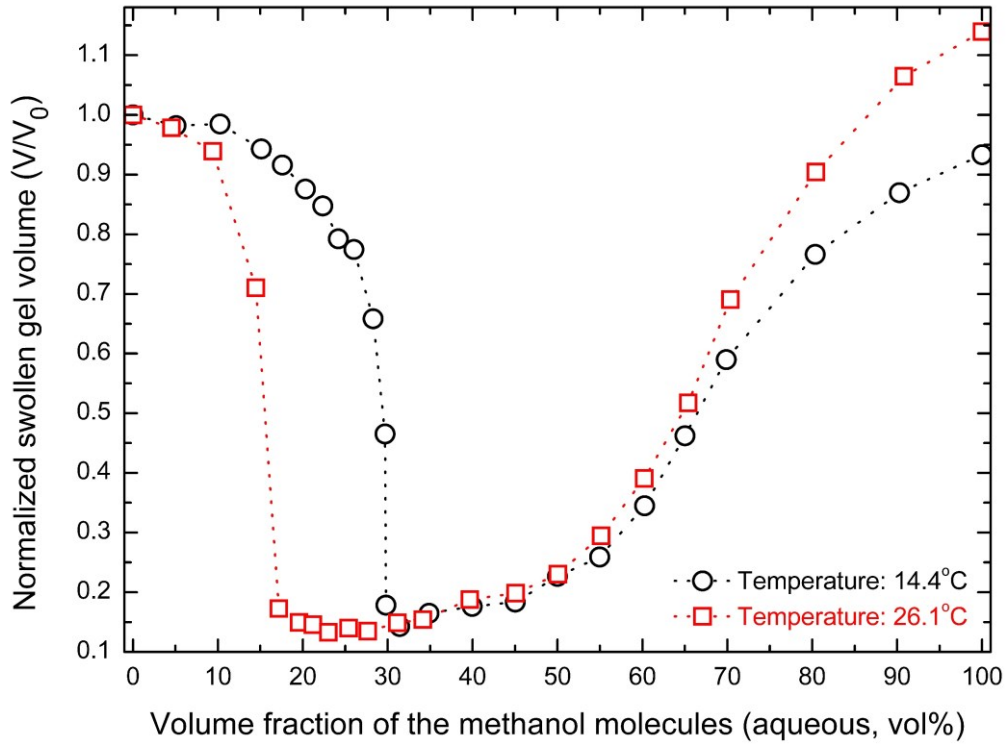


Figure 2.13(Figure 20) Cononsolvency transition of the same PNiPAAm macro-gel in methanol aqueous solutions under different temperatures. Data are extracted and reprocessed from [ref. \[102\]](#), note that the dotted lines in the figure are only used to guide eyesight.

Hirotsu et al. [\[102\]](#) reported swollen gel volume ratio in respect to dry state, V/V_{dry} for PNiPAAm macro-gels in the methanol-water mixtures under different temperatures. Here we replotted these data as normalized swollen gel volume ($\frac{V}{V_0} = \frac{V/V_{dry}}{V_0/V_{dry}}$) in **Figure 2.13**.

Crowther et al. [\[80\]](#) reported normalized swollen gel volume (V/V_0) of PNiPAAm micro-gel (containing 9% N,N'-methylenebisacrylamide (MBA) as crosslinkers) in 2-propanol aqueous solutions as a function of temperature. Here we replotted these data in **Figure 2.14**.

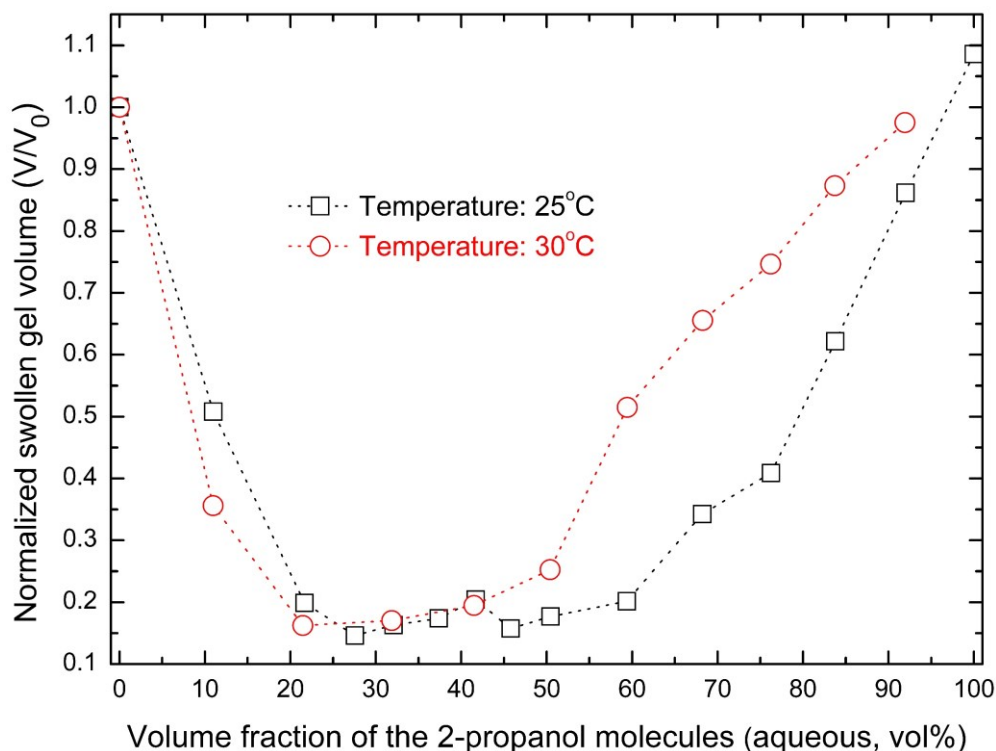


Figure 2.14(Figure 21) Normalized swollen gel volume (V/V_0) of the same PNiPAAm micro-gel in 2-propanol aqueous solutions as a function of temperature. Data are extracted and reprocessed from [ref. \[80\]](#), note that the dotted lines in the figure are only used to guide eyesight.

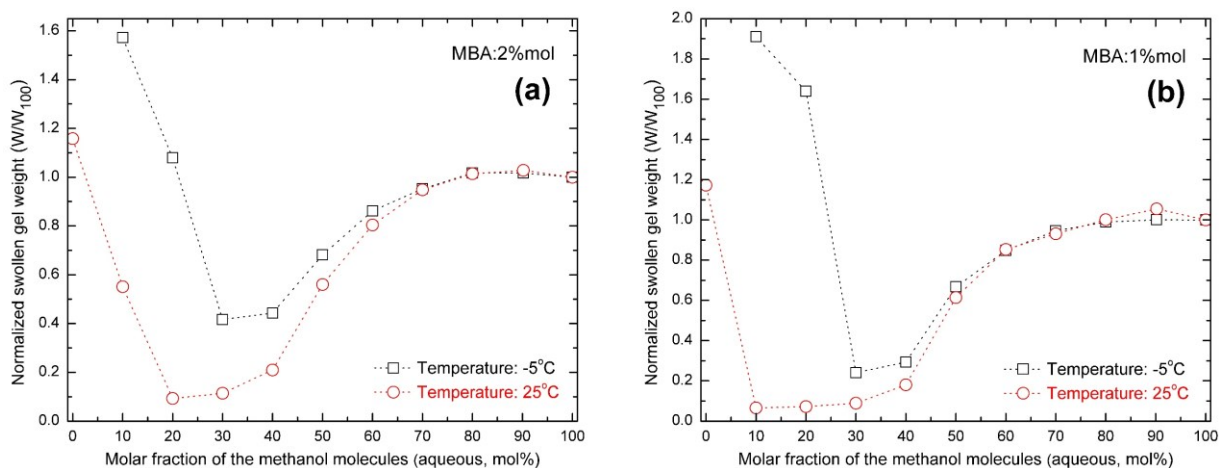


Figure 2.15(Figure 22) Normalized swollen gel weight(W/W_{100}) of two PNiPAAm macro-gels in methanol aqueous solutions as a function of temperature. Data are extracted and reprocessed from [ref. \[103\]](#), note that the dotted lines in the figures are only used to guide eyesight.

Walter et al. [\[103\]](#) reported swollen gel weight ratio (W/W_{dry}) of PNiPAAm macro-gel (containing 1%mol and 2%mol N,N'-methylenebisacrylamide(MBA) as crosslinkers) in methanol aqueous solutions as a function of temperature. Here we replotted these data as normalized swollen gel

weight ($\frac{W}{W_{100}} = \frac{W/W_{dry}}{W_{100}/W_{dry}}$) in **Figure 2.15**. Note that W_{100} is the micro-gel's swollen weight in pure methanol.

Biswas et al. [104] reported swollen gel weight ratio (W/W_{dry}) of PNiPAAm micro-gel (containing 6.67%wt N, N'-methylenebisacrylamide (MBA) as crosslinkers) in methanol aqueous solutions as a function of temperature. Here we replotted these data as normalized swollen gel weight ($\frac{W}{W_0} = \frac{W/W_{dry}}{W_0/W_{dry}}$) in **Figure 2.16**. Note that W_0 is the micro-gel's swollen weight in pure water.

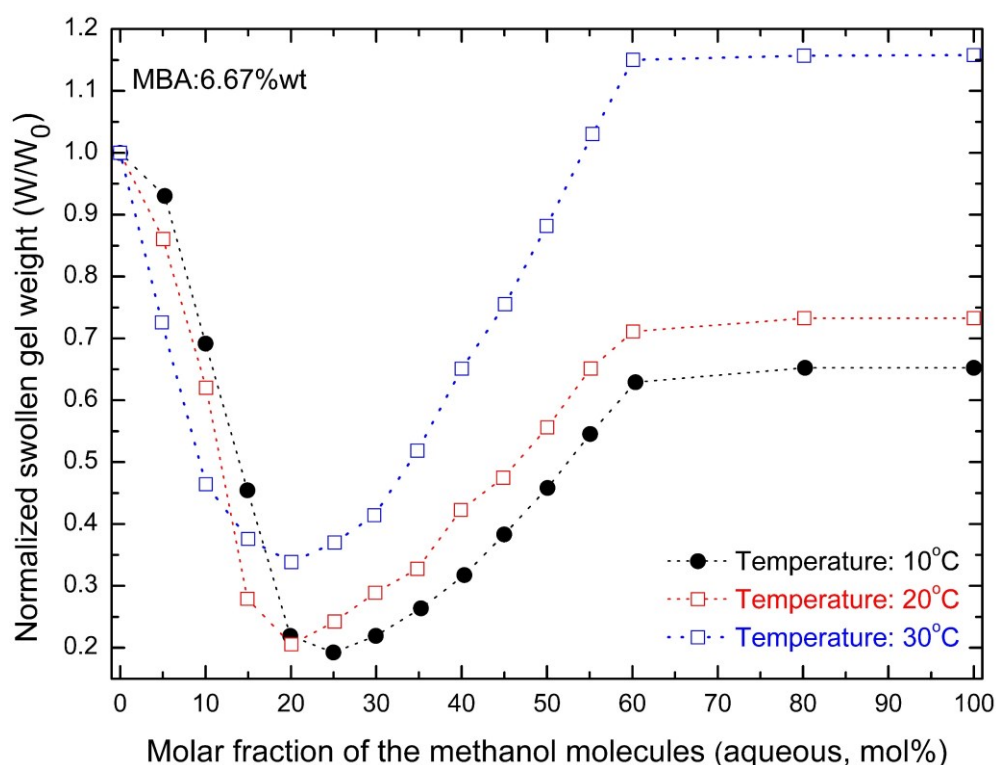


Figure 2.16(Figure 23) Normalized swollen gel weight(W/W_0) of the same PNiPAAm micro-gel in methanol aqueous solutions as a function of temperature. Data are extracted and reprocessed from **ref. [104]**, note that the dotted lines in the figure are only used to guide eyesight.

Chapter 3 The extended adsorption-attraction model

(Note: Some results presented in this chapter were already published by the author in the journal “Macromolecules, 2020, 53(7), 2323-2335”.)

3.1 Introduction

To understand phase-transition mechanism, a question not deeply discussed in **Chapter 2** is that what is the role of various polymer-solvent and cosolvent-solvent interactions in cononsolvency transition. For convenience sake, this question can be phenomenologically analyzed by a Flory-Huggins mean-field model [7, 8, 85] for polymers in a mixture of solvent and cosolvent with the following form:

$$G_{FH} = \frac{c \ln(c)}{N} + \phi_c \ln(\phi_c) + \phi_s \ln(\phi_s) + \chi_{pc} c \phi_c + \chi_{ps} c \phi_s + \chi_{cs} \phi_c \phi_s. \quad (3.1)$$

Here, the volume fraction of the polymers consisting of N monomers per chain in the solution is denoted by c , the volume fraction of the cosolvent is denoted by ϕ_c , and the volume fraction of the solvent is $\phi_s = 1 - c - \phi_c$. The free energy per volume is denoted by G_{FH} , and is given in units of $k_B T$. The phenomenological parameters χ_{pc} , χ_{ps} and χ_{cs} including of both excess enthalpic and excess entropic contributions, denote effective Flory-interaction parameters for the polymer-cosolvent interaction, the polymer-solvent interaction and the cosolvent-solvent interaction, respectively.

The condition for the two-phase coexistence of a tertiary polymer solution can be probed by a study of spinodal phase decomposition in terms of the second derivative ($D < 0$) of the free energy (G_{FH}), which corresponds to the surface of free energy (G_{FH}) being concave in mathematics. If the volume fractions c and ϕ_c are chosen as the independent composition variables, the condition for the spinodal phase decomposition of the tertiary system is expressed in terms of the second derivative (D) of the free energy G_{FH}

$$D = \left(\frac{\partial^2 G_{FH}}{\partial \phi_c^2} \right)_{c,T} \left(\frac{\partial^2 G_{FH}}{\partial c^2} \right)_{\phi_c,T} - \left(\frac{\partial^2 G_{FH}}{\partial \phi_c \partial c} \right)_T^2 < 0. \quad (3.2)$$

With the assumption of the χ -parameters defined above being independent of c and ϕ_c , we get:

$$D = \left(\frac{1}{Nc} + \frac{1}{\phi_s} - 2\chi_{ps} \right) \left(\frac{1}{\phi_c} + \frac{1}{\phi_s} - 2\chi_{cs} \right) - \left(\frac{1}{\phi_s} + \chi_{pc} - \chi_{ps} - \chi_{cs} \right)^2 < 0. \quad (3.3)$$

A typical solution of $D < 0$ for the spinodal decomposition (Eq.(3.3)) is $\chi_{cs} \ll 0$, $\chi_{cs} < \chi_{pc}$ and $\chi_{cs} < \chi_{ps}$ with a constraint of $\chi_{pc} < 0.5$ and $\chi_{ps} < 0.5$ for good solvent mixtures. According to the signatures behind the cononsolvency transition of various polymer systems, this case is the cononsolvency transition originating from strong attraction between two good solvents. This concept has recently been analyzed by Dudowicz et al. [85] who have shown that a strong negative Flory parameter

between the two solvents, χ_{cs} is necessary to obtain a demixing transition between the polymer and the associated solvent phase. A signature of this type of cononsolvency transition is that the associating solvent mixture functions as a real poor solvent for the polymer, ultimately driving the cononsolvency transition, and the result will be a solvent and cosolvent depleted polymer phase [82]. To my best knowledge, only organic-acid and organic-base solvents were reported for this type of cononsolvency in literature [105], such as cellulose acetate in aniline/acetic acid mixtures [106], poly(ϵ -caprolactone) in pyridine/formic acid or pyridine/acetic acid mixtures [107], and poly(methyl methacrylate) in pyridine/formic acid mixtures [107]. A detailed analysis for these real cases can be found in [section 3.4.2](#).

A second type of cononsolvency transition originates from the preferential/competitive adsorption between the better solvent and the polymers, a phenomenon recently discussed theoretically by Mukherji et al [35, 108]. This case corresponds to a solution ($D < 0$) of $\chi_{pc} < 0$, $\chi_{pc} < \chi_{ps}$ and $\chi_{pc} < \chi_{cs}$ with a constraint of $\chi_{cs} < 0.5$ and $\chi_{ps} < 0.5$ for the spinodal decomposition (Eq.(3.3)) for good solvent mixtures. The concept of preferential adsorption further assumes that the better solvent forms temporal bridges between monomers. A signature of this type of cononsolvency transition is that in the segregated phase of the polymer, the cosolvent is enriched in a coacervate phase [28, 40, 43-46]. Here, the common solvent is depleted only. As a realization of the preferential-adsorption concept in a recently published adsorption-attraction model [23, 24, 39], the preferential adsorption of polymer-cosolvent attraction was considered to be the sole driving force for the cononsolvency transition, while the effects of interactions between polymer and the solvent, and cosolvent-solvent were omitted. This allows for an analytic solution of the cononsolvency problem in cases of polymer brushes and solutions and explains the essential effect of the cononsolvency transition as a type-II phase transition [23, 24]. Nevertheless, it is worth noting that this model is still too simple to describe cononsolvency behaviors in real polymer systems accurately. In my previous study, see [Chapter 2](#), by a thermodynamic analysis we pointed out that an increasing demixing tendency between alcohol and water is correlated with an enhancement of the cononsolvency transition of PNiPAAm. In addition, both experiments [44, 79, 109, 110] and computer simulations [111] indicated that cosolvent-solvent interaction plays a significant role for the cononsolvency behavior of PNiPAAm.

The solution of $D < 0$ for the spinodal decomposition (Eq.(3.3)) also implies that the origin of the cononsolvency transition of the same polymer can be based on different transition mechanisms if the polymer is dissolved in different solvent mixtures. It should be noted that this behavior has been observed for a real polymer, namely, poly(methyl methacrylate) in pyridine/formic acid mixtures [107]. This is an example in which cononsolvency originates from a strong attraction between two solvents, while in chlorobutane/amyl acetate mixtures the cononsolvency transition originates from a preferential adsorption of chlorobutane on the polymer chains of poly(methyl methacrylate) [31].

In the above discussion, the Flory-Huggins mean-field model categorizes current knowledge of cononsolvency transition into two sub-types. However, this discussion is still a black-box analysis

and loses insight on the detail of microstructure of phase transition. In this chapter, to simplify our discussion, I focus on the cononsolvency transition originating from preferential adsorption between the better solvent and polymers. We extend the original adsorption-attraction model and discuss in depth the signatures behind the cononsolvency transition of polymers. The application of the theoretical model to polymer brushes and macrogels will be described first in [section 3.2](#). Then the model will be numerically solved and the physical meaning of the model parameters will be explained in [section 3.3](#). At last, the model will be applied to fit the experimental data and its validity is discussed in [section 3.4](#).

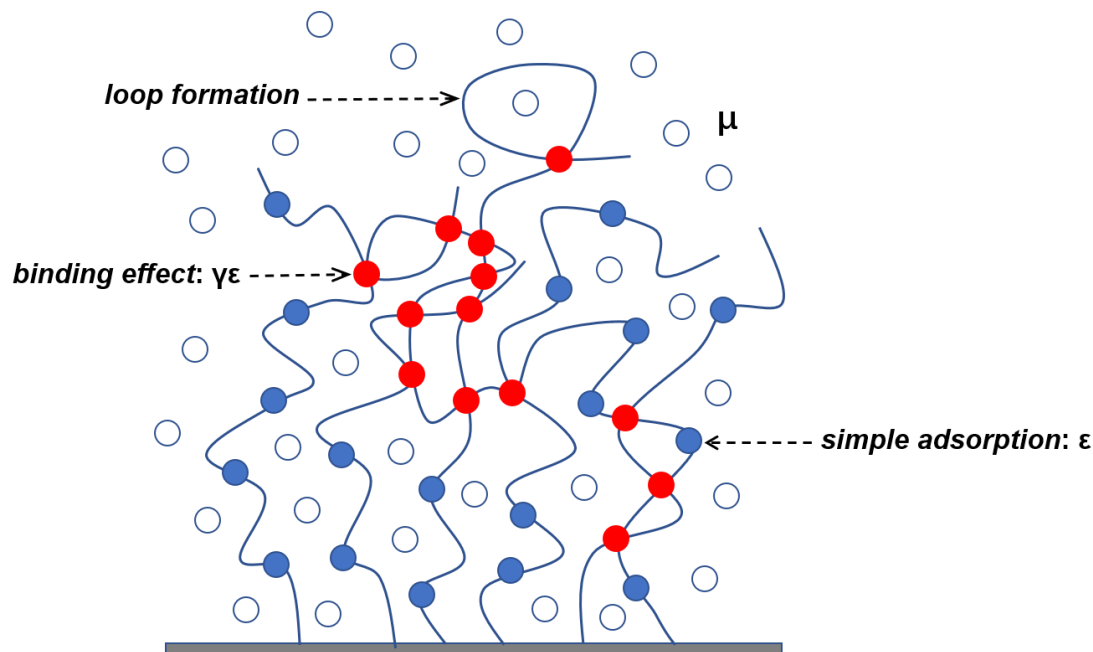
3.2 An extension of the adsorption-attraction model

In this section, we extend the adsorption-attraction model [\[23\]](#) which has already been briefly described in [section 2.3](#) of [Chapter 2](#). To have a better and deeper understanding of this model, if it is necessary some expressions will be rewritten and new interpretations will be given.

Preferential adsorption of the cosolvent onto polymer chains leads to an adsorption layer of cosolvent around polymers [\[39, 84, 112\]](#). We denote the probability that a monomer contacts with a molecule of the cosolvent by φ , which is the volume fraction of the cosolvent in the adsorption layer around the polymer. Obviously, that fraction also depends on the average volume fraction of the monomers c , which is approximated in the framework of mean-field or scaling models such as the Alexander-de Gennes approach [\[11\]](#) for brushes, and the Flory-Rehner approach [\[113\]](#) for polymer networks. The central assumption of this model is that cosolvent molecules can be shared by two or more monomers, which due to attractive interactions, decreases the free energy of the total system, regardless whether these monomers belong to the same chain or to different chains, see [scheme 3.1](#). Within the mean-field approximation this has been written in terms of a free energy per monomer unit as [Eq.\(2.4\)](#), here we rewrite it as:

$$f_{attr} = -2\gamma\varepsilon\varphi(1-\varphi)c, \quad (3.4)$$

where ε denotes the preferential-adsorption energy of one cosolvent molecule with respect to the polymer. Here and in the following we consider energies in units of $k_B T$ if not otherwise noted. Parameter γ represents the bridging efficiency of the molecular matching between monomer and cosolvent, it is noted that this interpretation for parameter γ is different from the original adsorption-attraction model [\[23\]](#), see [section 2.3](#) of [Chapter 2](#). For convenience but without losing generality, in this study γ can be treated as a constant with a value of $\gamma=1$ for PNIPAAm/alcohol/water system. Direct evidences supporting this central assumption from molecular-dynamic simulations [\[35, 97, 108\]](#) showed that a single chain can form loops due to preferential attraction between polymer and cosolvent. In addition, experimental evidences supporting this central assumption come from a Raman-spectroscopic study which investigated cononsolvency behaviors of linear poly(N-isopropylacrylamide) polymers in methanol-water mixtures, in which methanol molecules aggregate into clusters and behave like temporal bridges between polymer segments [\[114\]](#).



Scheme 3.1(Figure 24) An illustration of the concept of preferential adsorption of cosolvent on the polymer chains and cosolvent-assisted binding effect. Note that loop formation can also happen in the polymer brushes [97] when the grafting density is not high.

An implicit and necessary prerequisite behind the concept of a cosolvent-assisted temporary cross-linking effect in **Eq.(3.4)** is that the attraction strength between the cosolvent and polymer is stronger than alternate polymer-solvent interaction and cosolvent-solvent interaction, expressed by the excess energy $\varepsilon > 0$. This requirement is in line with the observation [115] that the Flory parameter between poly(vinylpyrrolidone) and short-chain alcohols is negative and the polymer exhibiting cononsolvency in alcohol water mixtures, in which case alcohol is the cosolvent and water is the solvent [64, 65]. In general, the excess energy (ε) depends both on temperature and monomer concentration. However, if the cononsolvency effect is dominated by the simple adsorption between cosolvent and monomer, as is the case when the cosolvent consists of alcohol molecules, ε can be treated as a constant. For example [116-119], the Flory parameter between polyethylene glycol and short-chain alcohols depends only marginally on the monomer concentration, and this dependence can be neglected when the alcohol chain length is longer than one carbon chain length. Here it is worth pointing out that a very crucial effect of parameter γ in **Eq.(3.4)** can be in systems where the cosolvent binds more specifically to the monomers, i.e. a binding/adsorption with a second monomer becomes unlikely ($\gamma \ll 1$), which leads to that the temporary-crosslinking energy, $\gamma\varepsilon$, is insufficient to reach a threshold [39] (in the order of about $1.0 k_B T$) that results in a phase transition. A candidate for such scenario can be poly(N,N-diethylacrylamide) in methanol-water and ethanol-water mixtures [45, 120]; when the threshold is overcome, phase transition happens, a case of this situation can be poly(N,N-diethylacrylamide) in propanol-water mixtures [45].

For a complete description of a particular system, the equation of state of the cosolvent including the adsorption on the polymer has to be considered. For the real case the cosolvent-solvent mixture is not ideal and neither is the solvent athermal with respect to the polymer. One aspect of varying

the size of the cosolvent is to change its mixing entropy along the polymer chains. We denote the ratio between the volume of a cosolvent molecule and a solvent molecule by λ like in **Eq.(2.5)**. For convenience we assume the molecular size of cosolvent being larger than or equalling to the molecular size of solvent, so that $\lambda \geq 1$, which is the common situation. This gives rise to an adsorption free energy per monomer according to the lattice model approximation **[23, 24]**:

$$f_{ads} = \frac{\varphi}{\lambda} \ln(\varphi) + (1-\varphi) \ln(1-\varphi) - \mu\varphi - \varepsilon \frac{\varphi}{\lambda}, \quad (3.5)$$

where μ represents the chemical potential change of the cosolvent when mixing with the solvent. In the preferential/competitive-adsorption process, the φ volume fraction of the solvent is replaced by the volume fraction of the cosolvent. On account of a desorption of the solvent from the polymer chain, the energy change (gain or loss) is $-\mu\varphi$ per monomer unit; and $-\varepsilon\varphi/\lambda$ is the energy loss due to adsorption of the cosolvent on the polymer chain per monomer unit. Note that the last term in **Eq.(3.5)** is different from **Eq.(2.5)**, see **section 2.3** of **Chapter 2**.

Another aspect is that an increasing demixing tendency between cosolvent and solvent is correlated with an enhancement of the collapse transition of the polymer, see **Chapter 2**. A convenient way to account for this effect on the polymer chains is to introduce a Flory-interaction-like term of the form:

$$f_{cs} = \chi_{cs} \varphi (1-\varphi), \quad (3.6)$$

where χ_{cs} denotes an effective Flory-parameter for the cosolvent-solvent interaction, i.e. a non-ideal cosolvent-solvent mixing interaction in the adsorbed layer. It is particularly noteworthy that the origin of the effective cosolvent-solvent interaction (χ_{cs}) can contain both excess enthalpic and excess entropic contributions, see **Chapter 2**. Reference values for the range of χ_{cs} of realistic systems can be estimated by semi-empirical models which are based on a broad range of experimental data; for further details about estimates of χ_{cs} we refer the reader to the **section 3.6.3**.

We use the following entropic free energy for a brush:

$$f_{brush} = t \frac{\sigma_d^2}{c^2} + \left(\frac{1}{c} - 1 - \nu\varphi \right) \ln(1 - c - \nu\varphi c), \quad (3.7)$$

where σ_d is the dimensionless grafting density of the polymer brush, the physical meaning of σ_d is the area fraction of flat substrate surface covered by the brush layer when polymer chains are stretched to sawtooth-shape-like conformations, thus there exists a constraint of $0 < \sigma_d \leq 1$, also see **Eq.(1.6)** in **section 1.2** of **Chapter 1**. The numerical prefactor t is of the order of one which accounts for the relation between the effective elastic energy of the chains in the brush and a chain simply stretched by fixing its ends. This corresponds to the mean-field Alexander-de Gennes approach **[11]**. The relation of $\sigma_d = \sigma A_m$ holds when grafting density σ , in the given units of *chains/nm²*, where A_m is the cross-sectional area of a monomer or Kuhn segment typically in the order of $\pi(0.3nm)^2$ **[73]**. The excess volume fraction in case of a full saturation of the polymer by cosolvent is given by ν . The

physical meaning of ν is that it describes the excluded-volume difference between the same monomer and the two good solvents. Note that the first term of Eq.(3.7) is a little bit different from Eq.(2.6), see section 2.3 of Chapter 2.

We use the following entropic free energy contribution for a macrogel network:

$$f_{gel} = \frac{3}{2} \frac{\alpha}{N_k c^{\frac{2}{3}}} + \left(\frac{1}{c} - 1 - \nu \varphi \right) \ln(1 - c - \nu \varphi c), \quad (3.8)$$

where N_k is the average number of Kuhn segments between two crosslinks in the network structure, α is the fraction of elastically effective chains in the network and can be considered as a material parameter characterizing the network structure and chemistry. The first term of Eq.(3.8) arises in the Flory-Rehner approach [113] for a network. For a phantom network model [9], we have:

$$\alpha = \frac{f-2}{f}, \quad N_m = N_k \left(\frac{f-2}{f} \right) x, \quad (3.9)$$

where N_m is the total number of Kuhn segments in the gel structure, f is the effect linking degree (functionality) for one crosslinker (or junction), and x is the number of chemical crosslinkers in the gel. For real polymer chains, on account of network defects such as loops and dangling ends, the effective linking degree for the chemical crosslinker seldom reaches the chemical functionality of the crosslinker [121].

We note that the solvent-cosolvent mixture within the brush/network is assumed to be in the same state as in the bulk phase and polymers are considered as substrate for binding cosolvent with short range interactions. This is very different to the model proposed by Opfermann et al. [19, 20] where the polymer phase is assumed as a homogeneous mixture of solvent, cosolvent and polymer. It can be shown that in the latter case a high negative Flory-interaction parameter between the cosolvent and the homogeneous polymer phase has to be assumed in order to quantitatively describe the brush collapse and corresponding simulation results [19, 20]. The difference between the two models has been thoroughly discussed in ref.[23]. Coming back to my formalism this means that the cosolvent-solvent interactions are mapped in the corresponding chemical potential, μ , on the one hand side, and onto the interaction parameter, χ_{cs} , in the adsorbed cosolvent phase, see Eq.(3.6).

It is now straightforward to introduce non-ideal mixing between the polymer and the solvents. Generally, in the preferential/competitive-adsorption process, the fraction of monomers with adsorbed cosolvent is given by φ and we call them “occupied”, then the rest fraction of monomers $1-\varphi$, which has adsorbed common solvent we call “bare”. The contribution of the non-ideal polymer-solvent-mixing for the free energy per monomer unit is given by

$$f_{int} = \left[\Delta \chi_{cs} \varphi + \chi_{ps} (1-\varphi) \right] \left[1 - g(\varphi) \right] (1 - c - \nu \varphi c). \quad (3.10.1)$$

Here, the expression $(1-c-\nu\varphi c)$ denotes the probability that a given monomer is not in contact with another monomer unit. Under this condition, $g(\varphi)$ (cosolvent volume fraction in the gel or brush layer) gives the probability that this monomer is in contact with cosolvent, and complementary, $1-g(\varphi)$, this monomer is in contact with a common solvent. We repeat that mean-field assumptions are consequently applied in this thesis. The first term in **Eq.(3.10.1)** denotes the excess interaction between an occupied monomer and the free common solvent molecules. We note that within the adsorption layer the interaction between cosolvent and common solvent is already taken into account in **Eq.(3.6)**. My numerical solution indicates that $\Delta\chi_{cs} \ll \chi_{cs}$ and this contribution can be in fact neglected in the experimental systems we discuss in this work. Eventually, χ_{ps} denotes the interaction when a bare monomer is exposed to the free common solvent molecules. This term represents the residual interaction of the polymer chain and the common solvent and thus represents the thermal solvent effect of the polymer.

For a real polymer system, the boundary condition $\rho \leq g(\varphi) \leq \varphi$ holds, where ρ is the volume fraction of cosolvent in the bulk outside the polymer phase. For a dilute polymer phase, such as polymer chains sparsely grafted on a surface as well as free polymer chains, the approximation $g(\varphi) \approx \rho$ is adequate, but this approximation is not valid for strongly confined polymer phases such as densely-grafted polymer brushes or highly-crosslinked polymer gels. An experimental observation [46] in the framework of a ^1H MAS NMR-spectroscopic study, which investigated the phase separation of poly (N-isopropylacrylamide) micro-gel in alcohol-water binary mixtures, revealed that the alcohol concentration in the confined solution is significantly higher than that in the free bulk solution. Moreover, alcohols of long carbon-chains are more significantly concentrated in the confined solution. In the current study we found that a simple mean-field approximation of $g(\varphi) \approx \rho$ was adequate to describe the cononsolvency transitions of sparsely grafted poly (N-isopropylacrylamide) brushes and sparsely-crosslinked macro-gels in alcohol aqueous binary mixtures. Effectively, we arrive at

$$f_{int} \approx \chi_{ps} (1-\varphi)(1-\rho)(1-c-\nu\varphi c). \quad (3.10.2)$$

Finally, the total free energy per monomer is approximated as follows for polymer brushes/ macrogels,

$$f(\varphi, c) = f_{attr} + f_{ads} + f_{cs} + f_{brush/gel} + f_{int}. \quad (3.11)$$

3.3 Numerical solution of the extended adsorption-attraction model

To obtain the equilibrium state, a minimization of the free energy $f(\varphi, c)$ with respect to the order parameter of the adsorption, φ , and the polymer concentration, c , has to be performed. We note that because of the non-linear coupling between cosolvent and monomers, **Eq.(3.4)**, **Eq.(3.7)**, **Eq.(3.8)** and **Eq.(3.10.2)** there exists no analytic solution for the general case. Minimization with respect to φ and c yields numerical solutions for the dimensionless brush thickness ratio $H/H_0 = c_0/c$, and di-

dimensionless macro-gel volume ratio $V/V_0 = c_0/c$ with respect to the chemical potential change of mixing of the cosolvent with the solvent, μ . We note that a minimization with respect to φ only leads to a free energy in an effective solvent that can be expressed as a concentration-dependent Flory-Huggins parameter [23, 24] $\chi(c)$.

In this section, we numerically solve the extended adsorption-attraction model, and the effects of each parameter on the shape of the cononsolvency-transition curve of polymer brushes are graphically presented in from **Figure 3.1a** to **Figure 3.1f**. To keep these figures as simple as possible, apart from the variation of the corresponding parameter as shown in each sub-figure, all other model parameters remained fixed as listed in **Table 3.1**. Several aspects are immediately visible from the numerical solutions:

First, it is particularly noteworthy that even though each parameter can influence the phase behaviour in a certain way in the extended adsorption-attraction model, due to a monomer-cosolvent-monomer triple contact (cosolvent-assisted temporary cross-linking effect), the dominant parameter is the free-energy loss (parameter $-\gamma\epsilon$), see **Eq.(3.4)**. If this effect is not counted (by setting $\gamma = 0$), the re-entrant property of cononsolvency transition is lost and thus cannot be numerically produced by the extended adsorption-attraction model. As we already pointed out in **section 3.2**, this viewpoint is critical to explain why poly(N,N-diethylacrylamide) does not show cononsolvency in methanol-water and ethanol-water mixtures [45, 120] while in propanol-water mixtures [45] occurs phase transition.

Second, as shown in **Figure 3.1a**, the size difference between cosolvent and solvent (upon variation of parameter λ while keeping the remaining parameters constant) can shift the collapse transition of polymers into the cosolvent-rich region.

Third, as shown in **Figure 3.1b**, the excluded-volume difference between the same polymer and two good solvents (parameter ν) plays an important role in regularizing the shape of the re-entrant transition curve. An asymmetric shape of the re-entrant transition curve has been observed in all currently available experimental observations, this is reflected first of all by a value $\nu > 0$.

Fourth, as shown in **Figure 3.1c**, the demixing tendency between cosolvent and solvent (parameter $\chi_{cs} > 0$) on the polymer chains plays a role in controlling the width of the cononsolvency transition.

Fifth, as shown in **Figure 3.1d**, the non-ideal mixing between polymer and solvent (parameter $\chi_{ps} > 0$) plays a role in shifting the collapse transition toward the lower-concentration region of cosolvent which is already verified by my previous study, see **Chapter 2**.

Sixth, as shown in **Figure 3.1e**, the polymer-cosolvent preferential adsorption (parameter ϵ) plays a dominant role for the strength of the collapse-transition for low concentrations of cosolvent (typically in the order of 10% volume fraction).

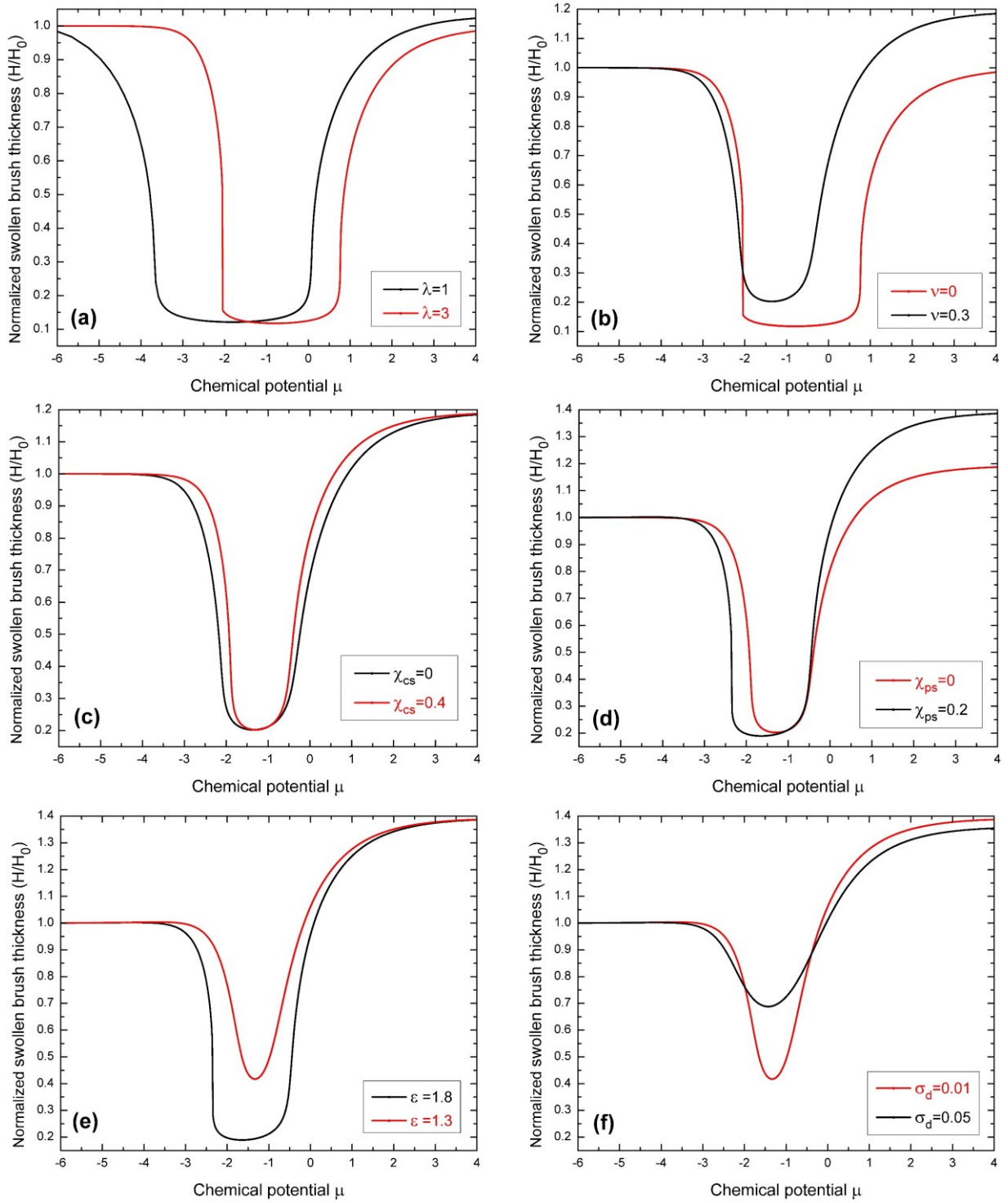


Figure 3.1(Figure 25) Illustration of the impact of the various model parameters on the predicted cononsolvency response of a polymer brush. The scaled brush thickness (H/H_0) is displayed as a function of chemical potential change of the cosolvent, μ : (a) for $\lambda = 1$ and $\lambda = 3$, (b) for $\nu = 0$ and $\nu = 0.3$, (c) for $\chi_{cs} = 0$ and $\chi_{cs} = 0.4$, (d) for $\chi_{ps} = 0$ and $\chi_{ps} = 0.2$, (e) for $\varepsilon = 1.3$ and $\varepsilon = 1.8$, (f) for $\sigma_d = 0.01$ and $\sigma_d = 0.05$. Note that apart from the variation of the corresponding parameter as shown in each sub-figure, all other model parameters remained fixed as listed in Table 3.1.

Table 3.1(Table 4) Parameter values used in numerically solving the extended adsorption attraction model from Figure 3.1(a) to Figure 3.1(f).

Figure number	σ_d	λ	ε	γ	t	ν	χ_{cs}	χ_{ps}
Figure 3.1a	0.01	change	1.8	1.0	1.0	0	0	0
Figure 3.1b	0.01	3	1.8	1.0	1.0	change	0	0
Figure 3.1c	0.01	3	1.8	1.0	1.0	0.3	change	0
Figure 3.1d	0.01	3	1.8	1.0	1.0	0.3	0.4	change
Figure 3.1e	0.01	3	change	1.0	1.0	0.3	0.4	0.2
Figure 3.1f	change	3	1.3	1.0	1.0	0.3	0.4	0.2

Finally, as shown in **Figure 3.1f**, when comparing **Eq.(3.7)** and **Eq.(3.8)**, we note that an increase of the grafting density of polymer brushes (parameters σ_d or σ) or an increase of the crosslink density of gels (parameter α/N_k) have the same effect in the cononsolvency transition, namely, the phase transition is weakened, but both grafting density and crosslink density have only a very small effect on the solvent composition at the minimum of the re-entrant curve, i.e. location of the maximum collapsed state. These facts have been reported in previous studies of PNiPAAm brushes (see **Chapter 2**), macrogels [103] and microgels [122]. We refer the reader to the **section 3.6.4** for additional details of data which are extracted and reprocessed from **refs.[103, 122]** for gels.

We conclude that each of the model parameters has qualitatively different impact on the cosolvent response of polymer brushes and gels. Moreover, the model parameters have clear physical meanings such as the size of cosolvent molecules, grafting density and miscibility of the solvents, which are independent of the model. This will be a crucial point of my comparison with experimental data.

3.4 Validation of the extended adsorption-attraction model

The chemical potential change, μ , plays a critical role in the preferential-adsorption model to determine the cononsolvency behaviours of polymers. To my best knowledge, previous studies have used the dilute solution model [35, 108] and the (pseudo) lattice gas model [23, 24, 39, 122] to estimate the chemical potential change. Although these chemical-potential models are sufficiently accurate to describe the general phase transition behaviors of the cononsolvency effect, on account of lacking a reasonable consideration of solvent-solvent interaction in these models, they may be still crude and insufficient to arrive at a detailed and comprehensive understanding of the roles of various interactions in the cononsolvency transition of polymers. For mixtures of different non-ionic components, to my best knowledge, the Margules model, Extended Van Laar model, Orye model, Wilson model and the Enthalpic Wilson model are good choices to estimate the chemical potential change upon mixing, the performance of these models was already investigated by **refs.[123, 124]**. For alcohol-water mixtures, the Enthalpic Wilson model [124] offers reasonable estimates of the chemical potential for each component, and has accurately (and rather successfully when compared to alternate models) reproduced the phase-separation behaviors of 1-butanol/water mixtures. Thus, in the present study we apply the Enthalpic Wilson model to compute chemical

potential changes; for additional details about this method, we refer the reader to the [sections 3.6.1-3.6.3](#).

The same as in [section 2.6](#) of [Chapter 2](#), in this chapter, we used the software package MATLAB with its unconstrained multivariable function to compute numerical solutions and least-square-fits to experimental data. For the numerical fit-procedure, some parameters of the extended adsorption-attraction model such as λ and ν remain fixed at their experimentally known values, this approach is a necessary requirement of the proposed extended adsorption-attraction model; while t is treated as a constant with a value of $t = 1/2$ since it showed little tendency to deviate in the fit procedure. We note that a variation of the value of t would also indicate a deviation from the Alexander-de Gennes model [\[11\]](#) which we assume here for simplicity. The parameters ε , f , χ_{cs} and χ_{ps} are treated as free parameters and are fitted in their physical ranges that have physical meanings. Then fitted values of these parameters ε , f , χ_{cs} and χ_{ps} are compared with known experimental facts to check the self-consistency of the extended adsorption-attraction model. Subsequently, the roles of polymer-solvent interactions and cosolvent-solvent interactions in the process of cononsolvency transition are discussed based on these fitted parameters.

3.4.1 Cononsolvency transition of polymer brushes and macro-gels in different alcohol-water mixtures

In [Figure 3.2](#) we display theoretical fits to experimental data of one and the same PNiPAAm brush in various alcohol-water mixtures, where the temperature is fixed at 25°C (Experimental data have already been reported in my previous study, see [Chapter 2](#)), [Table 3.2](#) shows the corresponding parameter values obtained in the numerical fit procedures. In [Figure 3.3](#) we display theoretical fits to the experimental data of one and the same PNiPAAm macrogel sample in various alcohol-water mixtures, where the temperature is fixed at 22°C, in [Figure 3.4](#) we display theoretical fits to the experimental data of one and the same PNiPAAm macrogel sample in various 1-propanol/water and DMSO/water mixtures, where the temperature is fixed at 25°C (Experimental data are extracted and reprocessed from [refs.\[40-42\]](#)). [Table 3.3](#) and [Table 3.4](#) show the corresponding parameter values obtained in the numerical fit procedures.

The resulting curves match the experimental data reasonably well. Most importantly from the results given in from [Table 3.2](#), [Table 3.3](#) and [Table 3.4](#), we imply that the parameter values are in line with the physical properties of PNiPAAm-alcohol-water tertiary mixtures: The strength of the preferential-adsorption energy ε between alcohol and polymer increases with the carbon-backbone length of the alcohol. This enhancement effect has been reported in the context of the attraction interactions between alcohol and other hydrophilic polymers such as poly(vinylpyrrolidone) [\[115\]](#), which as well exhibits the cononsolvency effect [\[64, 65\]](#). As for the same solvent mixtures, the current approach of the extended adsorption-attraction model requires that that parameters λ , ε and $\lambda\chi_{cs}$ are independent of polymer material architectures. This is verified for the cononsolvency transition of a PNiPAAm macro-gel and a brush in alcohol/water mixtures, see [Table 3.2](#), [Table 3.3](#) and [Table 3.4](#).

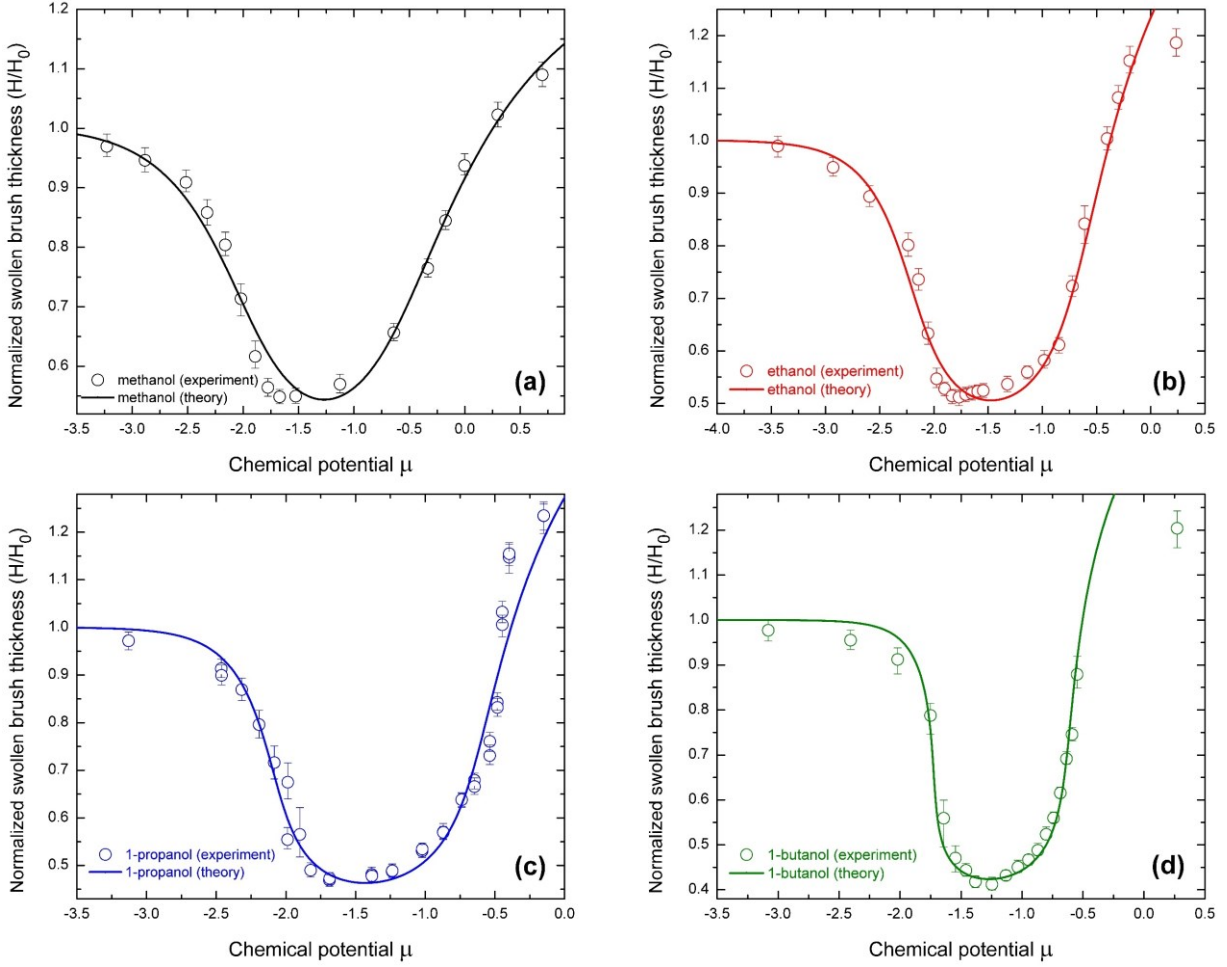


Figure 3.2(Figure 26) Cononsolvency transition of a single PNiPAAm brush sample in different alcohol aqueous solutions, at a temperature of 25°C: open circles are experimental results and solid lines are theoretical fits using the extended adsorption-attraction model. Parameters of the PNiPAAm brush are: grafting density $\sigma = 0.143 \text{ chains/nm}^2$, $M_n = 6.1 \times 10^4 \text{ g/mol}$, $M_w/M_n = 1.40$. The experimental data have already been reported in my previous study, see [Chapter 2](#).

Table 3.2(Table 5) Fit parameters for alcohol-water systems (polymer brush, $\sigma = 0.143 \text{ chains/nm}^2$, 25°C, Figure 3.2). We choose λ and ν from their experimental values. The first part of the value for $\lambda\chi_{cs}$ is estimated as its experimental value, the second part of the value for $\lambda\chi_{cs}$ is a correction to fit the experimental data. Experimental value of PNiPAAm-water interaction (χ_{ps}) is around 0.40.

Alcohol	λ	ϵ	ν	$\lambda\chi_{cs}$	χ_{ps}
methanol	2.2554	1.17	0.15	0.5609+0.35	0.25
ethanol	3.2587	1.25	0.20	1.2443+0.50	0.43
1-propanol	4.1443	1.32	0.23	2.5175+0.35	0.43
1-butanol	5.1004	1.45	0.27	3.8659+1.75	0.41

Previous studies pointed out that the origin of cononsolvency of PNiPAAm in alcohol-water mixtures could not be related to attractive alcohol-water interactions (see [Chapter 2](#)), and that the NH amide proton of PNiPAAm was as well unimportant in the polymer's cononsolvency transition

[81]. Thus, both experimental observations and theoretical analysis strongly imply that the origin of cononsolvency in this system has to be a hydrophobically driven adsorption of the alcohol molecules on the PNiPAAm polymer chains. This indication is particularly obvious for the cononsolvency transition of PNiPAAm brushes in 1-butanol/water mixtures. Actually, 1-butanol is not miscible with water at intermediate compositions at room temperature, thus only limited data of PNiPAAm brush thickness is available for these mixtures (see Chapter 2). Even though, in the very narrow water-rich regime (a volume fraction of 1-butanol is less than 10%), the PNiPAAm brushes can show a full landscape of cononsolvency transition, this peculiar phase-transition behavior can mainly be attributed to a hydrophobically driven adsorption of the 1-butanol molecules on the PNiPAAm polymer chains. It is particular worth noting that experiments of isomer effect of propanol and butanol in the cononsolvency transition of PNiPAAm brushes, further demonstrated this finding, see section 2.7 of Chapter 2.

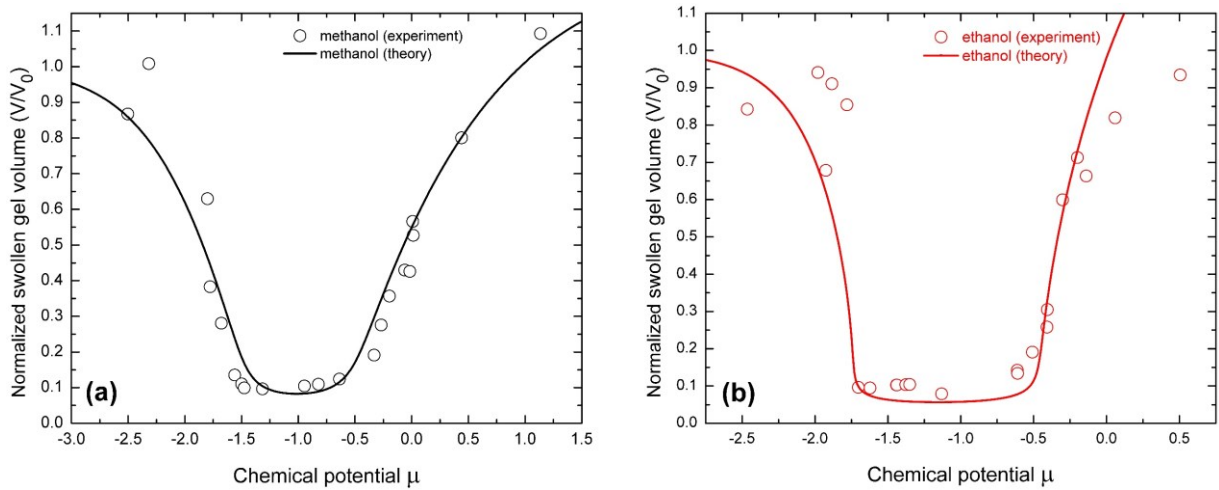


Figure 3.3(Figure 27) Cononsolvency transition of a single PNiPAAm macrogel sample in different alcohol aqueous solutions, at a temperature of 22 °C: open circles are experimental results and solid lines are theoretical fits using the extended adsorption-attraction model. Parameters of the PNiPAAm macrogel are: the total number of Kuhn segments in the gel structure is $N_m = 33.14 \text{ mmol}$, and the number of chemical crosslinkers is $x = 0.86 \text{ mmol}$. The maximum possible degree of linking for the chemical crosslinker is 4. The length of a Kuhn segment for gels in this study is chosen to be about four repeating units of PNiPAAm. Data are extracted and reprocessed from refs.[41, 42].

Table 3.3(Table 6) Fit parameters for alcohol-water systems (polymer macro-gel, 22°C, Figure 3.3). We choose λ and ν from their experimental values. The first part of the value for $\lambda\chi_{cs}$ is estimated as its experimental value, the second part of the value for $\lambda\chi_{cs}$ is a correction to fit the experimental data. Experimental value of PNiPAAm-water interaction (χ_{ps}) is around 0.40. The maximum possible degree of linking for the chemical crosslinker is 4, this condition requires the parameter value of $2 < f < 4$.

Alcohol	λ	f	ϵ	ν	$\lambda\chi_{cs}$	χ_{ps}
methanol	2.2517	2.30	1.17	0.08	0.5405+0.00	0.16
ethanol	3.2525	2.30	1.25	0.12	1.2557+0.00	0.30

In **Figure 3.5** we display theoretical fits to the experimental results of PNiPAAm brushes with different grafting densities in ethanol-water mixtures, while temperature is fixed at 25°C (Experimental data have already been reported in my previous study, see **Chapter 2**), **Table 3.5** shows the corresponding parameter values obtained in the numerical fit procedures. The fits match the experimental data reasonably well, and from **Table 3.5**, we infer that the resulting parameter values are in line with the physical properties of the PNiPAAm/ethanol/water tertiary mixtures. It is remarkable that the theoretical fits of the extended adsorption-attraction model show that with an increase of monomer concentration in the common solvent (in the case of polymer brushes: increase of grafting density), the interaction strength between water and monomers increases. A similar phenomenon has already been reported for a PNiPAAm micro-gel [103]. We note that this phenomenon can be related to the LCST transition of PNiPAAm which can be understood as a concentration-dependent χ -parameter [22, 76]. Thus, a higher grafting density can lead to an effective larger Flory parameter, χ_{ps} .

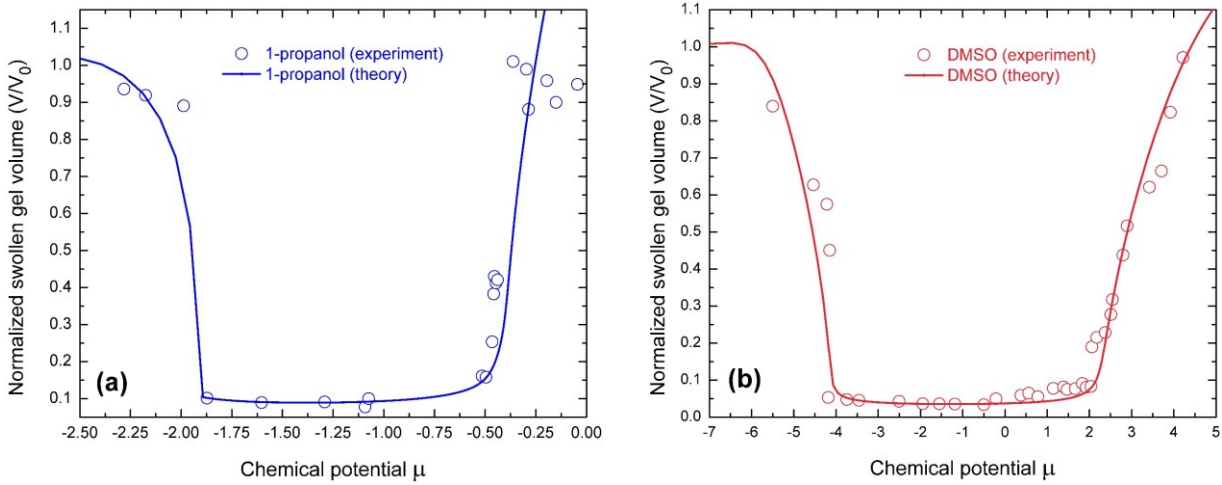


Figure 3.4(Figure 28) Cononsolvency transition of a single PNiPAAm macrogel sample in different alcohol aqueous solutions, at a temperature of 25 °C: open circles are experimental results and solid lines are theoretical fits using the extended adsorption-attraction model. Parameters of the PNiPAAm macrogel are: the total number of Kuhn segments in the gel structure is $N_m = 150 \text{ mmol}$, and the number of chemical crosslinkers is $x = 1.5 \text{ mmol}$. The maximum possible degree of linking for the chemical crosslinker is 4. The length of a Kuhn segment for gels in this study is chosen to be about four repeating units of PNiPAAm. Data are extracted and reprocessed from **ref. [40]**.

Table 3.4(Table 7) Fit parameters for 1-propanol/water and DMSO/water systems (polymer macro-gel, 25°C, Figure 3.4). We choose λ and ν from their experimental values. The first part of the value for $\lambda\chi_{cs}$ is estimated as its experimental value, the second part of the value for $\lambda\chi_{cs}$ is a correction to fit the experimental data. Experimental value of PNiPAAm-water interaction (χ_{ps}) is around 0.40. The maximum possible degree of linking for the chemical crosslinker is 4, this condition requires the parameter value of $2 < f < 4$.

Organic	λ	f	ϵ	ν	$\lambda\chi_{cs}$	χ_{ps}
1-propanol	4.1443	2.25	1.32	0.13	2.5175+0.00	0.43
DMSO	3.9357	2.25	1.70	0.06	-2.9443 -10	0.15

As noted already above, among the fit parameters of **Table 3.2** to **Table 3.5**, we fixed geometrical parameters λ and ν according to their experimental values. As shown from **Figure 3.2** to **Figure 3.5**, this resulted in a quite good fit performance of the model. The fit performance showed that the mean-field model can quantitatively describe cononsolvency transition of PNiPAAm brush and gel in various organic solvent/water mixtures. In particular, it is worth noting that the fit results in **Table 3.2** for the interaction parameter between water and PNiPAAm polymer (χ_{ps}) are nearly constant as it should be expected since only the cosolvent is changing. However, as shown in from **Table 3.2** to **Table 3.4**, for methanol and DMSO, a smaller value of χ_{ps} is required for an optimal fit of the experimental data. The reason for this somewhat specific behavior of methanol and DMSO with respect to the physical model is not clear. Even though, a candidate for the interpretation of this tendency of χ_{ps} is the disruption of a hydrogen bonding network between water molecules by the organic-solvent molecules: Organic-solvent molecules can be hydrated by water molecules to form hydrated clusters [125-128]. On account of much stronger enthalpic attraction between DMSO and water, between methanol and water (see **section 3.4.2** and **Figure 3.7**), the tendencies of forming clusters of hydrated DMSO and hydrated methanol become stronger. Thus, in DMSO/water and methanol/water mixtures, the ability to disrupt the hydrogen bonding network between water molecules significantly increases. This effect leads to a significant increase of translational entropy of water molecules, and the mixing entropy between polymer and water is increased, which improves the water molecule's solvent quality for the PNiPAAm polymer in the DMSO/water and methanol/water mixtures.

Among the data of from **Table 3.2** to **Table 3.5**, we note that the numerical fit values of $\lambda\chi_{cs}$ deviate from their experimental values, and this deviation is particularly obvious in the 1-butanol/water interaction and DMSO/water interaction. For 1-butanol/water interaction, this deviation may be attributed to the model which is used to estimate the experimental value. In the present study, the experimental value of $\lambda\chi_{cs}$ is estimated from the Enthalpic Wilson model for solutions of alcohol-water mixtures. However, it is reasonably expected that alcohol-water interaction on the polymer chains differ from their behaviors in solution. For more details regarding how we estimate the reference value of $\lambda\chi_{cs}$ in this study, we refer the reader to the **section 3.6.3**.

Table 3.5(Table 8) Fit parameters for the ethanol-water system (polymer brush, 25°C, Figure 3.5). We choose λ and ν from their experimental values. The first part of the value for $\lambda\chi_{cs}$ is estimated as its experimental value, the second part of the value for $\lambda\chi_{cs}$ is a correction to fit the experimental data. Experimental value of PNiPAAm-water interaction (χ_{ps}) is around 0.40.

Grafting density	λ	ϵ	ν	$\lambda\chi_{cs}$	χ_{ps}
0.143 chains/nm ²	3.2587	1.25	0.20	1.2443+0.50	0.43
0.103 chains/nm ²	3.2587	1.24	0.20	1.2443-0.25	0.35

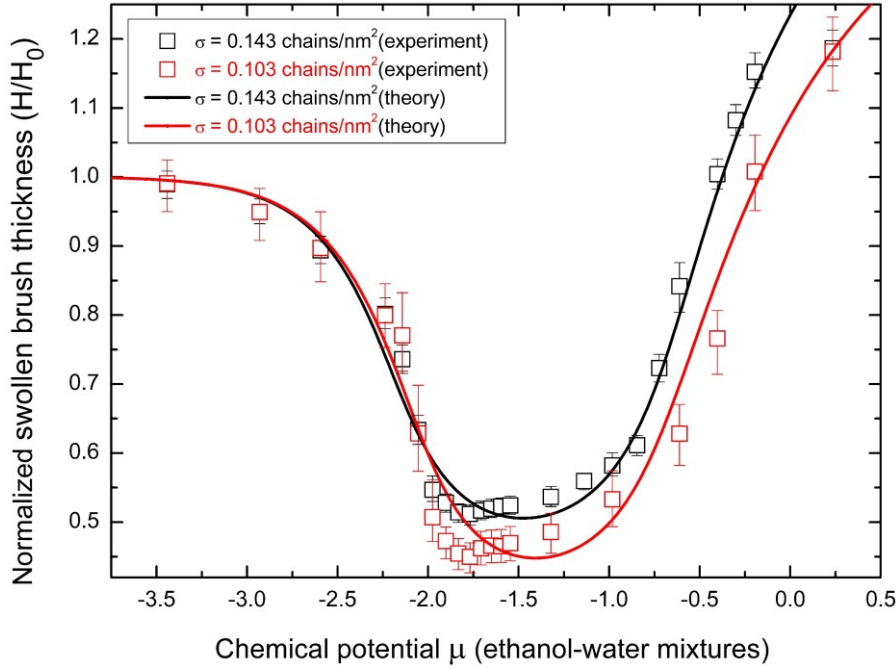


Figure 3.5(Figure 29) Grafting-density effect in the cononsolvency transition of PNiPAAm brushes in ethanol-water mixtures, at a temperature of 25°C: open squares are experimental results and solid lines are theoretical fits of the extended adsorption-attraction model. Parameters of the PNiPAAm brushes plotted in Figure 4 from top to bottom are: grafting density $\sigma = 0.143 \text{ chains/nm}^2$, $\sigma = 0.103 \text{ chains/nm}^2$. Both brushes contain polymers of identical molecular weight distributions: $M_n = 6.1 \times 10^4 \text{ g/mol}$, $M_w/M_n = 1.40$. The experimental data have been reported in my previous study, see [Chapter 2](#).

As for DMSO/water interaction, the deviation of $\lambda\chi_{cs}$ is too large and shall be mainly attributed to that the simplified model (Eq.(3.10.2)) neglects the effect of $\Delta\chi_{cs}$ which is defined in Eq.(3.10.1). It is worth pointing out that after including the effect of $\Delta\chi_{cs}$, all fitting parameter values become reasonable and are in physical ranges. Even though, the current approach of Eq.(3.10.1) still cannot quantitatively fit experimental data for cononsolvency transition of PNiPAAm macro-gels in DMSO/water mixtures. It is noted that the attraction strength between DMSO and water is not weak (see [section 3.4.2](#) and [Figure 3.7a](#)) and comparable to the preferential-adsorption strength between DMSO and PNiPAAm (see [Table 3.4](#)). It seems that DMSO-water attraction plays an important role in the cononsolvency transition of PNiPAAm. Nevertheless, the attraction between DMSO and water cannot be the dominant force to drive the phase transition of PNiPAAm polymer in DMSO-water mixtures, since attraction between DMSO and water cannot explain sol-gel behaviors [\[56\]](#) in the cononsolvency transition of hydrophilic polymers in the case of polymer solutions when the concentration of DMSO is very low. The cononsolvency of PNiPAAm in DMSO-water mixtures can be in principle explained based on the assumption of preferential adsorption of DMSO on the polymer chain and temporary crosslinking effect between monomers and DMSO molecules, nevertheless, we are aware that there also exist alternative approaches involving a different physical mechanism not known so far [\[44\]](#). We also note that the same issue arises when considering the effect of polyethylene glycol aqueous solutions on the cononsolvency transition of PNiPAAm gels [\[33\]](#). A

further study is in particular needed such as to check the role of binding effects of cosolvent-solvent clusters in the phase transition instead of a simple binding between cosolvent molecules and monomers; however, these topics are beyond the scope of this thesis.

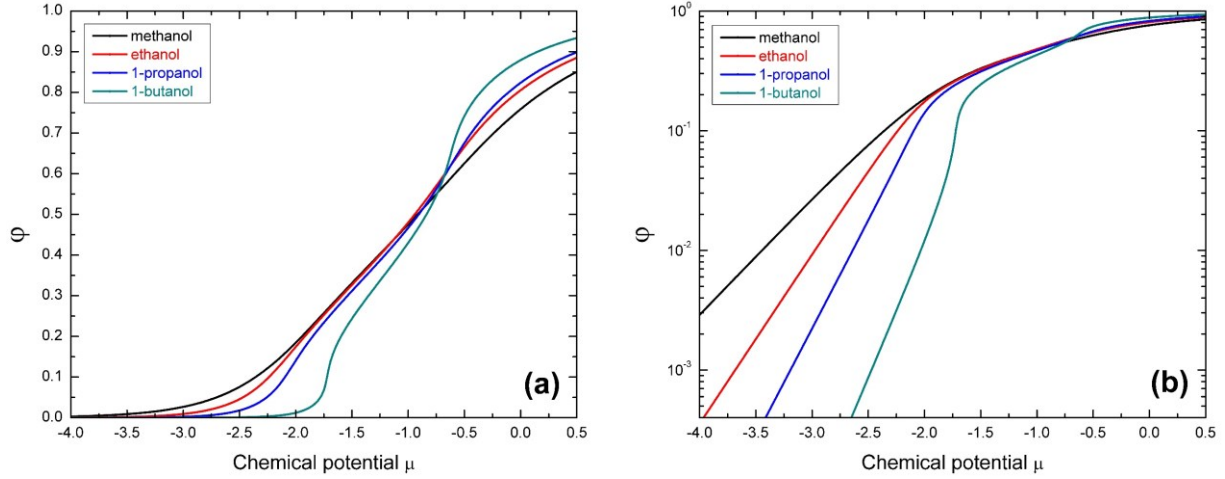


Figure 3.6(Figure 30) Cononsolvency transition of a PNiPAAm brush sample in different alcohol aqueous solutions, at the temperature of 25°C: ϕ as a function of the chemical potential is calculated by using the extended adsorption-attraction model to fit the experimental results shown in Figure 3.2. Figure 3.6a is a linear schematic dependence of ϕ on μ and Figure 3.6b is a schematic dependence of $\log_{10}(\phi)$ on μ . Parameters of the PNiPAAm brush are: grafting density $\sigma = 0.143 \text{ chains/nm}^2$, $M_n = 6.1 \times 10^4 \text{ g/mol}$, $M_w/M_n = 1.40$.

In **Figure 3.6**, the adsorption order parameter (the volume fraction of cosolvent, ϕ , adsorbed on the polymer chain) in the cononsolvency transition is evaluated. The evaluation is based on the numerical fit results of **Figure 3.2**. In **Figure 3.6**, an obvious discontinuous phase-transition behavior is observed for the cononsolvency transition of PNiPAAm in 1-butanol/water mixtures, while this behavior is not obvious in case of the other alcohol/water mixtures. These experimental observations are fully compatible with the predictions of a previous computer simulation study [39].

3.4.2 An analysis of the enthalpic interaction between cosolvent and solvent

In this section, we develop a mean-field approximation to estimate attraction strength between cosolvent and solvent based on enthalpy change of mixing these two solvents. This estimation is particularly helpful to determine the phase-transition mechanism of cononsolvency transition of PNiPAAm in DMSO-water mixtures. The peculiar cononsolvency-transition behavior of PNiPAAm in DMSO-water mixtures maybe originate from that the attraction strength between DMSO and water is comparable to the preferential-adsorption strength between DMSO and PNiPAAm, see **Figure 3.4**, **Figure 3.7a** and **Table 3.4**.

In short-chain alcohol and DMSO aqueous solutions, the interaction between alcohol and water molecules is dominated by alcohol-water hydrogen-bond formation [129, 130]. The total number of molecules in organic solvent-water binary mixtures is denoted as n , the molar fraction of organic

solvent is denoted by x , the volume ratio between one organic-solvent molecule and one water molecule is denoted by λ .

When an organic-solvent molecule's oxygen atom forms a bond with a water molecule's hydrogen atom, the corresponding probability is $\frac{1-x}{\lambda x+1-x}$ (volume fraction of water). There are nx organic-solvent molecules in the mixtures, therefore the maximum number of this kind of hydrogen bonds that can be formed is $nx \left(\frac{1-x}{\lambda x+1-x} \right) z_{co} + n(1-x) \left(\frac{\lambda x}{\lambda x+1-x} \right) \frac{z_{sh}}{2}$, where z_{co} is the number of oxygen atoms in one organic-solvent molecule that can form hydrogen bonds, z_{sh} is the number of hydrogen atoms in one water molecule that can form hydrogen bonds.

The corresponding probability for a water molecule's oxygen atom to form a hydrogen bond is $\frac{\lambda x}{\lambda x+1-x}$ (volume fraction of organic solvent). There are $n(1-x)$ water molecules in the mixtures, thus the maximum number of this kind of hydrogen bonds that can be formed is $n(1-x) \left(\frac{\lambda x}{\lambda x+1-x} \right) z_{so} + nx \left(\frac{1-x}{\lambda x+1-x} \right) \frac{z_{ch}}{2}$, where z_{so} is the number of oxygen atoms in one water molecule that can form hydrogen bonds, z_{ch} is the number of hydrogen atoms in one organic-solvent molecule that can form hydrogen bonds.

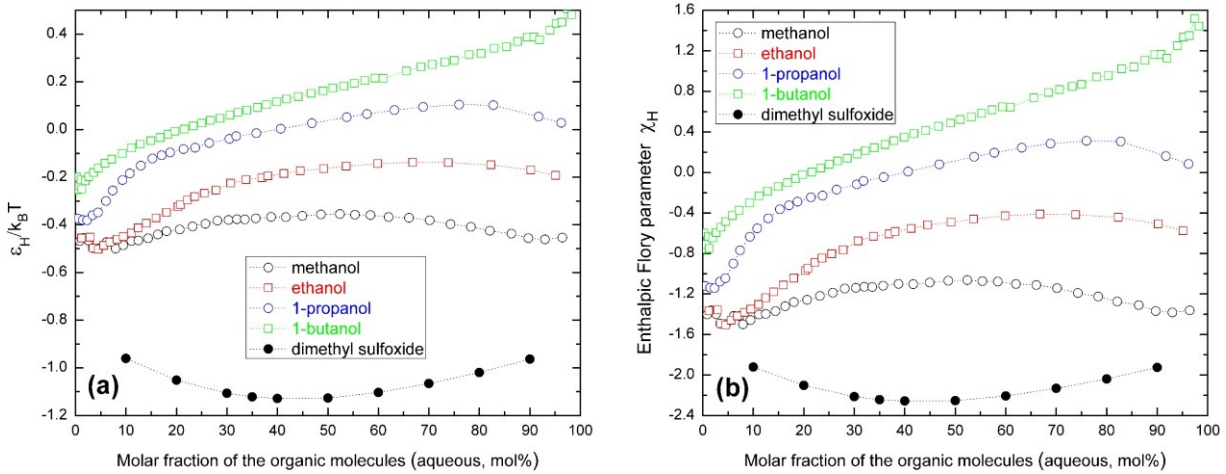


Figure 3.7(Figure 31) (a) Average energy change ε_H of the formation of one organic solvent-water hydrogen bond when mixing different organic solvents with water at the temperature of 25°C. (b) Enthalpic Flory parameter χ_H when mixing different organic solvents with water at the temperature of 25°C. Data are extracted and reprocessed from [refs.\[129, 130\]](#). Note that the dotted lines in the figures are only used to guide the eye.

Then the maximum number of hydrogen bonds that can be formed via contacts between organic solvent and water molecules is $n \left(z_{co} + \frac{\lambda z_{sh}}{2} + \lambda z_{so} + \frac{z_{ch}}{2} \right) \frac{x(1-x)}{\lambda x+1-x}$. Note that from a thermodynamics point of view, as long as isotope effects are neglected, these two kinds of hydrogen bonds formed by organic solvent/water interaction nearly don't have any difference. The molar enthalpy change

in the mixing is denoted as $\Delta_{mix}H_m$ and the average energy change of formation of one organic solvent/water hydrogen bond is denoted as ε_H . In the short-chain alcohol and DMSO aqueous solutions, the enthalpy changes of mixing of alcohol and water, DMSO and water are controlled by hydrogen-bonding formation between organic solvent and water molecules via sacrifice of hydrogen bonds from organic solvent-organic solvent and water-water interactions [129, 130], which yields a mean-field approximation:

$$\Delta_{mix}H_m \approx N_A \varepsilon_H \left(z_{co} + \frac{\lambda z_{sh}}{2} + \lambda z_{so} + \frac{z_{ch}}{2} \right) \frac{x(1-x)}{\lambda x + 1 - x}, \quad (3.12)$$

where N_A is the Avogadro constant. This implies

$$\varepsilon_H \approx \frac{2\Delta_{mix}H_m}{N_A (2z_{co} + 2\lambda z_{so} + \lambda z_{sh} + z_{ch})} \frac{\lambda x + 1 - x}{x(1-x)}. \quad (3.13)$$

Now we obtain the enthalpic Flory interaction parameter between organic solvent and water due to hydrogen bond formation, χ_H :

$$\chi_H \approx \frac{(2z_{co} + z_{ch}) \varepsilon_H}{k_B T}. \quad (3.14)$$

where k_B is the Boltzmann constant. $2z_{co} + z_{ch}$ is the maximum number of hydrogen bonds each organic solvent molecule can generate. Note that χ_H is different from the effective Flory-parameter between the two solvents $\chi_{cs, eff}$ of Eq.(2.9) and χ_{cs} of Eq.(3.6), which also include excess entropic contributions.

Note that for water, $z_{so} = 1$ and $z_{sh} = 2$; for methanol, ethanol, 1-propanol and 1-butanol molecules, $z_{co} = 1$ and $z_{ch} = 1$; for DMSO, $z_{co} = 1$ and $z_{ch} = 0$, data for $\Delta_{mix}H_m$ are extracted from refs.[129, 130]. Based on Eq. (3.13) and Eq. (3.14), the corresponding ε_H and χ_H as a function of the molar fraction of organic solvent are plotted in Figure 3.7, respectively. It is clearly shown that in Figure 3.7, at any fixed concentration of organic solvent, two simple order relations exist for ε_H and χ_H : “ $\varepsilon_H(\text{DMSO}, \text{H}_2\text{O}) < \varepsilon_H(\text{methanol}, \text{H}_2\text{O}) \leq \varepsilon_H(\text{ethanol}, \text{H}_2\text{O}) < \varepsilon_H(1\text{-propanol}, \text{H}_2\text{O}) < \varepsilon_H(1\text{-butanol}, \text{H}_2\text{O})$ ”, “ $\chi_H(\text{DMSO}, \text{H}_2\text{O}) < \chi_H(\text{methanol}, \text{H}_2\text{O}) \leq \chi_H(\text{ethanol}, \text{H}_2\text{O}) < \chi_H(1\text{-propanol}, \text{H}_2\text{O}) < \chi_H(1\text{-butanol}, \text{H}_2\text{O})$ ”. This is in accordance with the simple picture that longer carbon chain lengths of the alcohol increase its hydrophobic behavior. Figure 3.7 clearly shows that the attraction strength between organic solvent and water follows a simple order relation of “DMSO > methanol > ethanol > 1-propanol > 1-butanol”.

It has been reported that a strong cosolvent-solvent attraction can induce a cosolvency transition of poly(ϵ -caprolactone) in pyridine/formic acid or pyridine/acetic acid mixtures [107], and poly(methyl methacrylate) in pyridine/formic acid mixtures [107]. The strong attraction between pyridine and formic acid or acetic acid arises from the formation of a very strong “acid-base” type of hydrogen bonds.

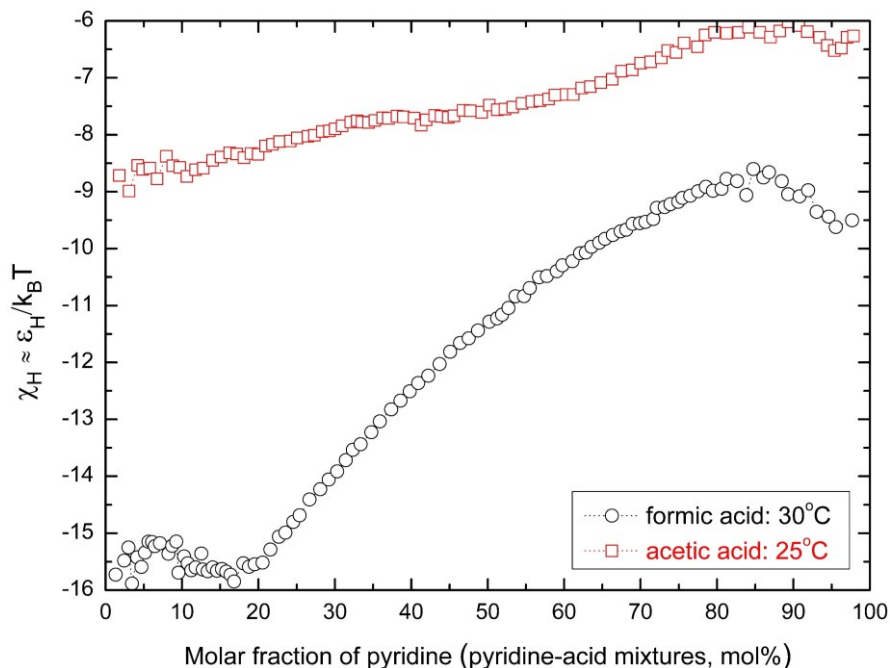


Figure 3.8(Figure 32) Average energy change ε_H of the formation of one pyridine-acid hydrogen bond, and enthalpic Flory parameter χ_H when mixing pyridine with different organic acids at the corresponding temperatures. Note that data are extracted and reprocessed from [ref. \[107\]](#).

Keep in mind that a pyridine molecule and a formic/acetic acid molecule can only generate one hydrogen bond of the “acid-base” type, respectively. By using the same method as discussed above, as shown in **Figure 3.8**, we quantify this strong attraction between the cosolvent and the solvent based on the concept of enthalpic Flory interaction parameter χ_H . Comparing the results in **Figure 3.7** and **Figure 3.8**, the differences are quite remarkable.

3.4.3 The window width of the cononsolvency transition

The window width of the cononsolvency transition, L , is defined as the molar-fraction gap of cosolvent concentration in which both the collapse and re-entry branches reach a predefined height. As sketched in **Figure 3.9a**, we follow Mukherji’s definition [\[131\]](#), in which the height is chosen as the half value between the minimum and the pure-water point on the cononsolvency-transition curve (the height is volume related).

Figure 3.9b presents the window width (L) for the cononsolvency transition of PNiPAAm polymer as a function of the experimental value of the effective Flory parameter ($\lambda\chi_{es}$) between cosolvent and water. For details behind the precise definition of the effective Flory parameter we refer the reader to the [section 3.6.3](#). In **Figure 3.9b**, it is obvious that there exists a monotonic relationship: a reduction of the window width of the cononsolvency transition is correlated with an enhancement of the demixing tendency between cosolvent and water. This monotonic relationship is also observed for the cononsolvency transition of a PNiPAAm brush in aqueous solutions of propanol and butanol isomers, see [section 2.7](#) of [Chapter 2](#). It is particularly noteworthy that this monotonic relationship also exists for other already-known neutral polymers which exhibit cononsolvency such

as poly(vinylpyrrolidone) [64, 65], poly(N, N-dimethylacrylamide) [99] and poly(acryloyl-L-proline methyl ester) [132]. What is more, computer simulations [82] also showed that a weakening of cosolvent-solvent attraction (equal to an increase of demixing tendency between cosolvent and solvent) can reduce the window width of cononsolvency transition. It is also noted that this tendency does not change when we use a definition of weight-related height [133] instead of a volume-related height [131].

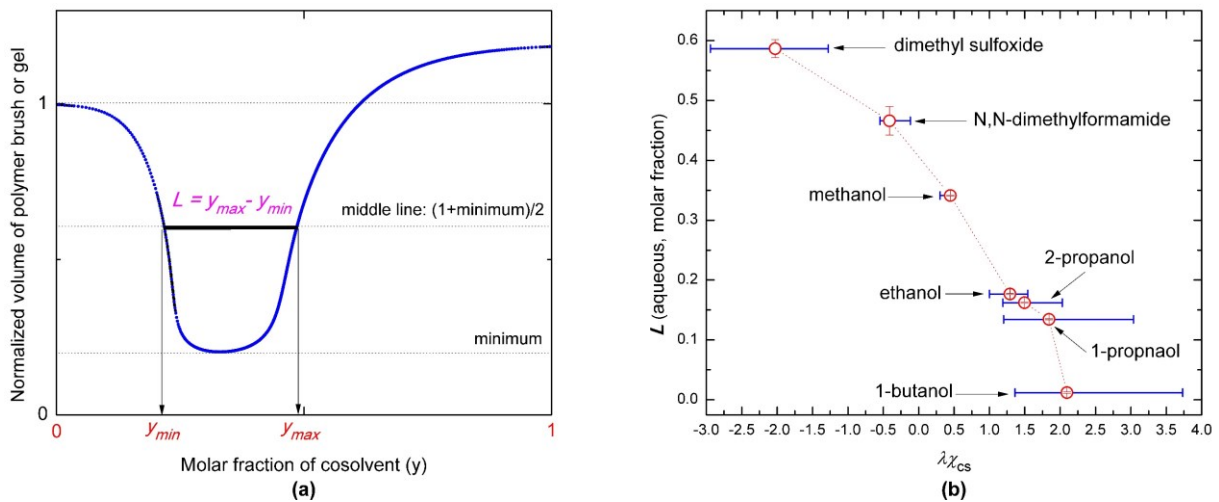


Figure 3.9(Figure 33) The window width (L) of the cononsolvency transition: (a) Sketch of the definition of window width using my theoretical model, see Figure 3.1c (for instance). (b) The width for cononsolvency transition of PNiPAAm polymers as a function of the experimental value of the effective Flory parameter between various cosolvents and water at a temperature close to 25°C. Data of the width are extracted and reprocessed from **Chapter 2** and refs.[40, 80, 122], data of the effective Flory parameter are extracted and reprocessed from refs.[87-89, 130, 134, 135]. Note that in the Figure 3.9a, the solid blue line is a typical cononsolvency-transition curve; in the Figure 3.9b the dotted line is a guide to the eye, and the blue error bars display the experimental uncertainties of the effective Flory parameter.

In **Table 3.2** and **Table 3.4**, the fit results of $\lambda\chi_{cs}$ show that a reduction of the width of the cononsolvency transition is correlated with an increase of the demixing tendency between cosolvent and solvent when the temperature is fixed. This is in agreement with a numerical prediction of the extended adsorption-attraction model: the width of the cononsolvency transition can be reduced by an enhancement of the tendency for demixing between cosolvent and solvent on the polymer chains, see **section 3.2** and **section 3.3**.

3.4.4 Pressure effect in the cononsolvency transition of PNiPAAm polymers

Experimental studies [136, 137] have reported that PNiPAAm mixed in alcohol-poor aqueous solutions shows a suppression of the cononsolvency effect at high hydrostatic pressure. We note that this pressure effect can be explained based on the suppression of the tendency to demix between cosolvent and water, and between polymer and water in the cononsolvency transition of PNiPAAm. During the process of mixing, alcohol molecules form hydrated clusters [125-128] and the excess molar volume of mixing ($\Delta V_{m,cs}$) is negative for short alcohol aqueous solutions [138].

This results in the fact that an increase of hydrostatic pressure favors hydration and thus a suppression of the demixing tendency between alcohol and water, it has been observed experimentally that an increase of pressure leads to a contraction of the immiscible gap of 1-butanol/water mixtures [139]. At very high hydrostatic pressure, the demixing tendency between alcohol and water is substantially suppressed, in the alcohol-poor regime maybe nearly all free alcohol molecules are captivated inside the water clusters through the hydration process. It has also been shown that pressure favors the hydration of polymer chains [140] and the formation of polymer/water hydrogen bonds at the cost of methanol/polymer bonds [136], so that effectively the water's solvent quality is improved for PNiPAAm polymers. This implies that for PNiPAAm at very high hydrostatic pressure in alcohol-poor aqueous solutions, the cosolvency effect is weakened and may be completely suppressed [136, 137].

The effect of the suppression of demixing between cosolvent and water, and between polymer and water in the cosolvency transition of PNiPAAm in alcohol-poor aqueous solutions, can be further rationalized by a synergistic effect of a reduction of the effective alcohol-water interaction on the polymer chains ($\Delta\chi_{cs}$) as well as a reduction of this interaction in bulk solvent mixtures excluding the polymer, as well as a reduction of the polymer-water interaction ($\Delta\chi_{ps}$). The reduction of the alcohol-water interaction in bulk solvent mixtures can be quantified in terms of a reduction of the chemical potential change of mixing ($\Delta\mu$). With an increase of hydrostatic pressure (ΔP), these reductions are approximated through the following relations [141]:

$$\begin{aligned}\Delta\mu &\sim \frac{\Delta P \Delta V_{m,cs}}{RT\rho} < 0 \\ \Delta\chi_{cs} &\sim \frac{\Delta P \Delta V_{m,cs}}{RT\phi(1-\phi)} \frac{1}{c} < 0 \\ \Delta\chi_{ps} &\sim \frac{\Delta P \Delta V_{m,ps}}{RT(1-\phi)(1-\rho)(1-c-\nu\phi c)} \frac{1}{c} < 0\end{aligned}\quad , \quad (3.15)$$

and applied to Eq.(3.5), Eq.(3.6) and Eq.(3.10.2), respectively; the meaning of $\Delta\mu$ is graphically presented in Figure 3.10. Here, $\Delta V_{m,cs}$ is the excess molar volume of mixing the alcohol with water, $\Delta V_{m,ps}$ is the excess molar volume of mixing the polymer with water, R is the gas constant and T is the thermodynamic temperature. It should be noted that $\Delta V_{m,ps}$ is negative when a hydrophilic polymer such as polyethylene glycol [142] is mixed with water. For additional details of estimating the pressure effect on the values of $\Delta\mu$, $\Delta\chi_{cs}$ and $\Delta\chi_{ps}$ in Eq.(3.15), we refer the reader to the sections 3.6.5-3.6.7, respectively.

According to Eq.(3.15), in the alcohol-poor regime, an increase of the hydrostatic pressure leads to a decrease of the Flory parameter for alcohol-water interaction on the polymer chains ($\Delta\chi_{cs}$), a decrease of the Flory parameter for polymer-water interaction ($\Delta\chi_{ps}$), and a reduction of the chemical potential change of mixing ($\Delta\mu$). We thus propose that in the language of the extended adsorption-attraction model, as expressed in Eq.(3.5), Eq.(3.6) and Eq.(3.10.2), these effects jointly weaken the collapse transition of PNiPAAm in the alcohol-poor regime. We find that for long-chain alcohol

aqueous solutions such as 1-propanol/water mixtures, when temperature and ΔP are fixed, $\Delta\chi_{cs}$ can be approximated as a constant, for additional details we refer the reader to the [section 3.6.6](#). Therefore, to qualitatively study the pressure effect in the cononsolvency transition, $\Delta\chi_{cs}$ and $\Delta\chi_{ps}$ in [Eq.\(3.15\)](#) are further simplified to be proportional to ΔP , this means if ΔP and temperature are fixed, $\Delta\chi_{cs}$ and $\Delta\chi_{ps}$ are approximated as constants.

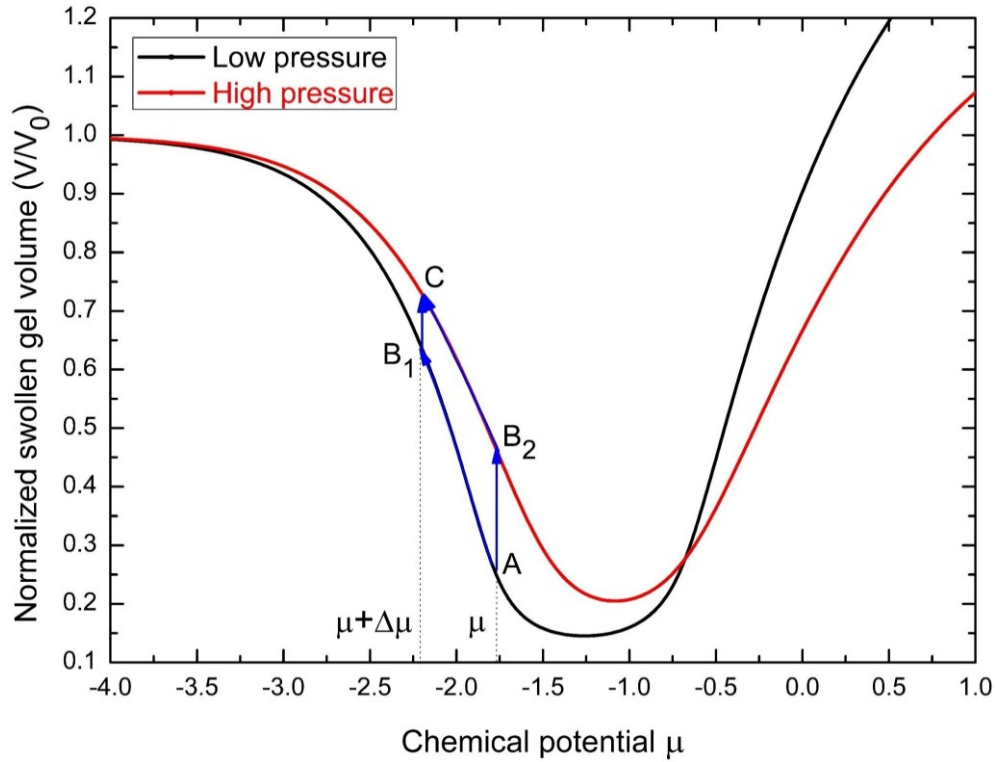


Figure 3.10(Figure 34) The effect of an increase of the hydrostatic pressure in the cononsolvency transition of polymers can be numerically decomposed into a synergistic effect on the effective Flory parameters for the cosolvent-solvent interaction (χ_{cs}), the polymer-solvent interaction (χ_{ps}), and a reduction of the chemical potential change of mixing μ , as implemented in the extended adsorption-attraction model. Note that apart from variations of χ_{cs} and χ_{ps} , the other parameters remained fixed (as shown in Table 3.6). The arrows in Figure 3.10 are eye guides for possible pathways when the cononsolvency system changes from the lower-pressure to the higher-pressure states.

Table 3.6(Table 9) Parameter values applied while numerically solving the extended adsorption-attraction model (Figure 3.10, polymer macrogel, temperature is fixed at 25°C.). As for the conditions of low pressure and high pressure, the parameter values are chosen to be qualitatively consistent with the system of PNIPAAm macrogel/methanol/water at the pressures of 100kPa and 140MPa respectively. For additional details of estimating the pressure effect on the values of $\Delta\chi_{cs}$ and $\Delta\chi_{ps}$, we refer the reader to the [sections 3.6.6](#) and [3.6.7](#).

Pressure	N_k	f	λ	ϵ	ν	$\lambda\chi_{cs}$	χ_{ps}
low pressure	200	2.5	2.2554	1.17	0.15	0.5609	0.25
high pressure	200	2.5	2.2554	1.17	0.15	0.20	0.15

It is noted that $\Delta\mu$ in the approach of **Eq. (3.15)** is independent of the order parameter of the adsorption (φ) and the polymer concentration (c), this allows us to decompose the overall pressure effect into two independent parts: first by a numerical solution of the extended adsorption-attraction model with respect to φ and c , the pressure effect on χ_{cs} and χ_{ps} can be graphically presented by curves such as shown in **Figure 3.10**; secondly the pressure effect on μ can be presented by a horizontal shift ($\Delta\mu$) on the curves. Here it is worth noting that in a numerical solution of the extended adsorption-attraction model, a simultaneous increase or decrease of χ_{cs} and χ_{ps} can result in a competing effect with each other for the collapse transition in the cosolvent-poor regime (as shown in **Figure 3.1c** and **Figure 3.1d**). As for the pressure effect in the alcohol-poor regime, we like to emphasize that for the reductions of alcohol-water interaction on the polymer chains ($\Delta\chi_{cs}$) and polymer-water interaction ($\Delta\chi_{ps}$) that have physical meanings (see **sections 3.6.6** and **3.6.7**), the cumulative effect of a simultaneous reduction of χ_{ps} and chemical potential ($\Delta\mu$, see **section 3.6.5**) exceeds the competing effect of a reduction of χ_{cs} .

Accordingly, by a numerical solution of the extended adsorption-attraction model, a graphical representation of the overall pressure effect in the cononsolvency transition of a polymer macrogel in solvent mixtures is presented in **Figure 3.10**. Note that except for a variation of χ_{cs} and χ_{ps} , all other parameters remained fixed when solving the equations (as shown in **Table 3.6**). In **Figure 3.10**, “A” represents the cononsolvency system at the lower-pressure state, “C” represents the cononsolvency system at the higher-pressure state, “B₁” and “B₂” represent possible intermediate states when the cononsolvency system changes from the lower-pressure to the higher-pressure states. By now it has been clear that if “A” represents the minimum for the collapse state of cononsolvency transition at the lower pressure, due to pressure change, “C” will represent the vicinity of the minimum for the collapse state at the higher pressure, then $\Delta\mu$ represents a shift of cosolvent concentration to a cosolvent-poor region.

The tendency of the transition curves shown in **Figure 3.10** is in line with experimental results of the pressure effect in the cononsolvency transition of PNiPAAm microgel as reported by Hofmann et. al [136]. In addition, this prediction was also verified by the influence of the hydrostatic pressure on the collapse behaviors of PNiPAAm polymers in the organic-solvent-poor regime of dimethyl sulfoxide-water mixtures [143]. It is particularly noted that an experimental study [61] of small-angle neutron scattering recently proved that the hydrophobic effect between PNiPAAm and solvents of methanol-water mixtures, is much weakened above a certain pressure (~150MPa). In previous study, see **Chapter 2**, we have already proved that the origin of cononsolvency transition of PNiPAAm in alcohol-water mixtures is the hydrophobic adsorption of alcohol molecules on the polymer chains, thus, the small-angle neutron scattering study [61] further directly supports my above theoretical analysis.

3.4.5 Cononsolvency transition of a single long polymer

Experimental studies [58, 59] reported that a single long PNiPAAm polymer chain shows strong cononsolvency phase-transition behaviors. To quantitatively explain its phase-transition behaviors in the theoretical scheme of the extended adsorption-attraction model, we use the following entropic free energy contribution for a single chain:

$$f_{\text{single}} = \left[\frac{3\beta^2}{2N_{ks}} - \frac{3\ln(\beta)}{N_{ks}} \right] + \left(\frac{1}{c} - 1 - \nu\varphi \right) \ln(1 - c - \nu\varphi c). \quad (3.16)$$

The first term in Eq.(3.16) is an approximation for the elastic energy of a stretched chain approximated by Flory approach in terms of a free energy per monomer unit, while the second term is the entropic free energy of mixing the polymer with solvents. The expansion factor β is defined by $\beta = R/R_0$, where R is the size of the single polymer chain and $R_0 \approx b_k \sqrt{N_{ks}}$ is its ideal-chain size with b_k being the size of a Kuhn segment and N_{ks} the chain length in unites of the polymer's Kuhn length b_k . Here, the average monomer volume fraction (c) for a single chain is defined as its volume occupation in the single-chain coil, $c = b^3 N/R^3$ with N being the chain length in the unites of the polymer's monomer size b . Since the second term in the first term of Eq.(3.16) is rather small for a long chain, for simplicity by using the leading-order approximation, we get an estimation,

$$f_{\text{single}} \approx \frac{3}{2} \frac{b}{b_k} (cN)^{-\frac{2}{3}} + \left(\frac{1}{c} - 1 - \nu\varphi \right) \ln(1 - c - \nu\varphi c). \quad (3.17)$$

As for a linear PNiPAAm polymer, the value of b_k/b is about 10.

In Figure 3.11, we display theoretical fits to published experimental data of poly(N-isopropylacrylamide) single chain in methanol–water mixtures, where the temperature is fixed at 20°C. Table 3.7 shows the corresponding parameter values obtained in the numerical fit procedures (experimental data are extracted and reprocessed from ref. [58]). The resulting fit curve matches the experimental data reasonably well. Most importantly from the results given in Table 3.7, we imply that the parameter values are in line with the physical properties of PNiPAAm-methanol-water tertiary mixtures. As for the same solvent mixtures, the current approach of the extended adsorption-attraction model requires that parameters λ , ε and $\lambda\chi_{cs}$ are independent of polymer material architectures. After eliminating the temperature effect, this is further verified for the cononsolvency transition of PNiPAAm single long chains, macrogels and brushes in methanol-water mixtures, see Table 3.2, Table 3.3 and Table 3.7.

Table 3.7(Table 10) Fit parameters for methanol-water systems (single polymer chain, 20°C, Figure 3.11). We choose λ and ν from their experimental values. The first part of the value for $\lambda\chi_{cs}$ is estimated as its experimental value, the second part of the value for $\lambda\chi_{cs}$ is a correction to fit the experimental data. Experimental value of PNiPAAm-water interaction (χ_{ps}) is around 0.40.

Alcohol	λ	ε	ν	$\lambda\chi_{cs}$	χ_{ps}
methanol	2.2493	1.17	0.00	0.7818+0.30	0.17

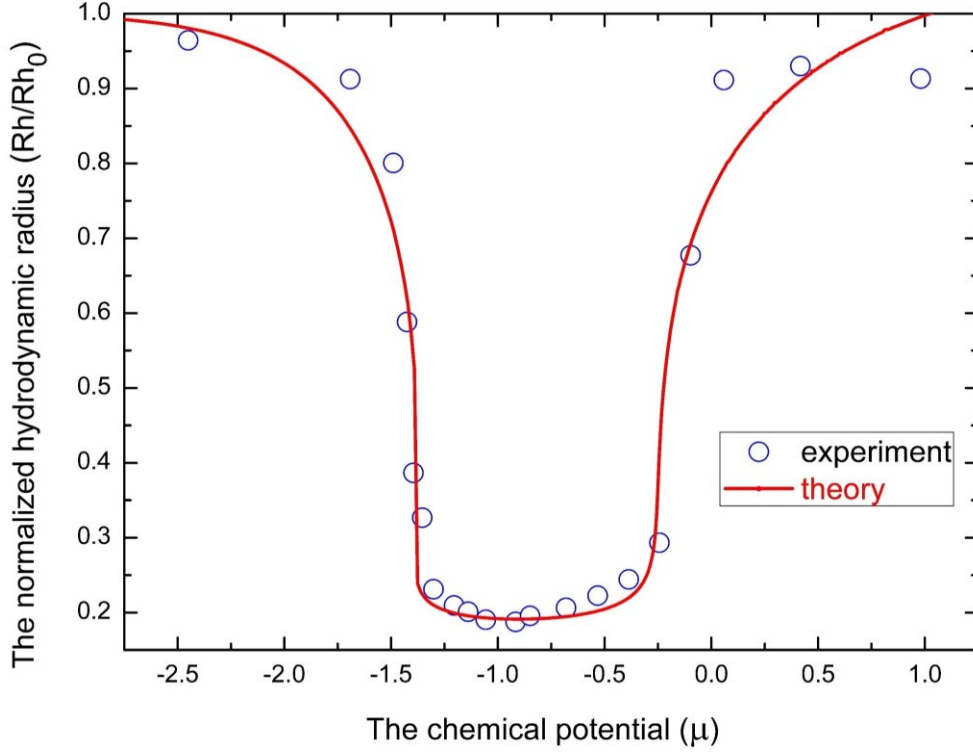


Figure 3.11(Figure 35) Cononsolvency transition of a single PNiPAAm chain in methanol aqueous solutions, at a temperature of 20°C: open circles are experimental results and solid lines are theoretical fits using the physical model. Parameters of the PNiPAAm are: $M_w = 2.63 \times 10^7$ g/mol, $M_w/M_n < 1.10$. The experimental data are extracted and reprocessed from [ref. \[58\]](#). The length of a Kuhn segment for single polymer chain in this study is chosen to be about ten repeating units of PNiPAAm.

Even though, we have to realize that the good performance of the current mean-field approach, also relies on that we choose the hydrodynamic radius rather than the radius of gyration to fit [Eq.\(3.16\)](#). It is important to remember that hydrodynamic radius is much suitable to be used to check a mean-field model for phase transition of a single long chain, this viewpoint has been already clearly pointed out by Sanchez [\[144\]](#) as early as four decades ago. Meanwhile, current mean-field approach does not well describe a short single polymer chain, since the conformation fluctuation is on the order of its coil dimension and monomer-concentration inhomogeneity becomes prominent.

3.5 Chapter summary

Both a theoretical analysis and experimental observations show that the phase-transition mechanism of cononsolvency depends on the relative strengths of various interactions in the polymer solutions. A cononsolvency transition can be driven by a strong cosolvent-solvent attraction or by the preferential adsorption of cosolvent onto the polymer. In this work, by using an extension of the adsorption-attraction model, we report on a comprehensive and quantitative theoretical study of the cononsolvency effect of neutral polymers such as PNiPAAm brushes, macro-gels and single long chains. The extended adsorption-attraction model is able to describe and predict the phase-transition behaviors of PNiPAAm brushes, gels and long single chain in various aqueous alcohol

solutions quantitatively. Besides the dominant roles of polymer-cosolvent preferential adsorption and the monomer-cosolvent-monomer triple contacts (cosolvent-assisted temporary cross-linking effect) that define the strength of the collapse-transition in the cosolvent-poor region, other effects are shown to be of relevance: The non-ideal mixing between polymer and solvent plays a role in shifting the collapse transition to the lower-concentration region of cosolvent, and an increase of the demixing tendency between cosolvent and solvent on the polymer chains reduces the window width of the cononsolvency transition. Using data from the literature we can show that the cononsolvency response of brushes, gels and single long polymer chain can be consistently described with the same model. Thus, also the swelling/deswelling behavior of PNiPAAm gels and single long chains with respect to cononsolvency is quantitatively described in this work. The used parameters are consistent with their microscopic interpretation.

In addition, weakening of the cononsolvency transition in cosolvent-poor aqueous solutions at high hydrostatic pressure can be explained by the suppression of demixing tendencies between cosolvent and water, and between polymer and water in the case of PNiPAAm. We note that the extended adsorption-attraction model can also be applied to other immobilized polymers such as polymeric micro-gels or dendrimers by only replacing the elasticity term in the free energy. Moreover, the concept of the extended adsorption-attraction model can be also re-cast and applied to systems of polymer solutions if polymer-solvent interactions and cosolvent-solvent interaction are considered.

As the phase-transition mechanism in the cononsolvency transition of polymers is still debated, this work contributes to the understanding of the underlying physical mechanism, which could help to develop quantitative models of smart responsive materials by harnessing the cononsolvency effect [145]. My theoretical approach can be refined and extended in several ways. Interesting would be the modification of the cononsolvency behavior by additional components in the solutions which can interfere with the cosolvent adsorption (regulatory solvents [24]), or which influence the thermal mixing behavior of the polymer.

3.6 Chapter appendix

3.6.1 Chemical potential change of mixing two components

The total Gibbs free energy of two species before mixing is $G_{initial}$ [5],

$$G_{initial} = n_1 \mu_1^* + n_2 \mu_2^*, \quad (3.18)$$

where n_1 and n_2 are the molar number of species "1" and "2" respectively, μ_1^* and μ_2^* are the chemical potential (molar Gibbs free energy) of pure species "1" and "2" respectively.

After mixing, in equilibrium, the total Gibbs free energy is G_{final} ,

$$G_{final} = n_1 [\mu_1^* + RT \ln(\gamma_1 x_1)] + n_2 [\mu_2^* + RT \ln(\gamma_2 x_2)], \quad (3.19)$$

where x_1 and x_2 are the molar fraction of species "1" and "2" in the mixture respectively; γ_1 and γ_2 are the activity coefficient of species "1" and "2" in the mixture respectively, they are functions of

temperature, pressure and composition change; R and T are the gas constant and the thermodynamic temperature respectively.

Then the mixing Gibbs free energy of species 1 and 2 is $\Delta_{mix}G$,

$$\Delta_{mix}G = G_{final} - G_{initial} = n_1RT \ln(\gamma_1 x_1) + n_2RT \ln(\gamma_2 x_2). \quad (3.20)$$

We note the following relations:

$$\begin{aligned} n &= n_1 + n_2 \\ x_1 &= \frac{n_1}{n} \\ x_2 &= \frac{n_2}{n} \\ x_1 + x_2 &= 1 \end{aligned} \quad (3.21)$$

where n is a constant. The molar mixing Gibbs free energy of species 1 and 2 is $\Delta_{mix}G_m$,

$$\frac{\Delta_{mix}G_m}{RT} = x_1 \ln(\gamma_1 x_1) + x_2 \ln(\gamma_2 x_2). \quad (3.22)$$

Then the chemical potential change of specie "1" in the mixing process is $\mu_{1,mix}$

$$\begin{aligned} \mu &= \frac{\mu_{1,mix}}{RT} = \frac{1}{RT} \left[\frac{\partial \Delta_{mix}G}{\partial n_1} \right]_{T,P} \\ &= \left[\ln(\gamma_1 x_1) + x_1 \left(\frac{\partial \ln(\gamma_1)}{\partial x_1} \right)_{T,P} \right] - \left[\ln(\gamma_2 x_2) + x_2 \left(\frac{\partial \ln(\gamma_2)}{\partial x_2} \right)_{T,P} \right], \end{aligned} \quad (3.23)$$

where P is the pressure. If we set $\gamma_1 = 1$ and $\gamma_2 = 1$, then the **Eq.(3.23)** reduces to lattice-model formula for the athermal chemical potential change as $\mu = \frac{\mu_{1,mix}}{RT} = \ln\left(\frac{x_1}{1-x_1}\right)$. Note that in **Eq.(3.23)**, μ is the dimensionless chemical potential change which is used in the **Eq.(3.5)** of **section 3.2**.

3.6.2 The Enthalpic Wilson model

For multi-species mixture systems, such as alcohol-water mixing, the Enthalpic Wilson model **[124]** can give quite good estimation of chemical potential for each component. For binary mixtures, the corresponding Enthalpic Wilson equations for the activity coefficients are given by:

$$\begin{aligned} \ln(\gamma_1) &= -\frac{x_2 \ln(A_{12}A_{21})}{(x_1 + A_{12}x_2)(x_2 + A_{21}x_1)} \times \left\{ 1 + x_1 \left(1 - \frac{1}{x_1 + A_{12}x_2} - \frac{A_{21}}{x_2 + A_{21}x_1} \right) \right\} \\ \ln(\gamma_2) &= -\frac{x_1 \ln(A_{21}A_{12})}{(x_2 + A_{21}x_1)(x_1 + A_{12}x_2)} \times \left\{ 1 + x_2 \left(1 - \frac{1}{x_2 + A_{21}x_1} - \frac{A_{12}}{x_1 + A_{12}x_2} \right) \right\} \end{aligned} \quad (3.24)$$

where A_{12} and A_{21} are constants and only dependent on temperature and pressure. The advantage of **Eq.(3.24)** is that A_{12} and A_{21} can be calculated by using experimental values of infinite dilution activity coefficient γ_1^∞ and γ_2^∞ **[88, 146]**. The relations between γ_1^∞ , γ_2^∞ and A_{12} , A_{21} are,

$$\ln(\gamma_1^\infty) = -\frac{\ln(A_{12}A_{21})}{A_{12}}$$

$$\ln(\gamma_2^\infty) = -\frac{\ln(A_{21}A_{12})}{A_{21}} \quad (3.25)$$

In practice, due to lack of reliable experimental values of infinite dilution activity coefficient for water in different mixtures [147, 148], we first need different semi-empirical activity-coefficient models such as PSRK method to accurately estimate the values of γ_1^∞ and γ_2^∞ by using DDB Software Package [149]. These calculated values are compared with their already-known reliable experimental values, then the suitable calculated values are chosen for these species that lack of reliable experimental values. Values of γ_1^∞ , γ_2^∞ , A_{12} and A_{21} for C₁-C₄ alcohol-water system are listed in Table 3.8 and Table 3.9. From Figure 3.12 to Figure 3.14, we show calculation results for molar mixing Gibbs free energy and chemical potential change.

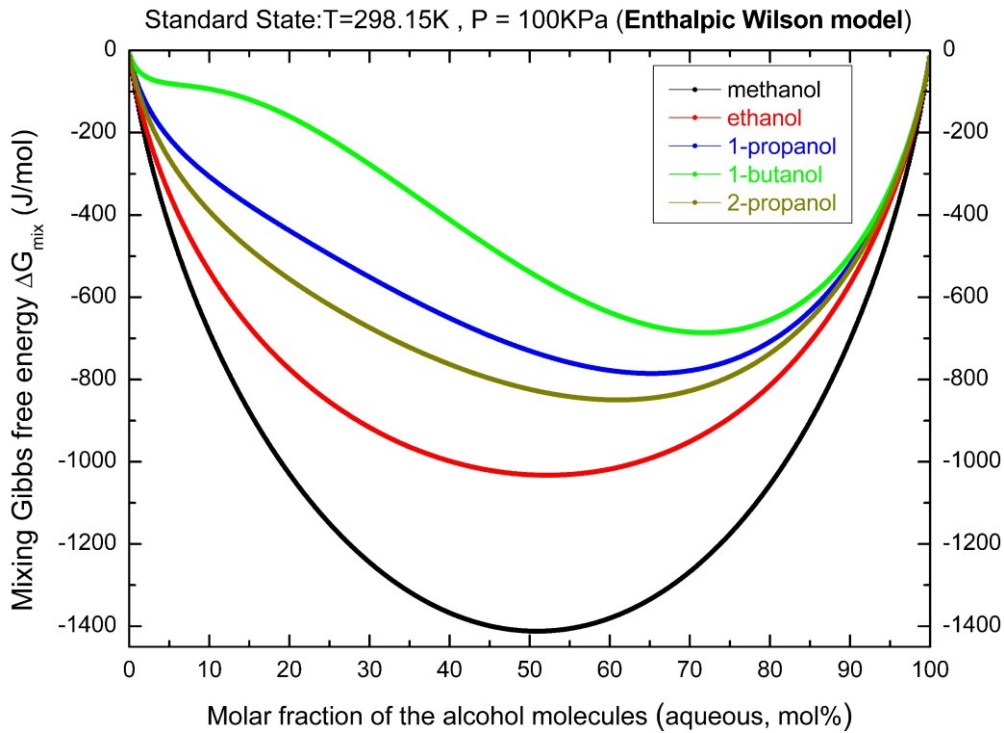


Figure 3.12(Figure 36) Molar Gibbs free energy of mixing for various alcohol/water mixtures at the standard state.

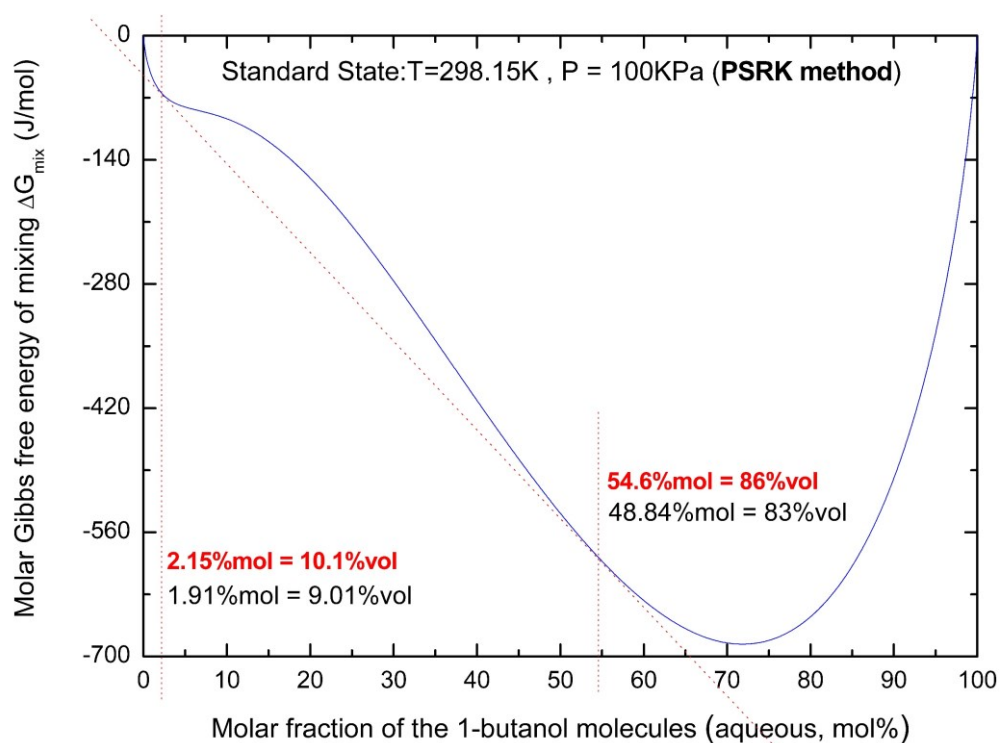


Figure 3.13(Figure 37) Molar Gibbs free energy of mixing for 1-butanol/water mixtures at the standard state: accurate mixture compositions for phase separation are 1.91%mol and 48.84%mol of 1-butanol, while the calculation values for phase separation are about 2.15%mol and 54.6% mol of 1-butanol.

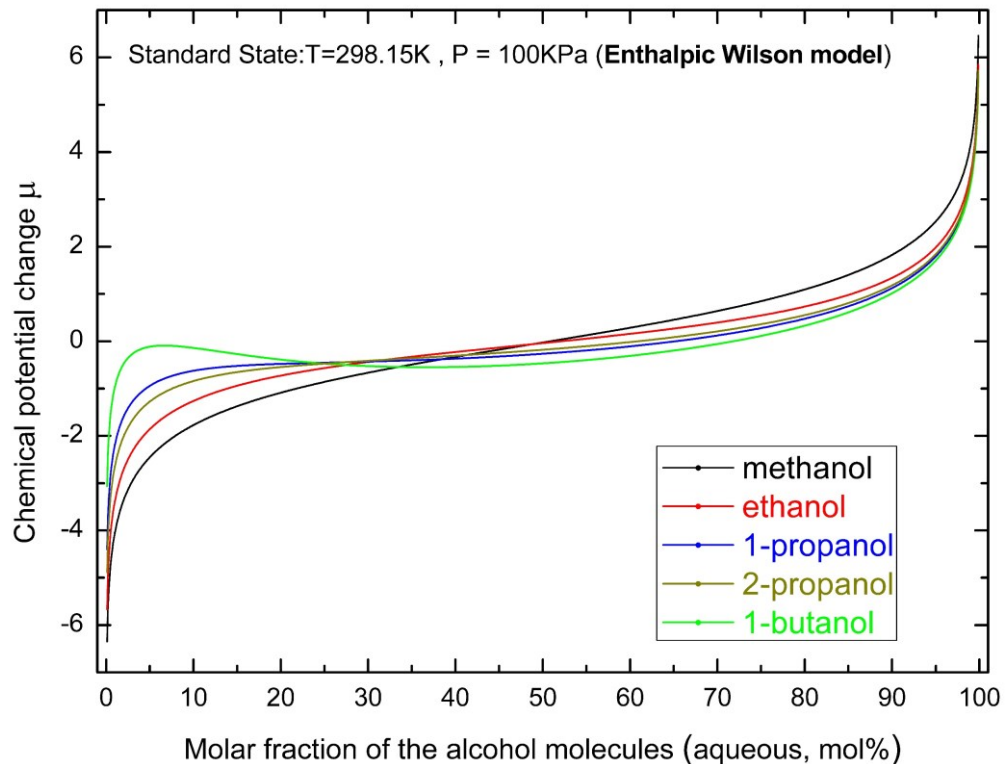


Figure 3.14(Figure 38) Chemical potential change of mixing for various alcohol/water mixtures at the standard state.

Table 3.8(Table 11) Values of γ_1^∞ , γ_2^∞ , A_{12} and A_{21} for different alcohol-water systems at the temperature of 298.15K (25°C).

[illegible]

Table 3.9(Table 12) Values of γ_1^∞ , γ_2^∞ , A_{12} and A_{21} for different alcohol-water systems at the temperature of 295.15K (22°C).

Temperature Air Pressure	295.15K 100KPa	symbol	"1" (alcohol)	"2" (water)																
			Methanol	Water		A_{12}		A_{21}		Calculation Methods	$\lambda_{XS}(\text{Mean})$	$\lambda_{XS}(\text{Maximum})$	$\lambda_{XS}(\text{Minimum})$							
		γ^∞	1.71678	1.54711		0.7364326468270750		0.9120432626254650		VTPR	0.4825	0.5405	0.4364							
			Ethanol	Water		A_{12}		A_{21}												
		γ^∞	3.51015	2.90148		0.6229247651272620		0.7342898618172030		MOSCED2005	1.1276	1.2857	1.0652							

Remarks: Due to lack of corresponding experimental reference values in literature for the condition of 22°C, here we used the method suitable for the condition of 25°C (as shown in **Table 3.8**) to calculate these values for the condition of 22°C. This approach is expected reasonable as the temperature difference between these two situations is marginal. The calculated values in **Table 3.9** and **Table 3.8** are consistent with each other.

3.6.3 Estimation of effective Flory-interaction parameter

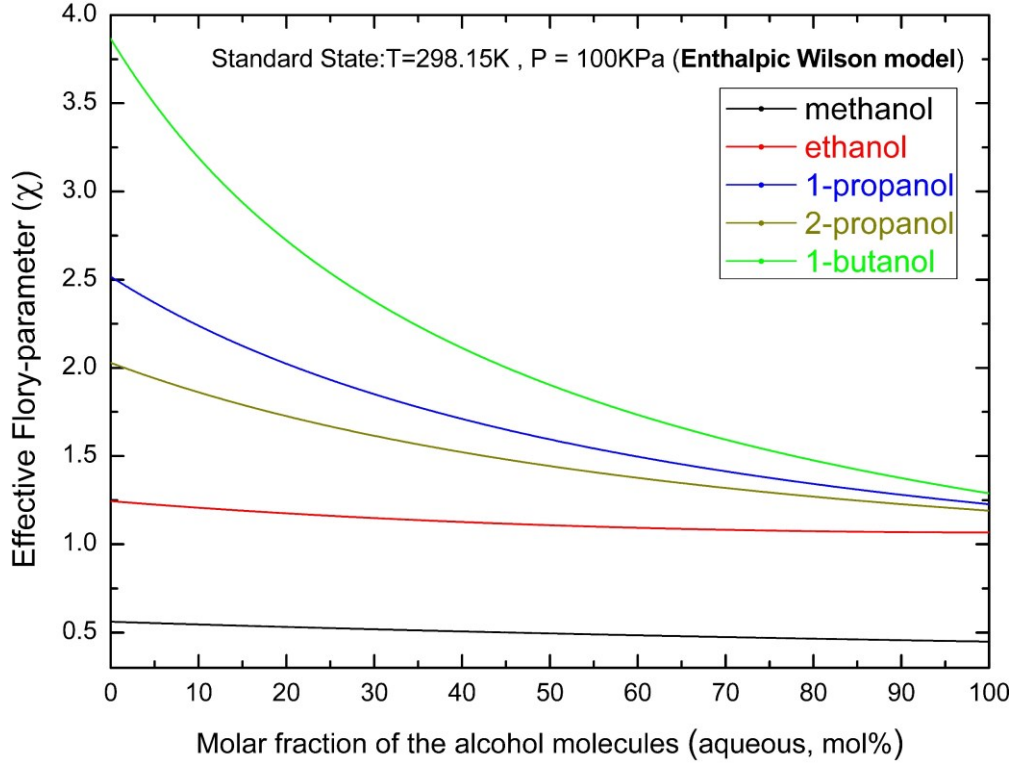


Figure 3.15(Figure 39) Effective Flory parameters for various alcohol/water mixtures at the standard state.

If we use the excess Gibbs free energy of mixing to estimate the interaction strength between species 1 and 2, the molar mixing Gibbs free energy $\Delta_{mix}G_m$ can be expressed as,

$$\frac{\Delta_{mix}G_m}{RT} = x_1 \ln(\gamma_1 x_1) + x_2 \ln(\gamma_2 x_2) = x_1 \ln(x_1) + x_2 \ln(x_2) + \chi x_1 x_2, \quad (3.26)$$

where χ is the effective Flory-interaction parameter. Then we get,

$$\chi = \frac{\ln(\gamma_1)}{x_2} + \frac{\ln(\gamma_2)}{x_1}, \text{ and} \quad (3.27)$$

$$-\frac{\chi}{\ln(A_{21}A_{12})} = \frac{1+x_1 \left(1 - \frac{1}{x_1 + A_{12}x_2} - \frac{A_{21}}{x_2 + A_{21}x_1} \right)}{(x_1 + A_{12}x_2)(x_2 + A_{21}x_1)} + \frac{1+x_2 \left(1 - \frac{1}{x_2 + A_{21}x_1} - \frac{A_{12}}{x_1 + A_{12}x_2} \right)}{(x_2 + A_{21}x_1)(x_1 + A_{12}x_2)}. \quad (3.28)$$

The right-hand side of Eq.(3.28) is a decreasing function in respect to argument x_1 when the boundary condition of $A_{12} > 0$, $A_{21} > 0$ is hold, and it has a boundary of $\left[\frac{1}{A_{21}}, \frac{1}{A_{12}} \right]$. Then we can get

$$\chi \in \left[-\frac{\ln(A_{21}A_{12})}{A_{21}}, -\frac{\ln(A_{12}A_{21})}{A_{12}} \right]. \text{ Note that Eq.(3.25), then we can get,}$$

$$\begin{aligned} \ln(\gamma_2^\infty) &\leq \chi \leq \ln(\gamma_1^\infty) \\ \ln(\gamma_2^\infty) &\leq \lambda \chi_{cs} \leq \ln(\gamma_1^\infty) \end{aligned} \quad (3.29)$$

in which $\lambda \geq 1$ is the volume ratio between a molecule of a component and a molecule of another different component in the binary mixtures, χ_{cs} is the conventionally used Flory-Huggins parameters. It is noted that $\chi = \chi_{cs, eff}$ which has already been estimated based on experimental data by Eq.(2.9). In Figure 3.15, we show calculation results for effective Flory-interaction parameter, the numerical calculation of χ is consistent with its experimental value $\chi_{cs, eff}$ also see Figure 2.6b.

3.6.4 Crosslink-density effect in the cononsolvency transition of poly(N-isopropylacrylamide) micro-gel and macro-gel

Zhu et al. [122] reported the average hydrodynamic radius, R_h of poly(N-isopropylacrylamide) micro-gels with different crosslink density in the dimethylformamide-water mixtures. Here we replotted these data as the normalized swollen gel volume ($\frac{V}{V_0} = \left(\frac{R_h}{R_{h,0}}\right)^3$) in Figure 3.16. Note that $R_{h,0}$ is the average hydrodynamic radius of poly(N-isopropylacrylamide) micro-gels in pure water, and V_0 is the micro-gel's swollen volume in pure water.

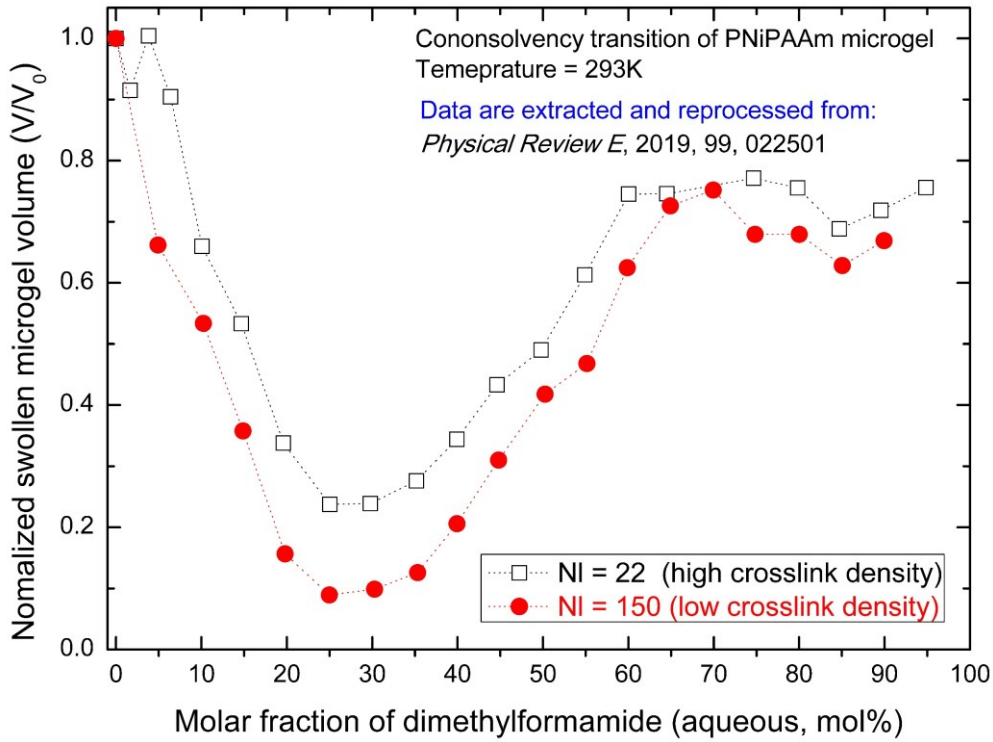


Figure 3.16(Figure 40) Crosslink-density effect in the cononsolvency transition of poly(N-isopropylacrylamide) micro-gel. Data are extracted and reprocessed from ref.[122], note that dotted lines in the figure are only used to guide eyesight.

Walter et al. [103] reported swollen gel weight ratio (W/W_{dry}) of PNiPAAm macro-gel (containing 1%mol and 2%mol N, N'-methylenebisacrylamide(MBA) as crosslinkers) in methanol aqueous solutions at the temperature of 298.15K. Here we replotted these data as the normalized swollen gel weight ($\frac{W}{W_0} = \frac{W/W_{dry}}{W_0/W_{dry}}$) in **Figure 3.17**. Note that W_0 is the macro-gel's swollen weight in pure water.

In **Figure 3.16** and **Figure 3.17**, experimental results show that when the crosslink density of gels is increased, the phase transition of poly(N-isopropylacrylamide) gels is weakened in dimethylformamide-water mixtures and methanol-water mixtures, but the crosslink density have only a very small effect on the solvent composition location of the maximum collapsed state. These observations are in line with the theoretical prediction of the extended adsorption-attraction model for polymer gels, more details see **section 3.2** and **section 3.3**.

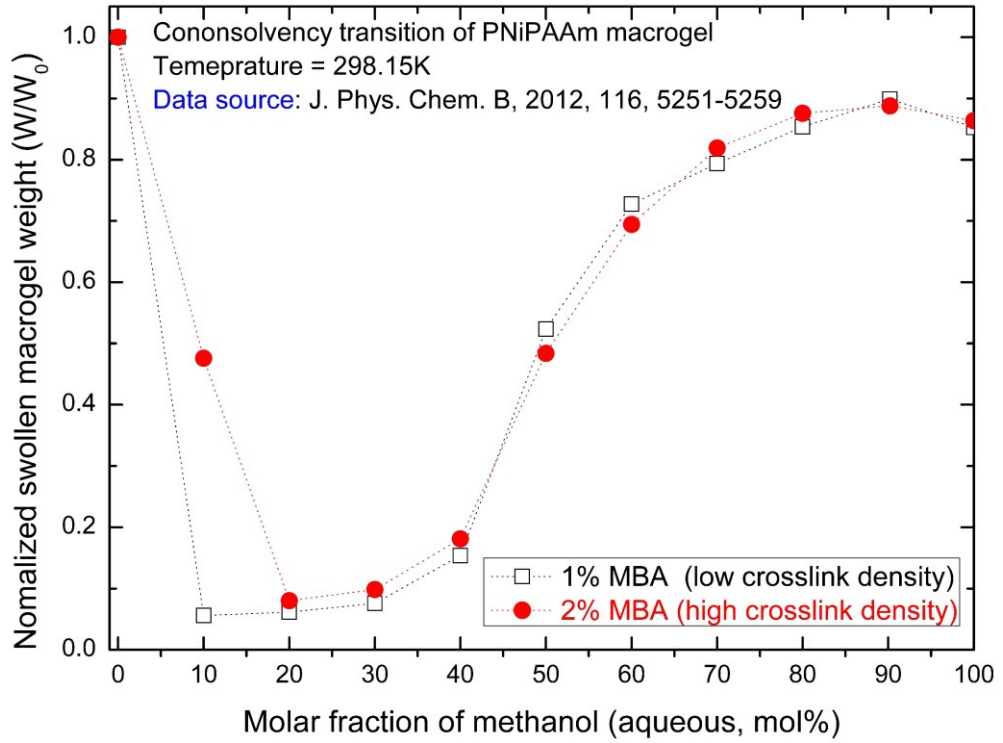


Figure 3.17(Figure 41) Crosslink-density effect in the cononsolvency transition of poly(N-isopropylacrylamide) macro-gel. Data are extracted and reprocessed from **ref.[103]**, note that dotted lines in the figure are only used to guide eyesight.

3.6.5 Pressure effect on the dimensionless chemical potential change (μ)

We note the fundamental thermodynamic relation [5],

$$dG_m = -S_m dT + V_m dP + \sum_i \mu_i dx_i, \quad (3.30)$$

where G_m is molar Gibbs free energy of the system, S_m is molar entropy of the system, V_m is molar volume of the system; μ_i and x_i are the i -th component's chemical potential and molar fraction respectively.

If temperature T and composition x_i are fixed, then the increase of molar Gibbs free energy of mixing $\Delta_{mix}G_m$, due to pressure effect can be expressed as,

$$d\Delta_{mix}G_m = \Delta V_m dP, \quad (3.31)$$

where ΔV_m is the excess molar volume of mixing. We get,

$$\Delta_{mix}G_m = \int \Delta V_m dP \approx \Delta V_m \Delta P. \quad (3.32)$$

Here, ΔP is an increase of pressure. Then the pressure effect on the dimensionless chemical potential change (μ) can be expressed as,

$$\Delta\mu = \frac{1}{RT} \left(\frac{\partial \Delta_{mix}G_m}{\partial x_1} \right)_{T, \Delta P} \approx \frac{\Delta P}{RT} \left(\frac{\partial \Delta V_m}{\partial x_1} \right)_{T, \Delta P}. \quad (3.33)$$

It is noted that for alcohol-water mixtures [138], in the alcohol-poor regime (when x_1 is small), Eq.(3.33) can be further approximated as,

$$\Delta\mu \sim \frac{\Delta P \Delta V_m}{RT x_1} \sim \frac{\Delta P \Delta V_m}{RT \rho}, \quad (3.34)$$

where x_1 , ρ are the molar fraction and volume fraction of the alcohol respectively. Note that ΔV_m is a **negative** quantity for short alcohol aqueous solutions [138], this means that if the pressure P is increased ($\Delta P > 0$), μ will decrease ($\Delta\mu < 0$).

3.6.6 Pressure effect on the cosolvent-solvent interaction (χ_{cs})

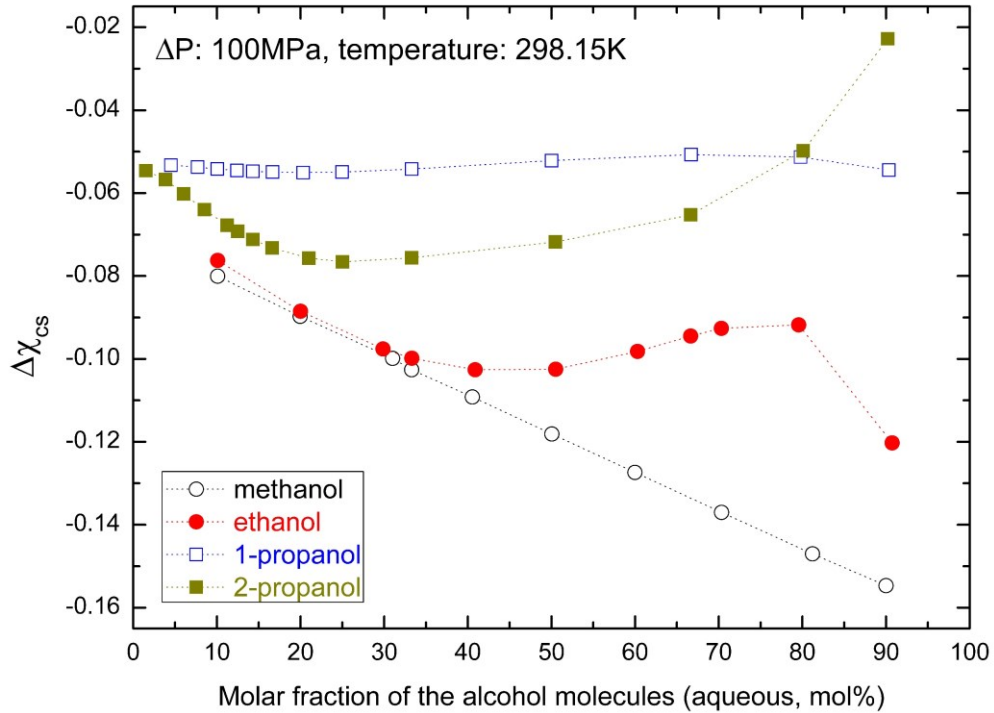


Figure 3.18(Figure 42) The reduction of cosolvent-solvent interaction ($\Delta\chi_{cs}$) as a function of various alcohol's molar fraction (x). Data are extracted and reprocessed from **ref.[138]**, note that dotted lines in the figure are guides to eyes.

The reduction of cosolvent-solvent interaction ($\Delta\chi_{cs}$) is estimated by using [141]:

$$\Delta\chi_{cs} \approx \frac{\Delta P \Delta V_{m,cs}}{RTy(1-x)}. \quad (3.35)$$

Here, $\Delta V_{m,cs}$ is the excess molar volume of mixing for short alcohol's aqueous solutions. ΔP is the increase of hydrostatic pressure. x and y are the molar fraction and the volume fraction of the alcohol in its aqueous solutions, respectively. For long-chain alcohol's aqueous solutions such as 1-propanol/water mixtures, when the temperature (T) and the increase of hydrostatic pressure (ΔP) are fixed, the reduction of cosolvent-solvent interaction ($\Delta\chi_{cs}$) can be approximated as a constant. By extracting and reprocessing data of $\Delta V_{m,cs}$ reported by Herráez [138], $\Delta\chi_{cs}$ as a function of various alcohol's molar fraction (x) is plotted in **Figure 3.18**. Note that, $\Delta V_{m,cs}$ also slightly depends on ΔP (not shown here), to simplify our discussion, in **Figure 3.18** we use the value of $\Delta V_{m,cs}$ at the standard pressure [138].

3.6.7 Pressure effect on the polymer-solvent interaction (χ_{ps})

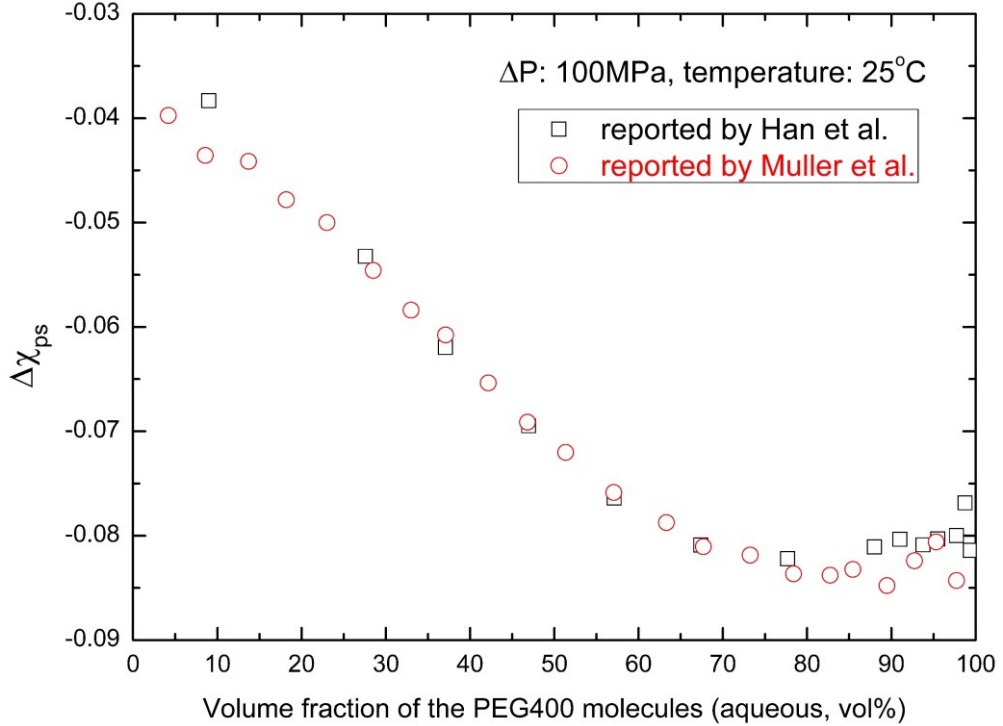


Figure 3.19(Figure 43) The reduction of polymer-solvent interaction ($\Delta\chi_{ps}$) as a function of PEG400's volume fraction (y). Data are extracted and reprocessed from Han [150] and Muller [151].

Similarly to **Eq.(3.35)**, the reduction of polymer-solvent interaction ($\Delta\chi_{ps}$) is estimated by using [141]:

$$\Delta\chi_{ps} \approx \frac{\Delta P \Delta V_{m,ps}}{RTy(1-x)}. \quad (3.36)$$

Here, $\Delta V_{m,ps}$ is the excess molar volume of mixing for a hydrophilic polymer's aqueous solutions. x and y are the molar fraction and the volume fraction of the hydrophilic polymer in its aqueous

solutions, respectively. By extracting and reprocessing data of $\Delta V_{m,ps}$ reported by Han [150] and Muller [151], $\Delta\chi_{ps}$ as a function of hydrophilic polymer PEG400's volume fraction (y) is plotted in **Figure 3.19**, in the plot we use the value of $\Delta V_{m,ps}$ at the standard pressure [150, 151]. It is expected that for other hydrophilic polymers such as poly(N-isopropylacrylamide) also have similar behaviors upon an increase of pressure (ΔP).

3.6.8 Chemical potential change of DMSO/water mixtures

As for DMSO/water mixtures, the Enthalpic Wilson model suitable for alcohol-water mixtures [124] does no longer correctly describe excess thermodynamic properties such as ΔG_m^E (**Figure 3.20**); in this thesis we use an improved interpolation method based on **ref.[134]** for DMSO/water mixtures. The interpolation formula for ΔG_m^E is

$$\frac{\Delta G_m^E}{RT} = a_1x + a_2x^2 + a_3x^3 + a_4x^4, \quad (3.37)$$

where the variable, x , is DMSO's molar fraction in its aqueous solutions; and R , T are gas constant and thermodynamic temperature respectively; and $a_1 = -2.97653$, $a_2 = 5.12261$, $a_3 = -2.55107$ and $a_4 = 0.39981$ are fit coefficients.

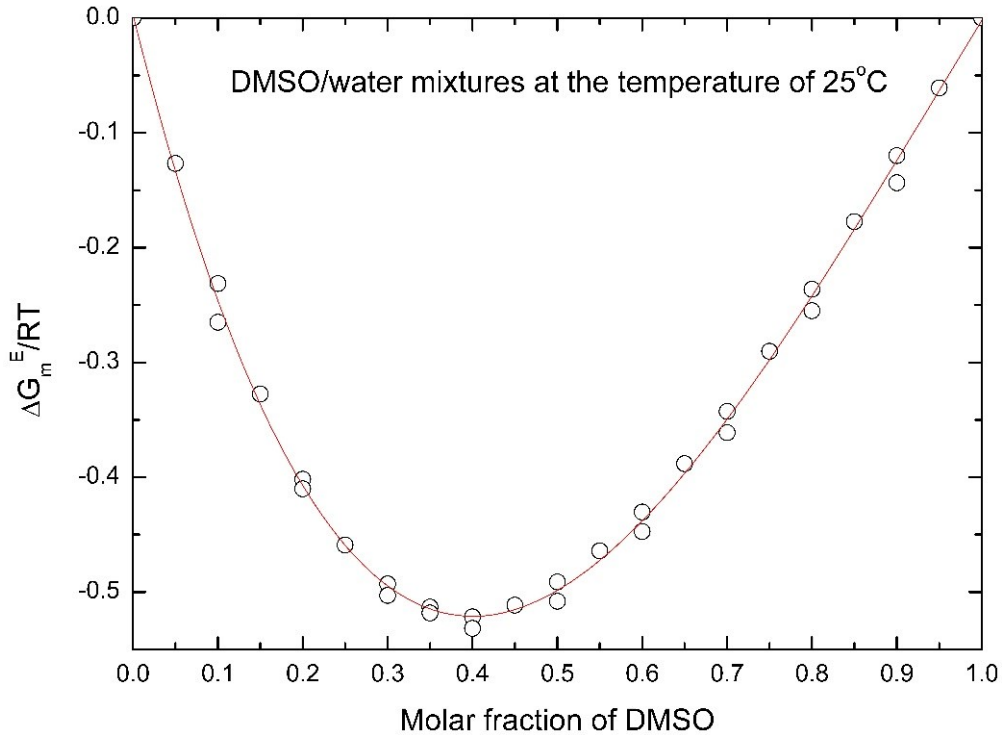


Figure 3.20(Figure 44) Molar excess Gibbs free energy as a function of molar fraction of DMSO in its aqueous solutions, when the temperature is at 25°C. Experimental data are extracted and reprocessed from **refs.[130, 134]**. Note that the solid line in the figure is a fit by using Eq.(3.37).

Then the chemical potential change of DMSO/water mixtures can be calculated by:

$$\begin{aligned}
\mu &= \frac{1}{RT} \left[\frac{\partial \Delta_{mix} G_m}{\partial x} \right]_{T,P} = \frac{1}{RT} \left[\frac{\partial \Delta_{mix} G_m^{id}}{\partial x} \right]_{T,P} + \frac{1}{RT} \left[\frac{\partial \Delta_{mix} G_m^E}{\partial x} \right]_{T,P} \\
&= \ln \left(\frac{x}{1-x} \right) + (a_1 + 2a_2x + 3a_3x^2 + 4a_4x^3)
\end{aligned} \tag{3.38}$$

Chapter 4 Gating the translocation of DNA through poly(N-isopropylacrylamide) decorated nanopores using the cononsolvency effect in aqueous environments

(Note: Some results presented in this chapter were already published by the author in the journal “Macromolecules, 2021, DOI: 10.1021/acs.macromol.1c00215”.)

4.1 Introduction

In **Chapter 2**, experimental investigations revealed that the thickness of a poly(N-isopropylacrylamide) brush on a flat surface exhibits in a switch-like change when a very small amount of alcohol (cosolvent) is added into the polymer-brush aqueous solutions. This switch effect is particularly significant when the alcohol is propanol isomers or butanol isomers. This phenomenon indicates that the cononsolvency of polymer brushes is a promising candidate for a switchable effect to mimic the opening or closing of cell-membrane channels, but so far this is merely a feasible idea implied by computer simulations [100, 152, 153] and not yet reported in any experimental investigation [154-156].

In this chapter, with the help of an emergent experimental method that based upon translocation dynamics of fluorescence DNA [66], we demonstrate that switchable nano-channels can be prepared by harnessing the cononsolvency transition in grafted polymers. The widening of the polymer decorated nano-channels occurs in a narrow window of about 5% volume fraction of ethanol in aqueous buffer solution. Furthermore, a quantitative method is provided to estimate the thickness of a polymer layer which is grafted around the rim of nanopores, and which cannot be directly measured by other already known analytic methods. PNiPAAm was chosen as a model polymer, experimental results quantitatively showed that polymers around the rim of nanopores show solvent-composition responsive behaviors in the range of metabolic pH values and room temperatures.

4.2 Methods

4.2.1 Preparation of polymer-grafted gold membrane

Track-etched polycarbonate membranes (Whatman, with nominal pore diameters equal to 50nm and thicknesses equal to 6 μ m), is only one-side coated with a thin layer of gold (EVA 300 Alliance Concept evaporator, thickness 50 nm, speed of deposit 0.2 nm). The polymer-grafted gold membrane is prepared by following the procedure: (1) The one-side gold-coated membrane (size is about 20mm \times 20mm) is cleaned with hydrochloric acid (HCl, ≤ 1.0 mol/L) for an hour at room temperature, then it is cleaned and rinsed in deionized water. (2) About 4 ml of 10 mg/ml (40mg) α -thiol ω -carboxylic acid terminated poly(N-isopropyl acrylamide) (Polymer Source products; molecular weight: $M_n = 1.5 \times 10^4$ g/mol, $M_w/M_n = 1.18$; and $M_n = 3.0 \times 10^4$ g/mol, $M_w/M_n = 1.25$.) in deionized water is reduced with 0.1 mmol (30mg) tris(2-carboxyethyl) phosphine hydrochloride (TCEP). Then the polymer solution is filtered by using 200nm-size PEFE filter. (3) The cleaned gold membrane is immersed in the filtered PNiPAAm solution and incubated 24-96 hours; the reaction temperature

is close to but lower than the LCST transition temperature of PNiPAAm (about 32°C). The pH of the reaction solution is neutral or a little bit basic. (4) After grafting reaction, to remove the non-reacted PNiPAAm and TCEP. The polymer-grafted gold membrane is immersed in deionized water reservoir at least 4 hours.

In the above protocol, we used the grafting-to method to prepare polymer-grafted membrane. The advantage of this approach is that the molecular weight and its distribution of a polymer layer can be well approximated to its free polymers in solution [157] in advance in contrast to grafting-from method, this is exact the case in my study when the polydispersity of polymer in solutions is narrow (close to 1.0), see **Table 4.1**. However, it is still impossible to measure the thickness of the polymer layer around the rim of nanopores by using current-known standard analytical methods. In this study, this problem is overcome based on a suction model by helps of translocation dynamics of fluorescence λ -DNA, see **section 4.2.2**. This allows us to estimate grafting density of polymers around the rim of nanopores.

Table 4.1(Table 13) Polymer grafting density of higher and lower grafted membranes with different molecular weight. In this study, we used a scaling approach to estimate grafting density. See **section 4.5.1** for the details of determining grafting density. The layer thickness is calculated based on the data of DNA translocation events which are measured at the temperature of 298 K.

sample name	grafting density (chains/nm ²)	layer thickness in tris-buffer solution (nm)	time of grafting reaction	molecular weight (M_n , g/mol)	PDI	polymer mor- phology
higher-graft-15K	~ 0.30	10.0 ± 1.0	96 hours	1.5 × 10 ⁴	1.18	brush
lower-graft-15K	~ 0.15	7.0 ± 0.1	48 hours	1.5 × 10 ⁴	1.18	brush
higher-graft-30K	~ 0.05	5.3 ± 0.1	72 hours	3.0 × 10 ⁴	1.25	mushroom
lower-graft-30K	<< 0.05	1.6 ± 0.1	24 hours	3.0 × 10 ⁴	1.25	mushroom

Nevertheless, it is necessary to properly design experiments to cross verify analysis based on my experiment measurement techniques. To qualitatively know grafting-density difference between two batch of grafted polymers, as for the lower-molecular-weight samples ($M_n = 1.5 \times 10^4$ g/mol, $M_w/M_n = 1.18$), first we used the fresh PNiPAAm solution to prepare higher grafting-density polymer and the grafting reaction time was 96 hours, then we re-used the “reacted” or “waste” PNiPAAm solution to prepare lower grafting-density polymer and the grafting reaction time was 48 hours. The methodology behind this approach is that: Polymer materials always have a molecular weight distribution. Because of the polymer chain’s huge size relative to its end functional groups and steric hindrance in the grafting reaction, shorter polymer chains prefer to react with the gold surface first, then turns to the longer polymer chains. Recently this phenomenon is revisited by **ref.[157]**. This approach is also designed to check the protocol’s reliability. As for higher-molecular-weight samples ($M_n = 3.0 \times 10^4$ g/mol, $M_w/M_n = 1.25$), the grafting reaction time for the lower-grafted sample is 24hours, and the grafting reaction time for the higher-grafted sample is 72 hours. The physical parameters of grafted membranes which are used in this study are listed in **Table 4.1**.

It is worth pointing out in advance that analysis results based on the suction model [66, 76, 158], are consistent with my experimental design in a somewhat intuitive way: the longer the time of grafting reaction and the higher the activity of the reactive solution, the thickness is higher for the grafted polymers when with the same molecular weight, see section 4.3.

4.2.2 Translocation experiments of fluorescence λ -DNA through nanopores

A dilute solution of λ -DNA (0.1 pM, 48 kbp) in Tris buffer solution (tris 10 mM, EDTA 1 mM and KCl 10 mM, pH \approx 7.6) fluorescently labeled with Yoyo-1 (Life Tech) filled the *cis*-chamber where the pressure was applied. A few hundred translocation events were observed simultaneously with a time resolution of 10ms, which was sufficient to resolve each translocation event. A cartoon depiction of a fluorescence λ -DNA translocating through a PNiPAAm-grafted nanopore, is shown in Scheme 4.1.

We analyzed the variation of the DNA translocation frequency per pore (f_{DNA}) with the gradient of pressure (P) where the pressure on the side of membrane without coating a gold layer is higher. My method is based on the well-proved statement of the so-called “suction model” [66, 76, 158]: In the strong confinement regime, the critical force to guide flexible linear polymer chains through nanopores is independent of the chain length. After a formulation of this statement under the condition of flow pressure, in the framework of the suction model, the translocation frequency is expressed as

$$f_{DNA} = k_1 \exp\left(-\frac{\Delta F}{k_B T}\right), \quad (4.1)$$

by assuming that DNA translocation is described as the travel of a flexible polymer through a free-energy landscape with a barrier of height ΔF and assuming the translocation process follows a Boltzmann statistic, which is already verified by computer simulations [159]. We note that the persistence length of DNA is about 50nm which is also the nanopore size in this study, thus a flexible-polymer-chain assumption for DNA in this study is reasonable. k_1 (s^{-1}) is the rate of incidence on the barrier. When k_1 is dominated by the presence of the barrier [66], $k_1 \propto J$ with J the solvent flux ($m^3 s^{-1}$). In the suction model, the energy barrier is $\Delta F = k_B T(J_c/J)$ and the translocation frequency f_{DNA} finally reads

$$f_{DNA} = k_2 \left(\frac{P}{P_c}\right) \exp\left(-\frac{P_c}{P}\right), \quad (4.2)$$

with k_2 being a proportionality factor (s^{-1}), $P_c = R_h J_c$ and $J_c = k_B T/\eta$. R_h is the hydrodynamical resistance of the pore equal to $8\eta L/\pi R_{eff}^4$ with L being the length of a pore ($L = 6\mu m$ in this study), R_{eff} the effective radius of pores, and η is the solvent viscosity (by assuming a Poiseuille law). In this study, η is treated as a constant since only a small change of ethanol concentration occurs in experiments. In practice, the effective radius of pores, R_{eff} is

$$R_{eff} = R_0 \left(\frac{P_{c,0}}{P_{c,eff}} \right)^{\frac{1}{4}}, \quad (4.3)$$

where $P_{c,0}$ and $P_{c,eff}$ are critical pressures of the blank membrane and when the same blank membrane is grafted with a polymer layer respectively; R_0 is the radius of nanopores without grafted polymers, in this study $R_0 = 25.0 \pm 1.0$ nm is the corresponding measured value using scanning electron microscopy.

The frequency f_{DNA} is calculated as

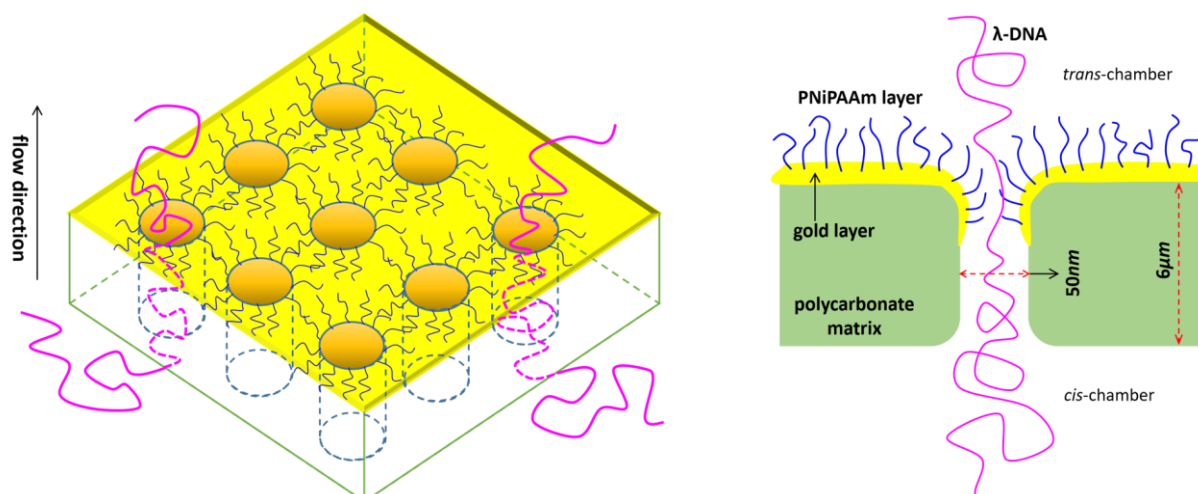
$$f_{DNA} = \frac{N_{DNA}}{\rho_{pore} A t}, \quad (4.4)$$

where N_{DNA} is the DNA translocation event through a fixed area ($A = 135 \mu m \times 135 \mu m$) of membranes and in a fixed period of time ($t = 30$ s), ρ_{pore} is the pore density with a value of $\rho_{pore} = 6 \times 10^8$ pores/cm² in this study. The average number of pores in the fixed area is about 1.1×10^5 , thus the number fluctuation of DNA translocation events observed in this study can be safely neglected. As shown in **Eq.(4.4)**, the number of translocation events (N_{DNA}) observed in this study only differs from the translocation frequency (f_{DNA}) by a constant multiplicatory factor. In the following we use N_{DNA} instead of f_{DNA} in discussion by convenience, since we are only interested in the relative variation of the frequency with respect to the buffer conditions. Thus, in this study the critical pressure (P_c) is obtained by fitting the nonlinear equation

$$N_{DNA} = k_3 \left(\frac{P}{P_c} \right) \exp \left(-\frac{P_c}{P} \right), \quad (4.5)$$

where k_3 is a constant for a given system.

If nanopores are grafted with polymer and the polymer has some responsive properties, with certain stimuli such as temperature change or solvent composition change, the conformations of the polymer changes and therefore the effective size of the nanopores. The useful information provided by the number of DNA translocation events (N_{DNA}) is that when the flow pressure (P) is fixed in the DNA translocation process and the effective size of nanopores changes (R_{eff}), then the number of DNA translocation event changes. This phenomenon can be used to estimate the swollen thickness of a polymer layer if it is grafted around the rim of nanopores. By using **Eq.(4.3)** and **Eq.(4.5)**, we can get the swollen thickness of the polymer layer that is grafted around the rim of nanopores by a relation of $H = R_{eff} - R_0$. It is also noted that we measure H under flow pressure, this leads to the estimated swollen thickness (H) which may not coincide with the swollen thickness of equilibrium polymer layers. Here, it is worth pointing out that the swollen thickness (H) of polymer layers around the rim of nanopores cannot be directly measured by any other known analytic methods.



Scheme 4.1(Figure 45) A cartoon of fluorescence λ -DNAs translocating through PNIPAAm-grafted nanopores: (left) A three-dimensional side view, (right) a longitudinal-sectional zoom-in view of a nanopore.

Therefore, the suction model clearly demarcates a boundary of an advantage and also a limit to my current approach to objectively measure the thickness of a polymer layer under flow pressure. We note that the driving force for DNA translocation can be an electric field [160], my experimental method can be easily extended to this case; however, this topic is beyond the scope of this thesis.

4.2.3 Method of identification and counting of DNA translocation events

We accomplished the counting of DNA translocation events (a kind of moving objects) using a customized algorithm to ensure objectivity as well as high reproducibility of the evaluation results including efficiency regarding their acquisition. The algorithm was coded in Python v3.7.3 (<https://www.python.org>) with numpy v1.16.4 (<https://numpy.org>) and OpenCV v4.1.1.26 (<https://openCV.org>).

Firstly, the video files are converted into raw image stacks by software such as ImageJ, which are fed into the program. Each image is then subjected to a noise-background subtraction considering a defined brightness percentage (noise-background strength, in my experiments it is about 13%). One problem in my experiments concerning the size of a real flash (a DNA translocation event). It is obvious that a flash is too small to be a real DNA translocation event in videos. Therefore, a threshold has to be defined to ignore too small closed contours (artefact DNA translocation event); this threshold is about a 5x5 pixel matrix in images in my video data. Then, images are processed by image blurring using a blur matrix, the blurring threshold is about a 18x18 pixel matrix for the blur matrix in my video data. The blurring is used to reduce interrupted object contours, which are determined next by a simple binary threshold routine. The contours are characterized by their center of mass, i.e. location within the image and size. This routine is repeated for all frame images unpacked from the video, thereby completing the time stack for each experiment. It is worth pointing out that artifacts arising from small but true objects are prevented by a minimum-size blurring threshold for the contours to be accepted.

One major problem in my experiments concerning the automatic identification of valid DNA translocation events, was the prolonged duration of single events exceeding that of one video frame. Accordingly, simple counting of contours in each single image will result in a significant over estimation of events. We therefore introduced another threshold parameter, namely the travel distance. Based on the individual flash size (a DNA translocation event), the travel distance value determines the distance, by which a DNA translocation is allowed to be displaced between consecutive image frames. Binding this value proportionally to the flash size seemed reasonable to us, since for bigger flashes, the inherent fluctuation within the determination of its center of mass for two consecutive frame images might be somewhat higher than for smaller flashes. Thus, we could successfully prevent an overcounting of DNA translocation events by only counting the objects that were sufficiently separated in terms of their location within consecutive frames and correctly identifying DNA translocation events lasting for several frames.

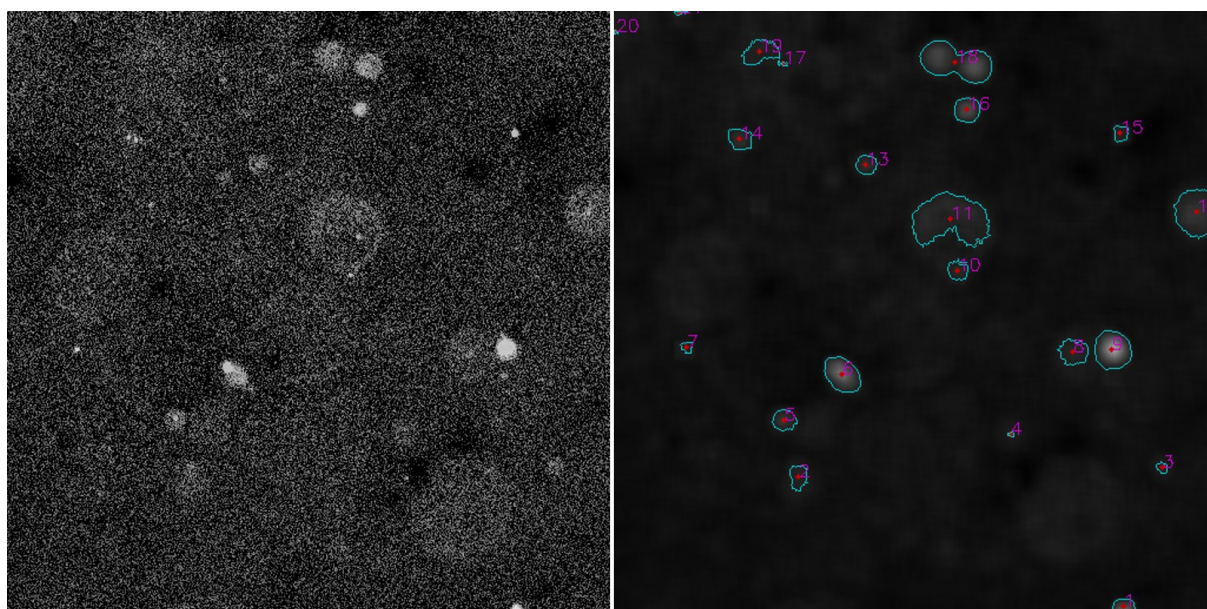


Figure 4.1(Figure 46) An example to determine the number of DNA translocation events: the left picture is an original image data and the right picture is the counting results for the left picture. Note that the vision size of video data (one frame) is fixed in an area of $A = 135\mu\text{m} \times 135\mu\text{m}$.

Noise-background strength would be quite different for different video data. To estimate the noise-background strength of each video as objectively as possible, firstly the smaller number of DNA translocation events (less than 250 in this study) of videos is accurately counted by human eyes, because it is very hard for human eyes to focus on and accurately count larger number of DNA translocation events. Then the Python code is used to estimate noise-background strength of these videos to make sure the counting results of Python code are as close as possible to the counting results of human eyes. Finally, the average noise-background strength of these videos is used to count the same batch experiments of videos which contain a larger number of DNA translocation event (more than 250 in this study). It is expected that this approach is reasonable since for the same batch of experiments, only an experimental parameter of pressure is changed in the experiments

and the contrast of each video is already adjusted at the same level and as clearly as possible for the same batch of experiments.

Figure 4.1 is an example to determine the number of DNA translocation events based on the algorithm applied in this study. This result is obtained by the following procedure: (I) Open the video in ImageJ(<https://imagej.net/Fiji>), subtract instrument background. (II) The video files are converted into raw image stacks with 32-bit depth by ImageJ. (III) The raw image stacks are fed into the program. Set noise-background subtraction for images, in this study it is 12%. Set a threshold that excludes an artefact DNA translocation event, this threshold is about a 5x5 pixel matrix in images in my video data. Set blur matrix for images, in this study the blurring threshold is about a 18x18 pixel matrix. Set the travel distance for DNA translocation event, in this study it is about 3 times of flash size. The program also needs to know the depth of raw image stacks, this value of depth shall be the same as the value of depth generated by ImageJ, in my study it is 32 bits by ImageJ. (IV) Run the program, the counting result will be marked on the images.

4.3 Results and discussion

4.3.1 Grafting density effect on the swollen behaviors of PNiPAAm polymers around the rim of nanopores

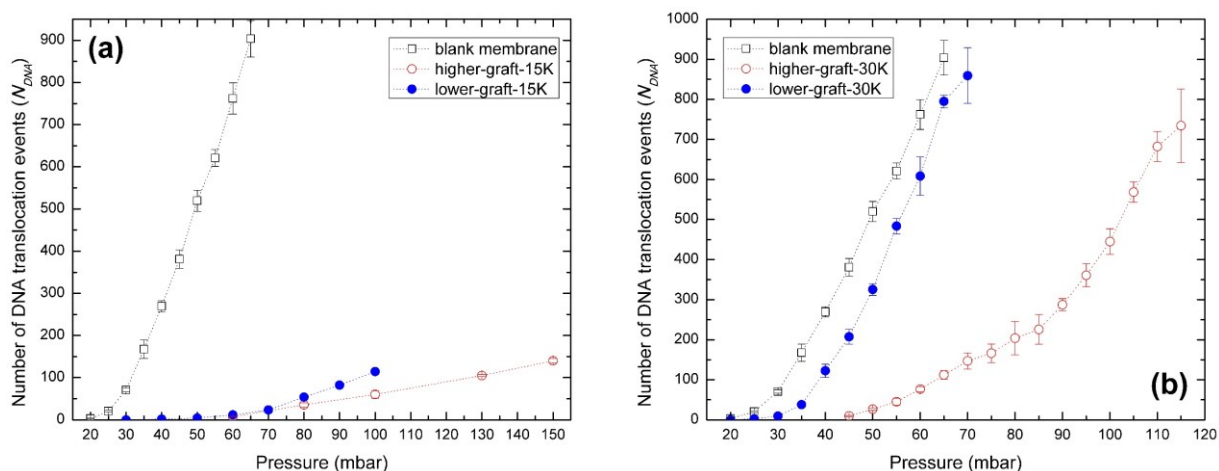


Figure 4.2(Figure 47) Number of DNA translocation events with respect to pressure in tris-buffer solutions when DNA translocates through nanopores. As for PNiPAAm-grafted nanopores: (a) Membranes of different grafting density with molecular weight of $M_n = 1.5 \times 10^4$ g/mol, $M_w/M_n = 1.18$; (b) Membranes of different grafting density with molecular weight of $M_n = 3.0 \times 10^4$ g/mol, $M_w/M_n = 1.25$. The size of blank nanopores is 50 nm and test temperature is 298 K. Note that the dotted lines in the figures are guides to eyes.

In **Figure 4.2**, we report translocation behaviors of DNA through nanopores in a tris-buffer solution. Considering the significant change of the number of DNA translocation events for those nanopores, the origin of this sudden change can be merely from the grafted PNiPAAm: because one reason is that the matrix material (polycarbonate) used to manufacture nanopores can't show solvent-composition responsive behavior; another reason is that when the concentration of ethanol is

lower than a threshold ($\approx 25\%$ vol in my study), my experiments show that the solvent quality effect on translocation behaviors of DNA is trivial (without showing these results). In **Figure 4.3**, we report translocation behaviors of DNA through shorter-chain polymer-grafted nanopores in a tris-buffer solution and 4.76%vol ethanol-buffer mixtures. In **Figure 4.4**, we report translocation behaviors of DNA through longer-chain polymer-grafted nanopores in a tris-buffer solution and various ethanol-buffer mixtures. In **Figures 4.2-4.4** we observe a consistent increase of DNA translocation efficiency with decreasing grafting density of the polymer layer, this is reflected by a larger gap of DNA translocation events between higher-density-grafted and lower-density-grafted membranes in various concentrations of ethanol. It clearly showed that polymers are grafted around the rim of nanopores.

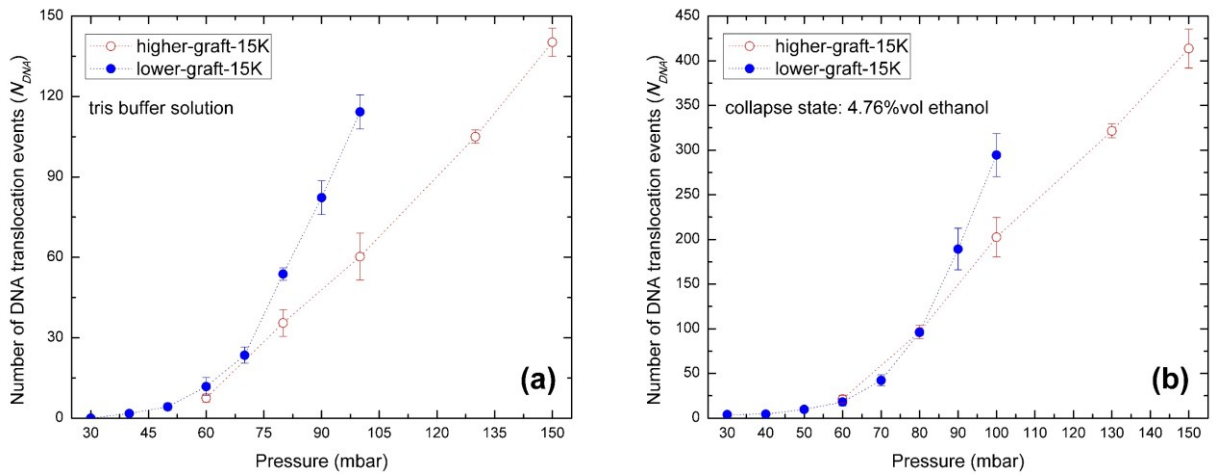


Figure 4.3(Figure 48) Number of DNA translocation events with respect to pressure when DNA translocates through nanopores with different polymer grafting density: (a) In tris-buffer solutions, (b) in 4.76%vol ethanol-tris-buffer mixtures. As for PNiPAAm-grafted nanopores, molecular weight of the PNiPAAm polymer is $M_n = 1.5 \times 10^4$ g/mol, $M_w/M_n = 1.18$. The size of blank nanopores is 50 nm and test temperature is 298 K. Note that the dotted lines in the figures are guides to eyes.

With the help of a scaling-law analysis, the morphology regimes of a polymer layer can be determined, for details see [section 2.2.4](#) and [section 4.5.1](#). In this study, by using grafting-to synthetic method, as for a shorter-chain PNiPAAm polymer ($M_n = 1.5 \times 10^4$ g/mol, $M_w/M_n = 1.18$), the grafted polymers exhibit a brush morphology. But for a longer-chain PNiPAAm polymer ($M_n = 3.0 \times 10^4$ g/mol, $M_w/M_n = 1.25$), the grafted polymers only reach a mushroom morphology in this study.

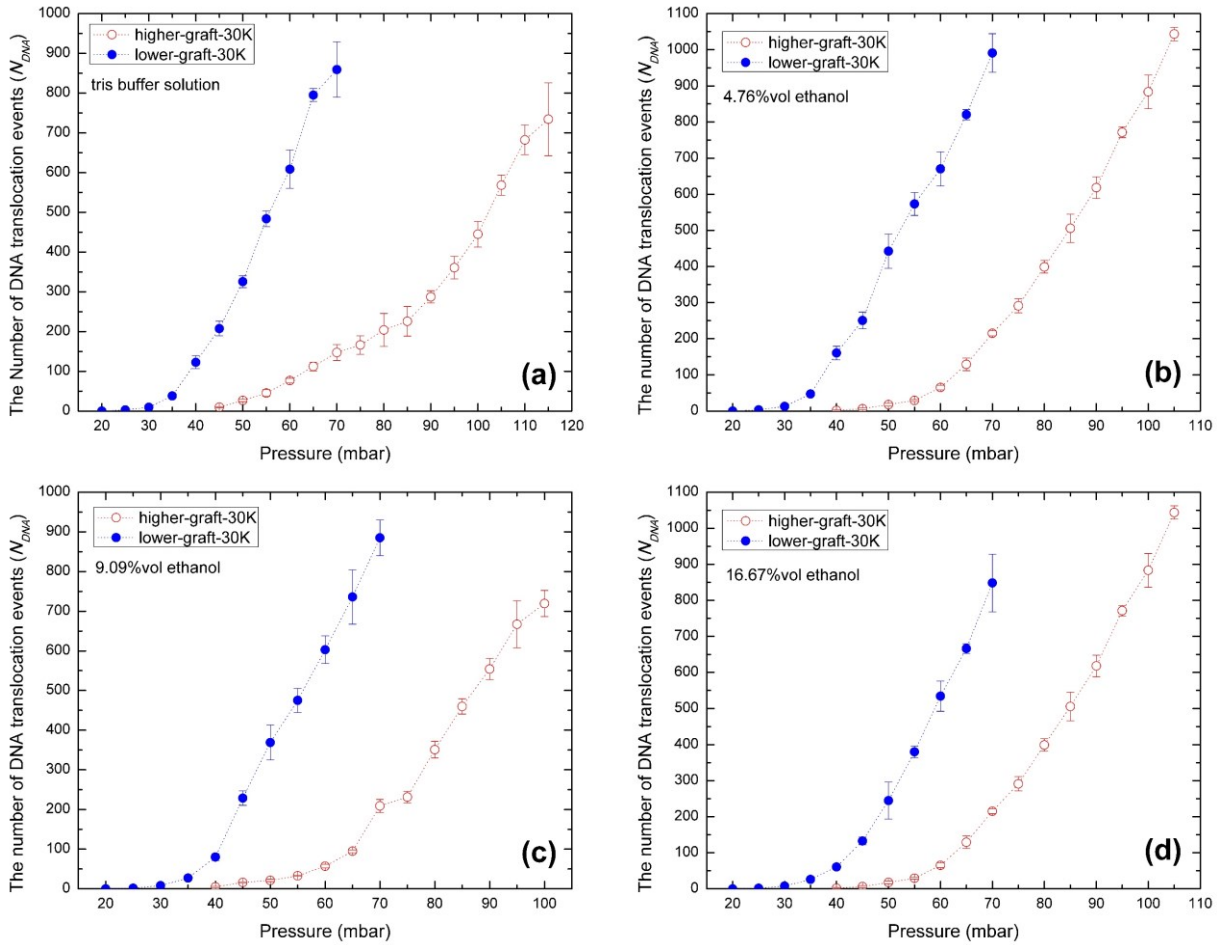


Figure 4.4(Figure 49) Number of DNA translocation events with respect to pressure when DNA translocates through nanopores with different polymer grafting density: (a) In tris-buffer solutions, (b) in 4.76%vol ethanol-tris-buffer mixtures. (c) In 9.09%vol ethanol-tris-buffer mixtures. (d) In 16.67%vol ethanol-tris-buffer mixtures. As for PNiPAAm-grafted nanopores, molecular weight of the PNiPAAm polymer is $M_n = 3.0 \times 10^4$ g/mol, $M_w/M_n = 1.25$. The size of blank nanopores is 50 nm and test temperature is 298 K. Note that the dotted lines in the figures are guides to eyes.

4.3.2 Switching effect of polymer chains around the rim of nanopores in the tri-buffer/ethanol mixtures

In **Figure 4.5**, we report the details for the cononsolvency behavior of higher-density and lower-density grafted PNiPAAm (shorter chain) around the rim of nanopores. Considering the obvious change of the number of DNA translocation events in 4.76%vol ethanol/tri-buffer mixtures and DNA translocation in a tri-buffer solution, the origin of this obvious change can be merely from solvent response of the grafted PNiPAAm. My results also show that when the ethanol composition is between 13% and 17%, the number of DNA translocation events recover to the same level as when the solvent is tris-buffer solution. As shown in **Figure 4.6**, the same behaviors are also observed for a longer polymer chain.

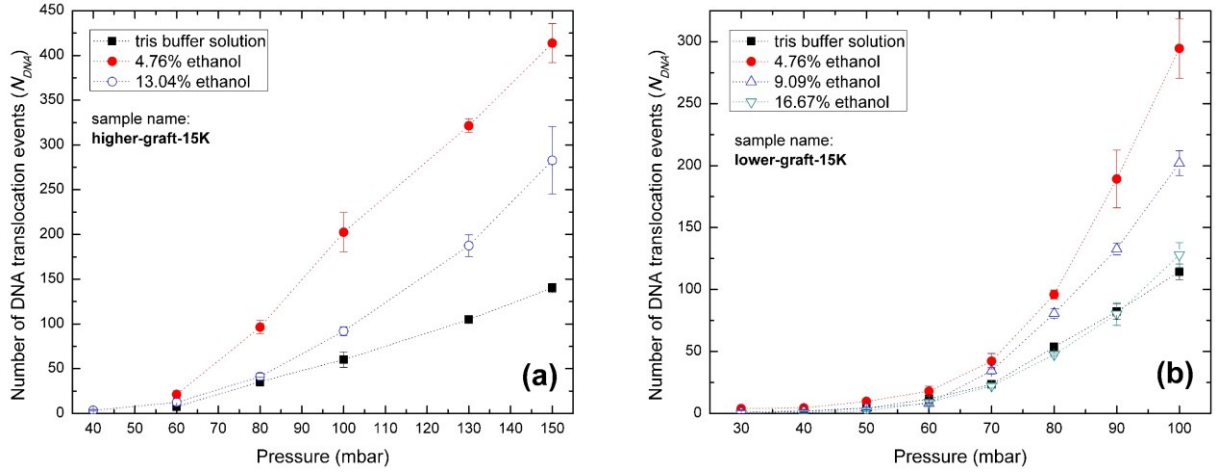


Figure 4.5(Figure 50) Number of DNA translocation events with respect to pressure in tris-buffer/ethanol mixtures, when DNA translocates through nanopores with different polymer grafting density: (a) For a higher grafting density of PNiPAAm-grafted nanopores, (b) for a lower grafting density of PNiPAAm-grafted nanopores. Molecular weight of the PNiPAAm polymer is $M_n = 1.5 \times 10^4$ g/mol, $M_w/M_n = 1.18$. The size of blank nanopores is 50 nm and test temperature is 298 K. Note that the dotted lines in the figures are guides to eyes.

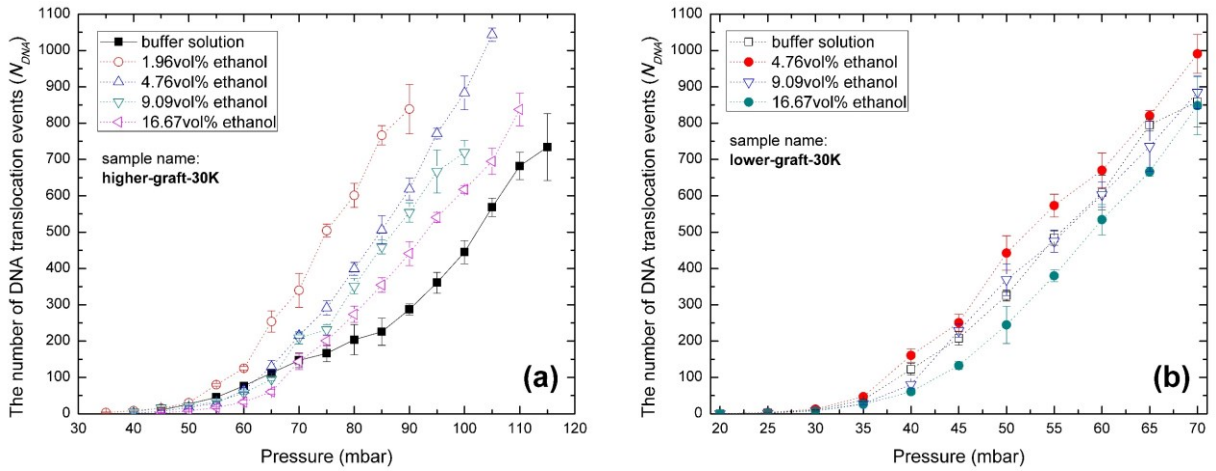


Figure 4.6(Figure 51) Number of DNA translocation events with respect to pressure in tris-buffer/ethanol mixtures, when DNA translocates through nanopores with different polymer grafting density: (a) For a higher grafting density of PNiPAAm-grafted nanopores, (b) for a lower grafting density of PNiPAAm-grafted nanopores. Molecular weight of the PNiPAAm polymer is $M_n = 3.0 \times 10^4$ g/mol, $M_w/M_n = 1.25$. The size of blank nanopores is 50 nm and test temperature is 298 K. Note that the dotted lines in the figures are guides to eyes.

As shown in **Figure 4.5** and **Figure 4.6**, the number of DNA translocation events first increases with an increase of ethanol concentration; when further increasing the ethanol concentration, the number of DNA translocation events decreases. This implies the size of the nanopores firstly increases under the stimuli of increasing ethanol concentration, then the nanopore size reduces under the stimuli of increasing ethanol concentration. This exactly indicates that grafted PNiPAAm shows

re-entrant signatures of cononsolvency transition in the ethanol/tris-buffer mixtures. This observation is also clearly supported by a study of the normalized number of DNA translocation events which is plotted in respect to the change of ethanol concentration under different driven pressures, see **Figure 4.7** and **Figure 4.8**. Solvent-composition responsive behaviors shown in **Figures 4.5-4.8** indicates that solvent-responsive behavior of grafted PNiPAAm can be used to control the size of nanopores. A cartoon depiction of ethanol-concentration induced phase transition of PNiPAAm layer around the rim of nanopore, is shown in **Scheme 4.2**. Interestingly, it is also worth noting that a similar behavior of re-entrant coacervation phase transition was also observed for free biopolymers (gelatin, type-B) in NaCl/alcohol/water mixtures with various pH values [161] where the solvent composition is quite similar to my study.

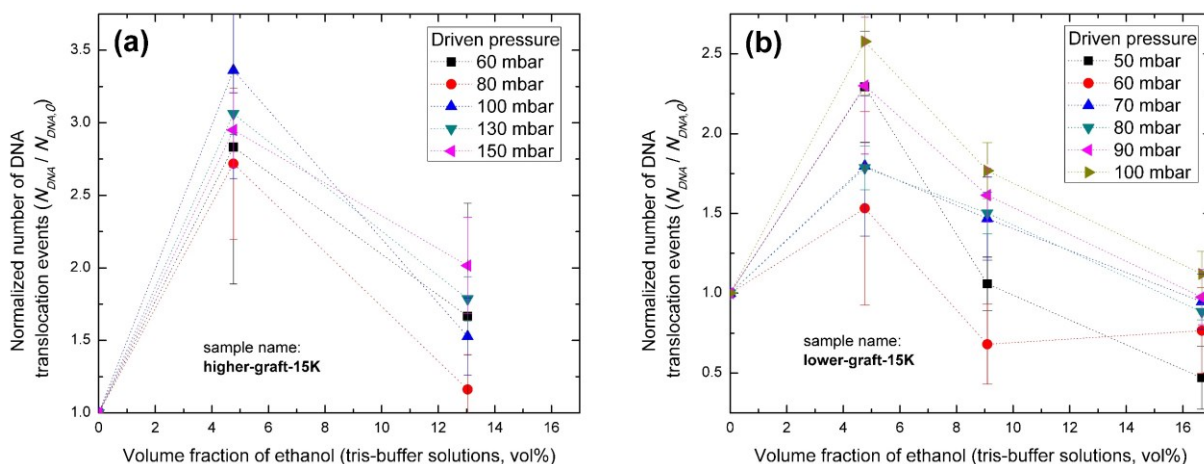


Figure 4.7 (Figure 52) The normalized number of translocation events is plotted with respect to ethanol concentration change under different driven pressure. (a) For a higher grafting density of PNiPAAm-grafted nanopores, data are already used in Figure 4.5a. (b) For a lower grafting density of PNiPAAm-grafted nanopores, data are already used in Figure 4.5b. Molecular weight of the PNiPAAm polymer is $M_n = 1.5 \times 10^4$ g/mol, $M_w/M_n = 1.18$. The size of blank nanopores is 50 nm and test temperature is 298 K. Not that the dotted lines in the figure are guides to eyes.

In **Figure 4.9**, by fitting the experimental results in **Figure 4.5** and **Figure 4.6** using Eq.(4.5), we quantitatively constructed diagrams for cononsolvency behaviors of grafted PNiPAAm around the rim of nanopores. From **Table 4.1**, we know that the polymer layers of short chains (**Figure 4.9a**) are in polymer-brush regime. In **Figure 4.9a**, it is observed that an increase of grafting density of PNiPAA brushes which are grafted around the rim of nanopores, weakens collapse transition of brush layer in ethanol/tris buffer mixtures. It is remarkable that even with a different geometric constraint, this phenomenon is the same as PNiPAAm brushes in ethanol/water mixtures on the flat surface (see **section 2.10** of **Chapter 2**), and this phenomenon is analytically predicted by the the extended adsorption-attraction model (see **Chapter 3**). Comparing phase behaviors of shorter and longer polymer chains, it is clear that the switching effect can be only realized by moderate-grafting-density polymer layers.

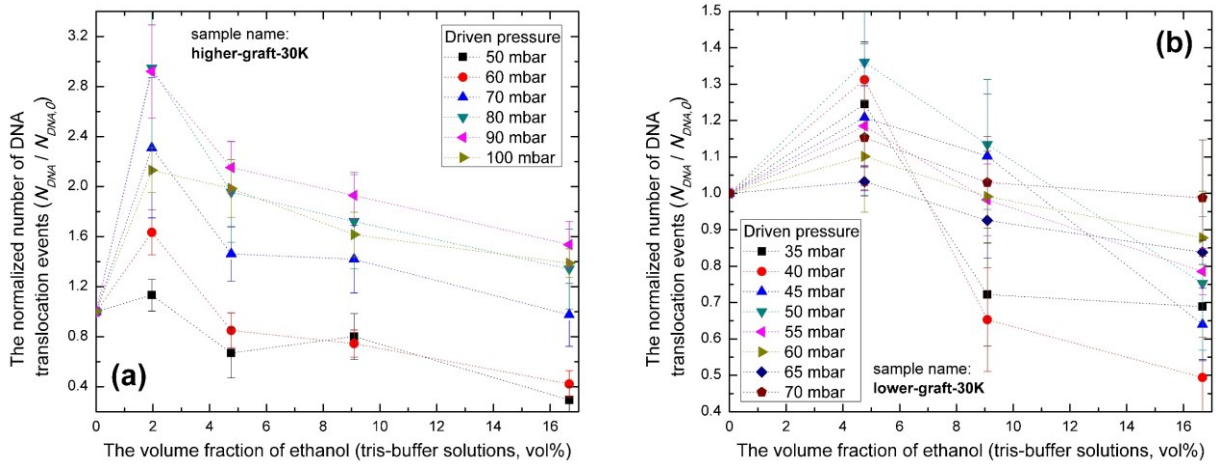


Figure 4.8(Figure 53) The normalized number of translocation events is plotted with respect to ethanol concentration change under different driven pressure. (a) For a higher grafting density of PNiPAAm-grafted nanopores, data are already used in Figure 4.6a. (b) For a lower grafting density of PNiPAAm-grafted nanopores, data are already used in Figure 4.6b. Molecular weight of the PNiPAAm polymer is $M_n = 3.0 \times 10^4$ g/mol, $M_w/M_n = 1.25$. The size of blank nanopores is 50 nm and test temperature is 298 K. Note that the dotted lines in the figures are guides to eyes.

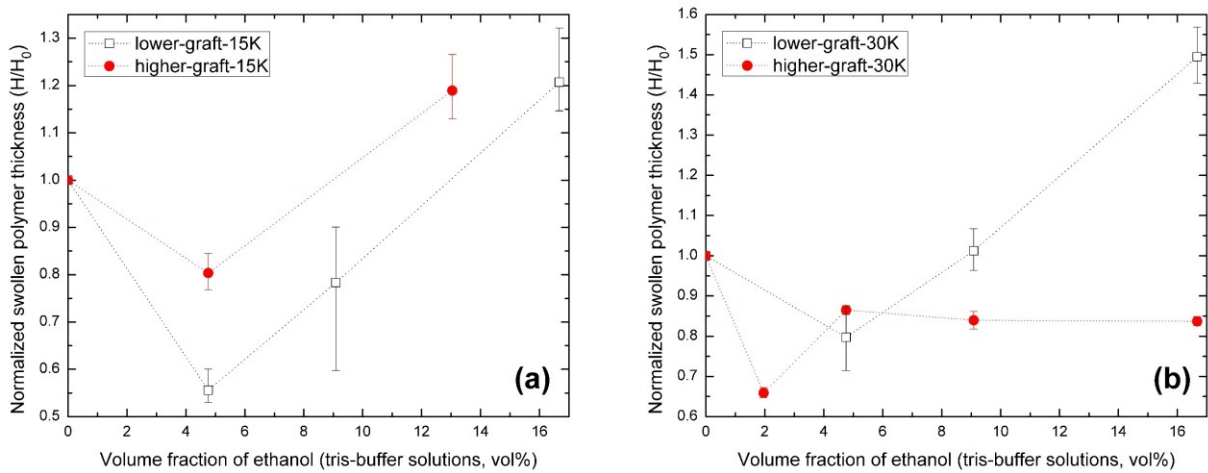
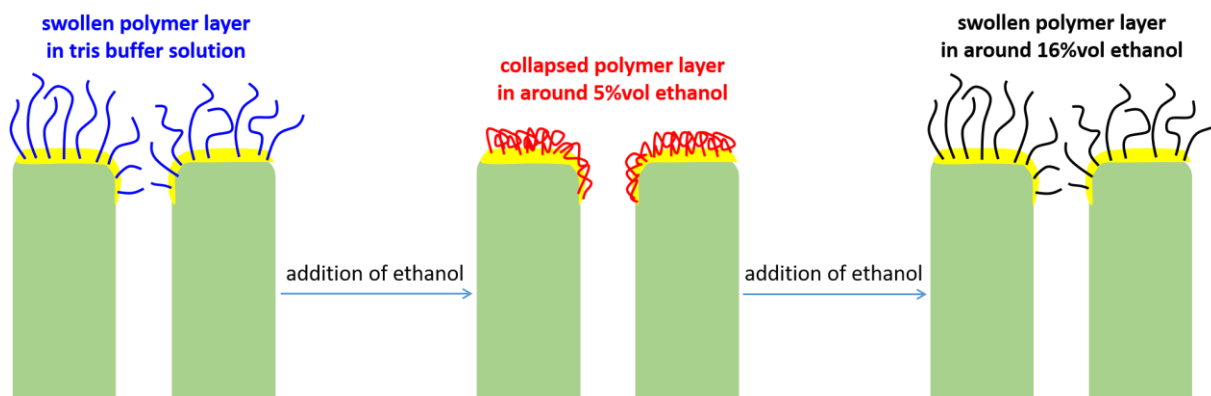


Figure 4.9(Figure 54) Ethanol-concentration responsive of grafted PNiPAAm polymer around the rim of nanopores. (a) Different grafting-density membranes with molecular weight of $M_n = 1.5 \times 10^4$ g/mol, $M_w/M_n = 1.18$; (b) Different grafting-density membranes with molecular weight of $M_n = 3.0 \times 10^4$ g/mol, $M_w/M_n = 1.25$. The size of nanopores is 50 nm and test temperature is 298 K. Note that the dotted lines in the figures are guides to eyes.

As for the phase behaviors of polymer chains with very low-grafting density as shown in **Figure 4.9b**, a decrease of grafting density weakens the collapse regarding the normalized swollen polymer thickness, this is quite different from brush behaviors as shown in **Figure 4.9a**. These observations are manifestations that phase behaviors of grafted polymers in a collapsed state (poor-solvent state) can be quite different from free polymers in solutions. Merely with a decrease of a grafted PNiPAAm polymer's grafting density, the swollen polymer chains can show various morphologies

such as collapsed brush, vertical phase segregation (coexistence of two phases) at a poor-solvent state, octopus-shape micelle and collapsed globule [51, 52]. In **Figure 4.9**, it is interesting to observe in my current experimental data that the grafting density has only a very small effect on the solvent-composition location of the maximum collapsed state, it doesn't matter whether or not the polymer layer is located in the brush regime; this phenomenon is also observed for polymer layers which are grafted on the flat surface. The observation in **Figure 4.9** is consistent with my previous study which investigated grafting-density effect for the cononsolvency transition of grafted PNiPAAm polymers on flat surfaces in ethanol-water mixtures, see **section 2.10** and **section 2.11** of **Chapter 2**.



Scheme 4.2(Figure 55) A depiction of ethanol-concentration induced phase transition of PNiPAAm layer around the rim of nanopore under the condition of flow pressure.

4.3.3 Switching effect of polymer brushes on the flat surface in the tri-buffer/ethanol mixtures

Although my DNA translocation experiments clearly indicated that the grafted PNiPPAm polymers around the rim of nanopores show signatures of re-entrant and switchable effect with respect to ethanol concentration, it is not clear whether these signatures are equilibrium behaviors, since my DNA translocation experiment is a kind of somewhat quasi-equilibrium method. Actually, few experiments reported that poly(N-n-propylacrylamide) [162] and PNiPAAm [163] show non-equilibrium phase-transition behaviors in the alcohol/water mixtures. To further check my observations in DNA translocation experiments, we used a well-developed in-situ Vis-spectroscopic ellipsometry method to study equilibrium swollen thickness of PNiPAAm brushes in ethanol/tris-buffer mixtures. The details of conducting ellipsometry experiments were already reported in my previous studies, see **section 2.2.3** of **Chapter 2**.

Typical real-time measurements of in-situ Vis-spectroscopic ellipsometry for swollen brush thickness of PNiPAAm in tris-buffer/ethanol mixtures are shown in **Figure 4.10a**. A summary of swollen thickness of polymer brushes with respect to ethanol concentration at various pH values of the buffer solution is plotted in **Figure 4.10b**. The ellipsometry study clearly indicates that PNiPAAm brushes show collapse behaviors with respect to an increase of ethanol concentration. As in cases of neutral and basic buffer solution, Figure 9b also indicates that at high concentration of ethanol, PNiPAAm brushes also show re-entrant behaviors, while in acidic buffer solutions this behavior disappears, currently the reason behind this difference is still unclear.

These ellipsometry observations qualitatively cross verified my DNA translocation experiments. However, it is also clear that the phase-transition window detected by translocation experiments through nanopores under non-equilibrium conditions differs from the phase-transition window detected by ellipsometry experiments in equilibrium. The main reason for this discrepancy may be attributed to the fact that the brush is subject to flow fields, osmotic pressure induced by the translocating DNA and hydrostatic pressure effects. From the theoretical description of the cononsolvency transition in brushes and in solutions [23, 24], it is known that densification of the polymer due to external forces shifts the cononsolvency transition to smaller cosolvent concentrations. What is more, it is remarkable that despite of the shift in the transition window, the reduction of relative height in the flat brush corresponds the change of the radius of the polymer-grafted nanopore when the grafting density is at the same level, see data of black squares in **Figure 4.9a** and red circles in **Figure 4.10b**, this can be analytically predicted by my previous theoretical studies for brush layers, see **Chapter 3**.

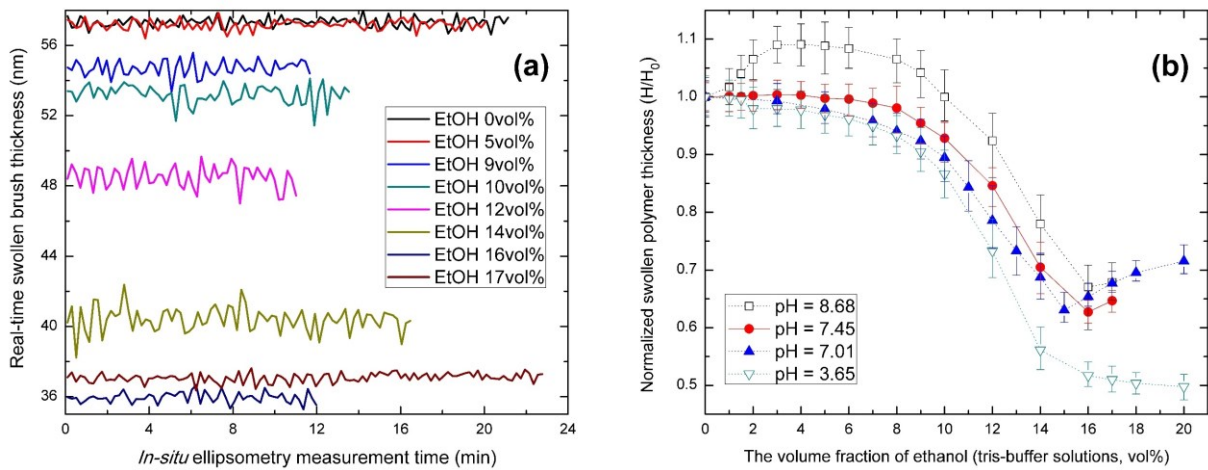


Figure 4.10(Figure 56) Swollen brush thickness of a PNiPAAM brush on a flat surface in ethanol/tris buffer mixtures. (a) Real-time swollen brush thickness of the PNiPAAM brush as a function of measurement time, pH value of the buffer is 7.45. (b) Average swollen brush thickness as a function of ethanol concentration obtained via in-situ Vis-ellipsometry at different pH values of buffer solutions. Parameters of the PNiPAAM brush are grafting density $0.143 \text{ chains/nm}^2$, $M_n = 6.1 \times 10^4 \text{ g/mol}$, and $M_w/M_n = 1.40$. Measurement temperature is at 25°C , note that the dotted lines in the Figure 4.10b are guides to eyes.

In **Chapter 3**, we have presented a thermodynamic model to understand the effect of huge hydrostatic pressure on the cononsolvency transition which also indicates a shift to smaller cosolvent concentrations. The fact that an increase of hydrostatic pressure (it is about equaling to an increase of flow pressure in this study) reduces the cosolvent chemical potential (μ). Based on my previous theoretical discussion, see **section 3.4.4** of **Chapter 3**, a reduction of cosolvent chemical potential (μ) further shifts the collapse state to a position where the cosolvent concentration is significantly lower. A reduction of cosolvent chemical potential (μ) by flow pressure is about, also see **Eq.(3.15)** and **Eq.(3.34)**,

$$\Delta\mu \simeq \frac{\Delta P \Delta V_m}{RTx}, \quad (4.6)$$

where ΔP is the increase of pressure on the polymer layer, ΔV_m is the excess molar volume of mixing cosolvent and solvent, R is the gas constant and T is the temperature, x is the cosolvent's molar fraction in solvent mixtures. In my DNA translocation experiments, it is expected that the hydrostatic pressure on the polymer layer which is grafted around the rim of nanopores (see **Scheme 4.1**), is significantly smaller than the hydrostatic pressure which is applied to the side of membrane without polymer layer. In my experiments, the hydrostatic pressure applied by the equipment on the side of membrane without polymer layer is at the order of 2bar (or 2.0×10^5 Pa). For the collapsed state of polymer layer in absence of flow pressure, the molar fraction of cosolvent (ethanol) is about $x = 0.05$ (volume fraction is about 0.15, see **Figure 4.10b**). As a rather overestimated choice of parameters for the polymer layer, $\Delta P = 1.0 \times 10^5$ Pa (this value is significantly higher than an estimated flow pressure on the polymer layer by using Hagen-Poiseuille equation, which is close to atmospheric pressure), $\Delta V_m = -1.0 \times 10^{-6} \text{ m}^3/\text{mol}$ [138], we get $\Delta\mu \approx -0.001$. This shift ($\Delta\mu \approx -0.001$) is too small that can be neglected, thus hydrostatic-pressure effect on the solvent is trivial and would not be the reason for the shift of phase-transition window in this study.

4.3.4 An attempt of numerical fit of experimental data using the extended adsorption-attraction model

Because it is hard to know how to exactly estimate chemical potential (μ) of mixing ethanol with tris buffer solution, here we just naively used a lattice-like formula to calculate chemical potential μ of experimental data (**Figure 4.9a**),

$$\mu = \ln\left(\frac{x}{1-x}\right) + C, \quad (4.7)$$

where x is the molar fraction of ethanol in the mixtures and C is a parameter that it represents the chemical-potential shift of ethanol/tris buffer solutions from ideal mixing. In this thesis, C is chosen to be $C = 3$ to obtain a good fit performance between experimental data and the extended adsorption-attraction model (see **Chapter 3**), the volume fraction of ethanol ρ in the model is roughly estimated by lattice model,

$$\rho = \frac{\exp(\mu)}{1 + \exp(\mu)}. \quad (4.8)$$

It seems that the experimental data (**Figure 4.9a**) can be well fitted by the extended adsorption-attraction model, see **Figure 4.11**. It is remarkable that fit values of model parameters (**Table 4.2**) are quite close to my previous report for ethanol-water mixtures, see **Chapter 3**. It is worth pointing out that the value of $C = 3$ in **Eq.(4.7)** is chosen to be quite arbitrary, it is obvious that the approach of **Eq.(4.7)** and **Eq.(4.8)** distorted the real situation in an unknown way. An improvement can be realized by considering osmotic-pressure effect generated by flow pressure on the polymer layer.

Even though, one still needs to know how to exactly estimate chemical potential (μ) of mixing ethanol with tris buffer solution. Currently this task is impossible to be achieved on account of the fact that thermodynamic data of this system is still unavailable.

Table 4.2(Table 14) Fit parameters for the ethanol-tris buffer system (polymer brush, 298 K, Figure 4.11). We choose λ and ν from their experimental values. The first part of the value for $\lambda\chi_{cs}$ is estimated as its experimental value, the second part of the value for $\lambda\chi_{cs}$ is a correction to fit the experimental data. Experimental value of PNiPAAm-water interaction (χ_{ps}) is around 0.40.

Grafting density	λ	ϵ	ν	$\lambda\chi_{cs}$	χ_{ps}
0.15 chains/nm ²	3.2587	1.23	0.20	1.2443+0.50	0.40

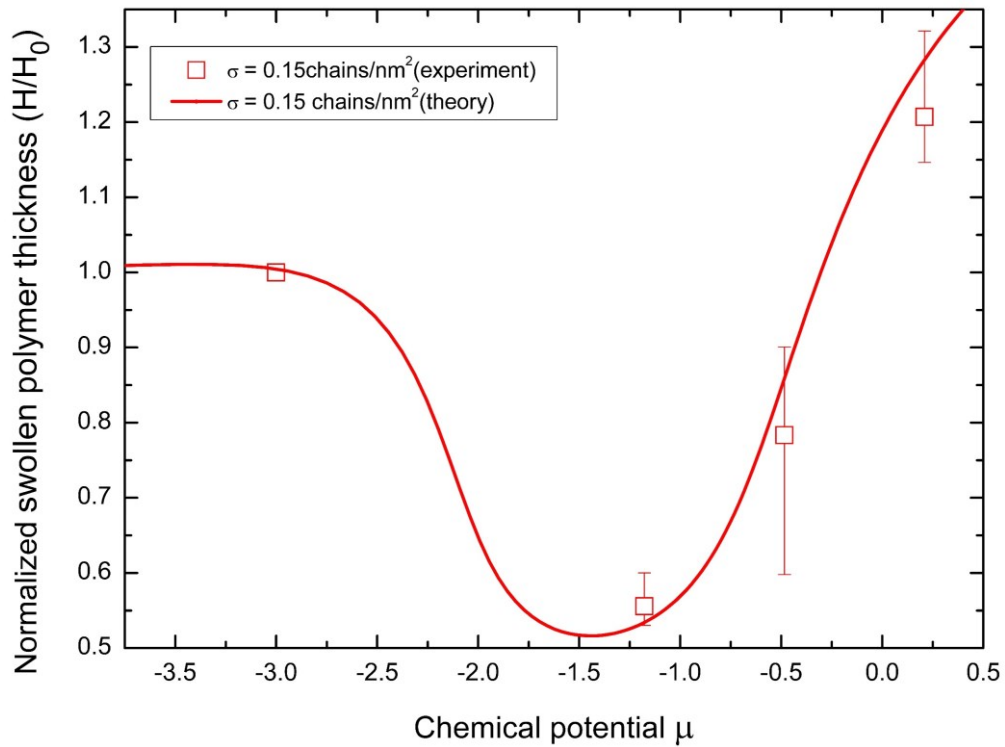


Figure 4.11(Figure 57) Cononsolvency responsive of grafted PNiPAAm polymer around the rim of nanopores. Molecular weight of the PNiPAAm polymer is $M_n = 1.5 \times 10^4$ g/mol, $M_w/M_n = 1.18$. The grafting density of polymer layers is around 0.15 chains/nm². The size of nanopores is 50 nm and the test temperature is 298 K.

4.4 Chapter summary

In this study, different molecular-weight PNiPAAm polymers are successfully grafted around the rim of solid-state nanopores by using grafting-to method. Regardless of chain length and grafting density of the grafted PNiPAAm polymers around the rim of nanopores, we demonstrate that small amounts of ethanol admixed to an aqueous solution can trigger the translocation of fluorescence DNA through polymer-decorated nanopores. We can identify the cononsolvency effect as being responsible for this observation which causes an abrupt collapse of the brush by increasing the alcohol content of the aqueous solution followed by a reswelling at higher alcohol concentration.

For the first time, we provide a quantitative method to estimate hydrodynamic thickness of a polymer layer which is grafted around the rim of nanopores. Regardless of the grafting density of a grafted PNiPAAM polymer layer around the rim of nanopores, in the alcohol-tris buffer mixtures, the polymer layer displays solvent-composition responsive behaviors in the range of metabolic pH values and room temperatures.

Although in this study PNiPAAM was chosen as a model synthetic polymer, we believe in that the conclusions made for PNiPAAM can be also in general extended to other synthetic polymers as well as to biopolymers such as gelatin [161] and elastin-like polypeptides [164]. As a proof of concept of using synthetic polymers to mimic biological functions of cell-membrane channels such as protein-induced transient pores in lipid membranes [165], my study clearly transpired that cononsolvency effect of polymers can be used as a novel trigger [166] to change the size of nanopores in analogy to the opening and closure of the gates of cell-membrane channels. What is more, in an application perspective, my study also shows that cononsolvency-controlled dynamic barrier on the nanoscale provides a new pathway for biomolecular separation and analysis such as ultra-filtration [167].

4.5 Chapter appendix

4.5.1 An estimation of grafting density

As for a grafted polymer layer, if it is in the brush regime, the following relation shall hold:

$$\begin{aligned} H_{swell} &\approx \frac{N}{g} D_{blob}, \\ D_{blob} &\approx \alpha g^{\nu_1} \end{aligned} \quad (4.9)$$

where H_{swell} is the swollen thickness of polymer layer, D_{blob} is the thermal blob size, g is the number of monomers in a thermal blob, and $\nu_1 = 0.588$ is the Flory exponent for a polymer chain in a good solvent. It is also noted that

$$D_{blob} \approx S = \frac{1}{\sqrt{\sigma}}. \quad (4.10)$$

Substitute Eq.(4.10) into Eq.(4.9), we get

$$\sigma \approx \left(\frac{H_{swell}}{N \alpha^{\frac{1}{\nu_1}}} \right)^{\frac{2\nu_1}{1-\nu_1}}. \quad (4.11)$$

Here, it is worth pointing out that Eq.(4.11) can be approximately used to determine a polymer layer's grafting density if we cannot directly measure thickness of a dry polymer layer, see Eq.(2.1) of Chapter 2.

4.5.2 The method of processing data

The mean value of DNA translocation event (N_{DNA}) is

$$N_{DNA} = \frac{1}{n} \sum_i^n N_{DNA,i} . \quad (4.12)$$

The error bar of DNA translocation event (ΔN_{DNA}) in this study is defined as its average absolute deviation instead of popular used standard deviation, because one could not naïvely assume that the data sample must comply to a “bell-shaped” statistical distribution such as Gaussian distribution. Another problem for standard deviation is that the population number of the data sample should not be too small (a general requirement is larger than 50). The average absolute deviation doesn't require a data sample to comply to a specific statistical distribution and doesn't have a restriction on population number in a data sample,

$$\Delta N_{DNA} = \frac{1}{n} \sum_{i=1}^n |N_{DNA,i} - N_{DNA}| . \quad (4.13)$$

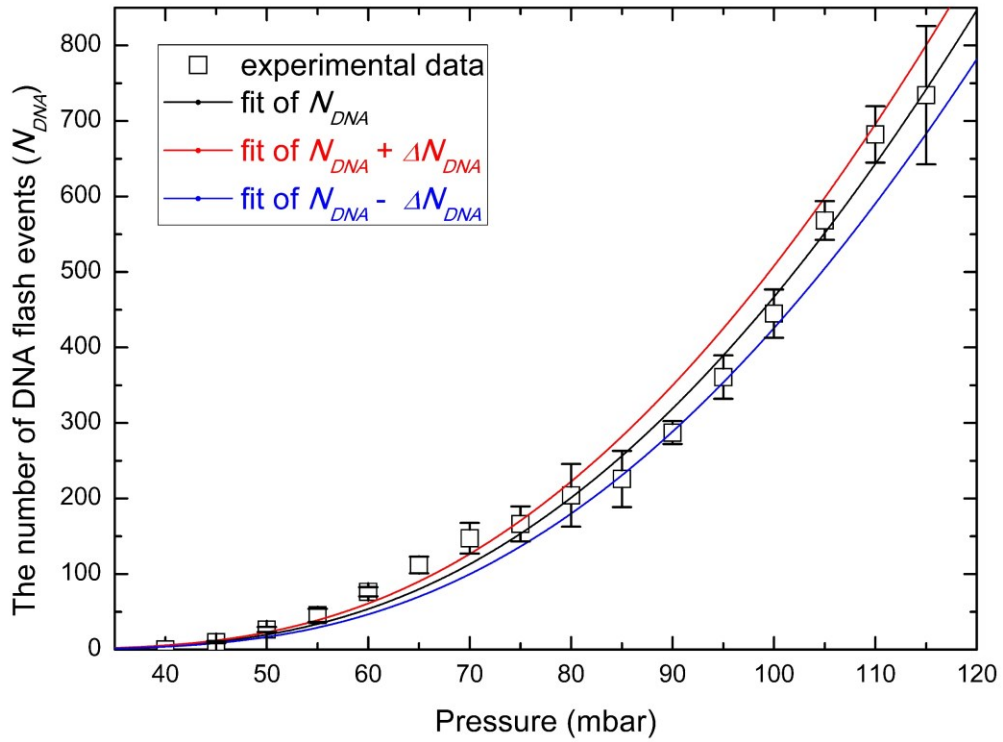


Figure 4.12(Figure 58) A graphic description how to get an error bar (ΔP_c) of a critical pressure by using Eq.(4.14).

The critical pressure (P_c) can be obtained by fitting the nonlinear equation Eq.(4.5), we rewrite it here,

$$N_{DNA} = k_3 \left(\frac{P}{P_c} \right) \exp \left(-\frac{P_c}{P} \right), \quad (4.14)$$

where P is the gradient of pressure applied in experiments. In practice, when P/P_c is small, **Eq.(4.14)** reduces to a linear equation,

$$N_{DNA} = \frac{k_3}{P_c} P - k_3. \quad (4.15)$$

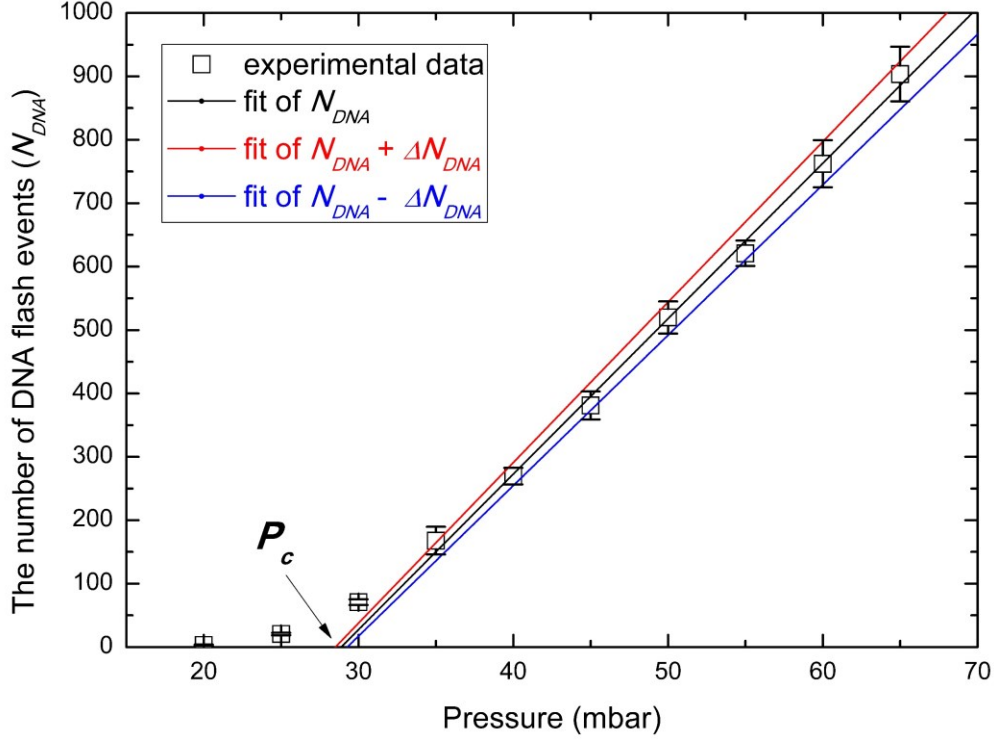


Figure 4.13(Figure 59) A graphic description how to get an error bar (ΔP_c) of a critical pressure by using **Eq.(4.15)**.

Therefore, a linear fit procedure of **Eq.(4.15)** is preferable when the data show an asymptotic linear behaviour between DNA translocation event (N_{DNA}) and the pressure (P), otherwise a non-linear fit procedure of **Eq.(4.14)** is a necessary choice. Note that k_1 in **Eq.(4.14)** and **Eq.(4.15)** is a constant for a given system. The key to get an error bar (ΔP_c) of the critical pressure is to use $N_{DNA} + \Delta N_{DNA}$, $N_{DNA} - \Delta N_{DNA}$ and N_{DNA} to fit **Eq.(4.14)** and **Eq.(4.15)**. **Figure 4.12** and **Figure 4.13** are examples of determining an error bar of a critical pressure by using **Eq.(4.14)** and **Eq.(4.15)**, respectively. In a practice of numerical fit procedures, the extrapolated values of critical pressure (P_c) by using **Eq.(4.14)** and **Eq.(4.15)** can be quite different, this phenomenon is an artefact. In physics, critical pressure (P_c) has to be always unique for a given system, therefore, to get a reasonable absolute value of critical pressure (P_c), a LINEAR fit of **Eq.(4.14)** should be always considered first. However,

it is also worth pointing out that when we follow the same equation (Eq.(4.14) or Eq.(4.15)) to process data, the estimated sizes of nanopores don't have obvious difference (Eq.(4.3)). This is because in Eq.(4.3), the ratio ($P_{c,0} / P_{c,eff}$) is independent of choosing Eq.(4.14) or Eq.(4.15).

Chapter 5 Concluding remarks and outlooks

5.1 *Concluding remarks*

Cononsolvency occurs if a mixture of two good solvents causes the collapse or demixing of polymers into a polymer-rich phase in a certain range of compositions of these two solvents. The better solvent is usually called cosolvent and another common solvent is called solvent. In this thesis, I experimentally investigated the cononsolvency effect of poly(*N*-isopropylacrylamide) (PNiPAAm) brushes at different grafting densities in aqueous alcohol mixtures. I have used Vis-spectroscopic ellipsometry measurements and proved the hypothesis that the cononsolvency transition of PNiPAAm brushes occurs as a volume phase-like equilibrium transition.

I found a strong collapse transition in PNiPAAm brushes followed by a reentry behavior as observed by ellipsometry measurements. Using a series of alcohols with increasing alkyl-chain length I have demonstrated that the cononsolvency effect is enhanced and shifted to smaller volume fractions of the alcohol. Particularly for the alcohol with increasing hydrophobic property this is correlated with an increasing tendency of demixing between the cosolvent and water. This is apparently in contrast to the hypothesis of strongly associative solvents being the origin of the cononsolvency effect. The hypothesis of preferential adsorption, on the other hand, can account for this case by assuming an increasing hydrophobically driven adsorption of the cosolvent on the polymer chains. The recently proposed adsorption-attraction model based on the concept of preferential adsorption, can be used to predict the corresponding phase-transition behavior. In particular the model predictions for variations of the grafting density is in agreement with the experimental findings. However, to reflect the imperfect mixing of the longer alcohols in water as well as finite miscibility of the polymers in the common solvent, extensions of the model have to be considered. I have shown that the simplest extension of the model taking into account the Flory-Huggins parameter for polymer and water can account for the qualitative changes observed for temperature changes in my experiments.

However, hydrophobically-driven preferential adsorption can be merely the phase-transition mechanism for cononsolvency transition of LCST polymers in organic solvent's aqueous solutions where the organic solvent is a better solvent. When water becomes a better solvent in cononsolvency transition, such as for cases of poly(*N*, *N*-dimethylacrylamide) and poly(2-(methacryloyloxy)ethyl phosphorylcholine) in alcohol-water mixtures, a preferential adsorption of water rather than alcohol should be considered as a candidate of phase-transition mechanism of cononsolvency transition. As for these cases, it may be suitable that the rationalization of preferential adsorption which is based on the competition between the two solvents in forming hydrogen bonds with the polymers.

Both a theoretical analysis and experimental observations show that the phase-transition mechanism of cononsolvency depends on the relative strengths of various interactions in the polymer solutions. A cononsolvency transition can be driven by a strong cosolvent-solvent attraction or by

the preferential adsorption of cosolvent onto the polymer. By an extension of the adsorption-attraction model, I report on a comprehensive and quantitative theoretical study of the cononsolvency effect of neutral polymers such as PNiPAAm brushes, macro-gels and single long chains. The extended adsorption-attraction model is able to describe and predict the phase-transition behaviors of PNiPAAm brushes, gels and long single chain in various aqueous alcohol solutions quantitatively. My analysis showed that besides the dominant roles of polymer-cosolvent preferential adsorption and the monomer-cosolvent-monomer triple contacts (cosolvent-assisted temporary cross-linking effect) that define the strength of the collapse-transition in the cosolvent-poor region, other effects are shown to be of relevance: The non-ideal mixing between polymer and solvent plays a role in shifting the collapse transition to the lower-concentration region of cosolvent, and an increase of the demixing tendency between cosolvent and solvent on the polymer chains reduce the width of the cononsolvency transition. Using data from my own experiments and literature I can show that the cononsolvency response of brushes, gels and single long polymer chain can be consistently described with the same model. Thus, also the swelling/deswelling behavior of PNiPAAm gels and single long chains with respect to cononsolvency is quantitatively described in this work. The used parameters are consistent with their microscopic interpretation. In addition, weakening of the cononsolvency transition in cosolvent-poor aqueous solutions at high hydrostatic pressure can be explained by the suppression of demixing tendencies between cosolvent and water, and between polymer and water in the case of PNiPAAm.

I also found that a consistent understanding of the LCST behavior of PNiPAAm together with the cononsolvency effect can be addressed using the concepts presented in this work. It is noted that both LCST and cononsolvency transitions of PNiPAAm polymers show behaviors of a type-II phase transition where the third virial coefficient is negative but the second virial coefficient stays positive in the free energy expansion. The reason behind this general phenomenon can be attributed to the fact that PNiPAAm achieves LCST transition by a kind of water-depleted physical crosslinking (attraction) of its hydrophobic side chains, while the polymer achieves cononsolvency transition by a kind of cosolvent-assisted physical crosslinking (attraction) of its side hydrophobic chains. Therefore, both phase transitions can indeed overlap with each other when temperature varies in the PNiPAAm/cosolvent/water solutions, such as PNiPAAm in the alcohol-water mixtures. The overlap of water-depleted and cosolvent-assisted physical crosslinkings can explain the phenomenon where LCST transition of PNiPAAm in cosolvent-water mixtures is enhanced by an increase of cosolvent concentration in the cosolvent-poor region.

An investigation of the grafting-density effect in the cononsolvency transition of grafted PNiPAAm polymers, showed that a decrease of grafting density at the collapse state when the temperature is fixed, the swollen polymer chains can show various morphologies such as collapsed brush and maybe octopus-shape micelles. In addition, my experimental results clearly showed that the strongest collapsed state can be only realized by moderate-grafting-density polymer brushes. My results display the universal character of the cononsolvency effect with respect to series of cosolvents and show that PNiPAAm brushes display a well-defined and sharp collapse transition. This is most pronounced for 1-propanol as cosolvent which is still fully miscible in water. Thus, switches

built from implementation of brushes in pores and similar concave geometries can be realized by harnessing the cononsolvency effect of stimuli-responsive polymers such as PNiPAAm.

Therefore, in this thesis, as an example of application of cononsolvency effect of grafted polymers, different molecular-weight PNiPAAm polymers are successfully grafted around the rim of solid-state nanopores by using grafting-to method. I demonstrate that small amounts of ethanol admixed to an aqueous solution can trigger the translocation of fluorescence DNA through polymer-decorated nanopores. I can identify the cononsolvency effect as being responsible for this observation which causes an abrupt collapse of the brush by increasing the alcohol content of the aqueous solution followed by a reswelling at higher alcohol concentration. For the first time, I provide a quantitative method to estimate hydrodynamic thickness of a polymer layer which is grafted around the rim of nanopores. Regardless of the grafting density of a grafted PNiPAAm polymer layer around the rim of nanopores, in the alcohol-tris buffer mixtures, the polymer layer displays solvent-composition responsive behaviors in the range of metabolic pH values and room temperatures. Although in this study PNiPAAm was chosen as a model synthetic polymer, I believe in that the conclusions made for PNiPAAm can be also in general extended to other synthetic polymers as well as to biopolymers such as proteins. As a proof of concept of using synthetic polymers to mimic biological functions of cell-membrane channels, my study clearly transpired that cononsolvency effect of polymers can be used as a trigger to change the size of nanopores in analogy to the opening and closure of the gates of cell-membrane channels.

In this thesis, in the case of weak cosolvent-solvent attraction, experimental observations for cononsolvency transition are successfully explained by a concept of preferential adsorption of the cosolvent onto polymer chains, this phase-transition mechanism has been confirmed by my experimental studies. Even though, it is worthy of pointing out that, the interpretation of the experimental observations in this thesis also heavily relies on the central assumption of the cosolvent-assisted temporary crosslinking effect that dominates the cononsolvency transition. This central assumption has been directly confirmed by molecular-dynamic simulations and it is consistent with all available experimental observations to date; however, so far, it is still lacking direct evidence in experimental studies for the central assumption. A feasible experimental way to prove this central assumption, is that finding cononsolvency transition of LCST polymers such as poly(N-isopropylacrylamide) in binary mixtures of two good organic solvents (such as two different alcohols), as this is an expectation that implied by the central assumption; however, these topics are beyond the scope of this thesis.

5.2 Outlooks: A preliminary discussion of the cononsolvency transition of polymer solutions

It is reported [56] that poly (vinyl alcohol) shows sol-gel behaviors (percolation transition) in DMSO-water mixtures when the concentration of DMSO is low. This phenomenon in principle can be explained by the assumption of preferential adsorption of DMSO molecules on polymer chains and DMSO-assisted temporary crosslinking effect between monomers. If we use the adsorption-attraction model presented in **Chapter 2** and **Chapter 3**, these models will require a rather strong

cosolvent-assisted binding effect between monomers ($\gamma\varepsilon$) to explain the strong and discontinuous transition of the polymer solution in the cosolvent-poor region. This explanation is an artifact since the cosolvent-assisted binding effect between monomers is almost independent of the polymer's topological structures when the chemistry of the monomer, the cosolvent and the solvent are given. Therefore, it is necessary to recast the concept of preferential adsorption for the case of polymer solution, and to consider additional elastic energy to accounting for sol-gel behaviors.

The elastic energy on accounting of forming a network by “crosslinkers” (cosolvent) in polymer solutions is roughly approximated in terms of a free energy per monomer unit by:

$$f_{elastic} = \frac{\alpha}{2N_k} \left[\frac{3}{c^{\frac{2}{3}}} - 3 + \ln(c) \right], \quad (5.1)$$

where N_k is the average number of Kuhn segments between two crosslinks in the network structure, α is the fraction of elastically effective chains in the network and can be considered as a topological parameter characterizing the network structure. The right hand side of **Eq.(5.1)** arises in the Flory-Rehner approach **[113]** for a network, the last logarithmic term is the correction term due to the volume change of the network. For a phantom network model **[9]**, we have:

$$\alpha = \frac{f-2}{f}, \quad N_m = N_k \left(\frac{f-2}{f} \right) n_b, \quad (5.2)$$

where N_m is the total number of Kuhn segments in the gel structure, f is the linking degree (functionality) for one crosslinker (or junction), and n_b is the number of “crosslinkers” in the network:

$$\frac{n_b}{N_m} = 2\varphi(1-\varphi). \quad (5.3)$$

For real polymer chains, if two monomers are bridged by a cosolvent, the linking degree naturally equals 4, for this case, the most common example is the system of PNiPAAm/alcohol/water. However, on account of network defects in particular dangling ends, the effective value of f is quite close to but larger than 2 for a temporary crosslinker (junction). Substituting **Eq.(5.2)** and **Eq.(5.3)** into **Eq.(5.1)**, we get:

$$f_{elastic} = \alpha^2 \varphi(1-\varphi) \left[\frac{3}{c^{\frac{2}{3}}} - 3 + \ln(c) \right]. \quad (5.4)$$

The following entropic free energy contribution for mixing in the polymer solution, keeping other terms the same as in **Chapter 3**, yields:

$$f_{mix} = \frac{\ln(c)}{N} + \left(\frac{1}{c} - 1 - \nu\varphi \right) \ln(1-c-\nu\varphi c), \quad (5.5)$$

where the excess volume fraction in case of a full saturation of the polymer by cosolvent is given by ν , and N is the polymer chain length. The physical meaning of ν is that it describes the excluded-volume difference between the same monomer and the two good solvents. The first term in **Eq.(5.5)** is the translational mixing entropy of polymer chains in the solution.

It is noted that because of the non-linear coupling between cosolvent and monomers in the above model, no analytic solution exists for the general case. Even though, to get some analytic insights from the model, we consider a case but without losing generality, i.e., $\nu = 0$, $\chi_{ps} = 0$ and $\Delta\chi_{cs} = 0$, we rewrite the model as:

$$f(\varphi, c) = \frac{\varphi}{\lambda} \ln(\varphi) + (1-\varphi) \ln(1-\varphi) - \mu\varphi - \varepsilon \frac{\varphi}{\lambda} + \chi_{cs}\varphi(1-\varphi) - 2\gamma\varepsilon\varphi(1-\varphi)c + \frac{\ln(c)}{N} + \left(\frac{1}{c} - 1\right) \ln(1-c) + \alpha^2\varphi(1-\varphi) \left[\frac{3}{c^{\frac{2}{3}}} - 3 + \ln(c) \right]. \quad (5.6)$$

In **Eq.(5.6)** the symmetry $\varphi \rightarrow 1-\varphi$ is only broken by the adsorption constant $\mu + \varepsilon/\lambda$. Obviously, the maximum contraction of the single polymer chain is reached for the case $\varphi \rightarrow 1/2$, where the temporary crosslinking effect reaches its maximum. We introduce the deviation from this half occupation of the chain by cosolvent by the variable δ defined by

$$\varphi = \frac{1}{2}(1-\delta). \quad (5.7)$$

Ignoring constant terms, under the constraint of $|\delta| < 0.3$ we obtain

$$f(\delta, c) \simeq -\frac{1}{2}\gamma\varepsilon(1-\delta^2)c + \frac{1}{4}\alpha^2(1-\delta^2) \left[\frac{3}{c^{\frac{2}{3}}} - 3 + \ln(c) \right] + \frac{1}{4}\chi_{cs}(1-\delta^2) + \frac{\ln(c)}{N} + \left(\frac{1}{c} - 1\right) \ln(1-c) + \frac{1}{2}\left(1 + \frac{1}{\lambda}\right)\delta^2 + \frac{1}{2}\left(1 - \frac{1}{\lambda} + \frac{\ln 2}{\lambda} - \ln 2\right)\delta + \frac{1}{2}\left(\mu + \frac{\varepsilon}{\lambda}\right)\delta. \quad (5.8)$$

The coupling of cosolvent with the single chain, the first and second terms in **Eq.(5.8)**, favors half-occupation of the polymer chain by the cosolvent (smaller value of $\delta \rightarrow 0$) because this leads to a maximum energy gain by sharing cosolvents. Minimizing the free energy in **Eq.(5.8)** with respect to δ yields

$$\gamma\varepsilon\delta c - \frac{\alpha^2}{2} \left[\frac{3}{c^{\frac{2}{3}}} - 3 + \ln(c) \right] \delta - \frac{1}{2}\chi_{cs}\delta + \left(1 + \frac{1}{\lambda}\right)\delta + \frac{1}{2}\left(1 - \frac{1}{\lambda} + \frac{\ln 2}{\lambda} - \ln 2\right) + \frac{1}{2}\left(\mu + \frac{\varepsilon}{\lambda}\right) = 0. \quad (5.9)$$

The equilibrium condition with respect to δ thus yields

$$\delta = -\frac{\frac{1}{2}\left(\mu + \frac{\varepsilon}{\lambda}\right) + \frac{1}{2}\left(1 - \frac{1}{\lambda} + \frac{\ln 2}{\lambda} - \ln 2\right)}{\gamma\varepsilon c - \frac{\alpha^2}{2} \left[\frac{3}{c^{\frac{2}{3}}} - 3 + \ln(c) \right] + \left(1 + \frac{1}{\lambda}\right) - \frac{1}{2}\chi_{cs}}. \quad (5.10)$$

Minimizing the free energy in **Eq.(5.8)** with respect to polymer concentration (c) reads

$$\delta^2 = 1 - \frac{c + \ln(1-c) - \frac{c}{N}}{\frac{\alpha^2}{4} \left(-2c^{\frac{1}{3}} + c \right) - \frac{1}{2} \gamma \varepsilon c^2}. \quad (5.11)$$

The formal solution for the equilibrium concentration of the polymer chain can be obtained implicitly using Eq.(5.10) and Eq.(5.11) by introducing the adsorption field, U , in the following form:

$$U = \frac{1}{4} \left(\mu + \frac{\varepsilon}{\lambda} + 1 - \frac{1}{\lambda} + \frac{\ln 2}{\lambda} - \ln 2 \right)^2. \quad (5.12)$$

Notice that with Eq.(5.10) and Eq.(5.11), we have an analytic construction for the adsorption field, U ,

$$U = \left\{ \gamma \varepsilon c - \frac{\alpha^2}{2} \left[\frac{3}{c^{\frac{2}{3}}} - 3 + \ln(c) \right] + \left(1 + \frac{1}{\lambda} \right) - \frac{1}{2} \chi_{cs} \right\}^2 \times \left[1 - \frac{c + \ln(1-c) - \frac{c}{N}}{\frac{\alpha^2}{4} \left(-2c^{\frac{1}{3}} + c \right) - \frac{1}{2} \gamma \varepsilon c^2} \right]. \quad (5.13)$$

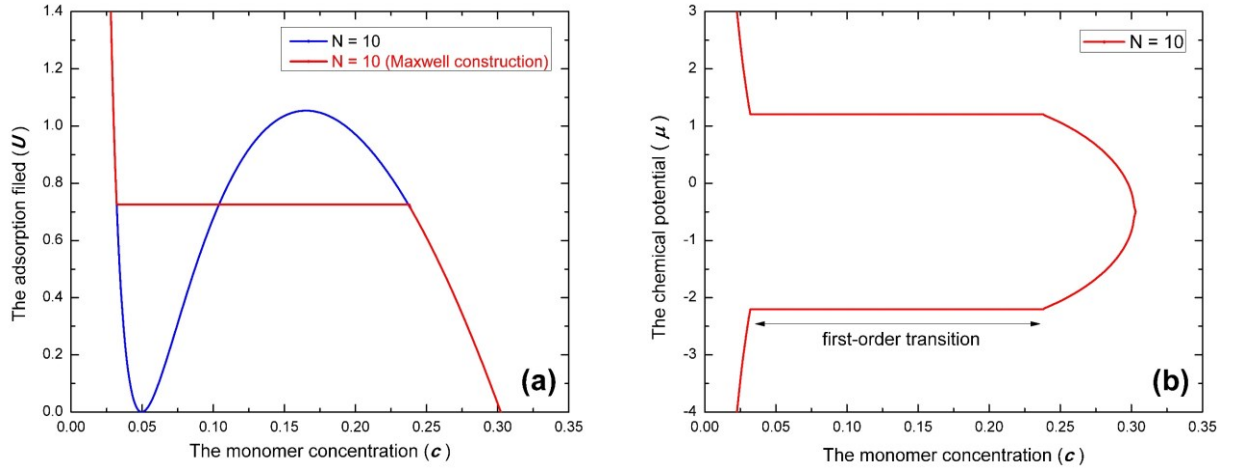


Figure 5.1 (Figure 60) (a) The adsorption field (U), is displayed as a function of monomer concentration (c). (b) The monomer concentration (c) is displayed as a function of chemical potential change of the cosolvent, μ . Model parameters used in the calculation are: $N = 10$, $\lambda = 1.0$, $\nu = 0$, $\gamma = 1.0$, $f = 4.0$, $\varepsilon = 0.5$, $\lambda \chi_{cs} = 0$, $\Delta \chi_{cs} = 0$ and $\chi_{ps} = 0$.

The symmetry of the simplified model, see Eq.(5.6), with respect to low and high cosolvent density transitions is captured by the fact that U represents the square of a function of cosolvent density with two solutions of chemical potential μ . It is noted that the function U , with respect to monomer concentration (c), always has a local minimum and a local maximum even for a very weak cosolvent-assisted binding effect between monomers ($\gamma \varepsilon$) and a very short polymer chain (N). This means that the true equilibrium results have to be obtained by the Maxwell construction through the instability; because for a given solvent composition (represented by solvent chemical potential μ), in the cononsolvency transition of polymer solutions, based on the phase rule, the system cannot have three coexisting equilibrium monomer concentrations (three coexisting phases). In Figure 5.1a,

as an example, we display the function U with respect to monomer concentration (c) and its Maxwell construction through the instability.

It is well accepted that an existence of a Maxwell construction is an indication of the first-order phase transition for a system [168], therefore, this indicates that the formulation of Eq.(5.8) for temporary network elastic energy indeed correctly captures sol-gel behaviors (percolation transition) of cononsolvency transition of polymer solutions such as poly (vinyl alcohol) in DMSO-water mixtures [56] when the concentration of DMSO is low. In Figure 5.1b, we show the analytical solution for the true equilibrium monomer concentration (c) with respect to solvent chemical potential (μ). The physical model also predicts that when the repulsion interaction between cosolvent and solvent becomes stronger, the range of cosolvent concentration for the collapse state of cononsolvency transition becomes narrower, see Figure 5.2; this prediction is already observed by studying cononsolvency of poly(vinylpyrrolidone) solutions in methanol-water and ethanol-water mixtures [64, 65].

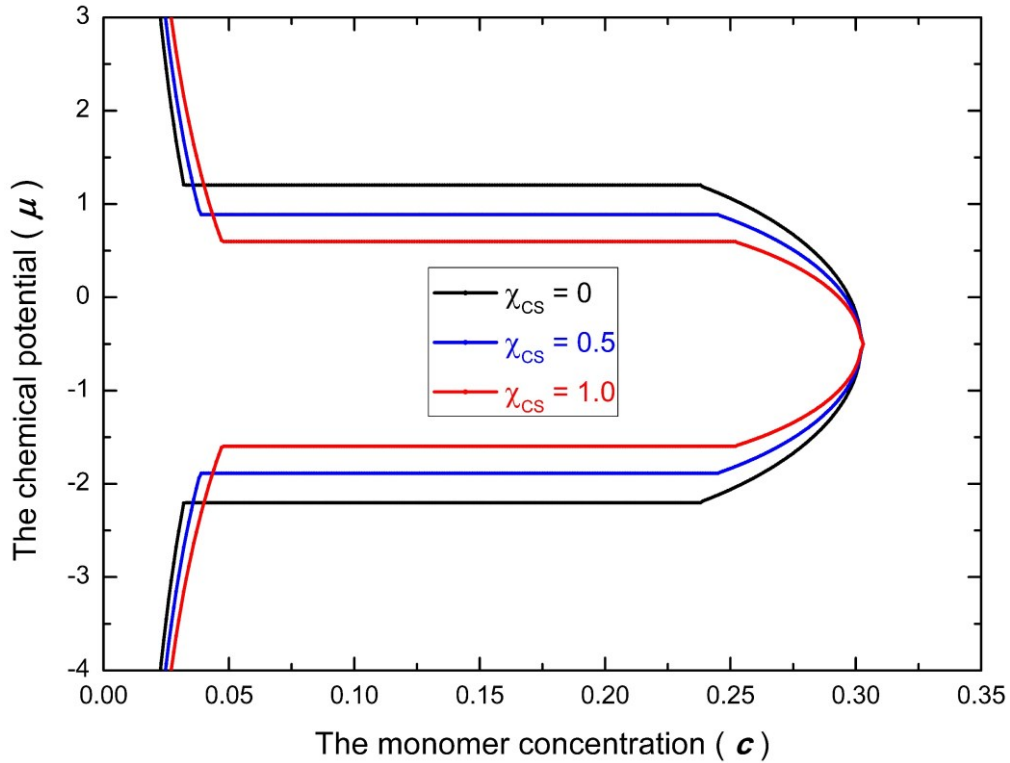


Figure 5.2(Figure 61) Illustration of the impact of cosolvent-solvent interaction on the predicted cononsolvency response of polymer solution. The monomer concentration (c) is displayed as a function of chemical potential change of the cosolvent, μ : A change of cosolvent-solvent interaction χ_{CS} , while other model parameters remained fixed as $N = 10$, $\lambda = 1.0$, $\nu = 0$, $\gamma = 1.0$, $f = 4.0$, $\varepsilon = 0.5$, and $\chi_{ps} = 0$.

On the one hand, it is noted that in a previous theoretical study [24] which discussed the cononsolvency transition of confined polymer solutions, an osmotic pressure per monomer (Π/c) was used to account for osmotic-pressure effects where only solvents can permeate through a membrane. The physical constraint of the study [24] is a little different from my current discussion which is for

unconfined polymer solutions. Even though, it is worth pointing out that polymer chains are confined by a membrane, the process of preferential adsorption of cosolvent onto polymer chains and cosolvent-assisted physical crosslinking between monomers would not differ much between confined and unconfined polymer solutions, since solvents molecules can go freely through the membrane and are adsorbed by polymer chains. The theoretical study [24] obviously underestimated the free energy of the confined polymer solutions, since the existence of network elastic energy is ignored. It is still questionable whether or not the theoretical approach of ref.[24] can even be applied to describe confined polymer solutions such as cytoplasm, where biomaterials such as RNA and proteins can aggregate and form network-like structures/aggregations [169, 170].

On the other hand, it is worth pointing out that my current approach (Eq.(5.4)) generates some unrealistic results. For example, if the value of cosolvent-assisted binding effect between monomers ($\gamma\varepsilon$) is chosen to be zero and other model parameters are kept the same as in Figure 5.1, the function U which is with respect to monomer concentration (c) still has a local minimum and a local maximum. This is unphysical, since if there is no preferential adsorption for two good solvents on the polymer chains, the solvent mixtures should behave like a conventional good solvent and there is no phase transition at all in this situation. Obviously, the current approach of Eq.(5.4), over-estimates the elastic energy of forming a network by “crosslinkers” (cosolvent) in polymer solutions. In mathematics, this issue can be overcome by an interpolation of combining Eq.(5.4) and Eq.(3.8) for network elastic energy, however, this naïve approach lacks of any physical foundation and should not be pursued. A further study which has a sound physical foundation is particularly needed in order to eliminate or at least mitigate these unrealistic side effects.

A further investigation on cononsolvency transition of polymer solutions and related systems is beyond the scope of this thesis, it will be discussed in another independent study.

References and notes

- [1] W.M. Babinchak, W.K. Surewicz, Liquid-Liquid Phase Separation and Its Mechanistic Role in Pathological Protein Aggregation, *Journal of Molecular Biology*, 432 (2020) 1910-1925.
- [2] S.F. Banani, A.M. Rice, W.B. Peeples, Y. Lin, S. Jain, R. Parker, M.K. Rosen, Compositional Control of Phase-Separated Cellular Bodies, *Cell*, 166 (2016) 651-663.
- [3] A.A. Hyman, C.A. Weber, F. Julicher, Liquid-liquid phase separation in biology, *Annual Review of Cell and Developmental Biology*, 30 (2014) 39-58.
- [4] Y. Shin, C.P. Brangwynne, Liquid phase condensation in cell physiology and disease, *Science*, 357 (2017).
- [5] P. Atkins, J.d. Paula, *Physical Chemistry* (9th Edition), W. H. Freeman Company, New York, 2009.
- [6] H. Falahati, A. Haji-Akbari, Thermodynamically driven assemblies and liquid-liquid phase separations in biology, *Soft Matter*, 15 (2019) 1135-1154.
- [7] P.J. Flory, Thermodynamics of High Polymer Solutions, *The Journal of Chemical Physics*, 9 (1941) 660-660.
- [8] M.L. Huggins, Solutions of Long Chain Compounds, *The Journal of Chemical Physics*, 9 (1941) 440-440.
- [9] M. Rubinstein, R.H. Colby, *Polymer Physics*, Oxford University Press, Oxford, 2003.
- [10] J.-M. Choi, A.S. Holehouse, R.V. Pappu, Physical Principles Underlying the Complex Biology of Intracellular Phase Transitions, *Annual Review of Biophysics*, 49 (2020).
- [11] P.-G. de Gennes, Polymers at an interface: a simplified view, *Advances in Colloid and Interface Science*, 27 (1987) 189-209.
- [12] D. Romeis, J.U. Sommer, Binary and Bidisperse Polymer Brushes: Coexisting Surface States, *ACS Applied Materials & Interfaces*, 7 (2015) 12496-12504.
- [13] S. Qi, L.I. Klushin, A.M. Skvortsov, M. Liu, J. Zhou, F. Schmid, Tuning Transition Properties of Stimuli-Responsive Brushes by Polydispersity, *Advanced Functional Materials*, 28 (2018) 1800745.
- [14] D. Mukherji, C.M. Marques, T. Stuehn, K. Kremer, Depleted depletion drives polymer swelling in poor solvent mixtures, *Nature Communications*, 8 (2017) 1374.
- [15] R. Wang, Z.-G. Wang, Theory of Polymers in Poor Solvent: Phase Equilibrium and Nucleation Behavior, *Macromolecules*, 45 (2012) 6266-6271.
- [16] R. Wang, Z.-G. Wang, Theory of Polymer Chains in Poor Solvent: Single-Chain Structure, Solution Thermodynamics, and Θ Point, *Macromolecules*, 47 (2014) 4094-4102.
- [17] A. Halperin, M. Kröger, F.M. Winnik, Poly(N-isopropylacrylamide) Phase Diagrams: Fifty Years of Research, *Angewandte Chemie International Edition*, 54 (2015) 15342-15347.
- [18] C. Scherzinger, A. Schwarz, A. Bardow, K. Leonhard, W. Richtering, Cononsolvency of poly-N-isopropyl acrylamide (PNIPAM): Microgels versus linear chains and macrogels, *Current Opinion in Colloid & Interface Science*, 19 (2014) 84-94.

- [19] M.G. Opferman, R.D. Coalson, D. Jasnow, A. Zilman, Morphological control of grafted polymer films via attraction to small nanoparticle inclusions, *Physical Review E*, 86 (2012) 031806.
- [20] M.G. Opferman, R.D. Coalson, D. Jasnow, A. Zilman, Morphology of polymer brushes infiltrated by attractive nanoinclusions of various sizes, *Langmuir*, 29 (2013) 8584-8591.
- [21] J. Shi, F. Yan, C. Wang, S. King, Y. Qiao, D. Qiu, Conformational Transitions of Dynamic Polymer Chains Induced by Colloidal Particles in Dilute Solution, *Macromolecules*, 53 (2020) 3052-3058.
- [22] V.A. Baulin, A. Halperin, Signatures of a Concentration-Dependent Flory χ Parameter: Swelling and Collapse of Coils and Brushes, *Macromolecular Theory and Simulations*, 12 (2003) 549-559.
- [23] J.-U. Sommer, Adsorption–Attraction Model for Co-Nonsolvency in Polymer Brushes, *Macromolecules*, 50 (2017) 2219-2228.
- [24] J.-U. Sommer, Gluonic and Regulatory Solvents: A Paradigm for Tunable Phase Segregation in Polymers, *Macromolecules*, 51 (2018) 3066-3074.
- [25] O. Matsarskaia, F. Roosen-Runge, F. Schreiber, Multivalent ions and biomolecules: Attempting a comprehensive perspective, *Chemphyschem*, 21 (2020) 1742-1767.
- [26] S. Kumar, I. Yadav, D. Ray, S. Abbas, D. Saha, V.K. Aswal, J. Kohlbrecher, Evolution of Interactions in the Protein Solution As Induced by Mono and Multivalent Ions, *Biomacromolecules*, 20 (2019) 2123-2134.
- [27] T.M. Birshtein, Y.V. Lyatskaya, Polymer brush in a mixed solvent, *Colloids und Surfaces A: Physicochemical and Engineering Aspects*, 86 (1994) 77-83.
- [28] K. Mukae, M. Sakurai, S. Sawamura, K. Makino, S.W. Kim, I. Ueda, K. Shirahama, Swelling of poly(N-isopropylacrylamide) gels in water-alcohol (C_1 - C_4) mixed solvents, *The Journal of Physical Chemistry*, 97 (1993) 737-741.
- [29] F. Tanaka, T. Koga, F.M. Winnik, Temperature-responsive polymers in mixed solvents: competitive hydrogen bonds cause cononsolvency, *Physical Review Letters*, 101 (2008) 028302.
- [30] B.A. Wolf, M.M. Willms, Measured and calculated solubility of polymers in mixed solvents: cononsolvency, *Die Makromolekulare Chemie*, 179 (1978) 2265-2277.
- [31] I. Fernández-Piérولا, A. Horta, Co-nonsolvency of PMMA, *Polymer Bulletin*, 3 (1980) 273-278.
- [32] S.M. Kim, Y.C. Bae, Co-nonsolvency effect of thermosensitive N-isopropylacrylamide nanometer-sized gel particles in water–PEG systems, *Polymer*, 54 (2013) 2138-2145.
- [33] T. Ishidao, M. Akagi, H. Sugimoto, Y. Onoue, Y. Iwai, Y. Arai, Swelling equilibria of poly(N-isopropylacrylamide) gel in aqueous polymer solutions, *Fluid Phase Equilibria*, 104 (1995) 119-129.
- [34] T. Ishidao, M. Akagi, H. Sugimoto, Y. Iwai, Y. Arai, Swelling behaviors of poly(N-isopropylacrylamide) gel in poly(ethylene glycol)-water mixtures, *Macromolecules*, 26 (1993) 7361-7362.
- [35] D. Mukherji, C.M. Marques, K. Kremer, Polymer collapse in miscible good solvents is a generic phenomenon driven by preferential adsorption, *Nature Communications*, 5 (2014) 4882.
- [36] P.-G. de Gennes, A second type of phase separation in polymer solutions, *Comptes rendus de l'Académie des sciences. Série II, Mechanics, Physics, Chemistry, Space sciences, Earth sciences*, 313 (1991) 1117-1122.

- [37] S. Bekiranov, R. Bruinsma, P. Pincus, Solution behavior of polyethylene oxide in water as a function of temperature and pressure, *Physical Review E*, 55 (1997) 577-585.
- [38] S. Bekiranov, R. Bruinsma, P. Pincus, A Primitive Model for Single-Chain/Aqueous-Solution Behavior of PEO under Pressure, *Europhysics Letters*, 24 (1993) 183-188.
- [39] A. Galuschko, J.-U. Sommer, Co-Nonsolvency Response of a Polymer Brush: A Molecular Dynamics Study, *Macromolecules*, 52 (2019) 4120-4130.
- [40] T. Ishida, Y. Hashimoto, Y. Iwai, Y. Arai, Solvent concentrations of dimethylsulfoxide-water and 1-propanol-water solutions inside and outside poly (N-isopropylacrylamide) gel, *Colloid and Polymer Science*, 272 (1994) 1313-1316.
- [41] T. Amiya, Y. Hirokawa, Y. Hirose, Y. Li, T. Tanaka, Reentrant phase transition of N-isopropylacrylamide gels in mixed solvents, *The Journal of Chemical Physics*, 86 (1987) 2375-2379.
- [42] Y. Hirokawa, T. Tanaka, Volume phase transition in a non-ionic gel, *AIP Conference Proceedings* 107(203) (1984) 203-208.
- [43] K. Nothdurft, D.H. Müller, T. Brands, A. Bardow, W. Richtering, Enrichment of methanol inside pNIPAM gels in the cononsolvency-induced collapse, *Physical Chemistry Chemical Physics*, 21 (2019) 22811-22818.
- [44] J. Wang, N. Wang, B. Liu, J. Bai, P. Gong, G. Ru, J. Feng, Preferential adsorption of the additive is not a prerequisite for cononsolvency in water-rich mixtures, *Physical Chemistry Chemical Physics*, 19 (2017) 30097-30106.
- [45] B. Liu, J. Wang, G. Ru, C. Liu, J. Feng, Phase Transition and Preferential Alcohol Adsorption of Poly(N,N-diethylacrylamide) Gel in Water/Alcohol Mixtures, *Macromolecules*, 48 (2015) 1126-1133.
- [46] N. Wang, G. Ru, L. Wang, J. Feng, ^1H MAS NMR studies of the phase separation of poly(N-isopropylacrylamide) gel in binary solvents, *Langmuir*, 25 (2009) 5898-5902.
- [47] Y. Yu, M. Cirelli, B.D. Kieviet, E.S. Kooij, G.J. Vancso, S. de Beer, Tunable friction by employment of co-non-solvency of PNIPAM brushes, *Polymer*, 102 (2016) 372-378.
- [48] Z. Zhang, A.J. Morse, S.P. Armes, A.L. Lewis, M. Geoghegan, G.J. Leggett, Effect of brush thickness and solvent composition on the friction force response of poly(2-(methacryloyloxy)ethylphosphorylcholine) brushes, *Langmuir*, 27 (2011) 2514-2521.
- [49] Q. Chen, E.S. Kooij, X. Sui, C.J. Padberg, M.A. Hempenius, P.M. Schon, G.J. Vancso, Collapse from the top: brushes of poly(N-isopropylacrylamide) in co-nonsolvent mixtures, *Soft Matter*, 10 (2014) 3134-3142.
- [50] S. Edmondson, N.T. Nguyen, A.L. Lewis, S.P. Armes, Co-nonsolvency effects for surface-initiated poly(2-(methacryloyloxy)ethyl phosphorylcholine) brushes in alcohol/water mixtures, *Langmuir*, 26 (2010) 7216-7226.
- [51] B.C. Choi, S. Choi, D.E. Leckband, Poly(N-isopropyl acrylamide) brush topography: dependence on grafting conditions and temperature, *Langmuir*, 29 (2013) 5841-5850.
- [52] C. Jentzsch, J.U. Sommer, Polymer brushes in explicit poor solvents studied using a new variant of the bond fluctuation model, *The Journal of Chemical Physics*, 141 (2014) 104908.

- [53] P.C. Nalam, L. Daikhin, R.M. Espinosa-Marzal, J. Clasohm, M. Urbakh, N.D. Spencer, Two-Fluid Model for the Interpretation of Quartz Crystal Microbalance Response: Tuning Properties of Polymer Brushes with Solvent Mixtures, *The Journal of Physical Chemistry C*, 117 (2013) 4533-4543.
- [54] G. Liu, G. Zhang, Reentrant Behavior of Poly(Nisopropylacrylamide) Brushes in Water–Methanol Mixtures Investigated with a Quartz Crystal Microbalance, *Langmuir*, 21 (2005).
- [55] R.M. Espinosa-Marzal, P.C. Nalam, S. Bolisetty, N.D. Spencer, Impact of solvation on equilibrium conformation of polymer brushes in solvent mixtures, *Soft Matter*, 9 (2013) 4045.
- [56] T.-H. Young, W.-Y. Chuang, Thermodynamic analysis on the cononsolvency of poly (vinyl alcohol) in water–DMSO mixtures through the ternary interaction parameter, *Journal of Membrane Science*, 210 (2002) 349-359.
- [57] R.O.R. Costa, R.F.S. Freitas, Phase behavior of poly(Nisopropylacrylamide) in binary aqueous solutions, *Polymer*, 43 (2002) 5879-5885.
- [58] G. Zhang, C. Wu, The Water/Methanol Complexation Induced Reentrant Coil-to-Globule-to-Coil Transition of Individual Homopolymer Chains in Extremely Dilute Solutions, *Journal of the American Chemical Society*, 123 (2001) 1376-1380.
- [59] G. Zhang, C. Wu, Reentrant coil-to-globule-to-coil transition of a single linear homopolymer chain in a water/methanol mixture, *Physical Review Letters*, 86 (2001) 822-825.
- [60] K.N. Raftopoulos, K. Kyriakos, M. Nuber, B.J. Niebuur, O. Holderer, M. Ohl, O. Ivanova, S. Pasini, C.M. Papadakis, Co-nonsolvency in concentrated aqueous solutions of PNIPAM: effect of methanol on the collective and the chain dynamics, *Soft Matter*, 16 (2020) 8462-8472.
- [61] B.-J. Niebuur, C.-H. Ko, X. Zhang, K.-L. Claude, L. Chiappisi, A. Schulte, C.M. Papadakis, Pressure Dependence of the Cononsolvency Effect in Aqueous Poly(N-isopropylacrylamide) Solutions: A SANS Study, *Macromolecules*, 53 (2020) 3946-3955.
- [62] K. Kyriakos, M. Philipp, C.H. Lin, M. Dyakonova, N. Vishnevetskaya, I. Grillo, A. Zacccone, A. Miasnikova, A. Laschewsky, P. Muller-Buschbaum, C.M. Papadakis, Quantifying the Interactions in the Aggregation of Thermoresponsive Polymers: The Effect of Cononsolvency, *Macromolecular Rapid Communications*, 37 (2016) 420-425.
- [63] K. Kyriakos, M. Philipp, J. Adelsberger, S. Jaksch, A.V. Berezkin, D.M. Lugo, W. Richtering, I. Grillo, A. Miasnikova, A. Laschewsky, P. Müller-Buschbaum, C.M. Papadakis, Cononsolvency of Water/Methanol Mixtures for PNIPAM and PS-b-PNIPAM: Pathway of Aggregate Formation Investigated Using Time-Resolved SANS, *Macromolecules*, 47 (2014) 6867-6879.
- [64] M. Guettari, A. Belaidi, S. Abel, T. Tajouri, Polyvinylpyrrolidone Behavior in Water/Ethanol Mixed Solvents: Comparison of Modeling Predictions with Experimental Results, *Journal of Solution Chemistry*, 46 (2017) 1404-1417.
- [65] M. Guettari, A. Aschi, R. Gomati, A. Gharbi, Structural transition of a homopolymer in solvents mixture, *Materials Science and Engineering: C*, 28 (2008) 811-815.
- [66] T. Auger, J. Mathe, V. Viasnoff, G. Charron, J.M. Di Meglio, L. Auvray, F. Montel, Zero-mode waveguide detection of flow-driven DNA translocation through nanopores, *Physical Review Letters*, 113 (2014) 028302.

- [67] X. Sui, Q. Chen, M.A. Hempenius, G.J. Vancso, Probing the collapse dynamics of poly(N-isopropylacrylamide) brushes by AFM: effects of co-nonsolvency and grafting densities, *Small*, 7 (2011) 1440-1447.
- [68] Y. Yu, R.A. Lopez de la Cruz, B.D. Kieviet, H. Gojzewski, A. Pons, G. Julius Vancso, S. de Beer, Pick up, move and release of nanoparticles utilizing co-non-solvency of PNIPAM brushes, *Nanoscale*, 9 (2017) 1670-1675.
- [69] S. Rauch, K.-J. Eichhorn, U. Oertel, M. Stamm, D. Kuckling, P. Uhlmann, Temperature responsive polymer brushes with clicked rhodamine B: synthesis, characterization and swelling dynamics studied by spectroscopic ellipsometry, *Soft Matter*, 8 (2012) 10260.
- [70] B. Zdyrko, K. Swaminatha Iyer, I. Luzinov, Macromolecular anchoring layers for polymer grafting: comparative study, *Polymer*, 47 (2006) 272-279.
- [71] C. Werner, K.-J. Eichhorn, K. Grundke, F.M. Simon, W. Grähler, H.J. Jacobasch, Insights on structural variations of protein adsorption layers on hydrophobic fluorohydrocarbon polymers gained by spectroscopic ellipsometry (part I), *Colloids and Surfaces A: Physicochemical and Engineering Aspects*, 156 (1999) 3-17.
- [72] W.J. Brittain, S. Minko, A structural definition of polymer brushes, *Journal of Polymer Science Part A: Polymer Chemistry*, 45 (2007) 3505-3512.
- [73] C. Xue, N. Yonet-Tanyeri, N. Brouette, M. Sferrazza, P.V. Braun, D.E. Leckband, Protein adsorption on poly(N-isopropylacrylamide) brushes: dependence on grafting density and chain collapse, *Langmuir*, 27 (2011) 8810-8818.
- [74] V.Y. Grinberg, T.V. Burova, N.V. Grinberg, A.P. Moskalets, A.S. Dubovik, I.G. Plashchina, A.R. Khokhlov, Energetics and Mechanisms of poly(N-isopropylacrylamide) Phase Transitions in Water-Methanol Solutions, *Macromolecules*, 53 (2020) 10765-10772.
- [75] C. Dalgicdir, F. Rodriguez-Ropero, N.F.A. van der Vegt, Computational Calorimetry of PNIPAM Cononsolvency in Water/Methanol Mixtures, *The Journal of Physical Chemistry B*, 121 (2017) 7741-7748.
- [76] P.-G. de Gennes, *Scaling Concepts in Polymer Physics*, Cornell University Press, Ithaca, NY, USA, 1979.
- [77] H. Kojima, Studies on the phase transition of hydrogels and aqueous solutions of thermosensitive polymers, *Polymer Journal*, 50 (2018) 411-418.
- [78] S. Backes, R. Von Klitzing, *Nanomechanics and Nanorheology of Microgels at Interfaces*, Polymers (Basel), 10 (2018).
- [79] I. Bischofberger, D.C. Calzolari, V. Trappe, Co-nonsolvency of PNIPAM at the transition between solvation mechanisms, *Soft Matter*, 10 (2014) 8288-8295.
- [80] H.M. Crowther, B. Vincent, Swelling behavior of poly-Nisopropylacrylamide microgel particles in alcoholic solutions, *Colloid and Polymer Science*, 276 (1998) 46-51.
- [81] F. Pooch, V. Teltevskij, E. Karjalainen, H. Tenhu, F.M. Winnik, Poly(2-propyl-2-oxazoline)s in Aqueous Methanol: To Dissolve or not to Dissolve, *Macromolecules*, 52 (2019) 6361-6368.
- [82] S. Bharadwaj, N.F.A. van der Vegt, Does Preferential Adsorption Drive Cononsolvency?, *Macromolecules*, 52 (2019) 4131-4138.

- [83] T. Zuo, C. Ma, G. Jiao, Z. Han, S. Xiao, H. Liang, L. Hong, D. Bowron, A. Soper, C.C. Han, H. Cheng, Water/Cosolvent Attraction Induced Phase Separation: A Molecular Picture of Cononsolvency, *Macromolecules*, 52 (2019) 457-464.
- [84] D. Mukherji, K. Kremer, Coil–Globule–Coil Transition of PNIPAm in Aqueous Methanol: Coupling All-Atom Simulations to Semi-Grand Canonical Coarse-Grained Reservoir, *Macromolecules*, 46 (2013) 9158-9163.
- [85] J. Dudowicz, K.F. Freed, J.F. Douglas, Communication: Cosolvency and cononsolvency explained in terms of a Flory-Huggins type theory, *The Journal of Chemical Physics*, 143 (2015) 131101.
- [86] Y. Marcus, Some thermodynamic and structural aspects of mixtures of glycerol with water, *Physical Chemistry Chemical Physics*, 2 (2000) 4891-4896.
- [87] G.S. Shealy, S.I. Sandler, The Excess Gibbs Free Energy of Aqueous Nonelectrolyte Solutions, *AIChE Journal*, 34 (1988) 1065-1074.
- [88] R.A. Dawe, D.M.T. Newsham, S.B. Ng, Vapor-liquid equilibriums in mixtures of water, 1-propanol, and 1-butanol, *Journal of Chemical & Engineering Data*, 18 (1973) 44-49.
- [89] R.F. Lama, B.C.-Y. Lu, Excess Thermodynamic Properties of Aqueous Alcohol Solutions, *Journal of Chemical & Engineering Data*, 10 (1965) 216-219.
- [90] J.-H. Chen, H.-H. Chen, Y.-X. Chang, P.-Y. Chuang, P.-D. Hong, Effects of cononsolvency on preferential adsorption phenomenon in poly(N-isopropylacrylamide) ternary solutions, *Journal of Applied Polymer Science*, 107 (2008) 2732-2742.
- [91] S.M. Kim, S.M. Lee, Y.C. Bae, Influence of hydroxyl group for thermoresponsive poly(N-isopropylacrylamide) gel particles in water/co-solvent (1,3-propanediol, glycerol) systems, *European Polymer Journal*, 54 (2014) 151-159.
- [92] X. Lang, E.X. Xu, Y. Wei, L.N. Walters, M.J.A. Hore, Isomeric and structural effects in polymer cononsolvent systems, *Polymer*, 170 (2019) 190-197.
- [93] F. Afroze, E. Nies, H. Berghmans, Phase transitions in the system poly(N-isopropylacrylamide)/water and swelling behaviour of the corresponding networks, *Journal of Molecular Structure*, 554 (2000) 55-68.
- [94] C.-H. Ko, K.-L. Claude, B.-J. Niebuur, F.A. Jung, J.-J. Kang, D. Schanzenbach, H. Frielinghaus, L.C. Barnsley, B. Wu, V. Pipich, A. Schulte, P. Müller-Buschbaum, A. Laschewsky, C.M. Papadakis, Temperature-Dependent Phase Behavior of the Thermoresponsive Polymer Poly(N-isopropylmethacrylamide) in an Aqueous Solution, *Macromolecules*, 53 (2020) 6816-6827.
- [95] T. Kogo, A. Shundo, C. Wang, K. Tanaka, Spatial Heterogeneity Accompanying Gel Formation of Poly(N-isopropylacrylamide) Aqueous Solution at a Temperature below Cloud Point, *Macromolecules*, 53 (2020) 10964-10971.
- [96] L.C. Moh, M.D. Losego, P.V. Braun, Solvent quality effects on scaling behavior of poly(methyl methacrylate) brushes in the moderate- and high-density regimes, *Langmuir*, 27 (2011) 3698-3702.
- [97] G. Park, Y. Jung, Many-chain effects on the co-nonsolvency of polymer brushes in a good solvent mixture, *Soft Matter*, 15 (2019) 7968-7980.

- [98] F. Wang, Y. Shi, S. Luo, Y. Chen, J. Zhao, Conformational Transition of Poly(N-isopropylacrylamide) Single Chains in Its Cononsolvency Process: A Study by Fluorescence Correlation Spectroscopy and Scaling Analysis, *Macromolecules*, 45 (2012) 9196-9204.
- [99] N. Orakdogan, O. Okay, Reentrant conformation transition in poly(N,N-dimethylacrylamide) hydrogels in water–organic solvent mixtures, *Polymer*, 47 (2006) 561-568.
- [100] C.-W. Li, H. Merlitz, C.-X. Wu, J.-U. Sommer, Nanopores as Switchable Gates for Nanoparticles: A Molecular Dynamics Study, *Macromolecules*, 51 (2018) 6238-6247.
- [101] H. Kojima, F. Tanaka, C. Scherzinger, W. Richtering, Temperature dependent phase behavior of PNIPAM microgels in mixed water/methanol solvents, *Journal of Polymer Science Part B: Polymer Physics*, 51 (2013) 1100-1111.
- [102] S. Hirotsu, Critical points of the volume phase transition in N-isopropylacrylamide gels, *The Journal of Chemical Physics*, 88 (1988) 427-431.
- [103] J. Walter, J. Sehart, J. Vrabec, H. Hasse, Molecular dynamics and experimental study of conformation change of poly(N-isopropylacrylamide) hydrogels in mixtures of water and methanol, *The Journal of Physical Chemistry B*, 116 (2012) 5251-5259.
- [104] C.S. Biswas, Q. Wang, B. Du, F.J. Stadler, Testing of the effect of parameters on the cononsolvency of random copolymer gels of N-isopropylacrylamide and N-ethylacrylamide in methanol-water mixed solvents by simple gravimetric method, *Polymer Testing*, 62 (2017) 177-188.
- [105] S.A. Chen, W.J. Lai, Polymer miscibility in mixed organic liquids having acid-base interaction—a modified two-dimensional approach, *Journal of Applied Polymer Science*, 23 (1979) 319-324.
- [106] E.W.J. Mardles, CCXCVIII.-The dissolution of substances in mixed liquids with special reference to colloids., *Journal of the Chemical Society, Transactions*, 125 (1924) 2244-2259.
- [107] A.K. Nandi, U.K. Sen, S.N. Bhattacharyya, B.M. Mandal, Co-nonsolvent systems for poly(ϵ -caprolactone) and poly(methyl methacrylate), *European Polymer Journal*, 19 (1983) 283-286.
- [108] D. Mukherji, C.M. Marques, T. Stuehn, K. Kremer, Co-non-solvency: mean-field polymer theory does not describe polymer collapse transition in a mixture of two competing good solvents, *The Journal of Chemical Physics*, 142 (2015) 114903.
- [109] I. Bischofberger, D.C. Calzolari, P. De Los Rios, I. Jelezarov, V. Trappe, Hydrophobic hydration of poly-N-isopropyl acrylamide: a matter of the mean energetic state of water, *Scientific Reports*, 4 (2014) 4377.
- [110] H. Yamauchi, Y. Maeda, LCST and UCST Behavior of Poly(N-isopropylacrylamide) in DMSO/Water Mixed Solvents Studied by IR and Micro-Raman Spectroscopy, *The Journal of Physical Chemistry B*, 111 (2007) 12964-12968.
- [111] S. Bharadwaj, P.B. Sunil Kumar, S. Komura, A.P. Deshpande, Kosmotropic effect leads to LCST decrease in thermoresponsive polymer solutions, *The Journal of Chemical Physics*, 148 (2018) 084903.
- [112] J. Heyda, A. Muzdalo, J. Dzubiella, Rationalizing Polymer Swelling and Collapse under Attractive Cosolvent Conditions, *Macromolecules*, 46 (2013) 1231-1238.

- [113] P.J. Flory, J. Rehner, Statistical Mechanics of Cross-Linked Polymer Networks I. Rubberlike Elasticity, *The Journal of Chemical Physics*, 11 (1943) 512-520.
- [114] R.-L. Zhao, K. Lin, X.-G. Zhou, S.-L. Liu, Solubility of Poly(N-isopropylacrylamide) in Aqueous Methanol from Raman Spectroscopy, *Acta Physico-Chimica Sinica*, 26 (2010) 1915-1922.
- [115] M.T. Zafarani-Moattar, F. Samadi, Determination of Solvent Activity in Poly(vinylpyrrolidone) + Methanol, + Ethanol, + 2-Propanol, + and 1-Butanol Solutions at 25°C, *Journal of Chemical & Engineering Data*, 49 (2004) 1475-1478.
- [116] X. Zheng, M.A. Anisimov, J.V. Sengers, M. He, Mesoscopic Diffusion of Poly(ethylene oxide) in Pure and Mixed Solvents, *The Journal of Physical Chemistry B*, 122 (2018) 3454-3464.
- [117] M.T. Zafarani-Moattar, N. Tohidifar, Vapor-Liquid Equilibria, Density, Speed of Sound, and Viscosity for the Poly(ethylene glycol) 400 + 1-Propanol and 1-Butanol Systems, *Journal of Chemical & Engineering Data*, 59 (2014) 4070-4080.
- [118] M.T. Zafarani-Moattar, N. Tohidifar, Vapor-Liquid Equilibria, Density, and Speed of Sound for the System Poly(ethylene glycol) 400 + Methanol at Different Temperatures, *Journal of Chemical & Engineering Data*, 51 (2006) 1769-1774.
- [119] M.T. Zafarani-Moattar, N. Tohidifar, Vapor-Liquid Equilibria, Density, Speed of Sound, and Viscosity for the System Poly(ethylene glycol) 400 + Ethanol at Different Temperatures, *Journal of Chemical & Engineering Data*, 53 (2008) 785-793.
- [120] C. Scherzinger, P. Lindner, M. Keerl, W. Richtering, Cononsolvency of Poly(N,N-diethylacrylamide) (PDEAAM) and Poly(N-isopropylacrylamide) (PNIPAM) Based Microgels in Water/Methanol Mixtures: Copolymer vs Core-Shell Microgel, *Macromolecules*, 43 (2010) 6829-6833.
- [121] S.S. Sheiko, A.V. Dobrynin, Architectural Code for Rubber Elasticity: From Supersoft to Superfirm Materials, *Macromolecules*, 52 (2019) 7531-7546.
- [122] P.W. Zhu, L. Chen, Effects of cosolvent partitioning on conformational transitions and chain flexibility of thermoresponsive microgels, *Physical Review E*, 99 (2019) 022501.
- [123] N.A. Gokcen, Gibbs-duhem-margules laws, *Journal of Phase Equilibria*, 17 (1996) 50-51.
- [124] S. Bruin, Activity Coefficient Relations in Miscible and Partially Miscible Multicomponent Systems., *Industrial & Engineering Chemistry Fundamentals*, 9 (1970) 305-314.
- [125] K. Lin, N. Hu, X. Zhou, S. Liu, Y. Luo, Reorientation dynamics in liquid alcohols from Raman spectroscopy, *Journal of Raman Spectroscopy*, 43 (2012) 82-88.
- [126] K. Udachin, S. Alavi, J.A. Ripmeester, Communication: Single crystal x-ray diffraction observation of hydrogen bonding between 1-propanol and water in a structure II clathrate hydrate, *The Journal of Chemical Physics*, 134 (2011) 121104.
- [127] A. Wakisaka, S. Mochizuki, H. Kobara, Cluster Formation of 1-Butanol-Water Mixture Leading to Phase Separation, *Journal of Solution Chemistry*, 33 (2004) 721-732.
- [128] S.S.N. Murthy, Detailed Study of Ice Clathrate Relaxation: Evidence for the Existence of Clathrate Structures in Some Water-Alcohol Mixtures, *The Journal of Physical Chemistry A*, 103 (40) (1999) 7927-7937.
- [129] D. Peeters, P. Huyskens, Endothermicity or exothermicity of water/alcohol mixtures, *Journal of Molecular Structure*, 300 (1993) 539-550.

- [130] H.L. Clever, S.P. Pigott, Enthalpies of mixing of dimethylsulfoxide with water and with several ketones at 298.15K, *The Journal of Chemical Thermodynamics*, 3 (1971) 221-225.
- [131] D. Mukherji, C.M. Marques, K. Kremer, Collapse in two good solvents, swelling in two poor solvents: defying the laws of polymer solubility?, *Journal of Physics: Condensed Matter*, 30 (2018) 024002.
- [132] A. Hiroki, Y. Maekawa, M. Yoshida, K. Kubota, R. Katakai, Volume phase transitions of poly(acryloyl-L-proline methyl ester) gels in response to water-alcohol composition, *Polymer*, 42 (2001) 1863-1867.
- [133] K. Mukae, M. Sakurai, S. Sawamura, K. Makino, S.W. Kim, I. Ueda, K. Shirahama, Swelling of poly(N-isopropylacrylamide) gels in water-aprotic solvent mixtures, *Colloid and Polymer Science*, 272 (1994) 655-663.
- [134] S.Y. Lam, R.L. Benoit, Some Thermodynamic Properties of the Dimethylsulfoxide-Water and Propylene Carbonate-Water Systems at 25 °C, *Canadian Journal of Chemistry*, 52 (1974) 718-722.
- [135] M. Cilense, A.V. Benedetti, D.R. Vollet, Thermodynamic properties of liquid mixtures. II. Dimethylformamide-water, *Thermochimica Acta*, 63 (1983) 151-156.
- [136] C.H. Hofmann, S. Grobelny, M. Erbkamp, R. Winter, W. Richtering, Influence of high-pressure on cononsolvency of poly(N-isopropylacrylamide) nanogels in water/methanol mixtures, *Polymer*, 55 (2014) 2000-2007.
- [137] B. Ebeling, S. Eggers, M. Hendrich, A. Nitschke, P. Vana, Flipping the Pressure- and Temperature-Dependent Cloud-Point Behavior in the Cononsolvency System of Poly(N-isopropylacrylamide) in Water and Ethanol, *Macromolecules*, 47 (2014) 1462-1469.
- [138] J.V. Herráez, R. Belda, Refractive Indices, Densities and Excess Molar Volumes of Monoalcohols + Water, *Journal of Solution Chemistry*, 35 (2006) 1315-1328.
- [139] Y. Aoki, T. Moriyoshi, Mutual solubility of n-butanol + water under high pressures, *The Journal of Chemical Thermodynamics*, 10 (1978) 1173-1179.
- [140] F. Meersman, J. Wang, Y. Wu, K. Heremans, Pressure Effect on the Hydration Properties of Poly(N-isopropylacrylamide) in Aqueous Solution Studied by FTIR Spectroscopy, *Macromolecules*, 38 (2005) 8923-8928.
- [141] P. Knychala, K. Timachova, M. Banaszak, N.P. Balsara, 50th Anniversary Perspective: Phase Behavior of Polymer Solutions and Blends, *Macromolecules*, 50 (2017) 3051-3065.
- [142] A. Eliassi, H. Modarress, G.A. Mansoori, Measurement of Activity of Water in Aqueous Poly(ethylene glycol) Solutions (Effect of Excess Volume on the Flory-Huggins χ -Parameter), *Journal of Chemical & Engineering Data*, 44 (1999) 52-55.
- [143] N. Osaka, M. Shibayama, Pressure Effects on Cononsolvency Behavior of Poly(N-isopropylacrylamide) in Water/DMSO Mixed Solvents, *Macromolecules*, 45 (2012) 2171-2174.
- [144] I.C. Sanchez, Phase Transition Behavior of the Isolated Polymer Chain, *Macromolecules* 12(5) (1979) 980-988.
- [145] D. Mukherji, C.M. Marques, K. Kremer, Smart Responsive Polymers: Fundamentals and Design Principles, *Annual Review of Condensed Matter Physics*, 11 (2020) 271-299.
- [146] V. Dohnal, D. Fenclová, P. Vrbka, Temperature Dependences of Limiting Activity Coefficients, Henry's Law Constants, and Derivative Infinite Dilution Properties of Lower (C₁-C₅) 1-Alkanols

- in Water. Critical Compilation, Correlation, and Recommended Data, *Journal of Physical and Chemical Reference Data*, 35(4) (2006) 1621-1651.
- [147] J. Haidl, V. Dohnal, Dilute Vapor Absorption: A New Accurate Technique for Measurement of the Limiting Activity Coefficient of Water in Hydrophobic Solvents of Lower Volatility, *Journal of Chemical & Engineering Data*, 62 (2017) 2713-2720.
- [148] J. Haidl, V. Dohnal, Activity Coefficients of Water at Infinite Dilution in Common Oxygenated Solvents, *Journal of Chemical & Engineering Data*, 65 (2020) 2790-2797.
- [149] DDB Software Package is recommended to calculate the values of γ_1^∞ and γ_2^∞ , DDBST GmbH, 2020, Hosted on Source Forge at <http://www.ddbst.de/software-package.html>
- [150] F. Han, J. Zhang, G. Chen, X. Wie, Density, Viscosity, and Excess Properties for Aqueous Poly(ethylene glycol) Solutions from (298.15 to 323.15) K, *The Journal of Chemical & Engineering Data*, 53 (2008) 2598-2601.
- [151] E.A. Muller, P. Rasmussen, Densities and excess volumes in aqueous poly(ethylene glycol) solutions, *The Journal of Chemical & Engineering Data*, 36 (1991) 214-217.
- [152] R.D. Coalson, A. Eskandari Nasrabad, D. Jasnow, A. Zilman, A Polymer-Brush-Based Nanovalve Controlled by Nanoparticle Additives: Design Principles, *The Journal of Physical Chemistry B*, 119 (2015) 11858-11866.
- [153] A.E. Nasrabad, D. Jasnow, A. Zilman, R.D. Coalson, Precise control of polymer coated nanopores by nanoparticle additives: Insights from computational modeling, *The Journal of Chemical Physics*, 145 (2016) 064901.
- [154] Y.A. Perez Sirkin, M. Tagliazucchi, I. Szleifer, Transport in nanopores and nanochannels: some fundamental challenges and nature-inspired solutions, *Materials Today Advances*, 5 (2020) 100047.
- [155] G. Perez-Mitta, M.E. Toimil-Molares, C. Trautmann, W.A. Marmisolle, O. Azzaroni, Molecular Design of Solid-State Nanopores: Fundamental Concepts and Applications, *Advanced Materials*, 31 (2019) e1901483.
- [156] R. Brilmayer, C. Forster, L. Zhao, A. Andrieu-Brunsen, Recent trends in nanopore polymer functionalization, *Current Opinion in Biotechnology*, 63 (2020) 200-209.
- [157] L. Michalek, K. Mundsinger, C. Barner-Kowollik, L. Barner, The long and the short of polymer grafting, *Polymer Chemistry*, 10 (2019) 54-59.
- [158] T. Zheng, M. Zhu, J. Yang, J. He, M. Waqas, L. Li, Revisiting the Flow-Driven Translocation of Flexible Linear Chains through Cylindrical Nanopores: Is the Critical Flow Rate Really Independent of the Chain Length?, *Macromolecules*, 51 (2018) 9333-9343.
- [159] H. Yong, H. Zhang, Y. Xie, H. Yang, Polymer linear transport in steady convergent microfluidics, *Soft Matter*, 9 (2013) 3565.
- [160] Q. Chen, J. Liu, A.E.P. Schibel, H.S. White, C. Wu, Translocation Dynamics of Poly(styrenesulfonic acid) through an α -Hemolysin Protein Nanopore, *Macromolecules*, 43 (2010) 10594-10599.
- [161] B. Mohanty, H.B. Bohidar, Systematic of Alcohol-Induced Simple Coacervation in Aqueous Gelatin Solutions, *Biomacromolecules*, 4 (2003) 1080-1086.

- [162] H. Kawasaki, T. Nakamura, K. Miyamoto, M. Tokita, T. Komai, Multiple volume phase transition of nonionic thermosensitive gel, *The Journal of Chemical Physics*, 103 (1995) 6241-6247.
- [163] N. Xue, X.-P. Qiu, V. Aseyev, F.M. Winnik, Nonequilibrium Liquid-Liquid Phase Separation of Poly(N-isopropylacrylamide) in Water/Methanol Mixtures, *Macromolecules*, 50 (2017) 4446-4453.
- [164] C.E. Mills, E. Ding, B.D. Olsen, Cononsolvency of Elastin-like Polypeptides in Water/Alcohol Solutions, *Biomacromolecules*, 20 (2019) 2167-2173.
- [165] R.J. Gilbert, M. Dalla Serra, C.J. Froelich, M.I. Wallace, G. Anderluh, Membrane pore formation at protein-lipid interfaces, *Trends in Biochemical Sciences*, 39 (2014) 510-516.
- [166] W.H. Binder, Polymer-induced transient pores in lipid membranes, *Angewandte Chemie International Edition*, 47 (2008) 3092-3095.
- [167] J. Yang, T. Zheng, A. Umair, L. Li, "Dead-End" Ultrafiltration: A Powerful Technique Utilizing "Coil-to-Stretch" Transition for Polymer Separation/Fractionation, *Macromolecules*, 53 (2020) 2396-2405.
- [168] U. Thiele, T. Frohoff-Hülsmann, S. Engelnkemper, E. Knobloch, A.J. Archer, First order phase transitions and the thermodynamic limit, *New Journal of Physics*, 21 (2019) 123021.
- [169] M.P. Hughes, M.R. Sawaya, D.R. Boyer, L. Goldschmidt, J.A. Rodriguez, D. Cascio, L. Chong, T. Gonen, D.S. Eisenberg, Atomic structures of low-complexity protein segments reveal kinked beta sheets that assemble networks, *Science*, 359 (2018) 698-701.
- [170] S. Boeynaems, S. Alberti, N.L. Fawzi, T. Mittag, M. Polymenidou, F. Rousseau, J. Schymkowitz, J. Shorter, B. Wolozin, L. Van Den Bosch, P. Tompa, M. Fuxreiter, Protein Phase Separation: A New Phase in Cell Biology, *Trends in Cell Biology*, 28 (2018) 420-435.

List of figures

- Figure 1.1**(Figure 1) A graphical plot of the mixture's Gibbs free energy (g) in respect to the composition vector of the liquid mixture (x). For simplicity, in the figure I plot the situation when the system only has two components. It is noted that if $x_d < x_l < x_c$, the system will undergo a phase separation when it goes to thermodynamic equilibrium. 5
- Figure 1.2** (Figure 2) A graphical plot of the Flory-Huggins free energy (G_{FH} , Eq.(1.3)) with respect to the volume fraction of polymer (c) for polymer solutions. It is noted that if $c \leq c_{dilute}$ or $c \geq c_{dense}$ there is no phase separation. Parameter used in the plot are $N = 100$ and $\chi_{ps} = 0.8$ 7
- Figure 1.3**(Figure 3) A graphical plot of the Flory-Huggins parameter (χ_{ps} , Eq.(1.8)) with respect to the volume fraction of polymer (c) for uniform polymer brushes. Note that in the plot I restrict the value of χ_{ps} in its conventional physical range ($0 \leq \chi_{ps} \leq 4.0$). 9
- Scheme 1.1**(Figure 4) A mechanism where phase transition of polymer occurs if one component (it is usually termed as cosolvent) of a binary solvent mixture displays a strong tendency to adsorb at the polymer and can form temporary crosslinks. 11
- Scheme 1.2**(Figure 5) Illustration of cosolvent-assisted loop formation on a single polymer chain. 13
- Scheme 2.1**(Figure 6) Preparation of PNiPAAm brushes on silicon substrates using the "grafting-to" approach. 18
- Figure 2.1**(Figure 7) Swollen brush thickness of a PNiPAAm brush in aqueous ethanol mixtures as a function of (a-c) measurement time and (d) ethanol fraction obtained via Vis-spectroscopic ellipsometry at the temperature of 25°C. Note that the dashed line in Figure 2.1d is only used to guide eyesight. The error bars in Figure 2.1d are neglected because they are quite small (around 0.5 nm). Parameters of the PNiPAAm brush are: grafting density $\sigma = 0.20$ chains/nm², $M_n = 5.02 \times 10^4$ g/mol, $M_w/M_n = 1.28$ 23
- Scheme 2.2**(Figure 8) Main cononsolvency transition regimes of a PNiPAAm brush in ethanol/water mixtures. 24
- Figure 2.2**(Figure 9) Normalized PNiPAAm brush thickness as a function of the volume fraction of cosolvent (a) Cononsolvency transition of the same PNiPAAm brush in different alcohol aqueous solutions, at the temperature of 25°C. Parameters of the PNiPAAm brush are: grafting density $\sigma = 0.143$ chains/nm², $M_n = 6.1 \times 10^4$ g/mol, $M_w/M_n =$

- 1.40. (b) A zoom-in of Figure 2.2a for the alcohol's volume fraction ranging from 0 to 25%. Note that the dotted lines in the figures are guides to the eyes.....25
- Figure 2.3**(Figure 10) Theoretical fits of cononsolvency behavior of the same PNiPAAm brush in different alcohol-water mixtures. The ideal chemical potential change has been calculated based on lattice model as $\mu = \ln(y/(1-y))$, where y is the molar fraction of alcohol. The parameters of the PNiPAAm brush are: grafting density $\sigma = 0.143$ chains/nm², $M_n = 6.1 \times 10^4$ g/mol, $M_w/M_n = 1.40$. While the numerical fit has been optimized in the full range of cosolvent volume fractions for short alcohols (Figure 2.3a), we restricted the fit to the collapse region for the longer alcohols (Figure 2.3b).26
- Figure 2.4**(Figure 11) Normalized PNiPAAm brush thickness as a function of the volume fraction of cosolvent: Cononsolvency transition of the same PNiPAAm brush in propanol isomer aqueous solutions, at the temperature of 25°C. Parameters of the PNiPAAm brush are: grafting density $\sigma = 0.143$ chains/nm², $M_n = 6.1 \times 10^4$ g/mol, $M_w/M_n = 1.40$. Note that the dotted line in the figure are guides to the eyes.27
- Figure 2.5**(Figure 12) Normalized PNiPAAm brush thickness as a function of the volume fraction of cosolvent (a) Cononsolvency transition of the same PNiPAAm brush in butanol isomer aqueous solutions, at the temperature of 25°C. Parameters of the PNiPAAm brush are: grafting density $\sigma = 0.143$ chains/nm², $M_n = 6.1 \times 10^4$ g/mol, $M_w/M_n = 1.40$. (b) A zoom-in of Figure 2.5a for the alcohol's volume fraction ranging from 0 to 25%. Note that the dotted and solid lines in the figures are guides to the eyes.28
- Figure 2.6**(Figure 13) Free energy change of mixing alcohols with water: (a) Molar Gibbs free energy change of mixing $\Delta_{mix}G_m$, when mixing different alcohols with water at the temperature of 25°C. (b) Effective Flory-interaction parameter between the two solvents χ_{CS} , when mixing different alcohols with water at the temperature of 25°C. Data are extracted and reprocessed from [refs. \[86-89\]](#), note that the dotted lines in the figures are only used to guide eyesight.29
- Figure 2.7**(Figure 14) Temperature effect on the cononsolvency transition of the same PNiPAAm brush in ethanol aqueous solutions under different temperatures: (a) Swollen brush thickness (unit in nanometre) as a function of temperature. (b) Normalized brush thickness (H/H_0) as a function of temperature. Parameters of the PNiPAAm brush are: grafting density $\sigma = 0.143$ chains/nm², $M_n = 6.1 \times 10^4$ g/mol, $M_w/M_n = 1.40$. Note that the dotted lines in the figures are guides to eyes.31
- Figure 2.8**(Figure 15) Normalized brush thickness (H/H_0) in the cononsolvency transition of a polymer brush as a function of the chemical potential change μ for $\chi_{ps}=0.3$, $\chi_{ps}=0.4$ and χ_{ps}

$\chi_{ps} = 0.5$. Note that in Figure 2.8 except changing the Flory-parameter χ_{ps} , other model parameters are fixed as $\sigma = 0.143$ chains/nm², $\gamma = 1.0$, $t = 1.0$, $\varepsilon = 1.5$, $\lambda = 3$ and $\nu = 0.2$ 32

Figure 2.9(Figure 16) Grafting-density effect in the cononsolvency transition of PNiPAAm brushes: (a) Cononsolvency transition of PNiPAAm brushes with different grafting densities in ethanol aqueous solutions, at the temperature of 25°C. The solid lines are numerical fits based on the adsorption-attraction model 23. (b) Reduced brush thickness in the collapsed state of PNiPAAm brushes vs. grafting density at the temperature of 25°C (in the 16% volume fraction of ethanol aqueous solutions). Parameters of the PNiPAAm brushes plotted in Figure 2.9a from above to bottom are: grafting density $\sigma = 0.214$ chains/nm², $M_n = 5.02 \times 10^4$ g/mol, $M_w/M_n = 1.28$; $\sigma = 0.143$ chains/nm², $M_n = 6.1 \times 10^4$ g/mol, $M_w/M_n = 1.40$; $\sigma = 0.103$ chains/nm², $M_n = 6.1 \times 10^4$ g/mol, $M_w/M_n = 1.40$ 33

Figure 2.10(Figure 17) Grafting-density effect in the cononsolvency transition of grafted PNiPAAm polymers in ethanol aqueous solutions, absolute swollen brush thickness at the temperature of 25°C: (a) with molecular weight of $M_n = 6.1 \times 10^4$ g/mol, $M_w/M_n = 1.40$ for all polymer layers; (b) with molecular weight of $M_n = 3.8 \times 10^4$ g/mol, $M_w/M_n = 1.38$ for all polymer layers. Note that the dotted lines in the figures are guides to eyes. 34

Figure 2.11(Figure 18) Grafting-density effect in the cononsolvency transition of grafted PNiPAAm polymers in ethanol aqueous solutions, normalized swollen brush thickness at the temperature of 25°C: (a) with molecular weight of $M_n = 6.1 \times 10^4$ g/mol, $M_w/M_n = 1.40$ for all polymer layers; (b) with molecular weight of $M_n = 3.8 \times 10^4$ g/mol, $M_w/M_n = 1.38$ for all polymer layers. Note that the dotted lines in the figures are guides to eyes. 35

Figure 2.12(Figure 19) Cononsolvency transition of the same PNiPAAm micro-gel in methanol aqueous solutions under different temperatures. Data are extracted and reprocessed from [ref. \[101\]](#), note that the dotted lines in the figure are only used to guide eyesight. 37

Figure 2.13(Figure 20) Cononsolvency transition of the same PNiPAAm macro-gel in methanol aqueous solutions under different temperatures. Data are extracted and reprocessed from [ref. \[102\]](#), note that the dotted lines in the figure are only used to guide eyesight. 38

Figure 2.14(Figure 21) Normalized swollen gel volume (V/V_0) of the same PNiPAAm micro-gel in 2-propanol aqueous solutions as a function of temperature. Data are extracted and reprocessed from [ref. \[80\]](#), note that the dotted lines in the figure are only used to guide eyesight. 39

Figure 2.15(Figure 22) Normalized swollen gel weight (W/W_{100}) of two PNiPAAm macro-gels in methanol aqueous solutions as a function of temperature. Data are extracted and

reprocessed from ref. [103] , note that the dotted lines in the figures are only used to guide eyesight.....	39
Figure 2.16 (Figure 23) Normalized swollen gel weight(W/W_0) of the same PNiPAAm micro-gel in methanol aqueous solutions as a function of temperature. Data are extracted and reprocessed from ref. [104] , note that the dotted lines in the figure are only used to guide eyesight.....	40
Scheme 3.1 (Figure 24) An illustration of the concept of preferential adsorption of cosolvent on the polymer chains and cosolvent-assisted binding effect. Note that loop formation can also happen in the polymer brushes [97] when the grafting density is not high.....	44
Figure 3.1 (Figure 25) Illustration of the impact of the various model parameters on the predicted cononsolvency response of a polymer brush. The scaled brush thickness (H/H_0) is displayed as a function of chemical potential change of the cosolvent, μ : (a) for $\lambda = 1$ and $\lambda = 3$, (b) for $\nu = 0$ and $\nu = 0.3$, (c) for $\chi_{cs} = 0$ and $\chi_{cs} = 0.4$, (d) for $\chi_{ps} = 0$ and $\chi_{ps} = 0.2$, (e) for $\varepsilon = 1.3$ and $\varepsilon = 1.8$, (f) for $\sigma_d = 0.01$ and $\sigma_d = 0.05$. Note that apart from the variation of the corresponding parameter as shown in each sub-figure, all other model parameters remained fixed as listed in Table 3.1.	49
Figure 3.2 (Figure 26) Cononsolvency transition of a single PNiPAAm brush sample in different alcohol aqueous solutions, at a temperature of 25°C: open circles are experimental results and solid lines are theoretical fits using the extended adsorption-attraction model. Parameters of the PNiPAAm brush are: grafting density $\sigma = 0.143 \text{ chains/nm}^2$, $M_n = 6.1 \times 10^4 \text{ g/mol}$, $M_w/M_n = 1.40$. The experimental data have already been reported in my previous study, see Chapter 2	52
Figure 3.3 (Figure 27) Cononsolvency transition of a single PNiPAAm macrogel sample in different alcohol aqueous solutions, at a temperature of 22°C: open circles are experimental results and solid lines are theoretical fits using the extended adsorption-attraction model. Parameters of the PNiPAAm macrogel are: the total number of Kuhn segments in the gel structure is $N_m = 33.14 \text{ mmol}$, and the number of chemical crosslinkers is $x = 0.86 \text{ mmol}$. The maximum possible degree of linking for the chemical crosslinker is 4. The length of a Kuhn segment for gels in this study is chosen to be about four repeating units of PNiPAAm. Data are extracted and reprocessed from refs.[41, 42]	53
Figure 3.4 (Figure 28) Cononsolvency transition of a single PNiPAAm macrogel sample in different alcohol aqueous solutions, at a temperature of 25°C: open circles are experimental results and solid lines are theoretical fits using the extended adsorption-attraction model. Parameters of the PNiPAAm macrogel are: the total number of Kuhn segments in the gel structure is $N_m = 150 \text{ mmol}$, and the number of chemical crosslinkers is $x = 1.5 \text{ mmol}$. The	

- maximum possible degree of linking for the chemical crosslinker is 4. The length of a Kuhn segment for gels in this study is chosen to be about four repeating units of PNiPAAm. Data are extracted and reprocessed from [ref. \[40\]](#)..... 54
- Figure 3.5**(Figure 29) Grafting-density effect in the cononsolvency transition of PNiPAAm brushes in ethanol-water mixtures, at a temperature of 25°C: open squares are experimental results and solid lines are theoretical fits of the extended adsorption-attraction model. Parameters of the PNiPAAm brushes plotted in Figure 4 from top to bottom are: grafting density $\sigma = 0.143 \text{ chains/nm}^2$, $\sigma = 0.103 \text{ chains/nm}^2$. Both brushes contain polymers of identical molecular weight distributions: $M_n = 6.1 \times 10^4 \text{ g/mol}$, $M_w/M_n = 1.40$. The experimental data have been reported in my previous study, see [Chapter 2](#). 56
- Figure 3.6**(Figure 30) Cononsolvency transition of a PNiPAAm brush sample in different alcohol aqueous solutions, at the temperature of 25°C: φ as a function of the chemical potential is calculated by using the extended adsorption-attraction model to fit the experimental results shown in Figure 3.2. Figure 3.6a is a linear schematic dependence of φ on μ and Figure 3.6b is a schematic dependence of $\log_{10}(\varphi)$ on μ . Parameters of the PNiPAAm brush are: grafting density $\sigma = 0.143 \text{ chains/nm}^2$, $M_n = 6.1 \times 10^4 \text{ g/mol}$, $M_w/M_n = 1.40$ 57
- Figure 3.7**(Figure 31) (a) Average energy change ε_H of the formation of one organic solvent-water hydrogen bond when mixing different organic solvents with water at the temperature of 25°C. (b) Enthalpic Flory parameter χ_H when mixing different organic solvents with water at the temperature of 25°C. Data are extracted and reprocessed from [refs.\[129, 130\]](#). Note that the dotted lines in the figures are only used to guide the eye.... 58
- Figure 3.8**(Figure 32) Average energy change ε_H of the formation of one pyridine-acid hydrogen bond, and enthalpic Flory parameter χ_H when mixing pyridine with different organic acids at the corresponding temperatures. Note that data are extracted and reprocessed from [ref. \[107\]](#). 60
- Figure 3.9**(Figure 33) The window width (L) of the cononsolvency transition: (a) Sketch of the definition of widow width using my theoretical model, see Figure 3.1c (for instance). (b) The width for cononsolvency transition of PNiPAAm polymers as a function of the experimental value of the effective Flory parameter between various cosolvents and water at a temperature close to 25°C. Data of the width are extracted and reprocessed from [Chapter 2](#) and [refs.\[40, 80, 122\]](#), data of the effective Flory parameter are extracted and reprocessed from [refs.\[87-89, 130, 134, 135\]](#). Note that in the Figure 3.9a, the solid blue line is a typical cononsolvency-transition curve; in the Figure 3.9b the dotted line is a guide to

the eye, and the blue error bars display the experimental uncertainties of the effective Flory parameter.	61
Figure 3.10 (Figure 34) The effect of an increase of the hydrostatic pressure in the cononsolvency transition of polymers can be numerically decomposed into a synergistic effect on the effective Flory parameters for the cosolvent-solvent interaction (χ_{cs}), the polymer-solvent interaction (χ_{ps}), and a reduction of the chemical potential change of mixing μ , as implemented in the extended adsorption-attraction model. Note that apart from variations of χ_{cs} and χ_{ps} , the other parameters remained fixed (as shown in Table 3.6). The arrows in Figure 3.10 are eye guides for possible pathways when the cononsolvency system changes from the lower-pressure to the higher-pressure states.	63
Figure 3.11 (Figure 35) Cononsolvency transition of a single PNiPAAm chain in methanol aqueous solutions, at a temperature of 20°C: open circles are experimental results and solid lines are theoretical fits using the physical model. Parameters of the PNiPAAm are: $M_w = 2.63 \times 10^7$ g/mol, $M_w/M_n < 1.10$. The experimental data are extracted and reprocessed from ref. [58] . The length of a Kuhn segment for single polymer chain in this study is chosen to be about ten repeating units of PNiPAAm.	66
Figure 3.12 (Figure 36) Molar Gibbs free energy of mixing for various alcohol/water mixtures at the standard state.	69
Figure 3.13 (Figure 37) Molar Gibbs free energy of mixing for 1-butanol/water mixtures at the standard state: accurate mixture compositions for phase separation are 1.91%mol and 48.84%mol of 1-butanol, while the calculation values for phase separation are about 2.15%mol and 54.6% mol of 1-butanol.	70
Figure 3.14 (Figure 38) Chemical potential change of mixing for various alcohol/water mixtures at the standard state.	70
Figure 3.15 (Figure 39) Effective Flory parameters for various alcohol/water mixtures at the standard state.	73
Figure 3.16 (Figure 40) Crosslink-density effect in the cononsolvency transition of poly(N-isopropylacrylamide) micro-gel. Data are extracted and reprocessed from ref.[122] , note that dotted lines in the figure are only used to guide eyesight.	74
Figure 3.17 (Figure 41) Crosslink-density effect in the cononsolvency transition of poly(N-isopropylacrylamide) macro-gel. Data are extracted and reprocessed from ref.[103] , note that dotted lines in the figure are only used to guide eyesight.	75

- Figure 3.18**(Figure 42) The reduction of cosolvent-solvent interaction ($\Delta\chi_{cs}$) as a function of various alcohol's molar fraction (x). Data are extracted and reprocessed from **ref.[138]**, note that dotted lines in the figure are guides to eyes. 76
- Figure 3.19**(Figure 43) The reduction of polymer-solvent interaction ($\Delta\chi_{ps}$) as a function of PEG400's volume fraction (y). Data are extracted and reprocessed from Han **[150]** and Muller **[151]**. 77
- Figure 3.20**(Figure 44) Molar excess Gibbs free energy as a function of molar fraction of DMSO in its aqueous solutions, when the temperature is at 25°C. Experimental data are extracted and reprocessed from **refs.[130, 134]**. Note that the solid line in the figure is a fit by using Eq.(3.37). 78
- Scheme 4.1**(Figure 45) A cartoon of fluorescence λ -DNAs translocating through PNiPAAm-grafted nanopores: (left) A three-dimensional side view, (right) a longitudinal-sectional zoom-in view of a nanopore. 84
- Figure 4.1**(Figure 46) An example to determine the number of DNA translocation events: the left picture is an original image data and the right picture is the counting results for the left picture. Note that the vision size of video data (one frame) is fixed in an area of $A = 135\mu m \times 135\mu m$ 85
- Figure 4.2**(Figure 47) Number of DNA translocation events with respect to pressure in tris-buffer solutions when DNA translocates through nanopores. As for PNiPAAm-grafted nanopores: (a) Membranes of different grafting density with molecular weight of $M_n = 1.5 \times 10^4 \text{ g/mol}$, $M_w/M_n = 1.18$; (b) Membranes of different grafting density with molecular weight of $M_n = 3.0 \times 10^4 \text{ g/mol}$, $M_w/M_n = 1.25$. The size of blank nanopores is 50 nm and test temperature is 298 K. Note that the dotted lines in the figures are guides to eyes. 86
- Figure 4.3**(Figure 48) Number of DNA translocation events with respect to pressure when DNA translocates through nanopores with different polymer grafting density: (a) In tris-buffer solutions, (b) in 4.76%vol ethanol-tris-buffer mixtures. As for PNiPAAm-grafted nanopores, molecular weight of the PNiPAAm polymer is $M_n = 1.5 \times 10^4 \text{ g/mol}$, $M_w/M_n = 1.18$. The size of blank nanopores is 50 nm and test temperature is 298 K. Note that the dotted lines in the figures are guides to eyes. 87
- Figure 4.4**(Figure 49) Number of DNA translocation events with respect to pressure when DNA translocates through nanopores with different polymer grafting density: (a) In tris-buffer solutions, (b) in 4.76%vol ethanol-tris-buffer mixtures. (c) In 9.09%vol ethanol-tris-buffer mixtures. (d) In 16.67%vol ethanol-tris-buffer mixtures. As for PNiPAAm-grafted nanopores, molecular weight of the PNiPAAm polymer is $M_n = 3.0 \times 10^4 \text{ g/mol}$, $M_w/M_n =$

- 1.25. The size of blank nanopores is 50 nm and test temperature is 298 K. Note that the dotted lines in the figures are guides to eyes.88
- Figure 4.5**(Figure 50) Number of DNA translocation events with respect to pressure in tris-buffer/ethanol mixtures, when DNA translocates through nanopores with different polymer grafting density: (a) For a higher grafting density of PNiPAAm-grafted nanopores, (b) for a lower grafting density of PNiPAAm-grafted nanopores. Molecular weight of the PNiPAAm polymer is $M_n = 1.5 \times 10^4 \text{ g/mol}$, $M_w/M_n = 1.18$. The size of blank nanopores is 50 nm and test temperature is 298 K. Note that the dotted lines in the figures are guides to eyes.89
- Figure 4.6**(Figure 51) Number of DNA translocation events with respect to pressure in tris-buffer/ethanol mixtures, when DNA translocates through nanopores with different polymer grafting density: (a) For a higher grafting density of PNiPAAm-grafted nanopores, (b) for a lower grafting density of PNiPAAm-grafted nanopores. Molecular weight of the PNiPAAm polymer is $M_n = 3.0 \times 10^4 \text{ g/mol}$, $M_w/M_n = 1.25$. The size of blank nanopores is 50 nm and test temperature is 298 K. Note that the dotted lines in the figures are guides to eyes.89
- Figure 4.7** (Figure 52) The normalized number of translocation events is plotted with respect to ethanol concentration change under different driven pressure. (a) For a higher grafting density of PNiPAAm-grafted nanopores, data are already used in Figure 4.5a. (b) For a lower grafting density of PNiPAAm-grafted nanopores, data are already used in Figure 4.5b. Molecular weight of the PNiPAAm polymer is $M_n = 1.5 \times 10^4 \text{ g/mol}$, $M_w/M_n = 1.18$. The size of blank nanopores is 50 nm and test temperature is 298 K. Not that the dotted lines in the figure are guides to eyes.....90
- Figure 4.8**(Figure 53) The normalized number of translocation events is plotted with respect to ethanol concentration change under different driven pressure. (a) For a higher grafting density of PNiPAAm-grafted nanopores, data are already used in Figure 4.6a. (b) For a lower grafting density of PNiPAAm-grafted nanopores, data are already used in Figure 4.6b. Molecular weight of the PNiPAAm polymer is $M_n = 3.0 \times 10^4 \text{ g/mol}$, $M_w/M_n = 1.25$. The size of blank nanopores is 50 nm and test temperature is 298 K. Note that the dotted lines in the figures are guides to eyes.91
- Figure 4.9**(Figure 54) Ethanol-concentration responsive of grafted PNiPAAm polymer around the rim of nanopores. (a) Different grafting-density membranes with molecular weight of $M_n = 1.5 \times 10^4 \text{ g/mol}$, $M_w/M_n = 1.18$; (b) Different grafting-density membranes with molecular weight of $M_n = 3.0 \times 10^4 \text{ g/mol}$, $M_w/M_n = 1.25$. The size of nanopores is 50 nm and test temperature is 298 K. Note that the dotted lines in the figures are guides to eyes.91

- Scheme 4.2**(Figure 55) A depiction of ethanol-concentration induced phase transition of PNiPAAm layer around the rim of nanopore under the condition of flow pressure..... 92
- Figure 4.10**(Figure 56) Swollen brush thickness of a PNiPAAm brush on a flat surface in ethanol/tris buffer mixtures. (a) Real-time swollen brush thickness of the PNiPAAm brush as a function of measurement time, pH value of the buffer is 7.45. (b) Average swollen brush thickness as a function of ethanol concentration obtained via in-situ Vis-ellipsometry at different pH values of buffer solutions. Parameters of the PNiPAAm brush are grafting density $0.143 \text{ chains/nm}^2$, $M_n = 6.1 \times 10^4 \text{ g/mol}$, and $M_w/M_n = 1.40$. Measurement temperature is at 25°C , note that the dotted lines in the Figure 4.10b are guides to eyes. 93
- Figure 4.11**(Figure 57) Cononsolvency responsive of grafted PNiPAAm polymer around the rim of nanopores. Molecular weight of the PNiPAAm polymer is $M_n = 1.5 \times 10^4 \text{ g/mol}$, $M_w/M_n = 1.18$. The grafting density of polymer layers is around 0.15 chains/nm^2 . The size of nanopores is 50 nm and the test temperature is 298 K..... 95
- Figure 4.12**(Figure 58) A graphic description how to get an error bar (ΔP_c) of a critical pressure by using Eq.(4.14). 97
- Figure 4.13**(Figure 59) A graphic description how to get an error bar (ΔP_c) of a critical pressure by using Eq.(4.15). 98
- Figure 5.1**(Figure 60) **(a)** The adsorption filed (U), is displayed as a function of monomer concentration (c). **(b)** The monomer concentration (c) is displayed as a function of chemical potential change of the cosolvent, μ . Model parameters used in the calculation are: $N = 10$, $\lambda = 1.0$, $\nu = 0$, $\gamma = 1.0$, $f = 4.0$, $\varepsilon = 0.5$, $\lambda\chi_{cs} = 0$, $\Delta\chi_{cs} = 0$ and $\chi_{ps} = 0$ 105
- Figure 5.2**(Figure 61) Illustration of the impact of cosolvent-solvent interaction on the predicted cononsolvency response of polymer solution. The monomer concentration (c) is displayed as a function of chemical potential change of the cosolvent, μ : A change of cosolvent-solvent interaction $\chi_{cs'}$ while other model parameters remained fixed as $N = 10$, $\lambda = 1.0$, $\nu = 0$, $\gamma = 1.0$, $f = 4.0$, $\varepsilon = 0.5$, and $\chi_{ps} = 0$ 106

List of tables

Table 2.1 (Table 1) Layer parameters (number-average molecular weight M_n , dry layer thickness h , and corresponding brush criteria such as critical grafting density σ^{**} , the radius of gyration of the chains in good solvent and poor solvent R_G and R_P respectively) of polymer films, which were used in this study.	20
Table 2.2 (Table 2) Solubility of PNiPAAm in short-chain polyols at the temperature of 25°C.	20
Table 2.3 (Table 3) Fitting parameters for the adsorption-attraction model.	26
Table 3.1 (Table 4) Parameter values used in numerically solving the extended adsorption attraction model from Figure 3.1(a) to Figure 3.1(f).	50
Table 3.2 (Table 5) Fit parameters for alcohol-water systems (polymer brush, $\sigma = 0.143$ chains/nm ² , 25°C, Figure 3.2). We choose λ and ν from their experimental values. The first part of the value for $\lambda\chi_{cs}$ is estimated as its experimental value, the second part of the value for $\lambda\chi_{cs}$ is a correction to fit the experimental data. Experimental value of PNiPAAm-water interaction (χ_{ps}) is around 0.40.....	52
Table 3.3 (Table 6) Fit parameters for alcohol-water systems (polymer macro-gel, 22°C, Figure 3.3). We choose λ and ν from their experimental values. The first part of the value for $\lambda\chi_{cs}$ is estimated as its experimental value, the second part of the value for $\lambda\chi_{cs}$ is a correction to fit the experimental data. Experimental value of PNiPAAm-water interaction (χ_{ps}) is around 0.40. The maximum possible degree of linking for the chemical crosslinker is 4, this condition requires the parameter value of $2 < f < 4$	53
Table 3.4 (Table 7) Fit parameters for 1-propanol/water and DMSO/water systems (polymer macro-gel, 25°C, Figure 3.4). We choose λ and ν from their experimental values. The first part of the value for $\lambda\chi_{cs}$ is estimated as its experimental value, the second part of the value for $\lambda\chi_{cs}$ is a correction to fit the experimental data. Experimental value of PNiPAAm-water interaction (χ_{ps}) is around 0.40. The maximum possible degree of linking for the chemical crosslinker is 4, this condition requires the parameter value of $2 < f < 4$	54
Table 3.5 (Table 8) Fit parameters for the ethanol-water system (polymer brush, 25°C, Figure 3.5). We choose λ and ν from their experimental values. The first part of the value for $\lambda\chi_{cs}$ is estimated as its experimental value, the second part of the value for $\lambda\chi_{cs}$ is a correction to fit the experimental data. Experimental value of PNiPAAm-water interaction (χ_{ps}) is around 0.40.....	55

Table 3.6 (Table 9) Parameter values applied while numerically solving the extended adsorption-attraction model (Figure 3.10, polymer macrogel, temperature is fixed at 25°C.). As for the conditions of low pressure and high pressure, the parameter values are chosen to be qualitatively consistent with the system of PNiPAAm macrogel/methanol/water at the pressures of 100kPa and 140MPa respectively. For additional details of estimating the pressure effect on the values of $\Delta\chi_{cs}$ and $\Delta\chi_{ps}$, we refer the reader to the sections 3.6.6 and 3.6.7	63
Table 3.7 (Table 10) Fit parameters for methanol-water systems (single polymer chain, 20°C, Figure 3.11). We choose λ and ν from their experimental values. The first part of the value for $\lambda\chi_{cs}$ is estimated as its experimental value, the second part of the value for $\lambda\chi_{cs}$ is a correction to fit the experimental data. Experimental value of PNiPAAm-water interaction (χ_{ps}) is around 0.40.....	65
Table 3.8 (Table 11) Values of γ_1^∞ , γ_2^∞ , A_{12} and A_{21} for different alcohol-water systems at the temperature of 298.15K (25°C).....	71
Table 3.9 (Table 12) Values of γ_1^∞ , γ_2^∞ , A_{12} and A_{21} for different alcohol-water systems at the temperature of 295.15K (22°C).....	72
Table 4.1 (Table 13) Polymer grafting density of higher and lower grafted membranes with different molecular weight. In this study, we used a scaling approach to estimate grafting density. See section 4.5.1 for the details of determining grafting density. The layer thickness is calculated based on the data of DNA translocation events which are measured at the temperature of 298 K.....	81
Table 4.2 (Table 14) Fit parameters for the ethanol-tris buffer system (polymer brush, 298 K, Figure 4.11). We choose λ and ν from their experimental values. The first part of the value for $\lambda\chi_{cs}$ is estimated as its experimental value, the second part of the value for $\lambda\chi_{cs}$ is a correction to fit the experimental data. Experimental value of PNiPAAm-water interaction (χ_{ps}) is around 0.40.....	95

Acknowledgements

Three years ago when I was determined to quit my job and went to Germany pursuing a PhD degree, for the first time I left my home country where I lived more than thirty years. I still clearly remember the day I arrived at the Dresden airport is April-02-2017, I were warmly welcomed by my colleagues Dr. Chanfei Su and Dr. Holger Merlitz in the airport. From the day on I started my life in Germany.

I am greatly indebted to one of my supervisors Prof. Dr. Jens-Uwe Sommer. Thank him for providing me an invaluable chance to finish my PhD study. Throughout my study, he has been supporting funding and mentoring for my theoretical study, while providing very insightful discussions and in partalr patience for my naïve in knowledge of Physics. I also would like to thank another supervisor Prof. Dr. Andreas Fery. Throughout my PhD study, he has been mentoring for my experimental study, and most important of all providing helps for my research collaboration in different groups of IPF Dresden.

Here I especially thank Dr. Petra Uhlmann, Dr. Sebastian Rauch and Dr. Eva Bittrich who taught me the knowledge of preparing polymer brushes appropriate for my PhD project and how to analyze them, as well as experimental skills of (in-situ) analysis and many other fundamentals of experimental work. I also thank Dr. Alexander Münch and other members in the group of Dr. Petra Uhlmann that helped me so much in many ways, not merely experimentally.

I gratefully thank our collaborator within the École normale supérieure de Lyon, Dr. Fabien Montel and Bastien Molcrette, who gave me a lot of support and hosted me during the research collaboration in Lyon. I also thank my colleagues Dr. Holger Merlitz who provided knowledge and valuable discussions that are beneficial to this work. Last, but not least, I would like to thank my family and friends for encouraging and supporting me during these years. All these people have been essential to the completion of my thesis.

List of publications

Publications during the period of PhD study

(The symbol “*” represents corresponding authors)

Huaisong Yong*, Bastien Molcrette, Marcel Sperling, Fabien Montel*, and Jens-Uwe Sommer*. *Regulating the Translocation of DNA through Poly(N-isopropylacrylamide)-Decorated Switchable Nanopores by Cononsolvency Effect*. **Macromolecules**, 2021, DOI: 10.1021/acs.macromol.1c00215.

Huaisong Yong*, Holger Merlitz, Andreas Fery, and Jens-Uwe Sommer*. *Polymer Brushes and Gels in Competing Solvents: The Role of Different Interactions and Quantitative Predictions for Poly(N-isopropylacrylamide) in Alcohol-Water Mixtures*. **Macromolecules**, 2020, 53(7), 2323-2335.

Huaisong Yong*, Eva Bittrich, Petra Uhlmann, Andreas Fery*, and Jens-Uwe Sommer*. *Co-nonsolvency transition of poly(N-isopropylacrylamide) brushes in a series of binary mixtures*. **Macromolecules**, 2019, 52, 6285-6293.

Huaisong Yong, Sebastian Rauch, Klaus-Jochen Eichhorn, Petra Uhlmann, Andreas Fery*, and Jens-Uwe Sommer*. *Co-nonsolvency Transition of Polymer Brushes: A Combined Experimental and Theoretical Study*. **Materials**, 2018, 11, 991.

Huaisong Yong, Sebastian Rauch, Klaus-Jochen Eichhorn, Petra Uhlmann, Andreas Fery*, and Jens-Uwe Sommer*. *Co-nonsolvency Transition of Polymer Brushes: A Combined Experimental and Theoretical Study*. Poster presentation at **16th DRESDEN POLYMER DISCUSSION: Concepts of Polymer Physics – From Soft Matter to Biological Systems**, 13th – 16th May, 2018, Meißen, Germany.

Other publications

Other publications that are unrelated to my PhD study can be found from my Google Scholar profile: <https://scholar.google.com/citations?user=iUtQp0wAAAAJ&hl=en>

Erklärung

Hiermit versichere ich, dass ich die vorliegende Arbeit ohne unzulässige Hilfe Dritter und ohne Benutzung anderer als der angegebenen Hilfsmittel angefertigt habe; die aus fremden Quellen direkt oder indirekt übernommenen Gedanken sind als solche kenntlich gemacht. Die Arbeit wurde bisher weder im Inland noch im Ausland in gleicher oder ähnlicher Form einer anderen Prüfungsbehörde vorgelegt.

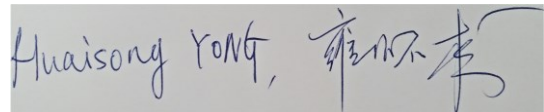
Die Dissertation wurde in der Zeit von April 2017 bis Dezember 2020 unter der Betreuung von Herrn Prof. Dr. Andreas Fery und Herrn Prof. Dr. Jens-Uwe Sommer am Leibniz-Institut für Polymerforschung Dresden e.V. in der Institut Theorie der Polymere und Abteilung Nanostrukturierte Materialien angefertigt.

Es haben keine früheren erfolglosen Promotionsverfahren stattgefunden.

Ich erkenne die Promotionsordnung der Fakultät Mathematik und Naturwissenschaften an der Technischen Universität Dresden vom 23. Februar 2011 an.

Dresden, December-15-2020

Signature

The image shows a handwritten signature in blue ink on a light gray background. The signature is written in a cursive style, with the name 'Huaisong Yang' in English and Chinese characters '杨怀松' (Yang Huaisong) in Chinese. The signature is written in a fluid, connected manner.